Response of the Indian and African monsoons to anthropogenic climate change

Marcellin Guilbert

To cite this version:

Marcellin Guilbert. Response of the Indian and African monsoons to anthropogenic climate change. Ocean, Atmosphere. Sorbonne Université, 2023. English. NNT : 2023SORUS454 . tel-04402683

HAL Id: tel-04402683
https://theses.hal.science/tel-04402683

Submitted on 18 Jan 2024

THESE DE DOCTORAT DE SORBONNE UNIVERSITÉ

École doctorale : 129 - Sciences de l'Environnement d'Île-de-France

Spécialité: Climatologie

Présentée par

Marcellin GUILBERT

Pour obtenir le titre de

DOCTEUR DE SORBONNE UNIVERSITÉ

Réponse des moussons indienne et africaine au changement climatique d'origine anthropique

Soutenance prévue le 20 Octobre 2023

Composition du jury :

M.	Francis CODRON	Président
Mme.	Elsa MOHINO	Rapportrice
M.	Hervé DOUVILLE	Rapporteur
M.	Robert JNGLIN WILLS	Examinateur
M.	Benjamin SULTAN	Examinateur
Mme.	Juliette MIGNOT	Directrice de thèse
M.	Pascal TERRAY	Directeur de thèse

Laboratoire d'Océanographie et du Climat: Expérimentation et Approches Numériques

Résumé

Les moussons se définissent par un renversement saisonnier des vents qui apporte plus de 80% des précipitations annuelles en Inde et au Sahel, qui en sont largement tributaires. Prévoir leur évolution sous l'effet de l'Homme, qu'on appelle la réponse anthropique, est donc d'une importance capitale d'autant plus que ces deux régions abriteront deux milliards d'habitants en 2100. Cependant, les prédictions de ces moussons que nous sommes capables de fournir sont accompagnées de fortes incertitudes portant sur l'amplitude et parfois sur le signe même de ces changements. En utilisant les simulations réalisées pour le 6^{eme} rapport du Groupe Intergouvernemental sur l'évolution du Climat (GIEC), nous cherchons à comprendre l'origine de ces incertitudes dans les modèles de climat.

La performance des modèles à reproduire l'évolution historique (1850-2014) est un facteur de confiance dans leur capacité à prévoir l'avenir. Cependant, ces évolutions historiques sont également marquées par des incertitudes. La première question à laquelle nous voulons répondre est donc: peut-on expliquer l'incertitude des modèles à simuler l'évolution des moussons indienne et sahélienne sur la période historique? Les erreurs que font les modèles par rapport aux observations sont appelées des biais et nous souhaitons tester l'hypothèse qu'ils sont susceptibles d'expliquer en partie les différentes réponses des moussons simulées par les modèles.

Nous traitons d'abord le cas de l'Inde, et suivant cette hypothèse, nous montrons que les biais de température des modèles dans l'océan Pacifique équatorial modulent la façon dont ils simulent la réponse historique de la mousson indienne. En effet, nous montrons qu'en modulant la réponse historique de l'océan Pacifique, les biais dans ce dernier affectent la mousson indienne via des mécanismes similaires à ceux qui lient l'ENSO (El Niño – Southern Oscillation) et la mousson en variabilité interannuelle.

Nous reproduisons ensuite la même étude pour la mousson sahélienne, où nous montrons que des biais de température dans tous les Tropiques sont fortement liés à la façon dont les modèles simulent son évolution historique. Cependant, nous n'identifions pas le mécanisme physique précis liant ce biais à la mousson sahélienne, mais montrons que cette dernière est fortement dépendante de la façon dont les modèles simulent la réponse du gradient inter-hémisphérique de température, ce qui est physiquement cohérent avec le rôle connu de ce gradient comme modulateur de la position de la zone de convergence intertropicale (ITCZ).

Dans la deuxième partie de nos investigations nous basculons dans les projections (2014-2100) basées sur un scénario pessimiste de fortes émissions et adressons la question suivante: quelles sont les sources d'incertitudes de la réponse forcée des moussons au sein des projections? Nous abordons cette fois le cas du Sahel en premier et lions la diversité des réponses à travers les modèles à deux facteurs: la réponse du gradient inter-hémisphérique de température et celle du Pacifique équatorial. Les mécanismes sous-jacents font intervenir une migration de l'ITCZ et une circulation de surface renforcée pour le premier, et une modulation de la circulation de Walker et des ondes tropicales pour le second. Via ces deux facteurs, nous expliquons 62% de l'incertitude des projections au Sahel.

Nous traitons finalement le cas du futur de la mousson indienne, et montrons que les incertitudes de celle-ci sont fortement liées à la réponse en température des déserts allant du Sahara au Pakistan, qui influencent également la réponse de la mousson sahélienne. En effet, plus la réponse en température est forte, plus le Heat Low sur les déserts sera prononcé ce qui renforce la circulation en surface des moussons.

Summary

The monsoons are defined by a seasonal reversal of winds that brings more than 80% of annual precipitation to India and the Sahel, which are largely dependent on them. Predicting their evolution under the influence of man - the so-called anthropogenic response - is therefore of the utmost importance, all the more so as these two regions will be home to two billion people by 2100. However, the monsoon projections we are currently able to provide are accompanied by major uncertainties concerning the amplitude and sometimes the very sign of these changes. Using recent simulations carried out for the 6^{th} report of the Intergovernmental Panel on Climate Change (IPCC), we seek to understand the origin of these uncertainties in climate models.

The performance of these models in reproducing historical trends (1850-2014) is a factor of confidence in their ability to predict the future. However, these historical trends are also marked by uncertainties. Consequently, the first question we want to answer is: can we explain the uncertainty of the models in simulating the evolution of the Indian and Sahelian monsoons over the historical period? Model errors in relation to an observed climatology calculated over a reference period of at least thirty years are called biases, and we wish to test the hypothesis that they may partly explain the different responses of the models.

We first consider the case of India, and following this hypothesis, we show that the climatological temperature biases of models in the equatorial Pacific Ocean modulate the way they simulate the historical response of the Indian monsoon. Indeed, we show that by modulating the historical response of the Pacific Ocean, climatological biases in the latter affect the Indian monsoon via mechanisms similar to those linking ENSO (El Niño - Southern Oscillation) and monsoon interannual variability.

We then reproduce the same study for the Sahelian monsoon, where we show that climatological temperature biases in all the Tropics are strongly linked to the way models simulate its historical evolution. We do not, however, identify the precise physical mechanism linking this bias to the Sahelian monsoon, but we do show that the latter is strongly dependent on the way models simulate the response of the inter-hemispheric temperature gradient, which is physically consistent with the known role of this gradient as a modulator of the position of the inter-tropical convergence zone (ITCZ).

In the second part of our investigations, we switch to projections (2014-2100) based on a pessimistic scenario of high emissions, and address the following question: what are the sources of uncertainty in the forced response of the monsoons within the projections? This time, we tackle the Sahel case first and link the diversity of responses across models to two factors: the response of the inter-hemispheric temperature gradient and that of the equatorial Pacific. The underlying mechanisms involve ITCZ migration and enhanced surface circulation for the first factor, and modulation of the Walker circulation and tropical waves for the second. These two factors account for 62% of the uncertainty in Sahel projections.

Finally, we look at the future of the Indian monsoon, and show that its uncertainties are strongly linked to the temperature response of deserts from the Sahara to Pakistan, which also influences the response of the Sahelian monsoon. Indeed, the stronger the temperature response, the more pronounced the thermal depression over the deserts, the stronger the monsoon surface circulation and hence the precipitation.

Keywords: Climate - Variability - Monsoon - Sahel - India - CMIP - Teleconnections - ENSO

Contents

List of Figures

List of Tables

General introduction

Introduction 1

At the time of writing this preamble on 9 May 2023, the Intergovernmental Panel on Climate Change (IPCC) sixth assessment report (AR6) states that global temperature at the surface of the Earth has risen by +1.1°C compared to pre-industrial values. The cause of this warming is unequivocal: mankind, through the use of fossil fuels and the accompanying emission of greenhouse gasses (GHGs), is playing the sorcerer's apprentice with the Earth. Beyond this global rise in temperature, other major changes are expected, notably in the water cycle and therefore rainfall intensity and distribution (AR6 chapter 8). In developed countries, what we once thought was only for others is now knocking on our door: the summer of 2022 in France was marked by unprecedented drought, forest's fires and water restrictions in many departments, and the winter was marked by a historical record of 32 days without significant rainfall. Monsoon regions, where annual rainfall is concentrated in the summer season, have long known the ravages of erratic rainfall. They are home to half of humanity, which rely heavily on rain-fed agriculture, and where the infrastructure to manage water resources is limited. Consequently, rainfall variations have dramatic consequences such as landslides, flooding, crop failure and drinking water scarcity.

In order to understand the consequences of our activities on the Earth equilibrium and to be able to act accordingly, climate models simulate future climates shaped by our emission choices. In a scenario where we pursue our current economic growth, it is very likely that global warming will exceed 4°C and could even exceed 5°C. While the models give relatively consistent results for global temperature, there are large uncertainties about changes in precipitation and the hydrological cycle, especially in monsoon regions (AR6 chapter 8). In this context and the particular cases of the Sahelian and Indian monsoons, we will try to answer the following question: what are the origins of model uncertainties in the Sahelian and Indian monsoons simulations and projections? The question may seem daunting at first, but the following introduction will equip us for the adventure that awaits us in the next chapters. We will begin by introducing the great machine of the climate system, its dynamics and the factors that shape it, both natural and anthropogenic. We will then present the place of the monsoons in this grand scheme and highlight their importance in more detail. Finally, we will explain how to put the Earth into a computer by presenting what climate models are, as well as the limitations associated with them. Here we go !

1.1 Did I hear climate?

Nothing is better to start than a quote, so let us turn to the wise words of Edward Lorenz to define climate: "Climate is what you expect, weather is what you get". Lorenz's quote gives a simplified yet powerful version of the precise definition of climate provided by the IPCC, which states that "climate in a narrow sense is the statistical description in terms of the mean and variability of relevant quantities over a period ranging from months to thousands or millions of years" (IPCC, 2021: Annex VII: Glossary). While surface air temperature and precipitation are the first key climatic quantities that come to mind, this thesis will also use other characteristics of the climate system such as wind and temperature at different atmospheric levels, as well as relative humidity, which all fall under the category of 'relevant quantities' mentioned by the IPCC. The most commonly used time interval to define climate is 30 years.

The thirty-year average of a climate variable provides a first-order description of its probability distribution at a given location and this will be the metric primarily studied in this thesis under the name of climatology. It is a simple but powerful tool that has, for example, enabled Wladimir Köppen to create one of the most famous global climate classifications (Koppen, 1936) using only precipitation and temperature (Figure.1.1). This classification defines the 5 major types of climate that we learn in middle school: tropical, dry, temperate, continental, and polar. Each type is then subdivided into subtypes based on variations in temperature and precipitation patterns, but this becomes the domain of specialized individuals such as geographers, hydrologists or climatologists...

It is possible to go further in the description of the probability distribution of a climate variable by using, for example, the second-order moment, namely the standard deviation, which corresponds to what is called climate variability. The best-known example of variability is the seasonality, which falls into the category of natural, but periodic, variability shaped by the tilt of the Earth's axis and its orbit around the Sun. However, there is a wide range of variability, the origins of which may be natural or forced, occurring on very different timescales, up to several millennia. Neverthelss, such definitions of the first two moments of the probability distribution of a climate variable are relevant in a stationary climate, or at least one that is stationary on the time scales of interest. It is not necessarily the case today because of the impacts of human activities on the climate and the rapid changes that they generate. As an example, Météo France reevaluates seasonal normal temperatures every ten years, which increase on average by 0.4°C due to the rapid global warming, so that a "normal" month of May today would have been considered exceptionally hot in the 1970s. Therefore, due to the rapid human-induced changes, these designations are potentially misleading, and it is important to place things in relation to a fixed reference. In our case, the reference will be the period around 1850, which we are using as an approximation of the pre-industrial era, and therefore a climate in which man has not yet had much impact.

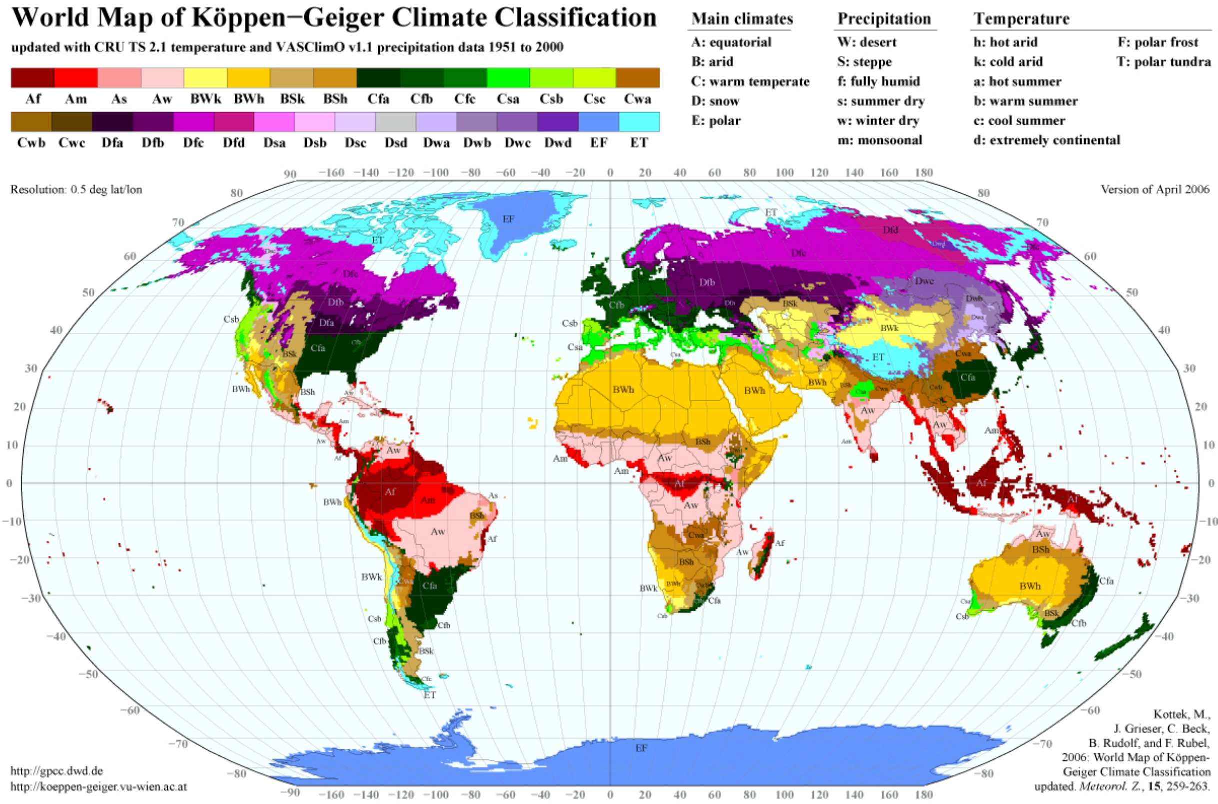

Figure 1.1: World map of Köppen climate classification (Kottek et al, 2006).

1.2 The climate system

1.2.1 Definition of the climate system

As always in sciences, the first step is to define the system under study. The climate system encompasses all the surface components of the Earth, namely the atmosphere, oceans, cryosphere, and continental surfaces, including the biosphere (Figure.1.2). The main object of study of climate sciences is the global energy (im)balance of this system, which has been greatly disrupted by human activities, resulting in modifications in all its components and in their interactions on large spatio-temporal scales. Of the five components of the climate system named above, three will be of particular interest to us in this thesis: the atmosphere, the oceans and the continental surfaces. We therefore describe them in more detail below, and it should be borne in mind that although we describe them individually, they are tightly coupled.

The atmosphere

The atmosphere is a layer of gasses that surrounds the Earth, extending from the surface up to about 10,000 km. It contains a complex mixture of gases, including nitrogen, oxygen, and water vapor, as well as trace amounts of other gases such as carbon dioxide, methane, and ozone. The atmosphere is responsible for regulating the Earth's temperature through the greenhouse effect (mainly due to the water vapor), which traps heat and keeps the planet warm enough to support life. Through its circulation and the water cycle, the atmosphere also participates in the redistribution of energy on Earth, as we will develop later. The troposphere, which is the first 10 km of the atmosphere and our subject of study, is both the air we breathe as well as the weather and the stage for our activities.

The oceans

The oceans cover about 70% of the Earth's surface and play a critical role in the climate system. They absorb and store large amounts of heat, carbon dioxide, and other gases from the atmosphere, and they transport heat, salt and nutrients around the globe through ocean currents. The oceans also affect the Earth's albedo (the amount of sunlight reflected back into space), and they provide habitat for a wide range of marine organisms.

Continental surfaces

The land surfaces include all non-frozen parts of the Earth's surface, including forests, grasslands, deserts, and urban areas. They interact with the atmosphere and oceans through processes such as evapotranspiration (the combined loss of water to the atmosphere through evaporation and transpiration by plants) and runoff, which affect the water cycle and can influence weather patterns.

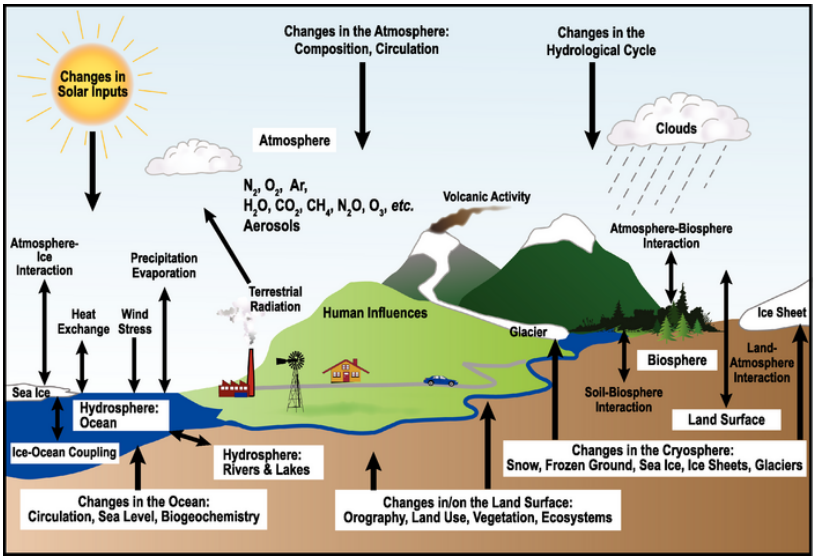

Figure 1.2: Components of the Climate System, Processes, and Interactions (IPCC, AR4).

1.2.2 Internal variability and external forcing

The state of the climate system and its related climate features, such as temperature or precipitation, may vary around its average state for two reasons: external forcings and internal variability. External forcings refers to any factors external to the Earth's climate system (as defined above) that can alter the balance of energy and induce shifts in temperature, precipitation, and other climate variables at both the global and regional scales. External forcing can be divided into two categories: natural and anthropogenic.

Natural forcing

Natural forcing includes phenomena like changes in solar radiation and volcanic eruptions, which can have significant effects on the Earth's climate. A well-known example is the variation in the distribution of solar radiation at the Earth's surface due to its rotation and the obliquity of its axis of rotation. This can be seen as a natural and periodic forcing that gives rise to the alternance of the day and the night and to the seasons we mentioned earlier, and is intrinsically linked to the monsoons as we will explain later. On much longer time scales (>10,000 years), variations in the Earth's orbital parameters also give rise to spectacular changes in the radiation received by the Earth. This forcing is responsible for the alternation between ice ages and interglacial periods. Finally, we can have more sporadic forcings, such as volcanic activity which leads to more abrupt and less predictable changes. As an illustration, the Pinatubo eruption in 1991 released large amounts of aerosols into the stratosphere, reflecting sunlight back into space and leading to a drop in average surface temperatures by about 0.5°C in the year following the eruption (Graft et al., 1993).

Anthropogenic forcing

Anthropogenic forcing refers to the impact of human activities on the climate system, such as deforestation, GHGs and aerosol emissions. These anthropogenic factors can cause long-term changes in the Earth's energy balance, some of which are counteracting and some of which are synergistic, but which ultimately lead to the global warming we are experiencing. We will give a detailed description of their effects on the climate and more specifically on the monsoons later in the introduction.

Internal variability

Internal variability refers to variations resulting from the interactions between the different components of the climate system, mainly the ocean and the atmosphere which are inherently unstable due to being fluids. These fluctuations can result in changes in temperature, precipitation, and circulation patterns. Internal variability is typically organized in large-scale perturbations from the mean state, with specific time and frequency characteristics called modes of variability. The most prominent mode of climate variability at interannual timescales is the El Niño-Southern Oscillation (ENSO) which is an irregular and coupled ocean-atmosphere phenomenon in the tropical Pacific that can affect precipitation patterns and temperatures worldwide for several months or a few years (AR6 chapter 4). In particular, El Niño events are associated with a global increase in the Earth's temperature that is superimposed on anthropogenic warming, leading to fears of severe heat waves when they occur, as expected for this summer of 2023. We will provide an overview of ENSO later in the introduction, when we describe the mechanisms explaining its global impacts, which will be extensively used in Chapters

3 and 4. The sum of internal variability and of the fluctuations due to natural forcing is known as natural variability.

How about a mix of all of them?

An important degree of complexity of the climate system is that internal variability, natural forcing and anthropogenic forcing can interact, amplify, or counteract each other at both the regional and global scales during some time intervals. This was the case in the early 2000s, when a combination of volcanic activity, low solar activity, and specific pattern of internal variability slowed down the warming trend over the period 1998-2012 compared to previous decades. Climate skeptics then claimed that global warming had stopped, and in a sense, we would have liked them to be right. However, it was actually just a temporary pause known as the global warming hiatus (Held, 2013;Deser et al., 2017), and recent observations show that warming has since resumed at a faster pace. This interplay illustrates why it is difficult to isolate and fully understand the specific impact of anthropogenic forcing on the climate, and consequently to anticipate the future. In light of these challenges, a range of statistical, dynamical and observational methods have been developed in order to separate the effects of internal variability and external forcings. These so-called detection and attribution approaches involve analyzing long-term observed trends and patterns, as well as simulations performed with climate models to understand the relative contributions of different factors to global temperature or precipitation changes. The notion of a climate model may seem unclear at the moment, but we will come back to it in detail later; for the moment let us assume that it is an (unperfect) digital representation of the Earth climate. The results from such methods are illustrated in Figure.1.3 which displays the relative impact of the different forcings on global warming trend over the 1951-2010 period (Morice et al., 2012).

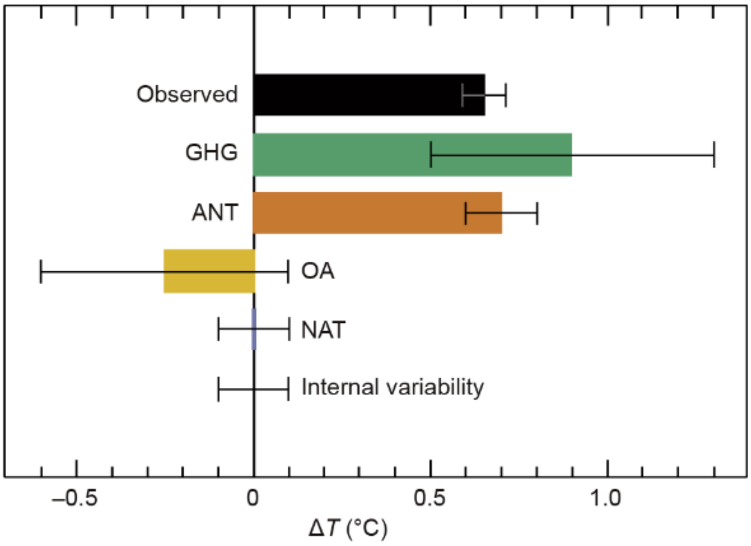

Figure 1.3: attribution of global warming trends over the 1951-2010 period to well-mixed GHGs, anthropogenic forcing which includes GHGs and anthropogenic aerosols (ANT), aerosols (OA), natural forcing (NAT) and internal variability. From Morice et al., 2012.

1.3 Energetics and dynamics of the climate system

1.3.1 Energy balance of the climate system

The Earth's radiative budget refers to the balance between incoming and outgoing radiations at the top of the Earth's atmosphere (Figure.1.4). The Earth receives energy from the sun in the form of shortwave radiation (primarily visible light) and radiates energy back into space in the form of longwave radiation (primarily infrared). We will first describe the integrated version of the Earth's radiative balance, i.e. its average on a global and annual scale, before refining this vision regionally and seasonally. This will allow us to introduce more rigorously the notion of season as well as the atmospheric and oceanic circulations that result from it. A tempting program that will open the highway to the monsoons, at last!

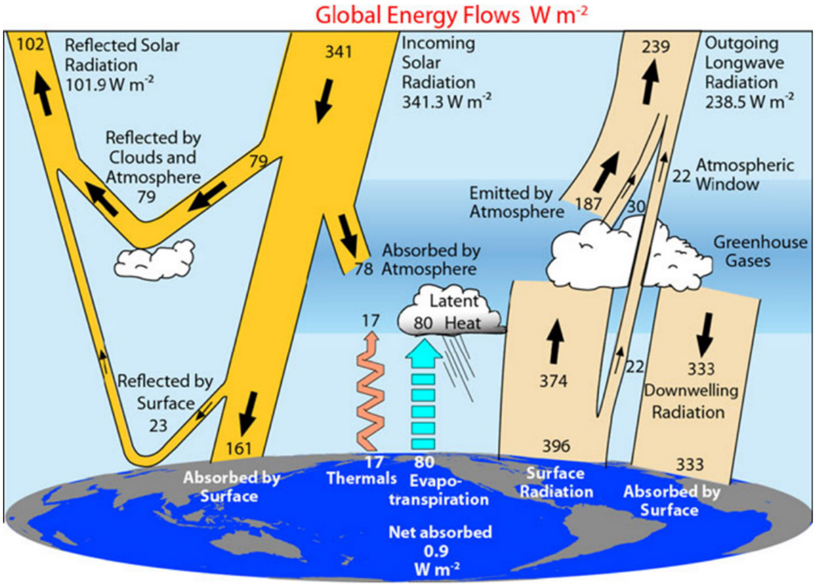

Figure 1.4: Schematic of the radiative balance of the Earth (provided by UCAR Center for Science Education).

The sun is the source of energy that powers the Earth (Figure.1.4). On a yearly and global average, it provides 341 $W.m^{-2}$ at the top of the Earth's atmosphere. The atmosphere absorbs 20% of the solar incident radiation and about 30% is reflected back to space by the atmosphere and earth's surfaces with a high albedo. As defined above, albedo is a quantity that refers to the ability of the Earth's surfaces, in particular the bright ones (clouds, deserts, ice) to reflect incident light .The remaining 50% is absorbed by the surface (both ocean, land and cryosphere). After absorbing solar energy, the surface will seek energy balance through three types of cooling: sensible heat, latent heat and black body radiation. The latter corresponds to the emission of infrared radiation in proportion to the surface temperature. However, the atmosphere contains species that strongly absorb infrared radiation, such as water vapor and GHGs. The atmosphere will then also try to reach energy balance, but its only way to do so is to emit infrared radiation in all directions. Some of this radiation then returns to the surface and constitutes a second source of heating, which is what we call the greenhouse effect. The greenhouse effect allows life to exist on Earth, because without it the average global temperature would be -18°C. However, by emitting GHGs through our activities, we amplify this second source of energy towards the surface, and the system seeks a new energy balance. All the cooling terms from the surface therefore increase, especially the infrared radiation emitted by the surface, which is accompanied by the rise in atmospheric temperature that we are currently experiencing. In fact this atmospheric rise of temperature is only a small (yet directly felt by humans) proportion of the excess of heat induced by the anthropogenic increase of the greenhouse effect: 90% of the excess of heat is stored in the ocean interior at depth. This may induce dynamical adjustments that can further modify the surface climate.

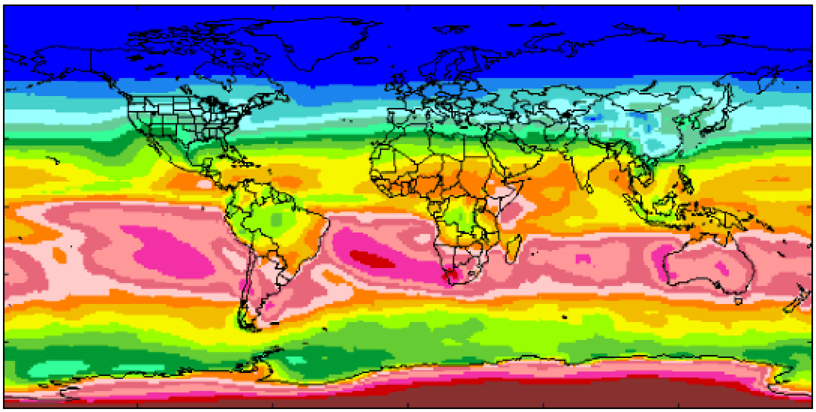

January 1984–1993

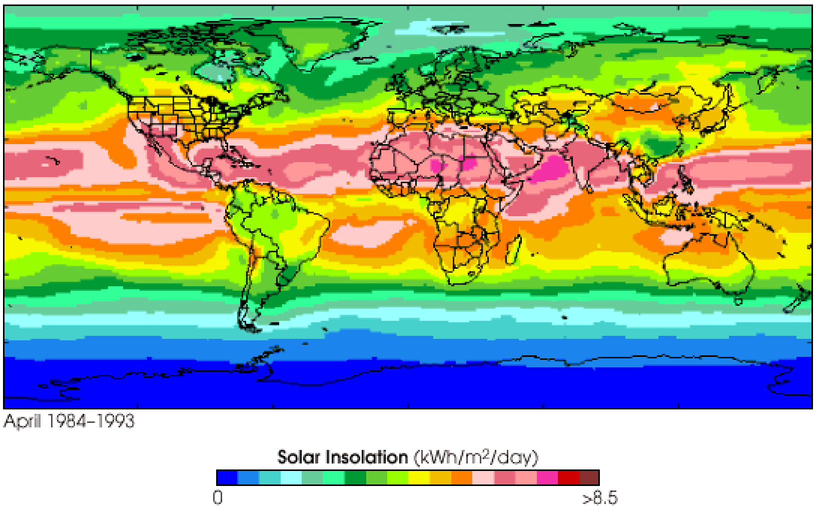

April 1984–1993

Figure 1.5: Solar insolation map averaged over ten year for January (top) and April (bottom) (Surface Meteorology and Solar Energy Project, NASA Langley Research Center, and the ISCCP Project.)

This integrated view of the Earth's radiative balance (and imbalance) hides a more complex reality if we remove time and space averaging. Firstly, keeping the annual average, the fact that the Earth is not flat (unless...) implies that the Equator receives more energy than the poles. There is therefore a spatial energy imbalance that will set in motion the oceanic and atmospheric masses to redistribute this energy surplus. Secondly, if we now look at monthly averages, because of the inclination of the Earth's axis of rotation in relation to its plane of rotation around the sun, the northern and southern hemispheres will successively receive more or less solar energy (Figure.1.5). This is what gives rise to the seasons as mentioned earlier; we speak of a boreal summer when the northern hemisphere receives more energy, and a boreal winter when it receives less. Thus, the energy imbalance at the Earth's surface also varies throughout the year, as do the atmospheric and oceanic circulations that accompany it. For example, the Indian and Sahelian monsoons are a feature of the boreal summer atmospheric circulation, but we will come back to this in detail later.

We now have the fundamentals on the radiative balance on Earth, its major variations in space and time and the accompanying imbalances, which set the oceans and the atmosphere in motion. Moving on, we will now describe these circulations and the way they redistribute energy, which will be a very useful foundation for discussing monsoons!

1.3.2 Dynamics of the climate system

If the redistribution of energy on Earth gives rise to oceanic and atmospheric circulations, one last detail crowns it all: the Earth turns! The Coriolis force is the result of the Earth's rotation for an observer at its surface. It is a central element that shapes the circulation of fluids on Earth. In the Northern Hemisphere, the Coriolis force is directed towards the east for an object moving northward and towards the west for an object moving southward. Conversely, in the Southern Hemisphere. The intensity of this force is zero at the Equator and increases with latitude, adding a little more complexity and beauty to the system (Figure.1.6). Indeed, rather than two cells connecting the Equator to the poles (left), we observe that a more complex structure emerges (right).

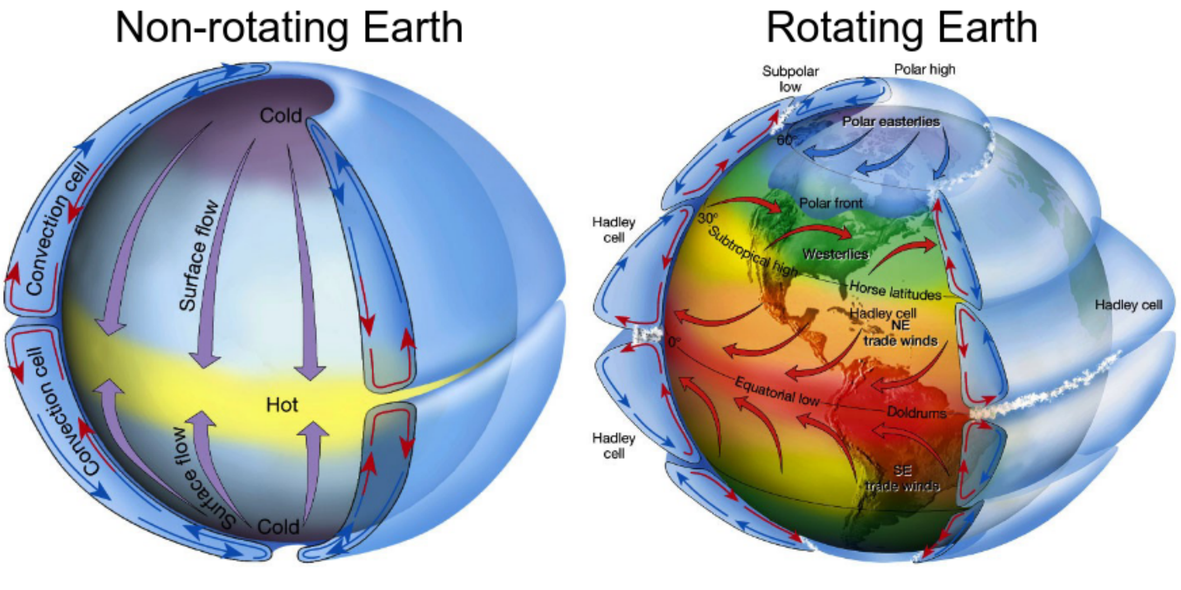

Figure 1.6: Diagram of atmospheric circulation on a non-rotating and rotating Earth (from Lutgens and Tarbuck, 2001).

As part of our work on monsoons, we are primarily interested in circulations within the Tropics. Therefore, within the set of atmospheric cells represented in Figure.1.6 we will primarily focus on the cells closest to the Equator, known as the Hadley circulation, and explain, among other things, why it does not extend to the poles. While this circulation broadly describes the meridional (north-south) circulation of the atmosphere in the Tropics, there is also a zonal (east-west) circulation called the Walker circulation, which completes the picture of large-scale tropical dynamics.

The Hadley circulation

As mentioned earlier, on an annual average, the surface of the Earth is heated more at the Equator than at higher latitudes. Consequently, the air at the Equator is warmer and less dense than the air at the poles which leads to a rising motion. As the air rises, it expands and cools, causing water vapor to condense, which releases latent heat into the atmosphere and forms clouds. In the lower layers, this rising motion creates a low-pressure zone near the Equator toward which surface winds converge. Due to the Coriolis force, these winds have an eastward component in both hemispheres and form the well-known trade winds. These winds are famous to sailors and were named as such due to their role in maritime commerce during the 16^{th} century. This region of low-level wind convergence and upward motion is called the InterTropical Convergence Zone (ITCZ). It corresponds to the region where precipitation is concentrated in the Tropics and is closely related to monsoons, as we will explain later. After reaching the upper-troposphere due to the upward motion, the air flows towards the poles, reducing its distance from the Earth's rotation axis and resulting in an increase in its zonal velocity in accordance with the conservation of angular momentum. This leads to the limit of its meridional extension at around 30° latitude in both hemispheres (Figure.1.6). Furthermore, it cools as it travels poleward and begins to sink back toward the surface which creates a high-pressure region known as the subtropical highs. These are closely linked to deserts, which are very common at these latitudes in both hemispheres. The descending air then flows back towards the Equator as surface winds, completing the trade winds and the Hadley cell.

This annual and zonal average view gives a rough outline of the Hadley circulation. However on a shorter timescale, we know that the Northern and Southern Hemispheres alternately experience a period of the year during which they receive an energy surplus. As the Hadley circulation arises from the need to redistribute this surplus, it is natural for it to exhibit seasonality in accordance with these variations (Figure.1.5). During the boreal summer, when the Northern Hemisphere has an excess of energy, the Hadley circulation deforms and loses its symmetry with respect to the Equator. The ITCZ shifts northward, and the cell in the Southern Hemisphere expands to the North and strengthens to intensify the energy transport towards this hemisphere (and conversely during boreal winter). Figure.1.7 shows a schematic of this seasonal circulation, with the alternating strength and expansion of the Hadley cells in each hemisphere depending on the season. At mid-latitudes, Figure.1.7 also suggests another rotational circulation in the meridian plane, called Ferrel circulation, which we will not focus on as our attention is on the Tropics, but which is in agreement with Figure.1.6

Figure.1.7 shows that with the seasons, the zone of convergence and ascent corresponding to the ITCZ, which has been said to be the heart of precipitation in the Tropics, moves on either side of the Equator. In boreal summer, it is located around 15°N . This latitude corresponds to the latitude of the Indian and Sahel monsoons. The latter can thus be interpreted as a regional manifestation of the ITCZ. We therefore understand one of the reasons why rainfall only exists during a particular season in the monsoon regions, which corresponds to the boreal summer in the case of India and the Sahel. The inter-hemispheric energy imbalance associated with the seasons is therefore a first mechanism at the origin of the monsoons, but it is not the only one and we must look for explanations on a regional scale to refine our vision as monsoons concern only some specific areas at subtropical latitudes. Before that however, as promised, we will explore the Tropics in the zonal direction and describe the Walker circulation!

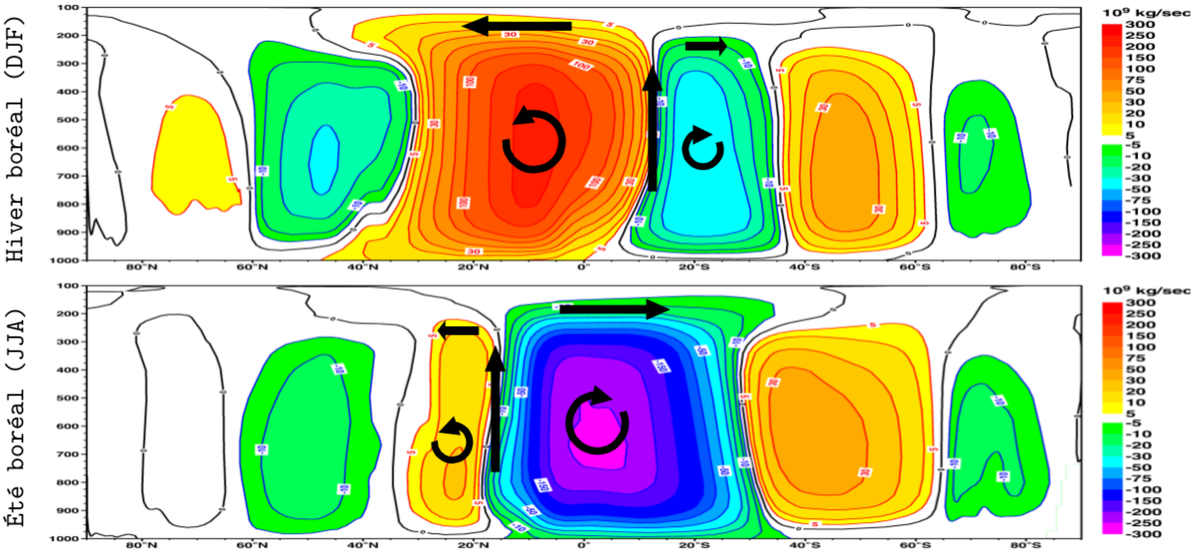

Figure 1.7: Zonal average of the stream function over 1979-2001 period from ERA40 reanalysis, north to the left and south to the right (extracted from Joly et al, 2009).

The Walker circulation

The Walker circulation is a convective cycle that originates from the interaction between the ocean and the atmosphere along the Equator, mainly in the Pacific Ocean. We have seen that the trade winds blow inexhaustibly in the Tropics from east to west as the Hadley cell returns to the Equator in the eastern part of the different oceanic basins. This causes warm surface waters to accumulate in the west of the basins with relatively cooler waters in the east due to the coastal upwelling systems. This gives rise to a sea surface temperature (SST) gradient along the Equator, accompanied by a gradient of Sea Level Pressure (SLP). As we are at the Equator, the Coriolis force is zero and the SLP gradient gives rise to a direct thermal circulation along the SLP gradient, which reinforces the trade winds. With the trade winds strengthened, we could start the loop we have just described again, this is called the Bjerknes feedback (J. Bjerknes, 1969).

Similarly to the Hadley circulation, the warmer temperature leads to a rising motion which releases latent heat into the atmosphere and forms large convective clouds. After reaching the upper troposphere, the air diverges from the ascending areas, cools and begins to sink back toward the surface, forming a zonally overturning circulation composed of several cells (Figure.1.8). Through the interaction of gradients of SST, SLP and trade winds along the Equator, the Walker circulation strongly depends on the ocean-atmosphere coupling and the thermocline depth in each oceanic basin which are crucial to understand its dynamics. Furthemore, through the interaction between the various cells that make up the Walker circulation, significant teleconnections are created within the Tropics which will be extensively explored in the rest of the manuscript.

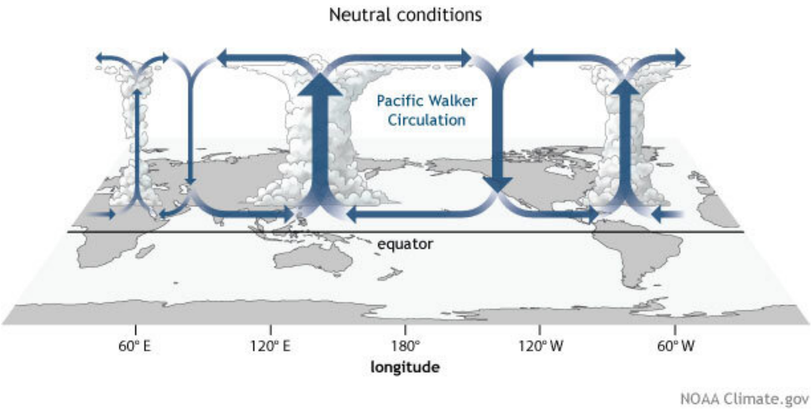

Figure 1.8: Schematic of the Walker circulation (provided by the NOAA).

So here we are with the meridional and zonal circulations in the Tropics. I promised you an explanation of ENSO at the beginning of the introduction, didn't I? The long awaited moment has come. The description of ENSO, the main mode of climate interannual variability, only comes now in the introduction because it is actually closely linked to the Walker circulation, as it is a modulation of the latter. ENSO is characterized by a warm (El Niño) or cold (La Niña) phase of the SSTs in the central and eastern Pacific. During an El Niño event, the warm SST anomalies reduce the equatorial SST gradient which induces a weakening of the trade winds by virtue of Bjerknes feedback and results in an eastward shift of the Pacific Walker cell. During a La Niña event, the opposite occurs, with stronger equatorial SST gradient and trade winds, and leads to changes in the other cells making up the Walker circulation as they are interconnected (Figure.1.9) This is why ENSO is able to generate very large-scale changes within the Tropics, called teleconnections, but even beyond since it also impacts the extra-tropics by locally perturbing the Hadley circulation and generating atmospheric waves in association with the zonal rainfall changes induced by ENSO (Trenberth et al., 1998).

Regarding monsoons, El Niño events are associated with unfavorable Sahelian and Indian monsoon conditions, while La Niña events are synonymous with intense precipitation (Webster et al., 1998; Janicot et al., 2001). By way of anecdote, it was while studying the Indian monsoon that Sir Gilbert Walker discovered the ENSO in the early 20^{th} century. The mechanisms linking this mode of variability to monsoons will be extensively explored in chapters 3 and 4 as very similar mechanisms seem to operate in the context of climate change. However, we will briefly discuss them here from an atmospheric point of view, to set the stage and get warmed up for what's to come. Firstly, by creating displacements in the ascending branches of the Walker circulation, ENSO is capable of creating a large-scale context that is more or less favorable for convection and therefore more or less favorable for precipitation in the Tropics. Secondly, ENSO modifies the release of latent heat into the atmosphere. These heating anomalies can then propagate in the Tropics in two forms: eastward and along the Equator as Kelvin waves, or westward as Rossby waves. The propagation of these anomalies, by locally altering the distribution of heat, is likely to modulate monsoon circulations.

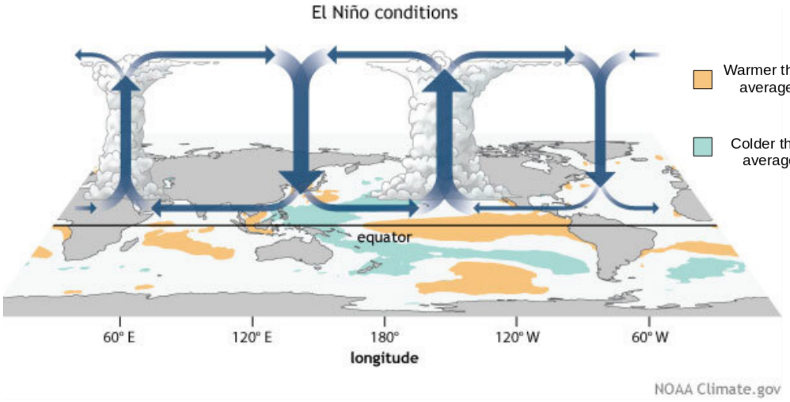

Figure 1.9: Schematic of the Walker circulation during El Niño event (provided by the NOAA).

1.4 It's monsoon time!

1.4.1 What are monsoons?

Finally in the heart of the matter you will tell me! Indeed, the time has come to talk about monsoons, and the first question that comes to mind is: what is it?

From an etymological perspective, the term "monsoon" comes from the Arabic word "mausim," which means "season" or "wind shift", which was used by sailors to designate the seasonal reversal of the winds over the Arabian Sea (Webster et al., 1998). Figure.1.10 illustrates this northeast-southwest wind inversion during the transition from boreal winter to boreal summer in the observations, which is particularly pronounced along the Indian coast and West Africa. During the Middle Ages, the Arab and Chinese sailors were known to use the monsoon winds to navigate across the Indian Ocean. This led to the establishment of trade routes between Asia, Africa, and Europe, which played a significant role in the development of the global economy. The concept of monsoons has been known and studied for thousands of years, with ancient civilizations in Africa, India, China, and Arabia developing their own systems of predicting and understanding monsoons. In the 17th century, European scientists began to study monsoons in more detail. One of the earliest and most notable researchers of monsoons was Edmund Halley, who proposed a theory for the origin of monsoons based on the differential heating of land and ocean surfaces. In the 19th and 20th centuries, advances in meteorology and atmospheric science led to significant breakthroughs in our understanding of monsoons. Scientists began to study the complex interactions between ocean currents, orography, atmospheric circulation patterns, convection, and regional climate systems that give rise to monsoons.

Now, for a modern definition of monsoons, we turn again to the wise words of the world's leading climate authority, the IPCC: «A monsoon is a tropical and subtropical seasonal reversal in both the surface winds and associated precipitation, caused by differential heating between a

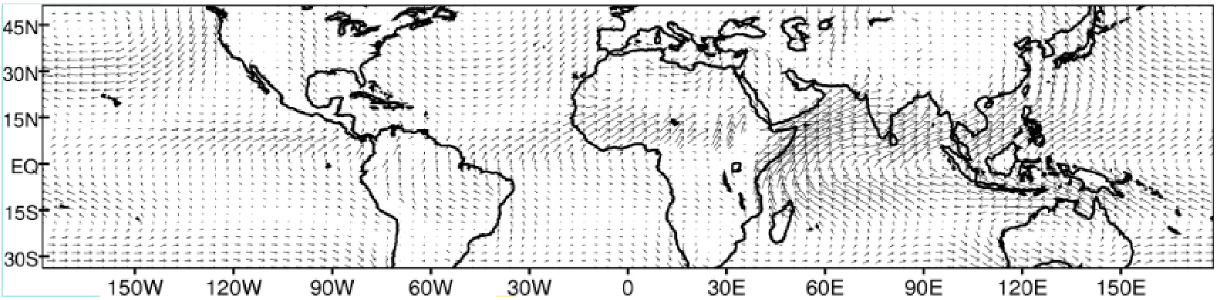

Figure 1.10: Seasonal change in lower tropospheric wind (925 hPa) between boreal summer and winter (JJA minus DJF). Winds are from ERA40 reanalysis (Source: The Global Monsoon Systems by WCRP).

continental-scale land-mass and the adjacent ocean» (IPCC, 2021: Annex VII: Glossary). If this definition is a bit simplistic, it has the merit of rebounding on the mechanisms we mentioned in the previous sections: once again, it is the redistribution of energy that puts things in motion! In fact, we can see monsoons as a regional manifestation of the large-scale dynamics we mentioned earlier. Monsoons are all at once: part of the ITCZ, part of the Hadley circulation, part of the Walker circulation and a transition zone between the Tropics and Subtropics. In this context of position at the interface of multiple large-scale dynamics, we understand that the sources of modulations are numerous and that the interactions are complex, which would deserve a slightly more detailed definition! Actually, we are a bit of a tease by using this definition found in the glossary, as AR6 provides a much more precise definition in the section on monsoons (IPCC, 2021: Annex V: Monsoons), it's tough love with the IPCC!

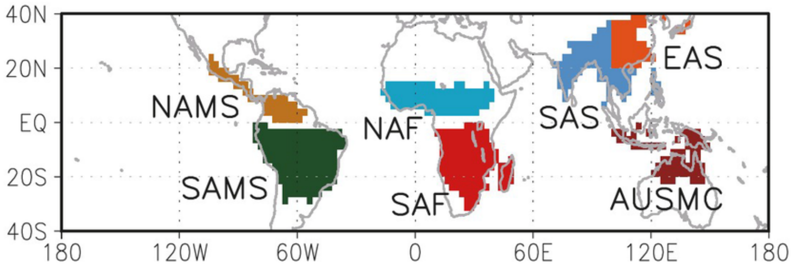

Figure 1.11: Land monsoon domains, as defined by Wang et al (2012).

While the Indian monsoon is the most famous, there are several monsoon systems across the globe and in both hemispheres. Various criteria have been established to define accurately monsoon domains, and in this manuscript we will adopt the following definition only based on rainfall: monsoon domain are areas where the precipitation difference between the local summer and winter is larger than $2.0 mm.day^{-1}$, and local summer precipitation exceeds 55% of the annual total precipitation (Wang et al., 2012). This criterion defines 7 monsoon domains which include more than half of humanity. Two of them are the subject of this thesis, namely the Sahelian monsoon which is part of the North African monsoon (NAF in Figure.1.11), and the Indian monsoon which is a part of the South Asian monsoon (SAS in Figure.1.11). Fluctuations in spatial extent and intensity of monsoons can have significant impacts on biodiversity, food security and economic development which we will discuss on a case-by-case basis for the Sahelian and Indian monsoons in the next subsections.

1.4.2 The Indian monsoon

Description and stakes

Figure.1.12 again shows the seasonal reversal of monsoon winds but in the specific case of India, and the dramatic changes in rainfall associated with it. The increase in summer precipitation is spectacular as the monsoon delivers 80% of the annual precipitation for most Indian regions. However the spatial distribution of precipitation is far from being homogeneous over the whole country (Figure.1.12) and is influenced by several factors, including the location and orientation of mountain ranges (Figure.1.13), prevailing wind patterns (Figure.1.12), and the distance from the sea.

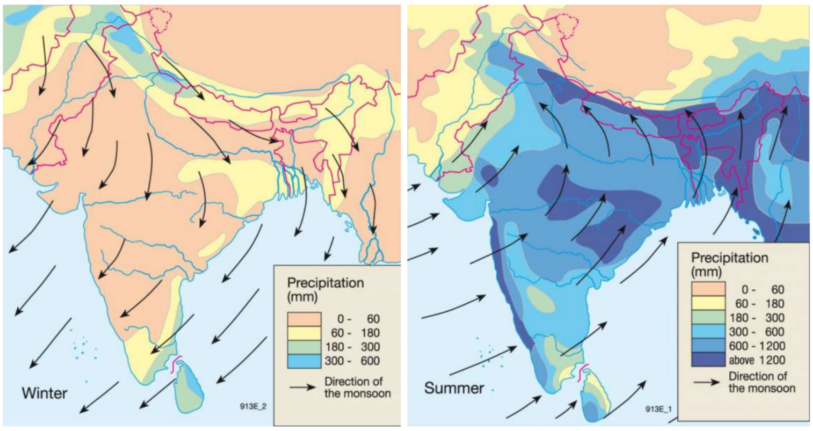

Figure 1.12: Map of surface winds and precipitation over India, left panel represents winter (October-January), right panel represents summer (June-September). Source: Diercke International Atlas.

Firstly, moisture-laden winds crossing the Indian Ocean are channeled towards the western part of the basin by the mountains of East Africa. The monsoon winds then continue their path towards the west coast of India, where they encounter the Western Ghats (Figure.1.13). This mountain range forces the air to rise and cool, leading to significant precipitation on the windward side of the mountain. This is known as the Foehn effect. The monsoon winds then continue over India, and a portion of them recharges with moisture while crossing the Bay of Bengal before encountering a fairly well-known mountain range called the Himalayas (Figure.1.13) in the northeastern part of India. Once again, due to the Foehn effect, very heavy precipitation strikes the region, which is the area with the highest rainfall in the country, with an average of over 2500 mm of rainfall per year. For comparison, the average annual rainfall in France is barely 850 mm of rainfall per year. Finally, as the monsoon winds cannot pass over the Himalayas due to their high altitude, they are deflected to the west and cross the Indo-Gangetic plains (Figure.1.13). This region combines favourable rainfall with a topography suitable for human activities. Thus, it is one of the most densely populated regions in the world and is considered as the most important agricultural region in India.

India, which was recently crowned as the most populous country in the world, with over 1.4 billion people, is fundamentally dependent on the monsoon which provides 80% of the annual rainfall as mentioned above. The monsoon rainfall replenishes India's water resources, including rivers, lakes, and reservoirs which serve as lifelines for irrigation, hydroelectric power generation, and domestic water supply. It is crucial for rain-fed agriculture as sufficient rainfall during the monsoon season ensures good

Figure 1.13: Topographic map of India.

soil moisture content and is the main source of water for irrigation, thereby ensuring agricultural productivity. Agriculture is still the backbone of the Indian economy and the country's food security. Indeed, it is a major contributor to India's GDP, accounting for around 18% and employing about 250 million people, which is more than the entire population of Pakistan or Brazil, respectively the 4^{th} and 5^{th} most populous countries in the world. Moreover, monsoon rains bring relief from the scorching heat of summer and aid in the dispersal of air pollutants, creating a more favorable living environment. This list of monsoon benefits is not exhaustive, but it helps to understand how important the monsoon is to India. Let us now tackle the dynamic structure and physical mechanisms of the monsoon to become real specialists!

Mean circulation

In a first simplistic approximation and as defined by the IPCC AR6, the Indian monsoon can be considered as a very large-scale land-sea breeze system oscillating seasonally rather than diurnally as the standard land-sea breeze systems (Figure.1.15). During the spring and summer, the continent warms up faster than the surrounding Indian Ocean and becomes warmer, creating a low-pressure zone over the Indian subcontinent. To fill this «void», the moisture-laden winds from the Indian Ocean rush into the subcontinent, rise over the heated landmass and finally cools, leading to the formation of precipitation. The sea breeze mechanism, although significant during the initial phase of the monsoon known as the onset, which occurs generally at the beginning of June, becomes insufficient to explain the persistence of the rainfalls once the monsoon has set in. It is then time to look up to find the complementary mechanism because the explanation is at the top! Indeed, the monsoon's sustenance stems from the release of latent heat through precipitation and the heating effect of the Tibetan plateau, culminating at an average altitude of 5 km, in the high troposphere. This heat release generates a similar situation to that at the surface, with a meridional temperature and pressure gradient between the Subtropics and the Equator in the upper troposphere, which feeds the anticyclonic circulation and the associated divergence in the upper troposphere. Thus, during the monsoon onset, it is the surface situation that starts the machine by "pushing" the circulation from below, while other mechanisms then take over and "pump" the circulation from the upper troposphere. This view still gives only a rough picture of the Indian monsoon and a regional explanation of its origins. It should be kept in mind that the monsoon is part of a planetary-scale phenomenon involving the northward migration of the ITCZ during the boreal summer as a part of the Hadley circulation, as well as the zonal Walker circulation. So while these regional mechanisms provide a local explanation for the origin of the Indian monsoon, it's just one piece of the larger puzzle that also involves global atmospheric circulation patterns and the migration of the ITCZ.

Lower-level circulation

Figure.1.12 illustrates the low-level circulation of the Indian monsoon, with the convergence of moisture-laden winds from the southwest over the Indian Ocean towards India during boreal summer and an opposite wind pattern during boreal winter. As we said earlier, winds then interact with the Indian topography to shape the spatial distribution of rainfall.

Upper-level circulation

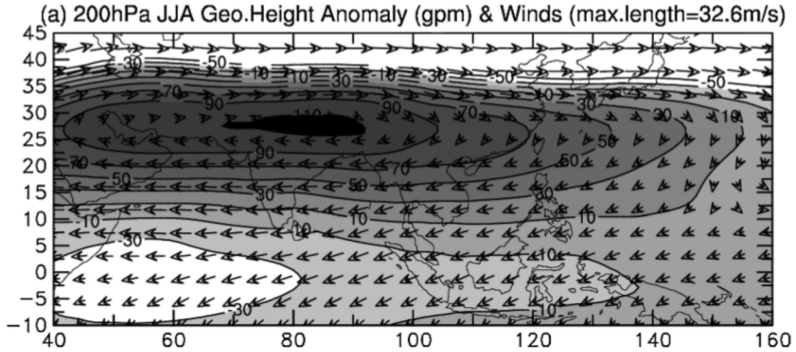

Figure 1.14: Climatology (1971-2000) of June-August geopotential height anomalies (shading in gpm, relative to the mean of the whole domain) and winds (arrows) at 200 hPa. From (Dai et al., 2013).

In response to the meridional temperature gradient in the upper troposphere, resulting from the release of latent heat and heating from the Tibetan Plateau, an anticyclonic circulation is established around 200-300 hPa over India. This anticyclonic circulation gives rise to the Tropical Easterly Jet (TEJ) around 15°N (Figure.1.14) concurring with the thermal wind relationship. This jet extends from East Asia to the west coast of Africa and only exists during the boreal summer. It is fed not only by the Indian monsoon but also by the Sahelian monsoon as we will see next. The southern branch of this anticyclonic circulation at higher levels is also an integral part of the meridional Hadley cell during boreal summer illustrated in Figure.1.7 (bottom panel). This illustrates the tight connection between the local Hadley cell and the Indian monsoon. The strength of the Tropical Easterly Jet (TEJ) can be used as a measure of monsoon dynamics' intensity since it is responsible for its formation. However, TEJ modulation can also influence the monsoon through the modulation of the vertical shear it induces, giving it an ambivalent role Dai et al., 2013).

In a nutshell

Figure.1.15 provides a summary of the main elements of the Indian monsoon circulation we have discussed above, but the complexity linked to the topography and the three-dimensional nature of the circulation must always be kept in mind. Here's a good thing done! Let's not stop here and strike while the iron is hot! For the next step, I propose a similar scenario but with a different actor: it's the turn of the Sahelian monsoon to present itself.

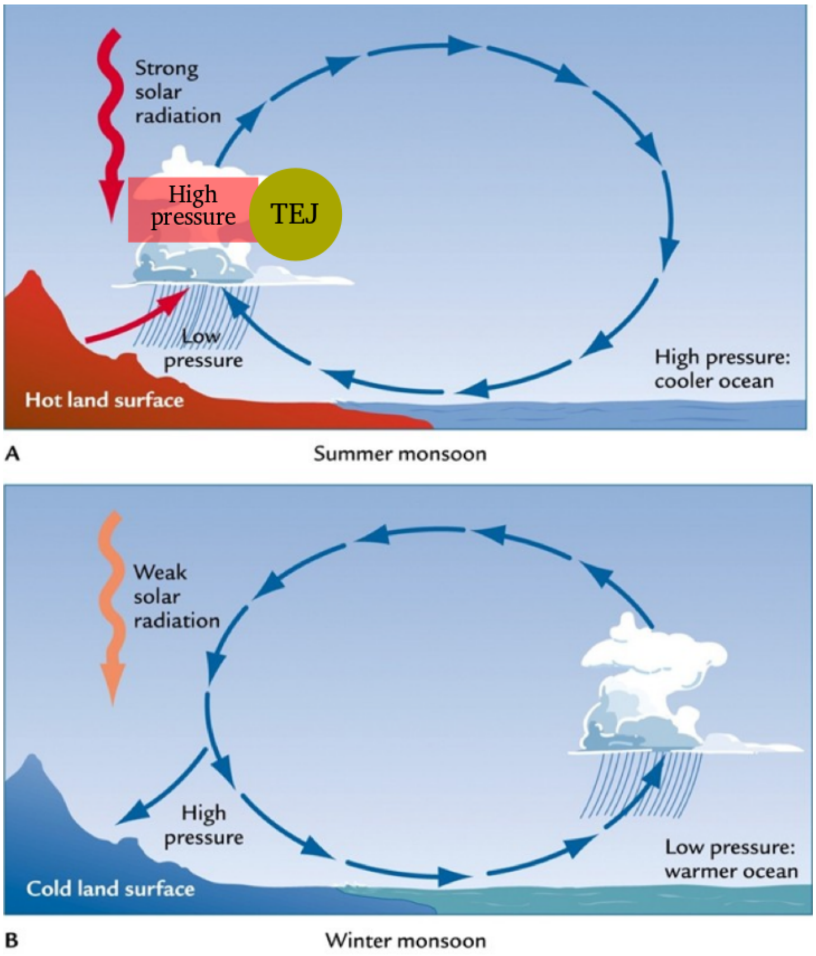

Figure 1.15: Conceptual diagram of the Indian monsoon circulation opposing summer and winter seasons.

1.4.3 The Sahel monsoon

Description and stakes

The Sahel is a region in West Africa which marks a transition zone between the Sahara desert to the north and the more fertile savannas and forests in equatorial Africa to the south. The origin of the name "Sahel" is not entirely clear, but it is believed to come from the Arabic word "sahil" which means "coast" or "shore". This is likely due to the fact that the Sahel region is located on the southern edge of the Sahara desert and is sometimes referred to as the "shore of the desert". The climate of the Sahel is generally dry, with a short rainy season lasting from June to September, which provides between 80% and 90% of the annual rainfall.

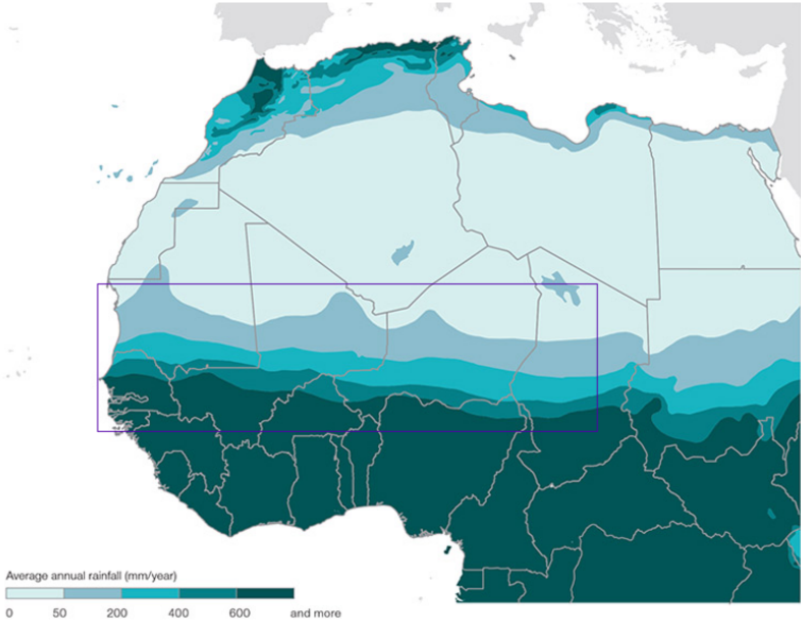

Figure 1.16: Annual average rainfall over north Africa. The purple box corresponds to the Sahel.(OECD, An atlas of the Sahara-Sahel:Geography, Economics, Politics; 2014).

We can see from Figure.1.16 that the spatial distribution of the annual precipitation is remarkably zonal: the further away from the Equator, the less it rains. This is in stark contrast with the complexity of the precipitation distribution that could be found in India (Figure 1.12). Can you recall what factors contributed to this complex pattern of precipitation over India? Yes, topography, I see that you've been paying attention! One of the peculiarities of the Sahel is that there are no major mountain ranges or massifs blocking the path of moisture-laden winds. It is a relatively flat region, with a remarkably zonal coastline, which results in a relatively uniform penetration of winds towards the north during the monsoon season, and therefore rainfall. The strong meridional precipitation contrast (Figure.1.16) has resulted in different livelihoods and settlement patterns, with nomadic herders being more common in the drier northern part, while sedentary farmers are more prevalent in the southern part. This North/South contrast in average annual precipitation is also reflected in its variability, as shown in Figure.1.17, where it can be observed that precipitation varies strongly from one year to another in the northern part of the Sahel.

According to the Food and Agriculture Organization (FAO) of the United Nations, the agriculture sector in the Sahel provides employment and

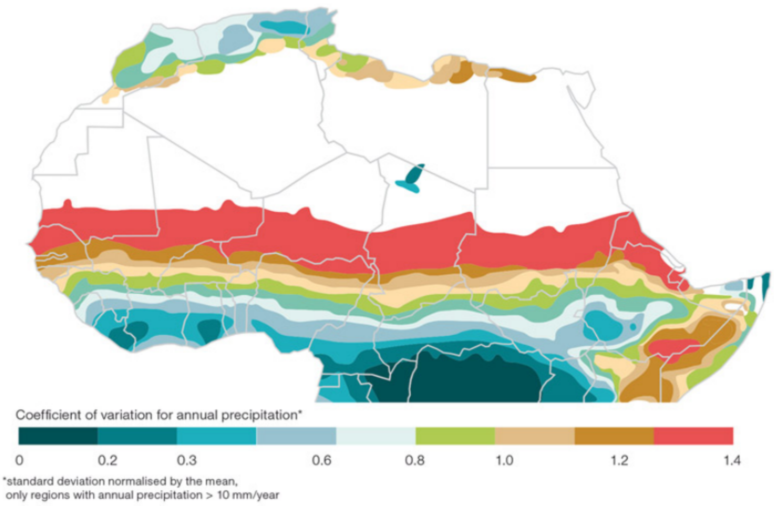

Figure 1.17: Coefficient of variation for annual precipitation calculated over 1901-2006 (standard deviation normalized by the mean). Extracted from An Atlas of the Sahara-Sahel (OECD, An atlas of the Sahara-Sahel:Geography, Economics, Politics; 2014).

income for around 80% of the population, including smallholder farmers and pastoralists, who rely on agriculture and natural resources for their livelihoods. A consequence is that the socio-economic situation of the Sahel region is closely linked to the intensity of the Sahelian Monsoon. As such, the monsoon rainfall is a critical factor in shaping the region's political and security landscape. Indeed, while the region has always been characterized by a complex and conflict-prone geopolitical situation, the large variations in rainfall amount that have occurred in recent decades (Biasutti, 2019) have certainly added fuel to the fire. By forcing farmers to adopt new practices, the changing monsoon rains have intensified competition for land and resources, generating waves of migration that further accentuate the geopolitical instability of the entire West Africa region. Insofar as the Sahel currently has 150 million inhabitants, with one of the highest growth rates on the planet which will bring the region to 350 million inhabitants by 2050, we realize the importance of the monsoon and the importance of understanding it for the local population. But enough chattering, let's draw up a portrait of this monsoon, which I am sure you are already passionate about!

Mean circulation

As was the case for its Indian counterpart, the Sahelian monsoon can be roughly described as a large-scale thermal breeze. At the beginning of summer, the SSTs of the Gulf of Guinea are cold compared to the continents, especially the Sahara north of the Sahel, which warms up intensely during this time of the year. The Sahara then becomes the seat of a large low-pressure zone called the Saharan Heat Low, leading to dry convection, which is limited in altitude by the subsiding branch of the Hadley circulation. As a consequence of the large meridional temperature gradient, moisture-laden winds from the Atlantic Ocean rush into the subcontinent and are "drawn" towards the thermal low pressure zone. These winds from the south eventually meet the winds from the Heat Low, known as the Harmattan. It is the convergence of these surface winds and the resulting upward movement that gives rise to the convective and rainy events that collectively form the Sahelian monsoon (Fig.1.18). Just like the Indian monsoon, the Sahelian monsoon can be seen as a part of the ITCZ and thus integrates into the global-scale atmospheric circulation and factors that can influence it such as the inter-hemispheric temperature gradient and energy imbalance (Schneider et al., 2014).

Lower-level circulation

Figure.1.18 illustrates the path of the winds to the Sahel during the monsoon season. Coming from the Atlantic Ocean, they cross the Equator due to the significant meridional thermal gradient, both inter-hemispheric and local. They then turn eastward due to the Coriolis force inversion and rush towards the lands, where they eventually meet the Harmattan around 15°N.

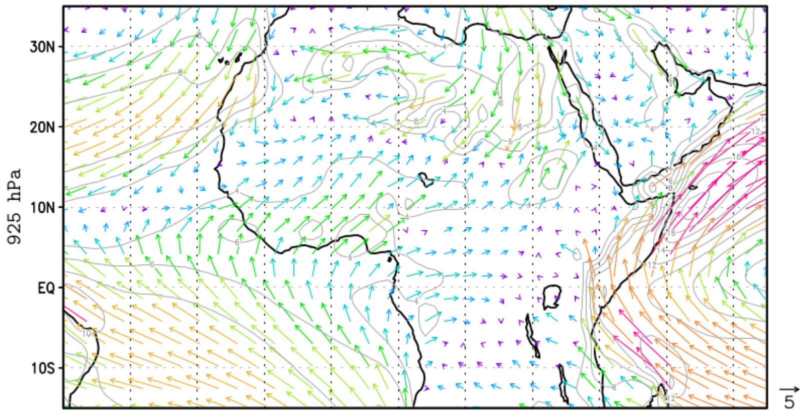

Figure 1.18: Mean June-August surface winds from ERA40 (1958-2001). Unit is $m.s^{-1}$. The isolines representing wind speed are drawn every $2m.s^{-1}$ starting from $4m.s^{-1}$. Colors from purple to red are proportional to the wind speed. Extracted from Joly et al (2008).

Upper-level circulation

In the mid-troposphere, the situation is a bit more complex than for the Indian monsoon. Around 600 hPa, we find the African Easterly Jet (AEJ) which originates from the thermal contrast between the very hot air masses coming from the Heat Low (45°C at the surface) and the relatively cooler air masses coming from the Gulf of Guinea (25°C at the surface). The AEJ plays a significant role in the development of thunderstorms and other convective systems in the region by providing a source of warm, moist air that can fuel these storms. Its average position is around 15°N (Figure.1.19).

In the upper troposphere, a familiar face can be found! We explained earlier that the strong pressure gradient near the tropopause resulting from the intense convection of the Indian monsoon gives rise to the TEJ (Tropical Easterly Jet). The situation is similar here, where the high pressures generated at high altitude by Sahelian convection will extend the TEJ from the Indian monsoon. Over the Sahel region, however, the TEJ is located between 5°N and 10°N, which is further south compared to its Indian counterpart. Due to its relationship with convection, the TEJ is an important factor in modulating the Sahelian monsoon. (Figure.1.19).

In a nutshell

Once again, a picture is worth a thousand words! Figure.1.20 summarizes the key elements of the circulation of the Sahelian monsoon! However,

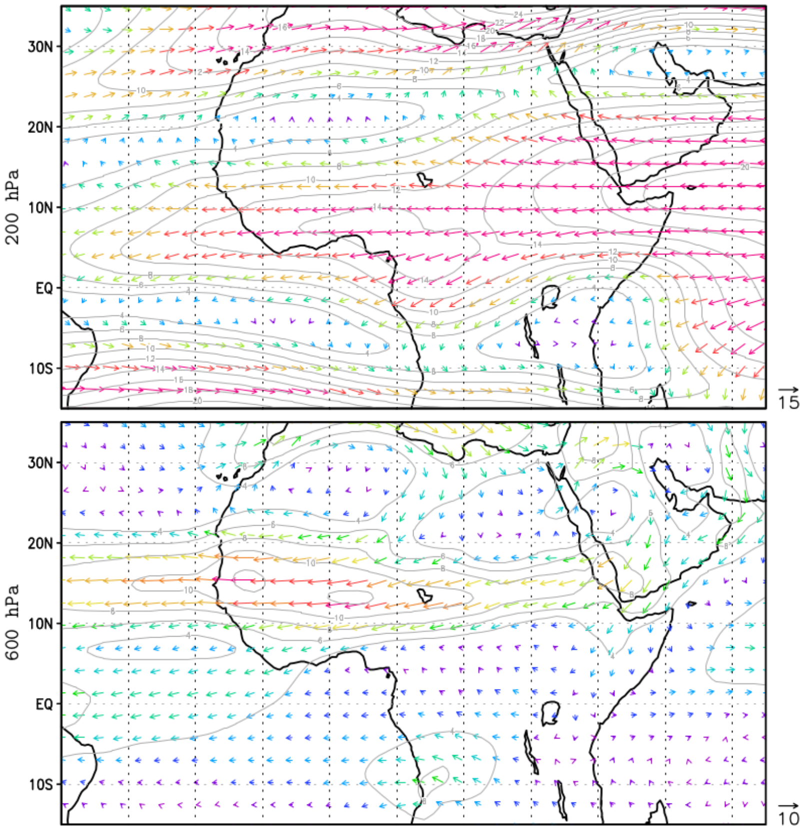

Figure 1.19: Mean June-August mid and upper-level winds from ERA40 (1958-2001). Unit is $m.s^{-1}$. The isolines representing wind speed are drawn every $2m.s^{-1}$starting from $4m.s^{-1}$. Purple to red colors are proportional to the wind speed. Extracted from Joly et al (2008).

for both monsoons, we have mentioned that the amount of precipitation is not the same every year, or even every decade. I understand that you are now curious about why this is the case, and the answers you are seeking are just ahead, with a section that will discuss the variability of the monsoon systems, their anthropogenic or natural origins, as well as the underlying mechanisms!

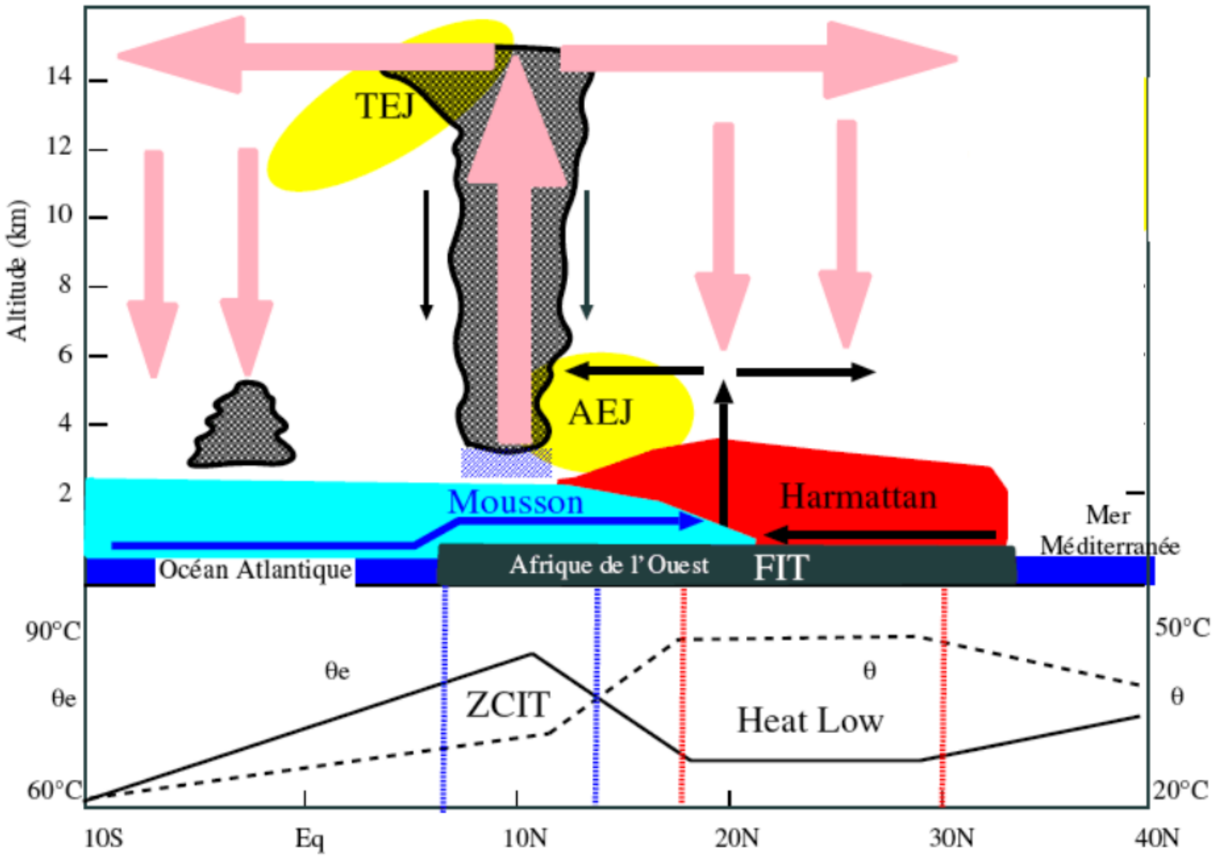

Figure 1.20: Conceptual diagram representing, on a zonal average, the key elements of the African monsoon during the boreal summer. Source: Manuel de météorologie tropicale, Beucher (2010).

1.5 Monsoons variability: from interannual to long-term trend

Monsoon variability refers to the fluctuations or changes that occur over time in the characteristics of the mean systems beyond the seasonal variations we have described above, with a particular focus on precipitation. These fluctuations in precipitation can occur over a wide range of time scales, and in particular from annual to multidecadal timescales. Typical timescales are a bit longer in the Sahel region, as illustrated in Figure.1.21. Such low-frequency variations in the amount of rainfall during the monsoon season can have dramatic consequences as both India and Sahel are largely dependent on it. In years to decades when the monsoon brings above-average rainfall, it can lead to flooding and landslides, causing loss of life and damage to property and infrastructure. On the other hand, in years of below-average rainfall, drought conditions can occur, leading to water scarcity, crop failures, and food insecurity.

In this thesis, we investigate long-term anthropogenic changes, whether they have already occurred or are yet to come, to answer a paradoxically simple and complex question: how do monsoons change? In reality, this question is a big investigation with many remaining grey areas. Generations of detectives have taken over from each other, leaving us with many clues, but also some inconsistencies. It is up to us to shed light on this matter. Fortunately, we are like Sherlock and Watson, aren't we?

To begin the investigation, the first step is to present very briefly some of the suspects and their operating methods. Although we will present them individually, keep in mind that complex relationships connect or oppose our suspects. In a later stage, we will present our investigation method and the uncertainties left by the investigators who came before us. Remember that we said at the beginning of the introduction that there are *a priori* two categories of suspects: those belonging to the natural variability gang, and those belonging to the anthropogenic forcing mob. We are trying to isolate the responsibility of the latter and understand how they act, but let us keep in mind that they are likely to interact.

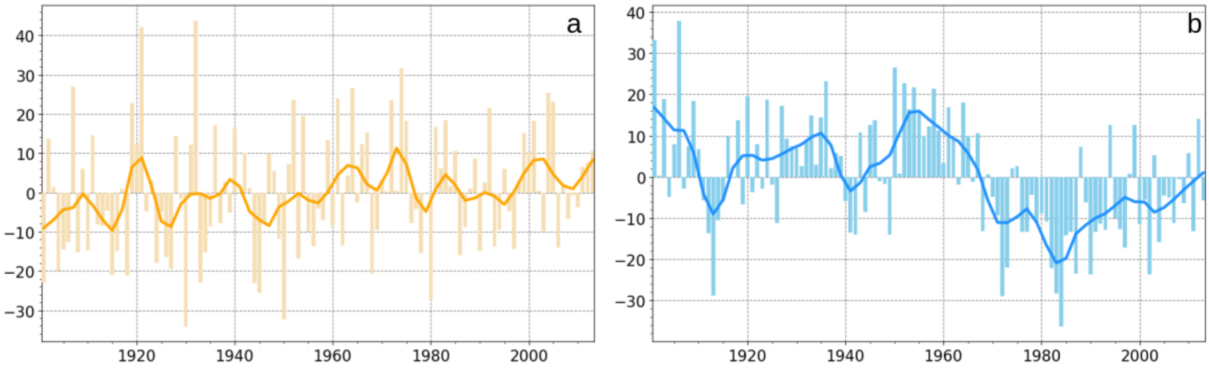

Figure 1.21: Anomalies (in %) of (a) Indian and (b) Sahelian rainfall compared to long-term average (1901-2012). The solid line represents the moving average over a 9-year interval (4 years before and 4 years after). The Indian panel uses Indian Meteorological Department (IMD) dataset and Sahel panel uses GPCP.

1.5.1 The natural variability gang

The members of this gang are numerous and operate on very variable time scales, but here only those identified by our predecessors as likely to exert long-term changes on monsoons will be presented (Biasutti, 2019;Huang et al., 2020).

The Interdecadal Pacific Oscillation (IPO): the Pacific kingpin

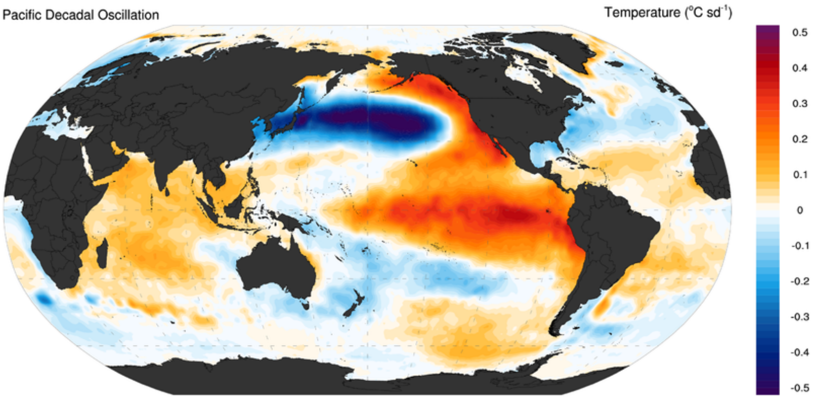

Figure 1.22: Photofit of the positive phase of the IPO (from Deser et al., 2010).

The Interdecadal Pacific Oscillation (IPO) refers to the long-term variability of the Pacific Ocean SSTs on a timescale of decades (20-30 years period, Power et al., 2021). The IPO is characterized by a pattern of warming and cooling phases in the tropical and northern Pacific Ocean, which can have significant impacts on global weather and climate patterns. During a positive phase of the IPO, the tropical Pacific Ocean experiences warmer-than-average SSTs, while the northern Pacific cools (Figure.1.22). The positive phase of the IPO is associated with more frequent El Niño events, which are associated with weaker than usual Indian and Sahelian monsoons as you already know ! Conversely for the IPO negative phase.

The Atlantic Multidecadal Variability (AMV) : the Atlantic ringleader

The Atlantic Multidecadal Variability (AMV) refers to the long-term variability of SSTs in the North Atlantic Ocean (Qin et al., 2020). The AMV is characterized by a fluctuation of several decades, with a typical duration of 60-80 years. During the positive phase of the AMV, the SSTs in the North Atlantic are warmer than average (Figure.1.23), while during the negative phase, the SSTs are cooler than average. During the positive phase of the AMV, there tends to be an increase in rainfall over the Sahel/Indian region and conversely for the negative phase (Biasutti, 2019;Sandeep et al., 2022). In climate models, and in the absence of external forcings, the AMV is typically associated with modulations of the Atlantic Meridional Overturning Circulation (AMOC) (e.g. Knight et al., 2005). Nevertheless, some have suggested that the AMV is also driven by changes in anthropogenic radiative forcing (Bellomo et al., 2021). The relative role of both is the topic of an active debate in the literature (Qin et al., 2020).

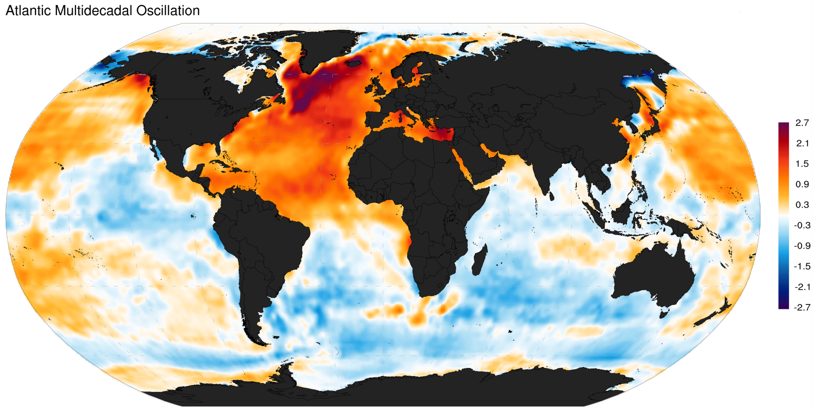
Atlantic Multidecadal Oscillation

Figure 1.23: Photofit of the positive phase of the AMV (from Deser et al, 2010).

Knowing what they look like and what is their relationship with monsoons will be enough for the rest of the day, so let's not dwell on their cases! Let's get down to business with the newcomers, who have gained notoriety over the past 150 years and are now among the most influential spheres of climate variability: the anthropogenic forcings.

1.5.2 The anthropogenic forcing mob

Aerosols: the chilly outlaw

Anthropogenic aerosols are tiny particles of solid or liquid suspended in the air, which are emitted by human activities such as burning fossil fuels, industrial processes, and transportation. They are not well-mixed and tend to stay close to where they were emitted.

Modus operandi:

First, they can absorb or scatter sunlight and reduce the amount of solar radiation that reaches the surface. This is called the direct effect of aerosols and leads to a cooling effect from which it gets its nickname. Historically, most aerosol emissions have occurred in the Northern Hemisphere due to earlier industrialisation. On a global-scale, this asymmetric distribution on the surface of the globe has been accompanied by an equally asymmetric cooling. Aerosols are thus able to modify the inter-hemispheric temperature gradient, which is reduced during the boreal summer. Remember that the Hadley cell deforms to redistribute the excess energy, resulting in the northward migration of the ITCZ in summer, of which the monsoons are a part? Great! The consequence of a reduction in this inter-hemispheric gradient is therefore a weaker northward migration of the ITCZ (Lau and Kim, 2010), which results in weaker precipitation over the monsoon areas. On a regional scale, aerosols are mostly emitted over continental surfaces, so the cooling they induce modifies the land/sea temperature gradient which is also one of the drivers of the monsoon. The monsoon circulation can therefore be slowed down, with less moisture-laden winds converging on the monsoon areas and therefore less precipitation (Bollasina et al., 2011;Biasutti, 2013). On a local scale, while the absorption of part of the sun's radiation by aerosols cools surface temperatures, it warms the atmospheric layer where they are concentrated, i.e. the first two kilometers of the atmosphere. This has the effect of reducing the temperature difference between the surface and the atmosphere. By now you know the drill: it is the differences in energy distribution that set the circulation in motion. As a result the circulation slows down, the atmosphere is said to be more stable and therefore less likely to generate precipitation (X. Li et al., 2018). Finally, aerosols have a second effect which is called indirect and corresponds to the modification of the formation and properties of clouds, due to the fact that they can serve as a condensation nucleus. This can change the albedo or the lifetime of clouds, leading to changes in the precipitation regime and the energetics of the climate system. We will leave this aspect aside during our work, but it is good to keep in mind that this indirect effect of aerosols has important implications for the climate system and suffers from high uncertainties (X. Li et al., 2018). This suspect therefore has a very broad scope, from global to local, but the evidence is consistent that they tend to reduce rainfall. Moving on to the other big fish in the climate underworld?

GHGs : the warming menace

GHGs are gases that absorb and reemit thermal infrared wavelengths, causing Earth's temperature to rise.

Modus operandi:

It is worth remembering that precipitation comes from the lifting of moisture-laden air masses to higher altitudes. On global average, the increase in temperature associated with GHGs is accompanied by an increase in absolute humidity under the Clausius-Clapeyron law at a rate of 7%/°C (Allan et al., 2020). If circulation remains unchanged, you might think that precipitation should increase by the same amount, and you would be right. However, simulations using climate models that only consider GHG forcing show an increase in precipitation of only 2-3%/°C, suggesting that GHGs are slowing down the circulation (Allan et al., 2020). Here we are touching upon the complexity of this forcing: it exerts contradictory effects on precipitation. If we understand that GHGs are likely to increase precipitation by increasing the water vapor content of the air, you may be wondering why they slow down circulation, and more specifically why they slow down monsoon circulation? No preferential treatment for suspects in this manuscript! So we'll use the same description as we used for aerosols, from the global to the local scale, to understand the effect of GHGs on monsoon circulation.

Firstly, and this is an argument we have already used previously, land heats up more quickly than the oceans' surface. In a simplistic view, as land surfaces represent 40% of the area in the Northern Hemisphere compared to 19% in the Southern Hemisphere, the Northern Hemisphere warms more than the Southern Hemisphere. This amplifies the inter-hemispheric gradient in the summer, which favors the northward migration of the ITCZ and promotes monsoon circulation, following the same reasoning as for aerosols' global effect. At the regional scale, the intensification of the land-sea temperature contrast is favorable to monsoon precipitation as it accentuates the local circulation by geostrophy (Chiang and Friedman, 2012;Zuo and Zhang, 2023).

But we still haven't presented anything that can reduce circulation, right? There it is! The reduction of circulation by GHGs is the result of opposing effects, and we will present here those that prevail and tend to reduce it. GHGs absorb and re-emit infrared radiation, leading to an increase in the amount of energy trapped in the atmosphere and consequently its temperature. This temperature increase is greater in the upper troposphere than in the lower troposphere, which implies again a reduction in the vertical temperature gradient. As a result, there is less energy difference between the vertical levels, and therefore less need for redistribution, which translates into enhanced atmospheric stability and less ascending motion. One last crucial point is that temperature changes over the oceans are not homogeneous, leading to changes in SST gradients and, thus, SLP gradients and surface winds. In the Pacific, for example, models predict that the eastern part of the basin will warm more than the western part, reducing the temperature gradient across the Pacific Ocean and thus the associated Walker cell. This example can be extended to other basins, and in reality, the entire Walker circulation, of which monsoons are an integral part, is slowed down (Wang et al., 2014;G. Li et al., 2017).

Land surface condition : the threat from below

Land surface conditions refer to the physical characteristics and properties of the Earth’s land surface, such as topography, soil type, vegetation cover, land use, and land cover.

Modus operandi:

Firstly, J. Charney et al., 1977 suggest that changes in surface conditions such as deforestation or land use change result in an increase in surface albedo, causing more incident radiation to be directly reflected rather than absorbed. This leads to a decrease in temperature over land and consequently of the temperature contrast between land and sea. Should I repeat once again that a weaker thermal contrast implies a weaker monsoon circulation because there is less need for energy redistribution? Secondly, trees and vegetation play a critical role in the hydrologic cycle by absorbing and storing water from the soil and the atmosphere, and releasing it back into the atmosphere through transpiration. Consequently, deforestation and land use change can lead to a decrease in soil moisture and a reduction in the transpiration rates of plants, which in turn can lead to a decrease in atmospheric humidity and a reduction in rainfall (Baldocchi, 2014; Chadwick et al., 2019).

What’s next?

You’ve become experts! You know about the mean state and variability of the Indian and Sahelian monsoons, the factors that can modify them, and some avenues for understanding how. However, an important question awaits before continuing the adventure. For those of you who have seen The Matrix, consider now that I am Morpheus: Do you choose the blue pill or the red pill? The blue pill ends your reading here, and you remain in the world of observations. You can study past climates, but your data is often scattered in time and space, and internal variability gives you headaches. The red pill takes you with me into the Matrix, more commonly known as the world of climate models. You can conduct experiments on a global scale, eliminate internal variability by conducting ensembles of simulations, and venture into seeing the future. However, I cannot promise a perfect world there; reproducing the climate system is not an easy task. Just like Neo, you’ve embraced the red pill, so let us embark on a journey to Wonderland. In the next and final part of this introduction, we will present what a climate model is, how it works, the issues it addresses, and its limitations. This will lead us to the questions that mark this thesis, especially those we have attempted to answer in Chapters 3 and 4: can we explain the uncertainty of models in explaining the historical changes in the Indian monsoon? Can we explain the uncertainty of models in projecting the Sahelian monsoon?

1.6 Climate models

1.6.1 History of climate models

In climate science, as in other scientific fields, experiments are the keystone of knowledge! The problem is that we've already started playing sorcerer's apprentice with the unique Earth we have, and now we need to do experiments to understand the poorly controlled one we've launched at full scale. So, to make up for the absence of "Earth2" and to provide a playground for our community, some brilliant scientists have reproduced the climate system on a computer.

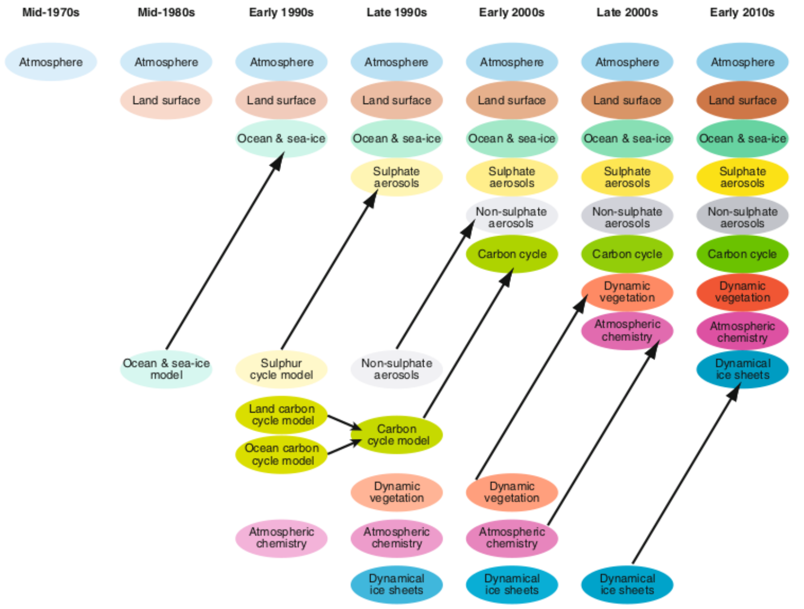

Figure 1.24: Chronology of climate model development from "Introduction to climate modelling" (Thomas Stocker, 2011).

This adventure began in 1922 with the first numerical weather prediction by Lewis Fry Richardson, who based his work on Bjerknes' assertion that changes in the state of the atmosphere could be predicted using a set of seven "primitive equations" and a precise initial state. Although the seven equations evoked by Bjerknes are still the ones used today, Edward Lorenz, who gave us the honour of the first words of this thesis, will prove him wrong about the initial conditions in the 1960s, thus introducing the notion of chaos into meteorology. It was not until the early 1950s and the development of the first computers that regional weather models really took off, notably under the impetus of John Von Neumann in the USA and Carl Gustaf Rossby in Sweden. After initially focusing on regional models, the first global atmospheric model was created in 1956 by Norman Philipps. The meteoric progress in computer science made it possible to make the models increasingly complex, and it was in 1976 that the first coupled global ocean-atmosphere circulation model (CGCM) was created. This achievement earned Syukuro Manabe and Klaus Hasselmann the Nobel Prize for Physics in 2021. Subsequently, several other laboratories developed their own CGCMs, making them more complex over time both in terms of resolution and physical processes taken into account (Figure.1.24), giving rise in 1995 to the international Coupled Models Intercomparison Project (CMIP), whose aim is to understand the dynamics of past and future climate and to serve as a scientific basis of the IPCC reports. In a sense, we are the heirs to this scientific heritage, since this thesis will use the results of the sixth iteration of this initiative: CMIP6.

In this brief history lesson, we have described the milestones that have marked the birth and development of climate models, but what do models look like when we look inside?

1.6.2 Anatomy of a CGCM

The primitive equations

To create a climate model, the first step is to establish the laws that regulate its different components, known as primitive equations. In the context of ocean-atmosphere circulation models, the foundation lies in the conservation of mass, momentum, and energy. Additional equations are required to describe the specific characteristics of each component and the variables that govern them. For instance, an equation for the conservation of moisture is necessary for the atmosphere, while one for the conservation of salinity applies to the ocean. In addition, an equation of state is needed to relate the thermodynamic variables in the different components of the climate system, such as the famous ideal gas law for the atmosphere. By counting these equations, as the conservation of momentum equation actually contains three equations (one per spatial direction), one can conclude that there are seven fundamental equations, as Bjerknes pointed out (V. Bjerknes, 1904).

I spare you here the formulation of these equations to prevent us all from having nightmares. They form such a complex set that there is no exact solution except in rare and simple cases. Models therefore seek an approximate solution through numerical methods that vary across the CGCMs. This represents a first cause of uncertainty. Nevertheless, I would like to remind you here that one million dollars is promised to whoever proves that a solution always exists for the conservation of momentum equations, enough to take a few years' vacation by the seaside!

The Earth through computer's eyes

The world is continuous and thus contains an infinite number of points, unlike computer memory which is finite. In order to overcome this problem, we need to transform the Earth into a discrete set that a computer can process. Since the Earth is three-dimensional, we will divide it into a set of "shoeboxes" called grid cells and the computer solves the primitive equations on such a mesh of grid cells (Figure.1.25). Note that there are now alternative grid forms, notably the icosahedral grid, which avoids certain pitfalls, but the idea remains the same.

The size and height of the grid cells define the spatial and vertical resolutions of the models, which currently averages 100 km, compared to 500 km in 1990, when the first IPCC report was published. The finer the resolutions, the more the models are able to account for small-scale phenomena and provide information at regional and local scales. However, increasing the resolution also results in an increase in processing

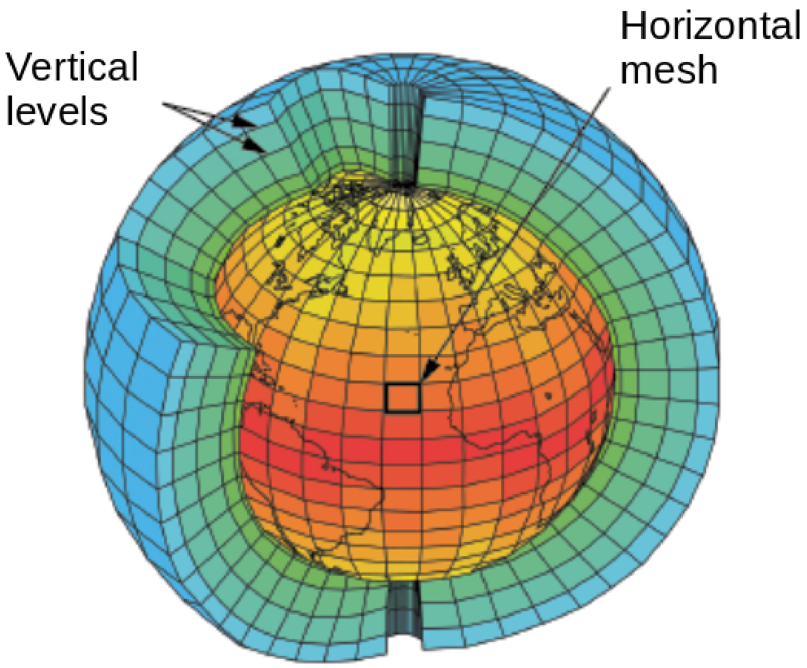

Figure 1.25: Representation of the three-dimensional mesh of the Earth. The colors represent temperature. Courtesy L. Fairhead, LMD.

time. In general terms, doubling the resolution of a model requires ten times more computing power to achieve the same processing time. Therefore, we cannot increase the resolution of models indefinitely, especially since these computations are very energy-consuming and carbon-emitting (Balaji et al., 2022). The same principle applies to time, which must be discretized into timesteps, which define a temporal resolution for the integration of the model. Therefore, we also understand that we cannot obtain as many states of the climate system as we would like, and that a compromise must be found between spatial and temporal resolutions and the physical processes represented in the model.

So far, there doesn't seem to be anything too serious, but hold on tight, troubles are about to rear their head. Indeed, an important question must surely be bothering you: what happens to phenomena that are smaller than the grid size, or shorter than the timestep? The models are unable to explicitly solve them, and yet they can not be neglected: clouds are very frequently smaller than one hundred kilometers and the condensation of water vapor occurs on an even smaller scale. This touches upon the "apple of discord" between modelers and is a prominent source of uncertainty in the results of climate models: the parameterization.

Parameterization of climate models

Parametrization refers to representing the average effect of complex physical processes that cannot be directly solved on the model's grid or resolution. Figure.1.26 illustrates some climate processes which typically need to be parameterized in current atmospheric models but such processes are also present in ocean models. The principle of parameterization is to express the averaged effect of phenomena that occur at unresolved scales in terms of variables and phenomena that the model explicitly resolves. This process therefore involves finding robust physical or statistical relationships between phenomena occurring at different spatiotemporal scales. Finding such relationships involves making ad-hoc approximations and assumptions about physics, as well as from a mathematical standpoint to ensure their tractability in models. An unresolved process is not linked to a unique parameterization, and modelers therefore make choices between the different relationships that exist, and thus between the different approximations that may have been made along the way. Additionally, the effectiveness of parameterizations is contingent upon the chosen spatio-temporal scales. Hence, a parameterization that yields favorable results for a spatial resolution of 100 km might not necessarily hold true for a resolution of 30 km. This highlights why increasing the spatial and vertical resolutions is not a definitive solution for generating better climate models as it often opens the need for a new parametrization. The variety of climate models thus partly finds part of its origins in the choice of unresolved phenomena that they choose to represent, as well as the parameterization they use to do so. These choices are a major source of uncertainties for the models (Hourdin et al., 2017).

Figure 1.26: A list of 20 climate processes and properties that typically need to be parameterised within global climate models (from MetEd, The COMET Program,UCAR).

In particular, the parameterization of a certain element of the climate system constitutes a thorn in the side of climatologists, and especially for us: clouds (Peatier et al., 2022). Clouds cover approximately two-thirds of the Earth's surface at any given time, yet, individual clouds can form and dissipate within minutes. Moreover, clouds can both warm and cool the planet depending on the type of cloud, their altitude and the time of day. This therefore requires parameterizations covering a very wide range of spatio-temporal scales, with phenomena ranging from microphysics to convection. In fact, clouds represent the biggest source of uncertainties in the projections made by models (Held and Soden, 2006;Vial et al., 2013;Schneider et al., 2017)(, and particularly in our case because they are inherently linked to precipitation and therefore to the monsoon. Beyond their direct link to precipitation, their impact on the Earth's radiative balance and the resulting feedbacks are capable of shaping patterns of future warming and precipitation.

The critical point of climate models is therefore their parameterization, particularly for clouds and thus precipitation. We now have one final point to address since we are studying the anatomy of a climate model. If the grid constitutes its skeleton, the primitive equations and parameterizations are the muscles that set it in motion, but how is it fed? What do we need to give it so that it can start working?

The inputs of a climate model

In meteorological forecasting, the initial state of the system is critical for making accurate predictions. Thus, after a dozen days at most we are no longer able to predict the realizations of the atmospheric system, due to uncertainties in the initial state: we have reached the limit of meteorological forecasting. Nevertheless, on longer time scales, the weather realizations tend to fluctuate around what is defined as an attractor in Lorenz chaos theory. In the context of ocean-atmosphere-cryosphere coupled system, this attractor represents the “climatological mean” as defined at the beginning of this manuscript. This attractor is independent of the initial state of the system, and studying climate change consists in investigating the possible changes of this attractor due to external constraints. This will be the main context of this thesis. Note that initial conditions may however be important for the climate trajectories on interannual to decadal timescales, consistently with the typical memory of the ocean and cryosphere. This is the topic of decadal predictions, which we will not tackle here.

One consequence of not providing an observed initial state is that the simulations we carry out with climate models have no reason to be in phase with the observations, even if the models were perfect and climate predictability unlimited. Thus the model could not follow the exact time sequence of weather events as they occur, it has for example no reason to reproduce the El Niño event of 1982-1983 at this timing. In practice, several (10-100) simulations with different initial states are performed, which is a huge advantage in the context of this manuscript as they provide one way of getting rid of the internal variability of the system (Lehner et al., 2020;Maher et al., 2021). Indeed, the models reproduce the low-frequency internal variability of the climate (more or less realistically), but with a random phase shift in climate models. Therefore, if we average multiple realizations of a given climate model that are initialized differently, we can easily “remove” the internal variability, which is not the case with observations with which we only have one realization. This is one of the major advantages of the models, which make it possible to isolate the anthropogenic component (Deser et al, 2020; Maher et al, 2021), and we will not fail to use this to our advantage in Chapters 3 and 4!

In our context, the most important inputs in climate models are external forcings, which are elements that cause variations in the amount of energy received (solar constant, aerosols) or trapped (GHGs) in the climate system. To accurately model past climates, a thorough understanding of both natural and anthropogenic external forcings and their temporal evolution is crucial. This mainly requires time series of CO_2, methane, aerosol, and nitrous oxide concentrations, which are then translated into radiative forcing. For projections, the same concept applies, except that instead of measuring past concentrations, scenarios are developed to imagine future concentrations depending on hypothetical economical and political considerations (Figure.1.27). As an illustration, the sixth report from the IPCC considers five main scenarios, ranging from the most pessimistic to the most optimistic regarding our future emissions, thereby creating a range of possible futures for the Earth.

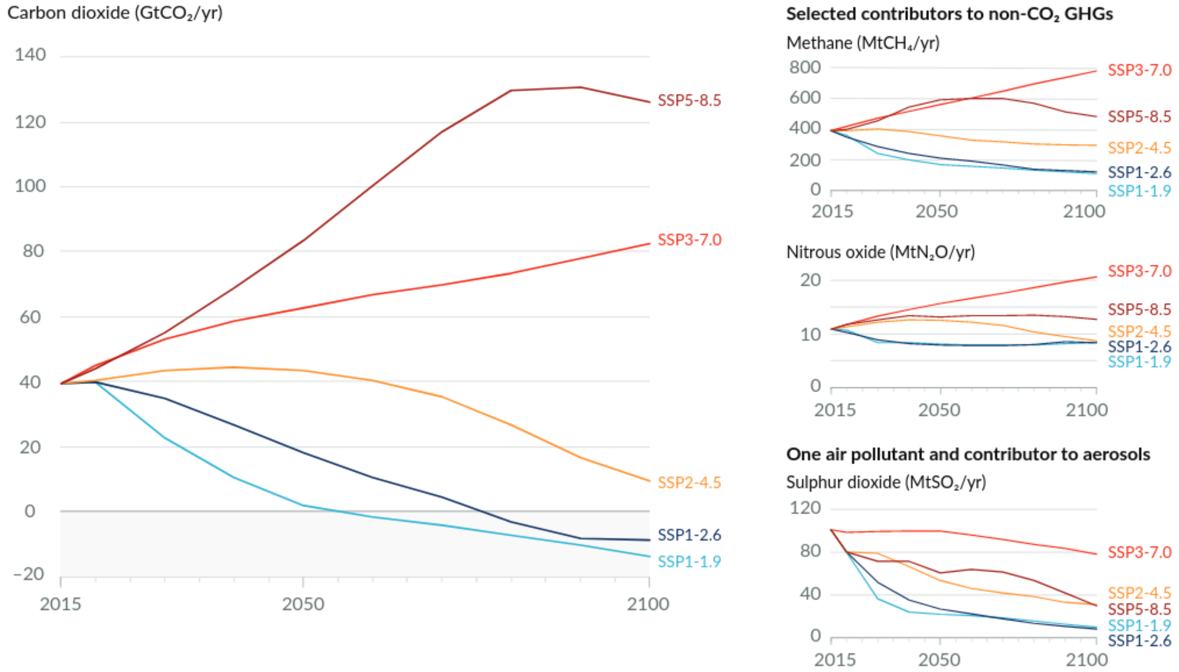

Figure 1.27: CO_2 ($GtCO_2$/yr), CH_4 ($MtCH_4$/yr), N_2O (MtN_2O/yr) and SO_2 ($MtSO_2$/yr)emissions are provided over the historical period and for six scenarios, along with the associated radiative forcing (from IPCC, 2021: Climate Change 2021: The Physical Science Basis.Contribution of Working Group I to the Sixth Assessment Report of the Intergovernmental Panel on Climate Change).

1.6.3 Climate models uncertainties

I promised you an imperfect world in which we could see the future and here we are about to play modern day Nostradamus. If astrology inspired his prophecies, we will for our part stick to using climate models. I leave it up to you to try his method and send me your results!

Figure.1.28 shows the sources of uncertainty concerning the future of precipitation at various time horizons, distinguishing the three contributors discussed in the previous sections of this introduction: internal variability, models and scenarios. At the global scale and at short and medium terms, we can see that the uncertainty of the future of precipitation is little linked to the scenario considered. This is due to the fact that at this time horizon, the forcings of the different scenarios are relatively similar and so are the impacts on climate variables. Moreover, this scenario uncertainty is considered irreducible from the point of view of climate science, since the scenarios are based on socio-economic decisions (Lehner et al., 2020).

Conversely, the uncertainty related to internal variability, which corresponds to the fact that a climate projection is uncertain at any given time in the future due the chaotic nature of the climate system, plays an

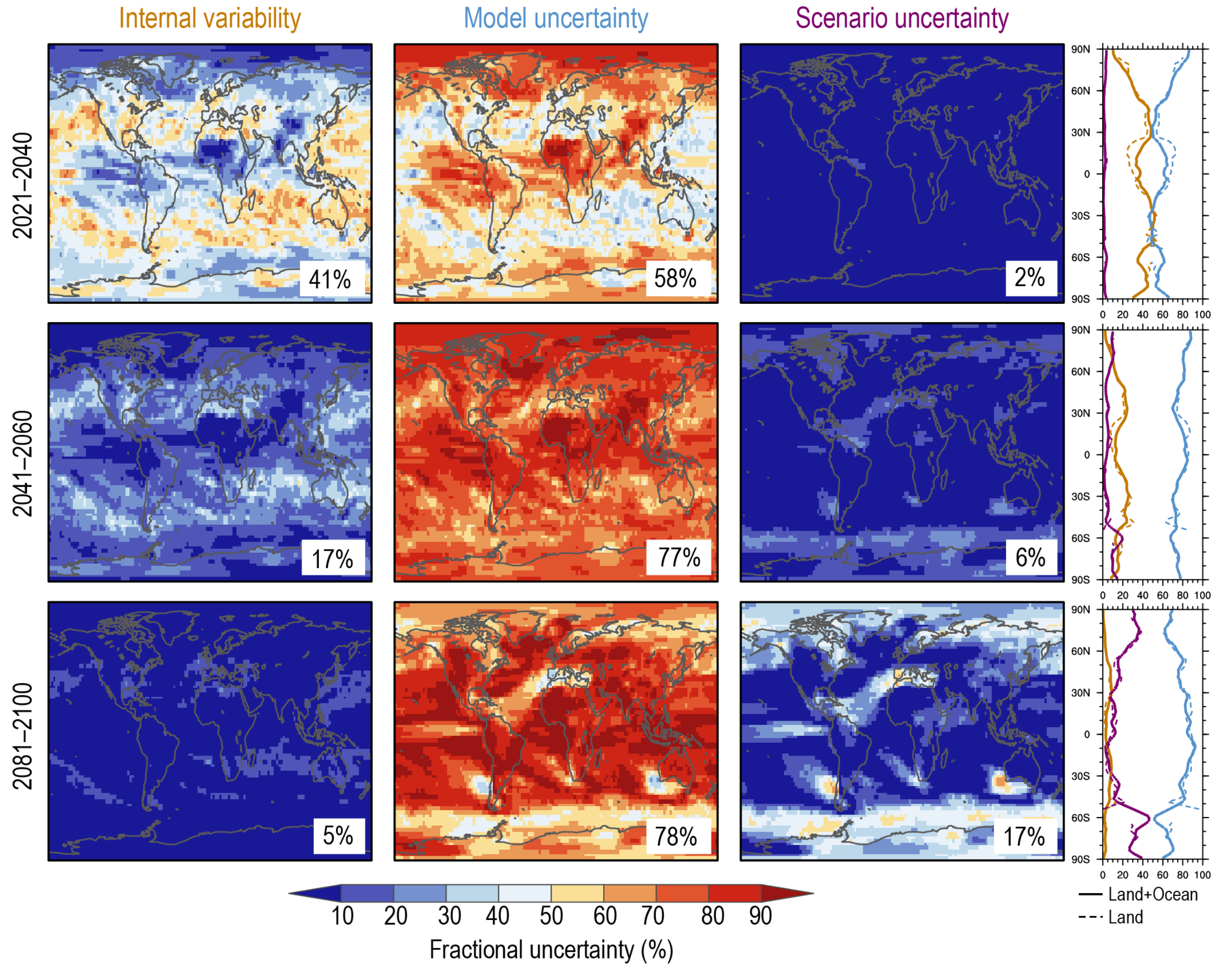

Figure 1.28: Geographical and zonal mean distribution of the percentage of variance explained by the three sources of uncertainty in CMIP6 projections of 20-year mean precipitation changes in 2021–2040 (top), 2041–2060 (middle) and 2081–2100 (bottom) relative to the 1995–2014 base period: Internal climate variability (left), model response uncertainty (middle) and scenario uncertainty (right, considering four plausible concentration scenarios: SSP1-2.6, SSP2-4.5, SSP3-7.0 and SSP5-8.5). Percentage numbers give the area-weighted global average value for each map. Right panels show the zonal mean fractions over both land and sea (solid lines) and over land only (dashed line). Source: Water Cycle Changes. In Climate Change 2021: The Physical Science Basis. Contribution of Working Group I to the Sixth Assessment Report of the Intergovernmental Panel on Climate Change.

important role in the short-term uncertainty but its role almost disappears at the end of the period. This uncertainty is intrinsically irreducible on long time scales after which information about the initial conditions has been lost, which corresponds to a decade at most for the climate system (Lehner et al., 2020).

But there is something that is valid on all time scales, and which is even more true the further into the future we go: the dominant uncertainty is that of the models. These uncertainties, as explained earlier, are related to structural differences between models arising from physical and numerical choices made by modeling centers, from which different responses to forcings arise both in the time and spatial dimensions. In principle, it is possible to reduce this uncertainty as it is simply related to the imperfection of the climate models. So this is rather good news: the most important uncertainty is the one we can control, at least theoretically! Now that we are convinced that focusing on the models is the best way to explore uncertainty about the future, it is time to look at what they project for the Indian and Sahelian monsoons and the associated discrepancies between models.

1.6.4 The fateful questions of this thesis

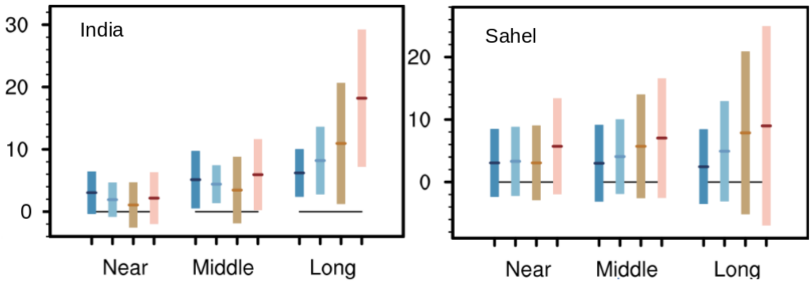

Figure 1.29: Indian (left panel) and Sahelian (right panel) monsoon precipitation change in near-term (2021–2040), midterm (2041–2060), and long-term (2080–2099) projections under SSP1–2.6, SSP2–4.5, SSP3–7.0, and SSP5–8.5 scenarios, relative to the climatology in 1995–2014 (unit: %). The thick horizontal lines represent the Coupled Model Intercomparison Project Phase 6 (CMIP6) multimodel ensemble, while the bars indicate the 10^{th} to 90^{th} percentile ranges (from Chen et al, 2020).

Figure.1.29 shows the relative evolution of Indian and Sahelian monsoon rainfall for different periods and scenarios, ranging from near- to long-term, and from a significant reduction in GHG emissions to an energy-intensive economy based on fossil fuels. In both regions, monsoon precipitation tends to increase over time, and the more emissive the scenario, the higher the increase. At first sight, this seems to be linked to the increase in absolute humidity, which is a consequence of the Clausius-Clapeyron relationship in a warming world (Z. Chen et al., 2020). On average, models predict a 20% increase in monsoon precipitation for the Indian monsoon and 10% for the Sahelian monsoon compared to current values. As a reminder, a drought or flood is considered to occur when precipitation differs by 10% from current climatology. For the high-emission scenarios, the future therefore looks more like a threat than a promise, although locally some regions may benefit from these changes. However, whether it is happiness or misfortune, a key-point is that there are strong uncertainties regarding these projections. For the Sahel region, they are such that we are not even sure whether we will experience a decrease or an increase in precipitation, or perhaps no change at all! These large uncertainties have persisted for many generations of models because of the complexity of simulating the monsoons, especially over West Africa (Monerie et al., 2017;Z. Zhang and Li, 2022). Although models have improved on average, the picture remains unclear and we need to make further progress in order to be able to implement adaptation policies, especially in the event that we do not reduce our emissions.

A first approach to better understand the uncertainties of projections could be summed up by this quote from Niccolo Machiavelli: “Whoever wishes to foresee the future must consult the past”. Indeed the robustness of the models’ performance over the historical period compared to observations seems to be a natural criterion to trust what they tell us about the future. However, strong uncertainties persist regarding the magnitude of the forced component of monsoon variability over the historical period, as illustrated by the significant long-term discrepancies among climate models when simulating Sahelian and Indian forced precipitation changes over the historical period (Figure.1.30). Knowing that these models are our main tool for making projections and that the anthropogenic forcings are becoming more and more important, the uncertainty on the historical forced response casts doubt on the reliability of the results produced by models, or at least, it is thought that being more accurate over the historical period could help reduce the uncertainties of the projection. From now on the question is fairly simple : can we explain the discrepancies about the historical anthropogenic response of the monsoons ? Despite all the efforts of the modelers and the convincing results obtained, the models still make errors not only in simulating the monsoons but throughout the climate system. One hypothesis we can make is that these errors compared to observations, called biases, are likely to influence the way the models respond to anthropogenic forcing, especially if these biases occur in "critical" areas for the monsoons. The first question that naturally arises is: do monsoon biases have an influence on how the models simulate the monsoons' forced response? In other words, is there a local explanation for the disagreement on the forced response of the monsoons? In a second step, the question can be extended to the whole world: can biases elsewhere on Earth have an influence on the anthropogenic response of the monsoons ? We explore those questions in Chapter 3, in which we will partially shed light on the origin of the model disagreement on the forced change of Indian monsoon by linking it to biases in the Pacific Ocean. To go beyond the article, we will extend this study to the case of the Sahel and analyze the limitations of the methodology used.

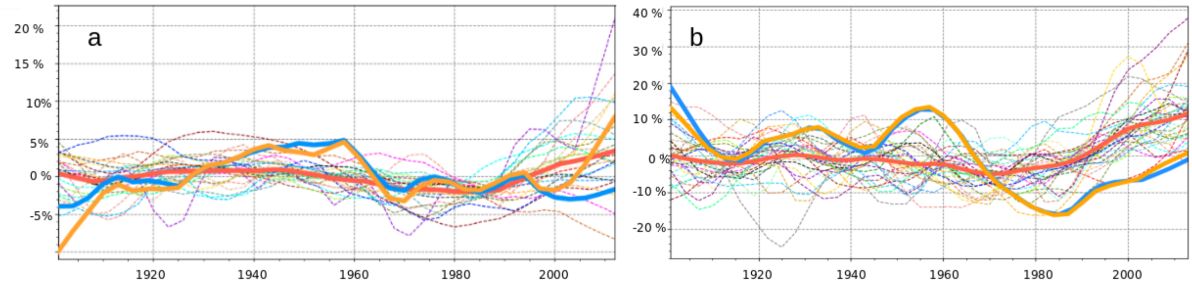

Figure 1.30: estimation of historical forced response of ISMR in CMIP6 models. It corresponds to low-pass filtered ISMR time series represented as normalized anomalies and expressed in % of the respective mean over 1901-2012 for each time series. The thin lines represent represent the multi-members average for all models with more than 1 member available from the CMIP6 repository (see supplementary Chapter 2), while bold lines represent the Multi-Model Ensemble mean (MMM) of the 25 historical members (red), the observed AIR (blue) and IMD (orange) indices, respectively.

A second approach consists in directly trying to understand what is uncertain within projections. Some studies have looked at the uncertainties within monsoons themselves: is it the change in monsoon circulation that is uncertain? Is it the change in humidity? The results show that the uncertainty in monsoon projections mainly comes from uncertainty in the changes in their circulation, known as uncertainty in the dynamic response of the monsoons (Roxy, 2017;Turner et al., 2020;Z. Zhang and Li, 2022). In contrast, the models tend to agree more on the thermodynamic response, which refers to changes in atmospheric humidity. In this thesis, we place the question a little differently and approach the problem as follows: what is uncertain in the projections and has an impact on the monsoon response simulated by the models? This involves looking for links between monsoon rainfall uncertainties and other regions on the globe, in order to understand whether it is due to uncertainties in remote regions, or whether the error is linked to local phenomena. Numerous studies have established links with uncertainties on SST changes, pointing mainly to the Atlantic Ocean for the Sahel and the Pacific Ocean for India

(Park et al., 2015;G. Li et al., 2017;Z. Zhang and Li, 2022). In Chapter 4 we focus on the case of the Sahel monsoon and revisit these sources of uncertainty in the light of a new methodology. We find that uncertainties on the future inter-hemispheric gradient as well as on the mean state of the Pacific Ocean are at the origin of more than 60% of the disagreement of the CMIP6 models on the Sahelian monsoon projections. To go beyond the article, we will also use this methodology on the Indian monsoon, which will allow us to understand once again the limits of our method.

We will not provide further details in the introduction, as its purpose is to entice you to read further! Chapters 3 and 4 will delve into the relevant literature in more details, addressing issues related to both historical period and projections. I know you're already excited! This first chapter is therefore concluded and will pave the way for the presentation of the data, simulations and methods we have used to establish our results.

Data and methods

Data and methods 2

We have presented the questions we want to answer, but in order to move from intention to realization a crucial question arises: how? Firstly, we need climate archives, i.e., a set of observed data that tells us what has happened since we began introducing anthropogenic forcing into the climate system. Ideally, these archives begin around 1850 and span the so-called 'historical period' (1850-present day). For our studies, we mainly need records of two variables: rainfall, and surface temperatures. These variables form the core of this thesis although we have also used a wide range of other oceanic and atmospheric variables to illustrate the physical processes explaining the observed and simulated rainfall and temperature evolutions as will be detailed below. Secondly, in order to study the monsoons' response to anthropogenic forcing, we have chosen to make extensive use of climate models. This will allow us to revisit the past as well as to explore the possible futures. As we have already presented the concept of climate modeling in Chapter 1, we will focus here on the international modeling initiative which provides us with all the climate simulations used in this thesis: CMIP6. Finally, after presenting the simulations and validation datasets, we will give a quick overview of the statistical methods that will allow exploiting them efficiently as the number of models and simulations available in CMIP6 is now quite impressive. The opportunity to travel to the land of statistics that you have always dreamed of!

2.1 Validation datasets

2.1.1 A global portrait of precipitation

The Global Precipitation Climatology Project (GPCP, Adler et al., 2003) is a set of monthly data on global precipitation with a spatial resolution of 2.5° latitude x 2.5° longitude. The dataset is based on a combination of satellite observations and surface measurements and covers the period from 1979 to present. It is an extremely valuable dataset, as it provides a global record of precipitation by combining several types of observations, which improve its reliability. In view of these qualities, it will serve as a global reference for present-day precipitation climatology (1979-2014) when assessing the model's performance and to define the global precipitation bias of climate models in our studies. However, it does not go back very far in time, which poses a problem for the analysis of long-term trends such as the anthropogenic response of monsoons.

GPCP dataset is available on National Oceanographic and Amospheric Administration (NOAA) website:

https://psl.noaa.gov/data/gridded/data.gpcp.html

2.1.2 The case of Indian rainfall

Since no long-term trends can be estimated with GPCP, we supplement our validation sets with two new long-term datasets specific to India:

All-India Rainfall index (AIR)

AIR (Parthasarathy et al., 1994) provides information about the amount of rainfall received over India from 1871 to present day. The dataset is maintained by the Indian Institute of Tropical Meteorology (IITM) and consists of an area-weighted mean from a fixed ensemble of 306 rain gauge stations over India, excluding the hilly regions.

India Meteorological Department (IMD)

IMD (Mohapatra et al., 2018) index provides detailed and local information about the amount of rainfall received over India from 1901 to present day. From this dataset, another All-India rainfall index has been computed, also as an area-weighted mean, but based on about 6329 stations, with at least 90% data availability over the period.

IMD rainfall dataset is available on IMD website : https://cdsp.imdpune.gov.in/

These two indices provide useful time series detailing the long-term evolution of rainfall in India. However, these datasets have limitations. For instance, the limited number of rain gauges for AIR does not guarantee a good spatial sampling of precipitation in India, especially as we have shown that spatial variability in precipitation is substantial (Figure.1.12). On the other hand, IMD has a much larger number of stations, but does not provide data for every time step (up to 10% of missing data), which does not guarantee the temporal consistency of the series. These imperfections in the datasets can lead to inconsistencies in precipitation trends in India (Lin and Huybers, 2019;Singh et al., 2019), especially in the recent period, as will be discussed in Chapter 3. Observations are therefore not perfect! This is partly why it is difficult to assess the impact of human activity on the monsoons. Another tool for assessing this impact is climate models, which are also far from perfect, as we have already said, but which provide a complementary vision and are just as valuable!

2.1.3 The case of Sahel rainfall

We also complement GPCP with two long-term datasets. They are not specific to the Sahel, but still allow long-term trends to be estimated:

The Global Precipitation Climatology Centre (GPCC)

The GPCC dataset uses the complete GPCC station database (64.400 stations with at least 10 years of data) available at the time of analysis (Rudolf et al., 1994). This land dataset provides monthly outputs with a spatial resolution up to 2.5° latitude x 2.5° longitude, available from 1891 to 2023.

GPCC dataset is available on NOAA website :

https://psl.noaa.gov/data/gridded/data.gpcc.html

The DELAWARE dataset

The DELAWARE dataset is primarily based on observation-station records that were compiled, for the most part, from several publicly available sources such as the Global Historical Climatology Network dataset (Peterson and Vose, 1997), the Global Historical Climatology Network Monthly Version 3 dataset (Lawrimore et al., 2011), the Daily Global Historical Climatology Network archive (Menne et al., 2012), and the Global Surface Summary of Day. It provides monthly outputs from 1901 to 2014 on a 0.5° latitude x 0.5 ° longitude global grid, but again only for land areas.

DELAWARE dataset is available on NOAA website :

https://psl.noaa.gov/data/gridded/data.UDel_AirT_Precip.html

2.1.4 A global portrait of surface temperature

To describe global surface temperatures and assess the models temperature biases, we will use data from ERA-Interim (ERAi, Dee et al., 2011), which are global atmospheric reanalyses. What is a reanalysis, you might ask ?

Climate reanalysis is a method of optimally combining historical observations from a variety of sources, including weather stations, satellites and ocean buoys, with atmospheric models to create a record of past weather and climate. It provides a fairly long-term and high-resolution dataset of various atmospheric and surface variables, including surface temperature. However, it should be borne in mind that combining observations and models makes one vulnerable to the errors of each. Indeed, as we have said, observations may be limited in quantity or quality, and models may not correctly reproduce all the physical processes at work. As precipitation is more difficult to observe and model than temperature, precipitation products from ERAi may be subject to greater uncertainty and bias compared to temperature products. This is why we will only use reanalyses in the case of surface temperatures. This dataset will serve as a global surface temperature reference for the present-day climatology (1979-2014), allowing us to define the global surface temperature bias of climate models. Like GPCP, this dataset does not go back very far in time and therefore cannot be used to assess long-term trends. The spatial resolution of the ERAi is approximately 80 km and we used monthly outputs.

ERAi dataset is publicly accessible upon registration on the European Centre for Medium-Range Weather Forecasts (ECMWF) data portal : https://www.ecmwf.int/

2.2 CMIP6

As mentioned earlier, CMIP6 (Eyring et al., 2016) is a collaborative effort among the international climate modeling community and is the latest in a series of intercomparison projects that have been conducted over the past few decades. The goal of CMIP6 is to provide a state-of-the-art set of coordinated climate model simulations that can be used to better understand the drivers of climate change under different GHGs emission scenarios. CMIP6 generates the protocol for a set of standard simulations that each model runs. This allows results to be directly comparable across different models, to see where models agree and disagree on past and future changes. Last but not least, CMIP6 also provides detailed and comprehensive documentation on the simulations and coupled models participating in the initiative. In our work, we have used the monthly outputs of about forty models (see Table.2.1) both for the historical period and for the projections with the highest emission scenario (SSP5-8.5). We also derived some important dynamical diagnostics such as the streamfunction and the velocity potential from the wind variables output from CMIP6. The methods to obtain these diagnostics are detailed in the methods sections of Chapters 3 and 4

CMIP6 data are publicly available upon registration on the data portal of the Earth System Grid Foundation :

https://esgf-node.ipsl.upmc.fr/search/cmip6-ipsl/

Table 2.1: Climate Models

Model Name	Modeling Center	Spatial Resolution	Chapter 3	Chapter 4
ACCESS-CM2	CSIRO, Australia	1.875° x 1.25°	Yes	Yes
ACCESS-ESM1-5	CSIRO, Australia	1.875° x 1.25°	Yes	Yes
AWI-CM-1-1-MR	AWI, Germany	0.9375° x 0.9375°	No	Yes
BCC-CSM2-MR	BCC, China	1.125° x 1.125°	Yes	Yes
BCC-ESM1	BCC, China	2.815° x 2.815°	Yes	No
CAMS-CSM1-0	CAMS, China	1.125° x 1.125°	Yes	Yes
CanESM5	CCma, Canada	2.8125° x 2.8125°	Yes	Yes
CAS-ESM2-0	CAS, China	1.4° x 1.4°	Yes	Yes
CESM2	NCAR, USA	1.25° x 0.9375°	Yes	Yes
CESM2-WACCM	NCAR, USA	1.25° x 0.9375°	Yes	Yes
CMCC-CM2-HR4	CMCC, Italy	1.25° x 0.9375°	Yes	No
CMCC-CM2-SR5	CMCC, Italy	1.25° x 0.9375°	Yes	Yes
CNRM-CM6-1	CNRM-CERFACS, France	1.4° x 1.4°	Yes	Yes
CNRM-ESM2-1	CNRM-CERFACS, France	1.4° x 1.4°	Yes	Yes
E3SM-1-1	E3SM-Project, DOE, USA	1.0° x 1.0°	Yes	Yes
EC-Earth3	EC-Earth consortium	0.7° x 0.7°	No	Yes
FGOALS-f3-L	CAS, China	1.0° x 1.0°	Yes	Yes
FIO-ESM-2-0	FIO, China	1.875° x 1.25°	Yes	Yes
GFDL-CM4	NOAA-GFDL, USA	1.25°x1.0°	Yes	Yes
GFDL-ESM4	NOAA-GFDL, USA	1.25°x1.0°	Yes	Yes
GISS-E2-1-G	NASA-GISS, USA	2.5° x 2.0°	Yes	Yes
GISS-E2-1-H	NASA-GISS, USA	2.5° x 2.0°	Yes	Yes
HadGEM3-GC31-LL	MOHC, UK	1.875° x 1.25°	Yes	Yes
HadGEM3-GC31-MM	MOHC, UK	0.83° x 0.55°	No	Yes
INM-CM5-0	INM, Russia	2.0° x 1.5°	Yes	Yes
IPSL-CM5A2-INCA	IPSL, France	3.75° x 3.75°	Yes	No
IPSL-CM6A-LR	IPSL, France	2.5° x 1.125°	Yes	Yes
KACE-1-0-G	NIMS-KMA, Korea	1.875° x 1.25°	Yes	Yes
MIROC-ES2L	MIROC, Japan	2.8° x 2.8°	Yes	Yes
MIROC6	MIROC, Japan	1.4° x 1.4°	Yes	Yes
MPI-ESM-1-2-HAM	Hammoz Consortium	1.875° x 1.875°	Yes	No
MPI-ESM1-2-LR	MPI, Germany	1.875°x 1.25°	No	Yes
MPI-ESM1-2-HR	MPI, Germany	0.9375° x 0.9375°	No	Yes
MRI-ESM2-0	MRI, Japan	1.125° x 1.125°	Yes	Yes
NESM3	NUIST, China	1.875° x 1.875°	Yes	No
NorCPM1	NCC, Norway	2.5° x 1.875°	Yes	No
NorESM2-LM	NCC, Norway	2.5° x 1.875°	Yes	Yes
SAM0-UNICON	SNU, Korea	1.25° x 0.9375°	Yes	No
TaiESM1	AS-RCEC, China	1.875° x 1.25°	Yes	Yes

2.3 Methods

Climate, as defined in the introduction, is described to first order using variables averaged over a long period (around thirty years). In our studies, we have been interested in the changes in this mean state both over the historical period and in the future, which we define in the simplest way as a difference between the end and the beginning of the studied periods. From this definition, we obtained as many values of change as models used because of their diversity. This inter-model spread in the climate response is one of the main focuses of this work.

But we are going one step further. I said in the introduction that we would take advantage of the fact that models often have several realizations for each period, remember? In fact, for each of the models, we have calculated the change for all the available members, which we have then averaged together, enabling us to obtain the best possible estimate of the forced response for each of the models (number of members in Appendices 1 and 2). We have therefore reduced the influence of internal variability on the inter-model spread as much as possible, in order to focus on the different responses of the models to anthropogenic forcing (Kay et al., 2015;Deser et al., 2020).

In our quest for explanations, we had to explore the jungle of CMIP6 models that not even Indiana Jones dared to venture into. To do so, we equipped ourselves with a powerful but potentially misleading arsenal: statistics. In one of his books on climate variability, Hans von Storch said in typical German humour: "The history of misuses of statistics is as long as the history of statistics itself" (Von Storch and Navarra, 1999). So to try to prove him wrong, or at least not to prove him right, we have multiplied the methods, the domains and tried to assess the statistical significance of the results in different ways. Statistical significance is a measure of the likelihood that the result of a statistical test is due to chance, and while it lends robustness to a statistical test, it does not always ensure practical (physical) value beyond the world of mathematics. In addition, we have used statistical methods that assume independence of realizations, or at least perform better under this context. However, this assumption is not entirely verified by the climate models that sometimes share the same ocean or atmosphere components.

In the rest of this section we will describe the two main statistical methods we have used, as well as their limitations. Many of the statistical methods and significance tests used are part of the NCSTAT software developed by our benefactor Pascal Terray. A detailed documentation can be found on his personal webpage, which includes a detailed description of the methods, associated references, as well as numerous other tools besides those we used in our work.

Despite their limitations, the statistical tools have been of great help in navigating the models, their countless variables and the relationships that link them. While banning such tools would be excessive, caution is always warranted when analyzing statistical results. To avoid pitfalls and because we remain climate scientists, we systematically looked for physical mechanisms that could underlie and explain the statistical relationships we found.

2.3.1 Trends, regressions and correlations

To estimate trends, we used locally weighted regression also called LOESS (Cleveland and Devlin, 1988), which is a nonparametric method for fitting a smoothed regression curve to data through local smoothing, in a moving fashion analogous to a moving average. We have applied LOESS with a moving time window of 20 years in some time series in Chapters 3 and 4, and call them "low-pass filtered", as LOESS eliminates fluctuations with periodicities of less than 20 years in such a configuration.

The most fundamental tools that will be widely used in our studies are correlations and linear regressions (Von Storch and Navarra, 1999). These methods are used to identify and quantify the relationships between two sets of data. If the most common case is to work on time series, it should nevertheless be borne in mind that throughout this thesis we'll be working on series of "model" dimension. First, we need to define indices that characterize an element of the climate system, which can be spatial averages of certain variables, and we calculate them for each of the models. Consequently, these methods depend on our ability to define indices that represent the phenomenon we wish to study. Once these indices have been computed, we regress them on all sorts of variables, meaning that we look for the best-fitting line or curve that represents the relationship between the variables across the models. If not specified, statistical significance from regressions/correlations is obtained by conducting a Student's t-test. This test is based on the assumption that the data follows a Gaussian distribution, which we assume to be true throughout our studies. Beyond the necessity of using relevant indices, it is important to note that correlation does not imply causality. The physical mechanisms we will develop in the upcoming chapters will aim to untangle the underlying causal relationships of the correlations, while also ensuring that we are not dealing with a statistical artifact.

In the case of monsoons, the definition of precipitation indices derives directly from the monsoon domains shown in Fig.1.11, which are based on observations. However, describing model biases and/or future changes on the basis of indices, and therefore spatial averages, implies a certain spatial homogeneity of the quantity studied. Nevertheless, there is no reason why model uncertainties should be homogeneous within monsoon domains. Furthermore, it is not certain that the definition domains based on observations are adapted to the monsoon as represented by the models, given the biases they may suffer from. Consequently, there is no guarantee that the examination of an index averaging over these domains is relevant. Fortunately, we have a secret card up our sleeve: Maximum Covariance Analysis (MCA), also known as Singular Value Decomposition (SVD). This technique will allow us to free ourselves from the definition of indices for monsoon domains, and enable us to find spatial patterns that maximize monsoon uncertainty and its interaction with other variables.

2.3.2 Maximum Covariance Analysis (MCA)

This section will explain the idea, pitfalls and safeguards behind MCA. However, for the more curious, we develop some calculations at the end of this section and full details are available in Bretherton et al., 1992! MCA is actually a generalization of Principal Component Analysis (PCA), which, rather than studying the variability of a dataset, extends this concept and studies the covariability between two datasets. The aim of MCA is to identify coupled modes of variability between two fields. In our case, we use a «model» dimension rather than a time dimension, as we want to describe the statistical relationships between the inter-model spread of precipitation changes with other variables. MCA results in pairs of spatial structures and associated expansion coefficients, which constitute a MCA mode that explain the most covariance between these two fields along the "model" dimension. Mathematically, the expansion coefficients of one MCA mode form a pair of Singular Variables (SV), one for each field, that evolve jointly and which describe a certain covariance fraction, quantified by the Squared Covariance Fraction (SCF). Each MCA mode describes part of the covariance matrix between the two fields, just as PCA mode describes part of the variance of one field. As illustrated in Figure.2.1, two types of maps can be obtained from a pair of SVs defining a MCA mode :

Homogeneous map

Map of regressions of a field onto the standardized SV of the same field. This map allows visualizing the spatial structure that the SV represents within its original field.

Heterogeneous map

Map of regressions of a field onto the standardized SV of the other field. It shows the extent to which the values of the second field can be 'predicted' from the SV of the first field.

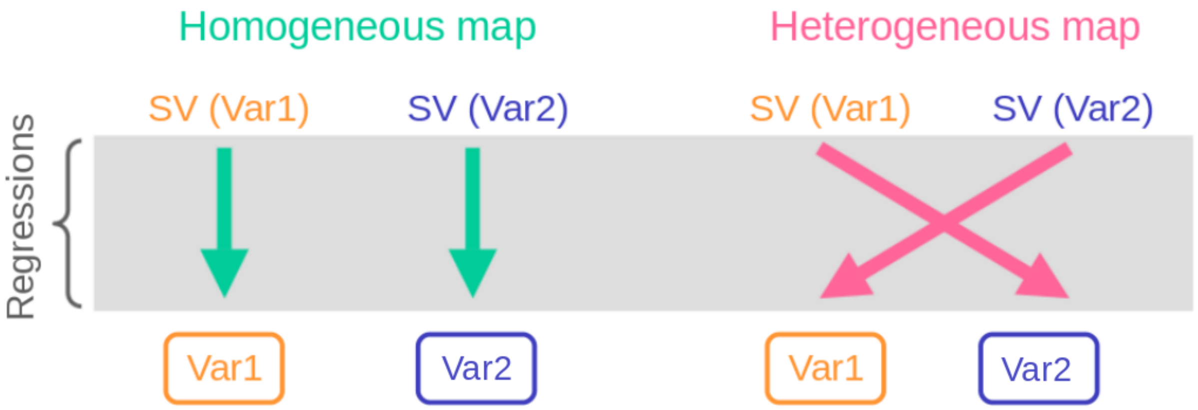

Figure 2.1: Homogeneous and heterogeneous maps from MCA.

Limits and safeguards

While we have presented this technique as a secret card up our sleeve, it is not magical and has some important limitations. Firstly, no matter what the datasets are, and even if they are perfectly independent, MCA will yield modes of co-variability. As a result, it will be essential for MCA, more than for any other statistical method used in this thesis, to check the significance of the results in order to ensure their robustness. We present the robustness metrics associated with MCA in the following paragraph, and will also use complementary regression analyses based on other simpler indices to test the reliability of the results. Secondly, because in our case we have only few models compared to the spatial size of the domains of interest (typically 8,000 grid points if we consider phenomena on a global scale), the covariance matrix is singular and its decomposition into MCA modes is not unique. For this reason, we only focus on the 1st mode from the MCAs. By doing so, we also avoid the problems of interpretation related to the orthogonality constraints, inherent to the higher MCA modes (Cherry, 1997).

Relevant measure of the physical significance of the patterns obtained with MCA is given by the fraction of domain-integrated variance of each field explained by the SVs. This metric quantifies how well each pattern retrieves the variability of the original fields. Furthermore, the SCF is used for comparing the relative importance of modes in a given MCA while the correlation value between the 1st SVs of the two fields and the Normalized root-mean-square Covariance (NC) allows us to assess more quantitatively how the coupled patterns associated with a MCA mode are related (Y. Zhang et al., 1998). Finally, for all these metrics, confidence levels can be estimated using a blockwise bootstrap procedure and this approach will be used to assess the robustness of the MCA modes.

The mathematicians' corner

If you venture here, you love mathematics and you're probably angry with me for depriving you of the primitive equations in the introduction. Fortunately, now is the time for reconciliation! Here are a few details on the mathematical problem behind MCAs.

First, we consider two data matrices X [m ×n] and Y [q ×n], where n is the number of models and m and q are respectively the number of grid points for each pattern. Then, we choose an arbitrary pattern in the x domain which is represented by a unit column vector of size m called u. We do the same in the y domain and define v as a unit column vector of size q representing a pattern of the y field.

As a reminder, we are looking for the pair of patterns that interact the most. We are therefore looking for the projection of data X and Y onto a x-pattern and a y-pattern that maximize covariance. Mathematically, this corresponds to finding an optimal u and v that maximize covariance:

$$c = cov(u^t X, v^t Y)$$
$$c = \frac{1}{n-1}(u^t X (v^t Y)^t)$$
$$c = u^t C_{XY} v \text{ with } C_{XY} = \frac{1}{n-1} X Y^t$$

The maximum c is obtained from the leading mode of the SVD of C_{XY}, resulting in a x-pattern called u1 (the first SV of X), and a y-pattern called v1 (the first SV of Y), and $c = \sigma_1$, the first singular value. Each SVD mode explains an amount σ_k of the overall squared covariance in C_{XY}. Thus, it is useful to think of the importance of the SVD modes in MCA in terms of their squared covariance fraction (SCF) as we mentioned earlier.

RESULTS

Inter-model Spread of Historical Indian and Sahelian Monsoon Rainfall Change in CMIP6

3

The objective of this chapter is to study the inter-model spread of the Indian Summer Monsoon (ISM) and the Sahel monsoon responses to anthropogenic forcing over the historical period (1850-2014). In particular, we aim at assessing and understanding whether the diversity of evolution of precipitation in two monsoon regions as simulated by the models over the historical period are related to local or remote climatological biases of the models. The results obtained on the ISM were the topic of an article published in Journal of Climate in 2023 (see section 3.2) and are summarized below. The focus on the Sahel monsoon, which is more difficult, is detailed in section 3.3.

3.1 Inter-model Spread of Historical Indian Monsoon Rainfall Change in CMIP6: objectives and summary

This chapter is based on a large set of 34 coupled models from the CMIP6 exercise, comprising between 1 and 50 members each (see Annex 1). Firstly, we show, for the first member of each model, the filtered time series (with a LOESS smoother, see Chapitre 2) of summer monsoon (June to September) precipitation over India, focusing only on low-frequency variability greater than 20 years. This allows us to highlight the fact that there is an inter-model spread that increases significantly towards the end of the period (1990-2014). However, at this stage, a question arises: is this spread related to internal variability or forced response of the Indian monsoon? As we announced in Chapter 2, we can damp the internal variability of the models by averaging over the available members. Therefore, by plotting the same series as before, but averaging all available members for models with at least two members (25 models out of 34), we can visualize the best estimation of the anthropogenic response of each model over time. This allows us to demonstrate that the inter-model spread is identical as when considering only one member per model, which implies two things: (i) the low-frequency filtering largely removes internal variability even with only one member, and (ii) the inter-model spread is due to the forced response of the monsoon and the way each model responds specifically to the external forcing. We have also emphasized some disagreement among the observation series, particularly towards the end of the period, which indicates that there may be large uncertainties in the data derived from observations as well. Finally, we show that the inter-model spread of the historical response of the monsoon is primarily linked to the circulation response, particularly the meridional wind component and its vertical shear.

At this stage, we propose to test the following hypothesis: Can model's biases in tropical precipitation and surface temperature, locally or remotely, influence the forced response of the Indian monsoon? While the influence of biases on the future response of the Indian monsoon has already been studied (G. Li et al., 2017), a possible link with the historical change remains an open question.

The first step is to look for an explanation at the local scale, focusing on the in-situ biases of surface temperature and precipitation over India. However, we demonstrate that there is no significant relationship with these local variables despite the seasonal cycle of ISM rainfall being commonly used as a metric for selecting CMIP models and their associated projections of ISM. Therefore, we go one step further and look for remote links, and we choose to focus mainly on the Tropics taking into account the well-known teleconnections of ISM with different tropical modes of interannual variability, especially ENSO (see Chapitre 1). The second step, then, is to review the tropical temperature and rainfall biases and the diversity of the models responses over the historical period for these two variables before searching for possible relationships with the inter-model spread of Indian monsoon change. Biases and responses are characterized by two metrics respectively: the multi-model mean and the inter-model standard deviation, which represents the inter-model spread. Evaluating the temperature/rainfall biases and changes over the historical period gives us the opportunity to compare the results of CMIP6 with previous exercises, in particular CMIP5. After describing the temperature and rainfall mean-state changes, we are placing particular emphasis on areas where there is a large inter-model spread of both bias and response, as these are likely to generate uncertainties in the historical response of the ISM.

We then use MCAs and find that precipitation and surface temperature biases in the tropical Pacific Ocean are responsible for an almost homogeneous modulation of the historical response of the ISM. We therefore focus on the Pacific Ocean and show that the local biases in precipitation and temperature are strongly coupled there, primarily of oceanic origin in the sense that point-wise correlations between rainfall and SST biases in the tropical Pacific are high and positive, meaning that precipitation bias are likely generated by the biases in local SST

Furthermore, we found that the bias in SST gradient along the equatorial Pacific drives the inter-model spread in the historical response of the Indian monsoon. The question now is: how does this bias manage to influence the response of the Indian monsoon? We demonstrate that there is a positive and significant correlation between the bias and the historical response of the equatorial Pacific SST gradient. In other words, models with an El Niño-like (too weak) SST gradient tend to produce a historical response that is also El Niño-like (reduction of SST gradient) and vice-versa. This modulation of SSTs in the equatorial Pacific has an impact on the historical response of the Indian monsoon in two ways. Firstly, it induces a shift in the Walker circulation, creating an unfavorable context for convection in the case of an El Niño-type bias, and conversely. Secondly, by modifying the release of latent heat, the equatorial Pacific coupled response generates anomalies in the upper troposphere that propagate towards India in the form of Rossby waves, altering the ISM atmospheric circulation response, and thus, indo-pacific precipitation patterns.

3.2 Article *in extenso*, published in Journal of Climate

Additional material for this article can be found in the first section of the appendix!

Intermodel Spread of Historical Indian Monsoon Rainfall Change in CMIP6: The Role of the Tropical Pacific Mean State

Marcellin Guilbert,[a] Pascal Terray,[a] and Juliette Mignot[a]

[a] *Laboratoire d'Océanographie et du Climat: Expérimentations et Approches Numériques, Institut Pierre-Simon Laplace, Sorbonne Université/CNRS/IRD/MNHN, Paris, France*

(Manuscript received 3 August 2022, in final form 15 February 2023, accepted 21 February 2023)

ABSTRACT: Robust projections of the Indian summer monsoon rainfall (ISMR) are critical as it provides 80% of the annual precipitation to more than 1 billion people who are very vulnerable to climate change. However, even over the historical period, state-of-the-art climate models have difficulties in reproducing the observed ISMR trends and are affected by a large intermodel spread, which questions the reliability of ISMR projections. Such uncertainty could come from internal variability or model biases. Here, we study the impact of the latter on the historical forced change of ISMR in 34 models from CMIP6. First, we show that models' biases over India do not significantly impact how they simulate the historical change of ISMR. However, we do find statistically significant relationships between ISMR historical forced changes and remote rainfall and temperature biases within the tropics by using a maximum covariance analysis (MCA). Our results highlight the key role of tropical Pacific sea surface temperature (SST) mean state biases as an important source of intermodel spread in the ISMR change. The physical mechanisms underlying these statistical relationships between ISMR change and the intermodel spread of Pacific SST biases are finally explored. We found that models having El Niño/La Niña–like mean SST bias in the Pacific tend to exhibit El Niño/La Niña–like changes over the historical period, impacting ISMR through a shift in the Walker circulation and Rossby wave propagation across the Pacific.

KEYWORDS: Monsoons; Climate change; ENSO

1. Introduction

Indian summer monsoon rainfall (ISMR) plays a critical role for India as it provides up to 80% of the annual precipitation from June to September (Ramage 1971; Jain and Kumar 2012) in a country that represents about 20% of today's world population. ISMR changes have profound impacts on local livelihood, economic development, and social stability. As an illustration, in 2002, India suffered an unusually weak summer monsoon with a 20% ISMR decrease. This resulted in billions of dollars in economic damages (Gadgil et al. 2004) and affected more than a billion people through drinking and sanitation. In this context, the weakening trend of the Indian summer monsoon at the end of the twentieth century and its possible recovery during the last 20 years are of great concern for India (Raghavan et al. 2016; Jin and Wang 2017).

Consequently, predicting ISMR evolution is critically important for India, and the Indian government launched the "Monsoon Mission" in 2012, a national initiative which aims to tackle scientific and economic challenges raised by the predictability and future of the Indian monsoon (Rao et al. 2019). One of the major achievements of this ongoing project is that an Indian coupled model [Indian Institute of Technology Madras Earth System Model, version 2 (IITM-ESMv2)] contributed to phase 6 of the Coupled Model Intercomparison Project (CMIP6) (Swapna et al. 2018). More generally, the will to better understand monsoon variability at different time scales is illustrated by the coordination of a monsoon-dedicated international cooperation program in CMIP6 called the Global Monsoon Model Intercomparison Project (Zhou et al. 2016).

Understanding the unfolding challenges of the future ISMR evolution relies on coupled atmosphere–ocean general circulation models (CGCMs) and climate projections. However, even over the historical period, large uncertainties remain about the ability of CGCMs to reproduce ISMR seasonal cycles and trends (Saha et al. 2014; Annamalai et al. 2017). To improve the reliability of CGCMs, it is necessary to identify the factors that are responsible for their inaccuracy in reproducing the evolution of the ISMR over the historical period and to distinguish between the part of this failure that is related to systematic errors and other factors such as internal variability.

In terms of radiative forcing, the first main anthropogenic forcing is the increase of atmospheric GHGs. The thermodynamic effect of GHGs on precipitation refers to the increase of precipitable water in the atmosphere induced by the increase in temperature. This implies that moisture convergence must increase in response to global warming if one assumes unchanged atmospheric circulation. This is called the "wet-get-wetter" mechanism (Vecchi and Soden 2007). The impact of GHG forcing on circulation is also of critical importance. In recent decades, the Indian subcontinent has warmed faster than the Indian Ocean (IO), thereby reinforcing the meridional thermal gradient

---

Denotes content that is immediately available upon publication as open access.

Supplemental information related to this paper is available at the Journals Online website: https://doi.org/10.1175/JCLI-D-22-0585.s1.

Corresponding author: Marcellin Guilbert, marcellin.guilbert@locean.ipsl.fr

DOI: 10.1175/JCLI-D-22-0585.1

in the lower troposphere, which enhances ISMR (Lau and Kim 2017; Singh et al. 2019; Jin et al. 2020). However, reducing GHGs' impact over ISMR to surface temperature gradient would be erroneous (Ma and Yu 2014; Lau and Kim 2017). Indeed, latent heating also modulates the land–ocean thermal contrast and the monsoon circulation in the mid–upper troposphere according to the thermal wind relationship (Dai et al. 2013). This overview illustrates the complexity of ISMR response to GHG forcing and possible sources of uncertainty in the way models represent the evolution of ISMR.

The second main anthropogenic forcing is the increase of atmospheric aerosols, which have on average a cooling effect at the surface (Ming et al. 2011). Aerosol emission rose sharply during the 1950s in the Northern Hemisphere, leading to an asymmetric cooling at the end of the twentieth century. This cooling may have caused a reduction in the summer interhemispheric energy imbalance resulting in an equatorward shift of the intertropical convergence zone (ITCZ) and hence of ISMR (Salzmann et al. 2014; Polson et al. 2014). At the regional scale, aerosols have furthermore compensated for GHG-induced temperature increases over South Asia, but not over the IO (Lau and Kim 2017; Li et al. 2018; Singh et al. 2019; Seth et al. 2019), leading to a reduced land–sea thermal contrast, which has contributed to slowing down the monsoon circulation and led to a decrease in precipitation during the twentieth century (Li et al. 2015). Even if the direct effect is dominant, the indirect effect of aerosols, which refers to changes induced in clouds' radiative properties, their frequency, and their lifetimes, should not be overlooked. Indeed, CGCMs including both processes tend to reproduce better temperature and precipitation records over the twentieth century (Wilcox et al. 2013; Wang et al. 2015).

In addition to uncertainty coming from these complex processes, the recent ISMR changes in models may also be significantly influenced by internal variability (Huang et al. 2020). The interdecadal variability of the IO SST, which refers to a basinwide warm (cold) phase, is linked to ISMR through increased (decreased) southwesterly winds (Vibhute et al. 2020). The interdecadal Pacific oscillation (IPO), which is characterized by a tropical Pacific warmer or colder than average, also has remote impacts on ISMR variations (Chinta et al. 2022). The positive IPO phase weakens the Walker and Hadley circulations, which results in decreased ISMR (Joshi and Kucharski 2017). A transition from a cold to a warm phase of the IPO is thus another factor that may have contributed to the drying trend of ISMR over the last half of the twentieth century (Salzmann and Cherian 2015; Huang et al. 2020).

The relative roles of these different factors may not be stationary in time, both in the observations and CGCMs, and they may be altered in the latter due to systematic errors in simulating Indian summer monsoon (ISM) (Hurley and Boos 2013; Annamalai et al. 2017; Terray et al. 2018) or because of missing key physical processes, for example, those related to clouds (Oueslati et al. 2016). As noted by Oueslati et al. (2016), present-day climatological biases in specific humidity and profile of vertical velocity are important sources of intermodel spread in the tropics, both over land and ocean, in CMIP5 models. The parameterizations of convection or orography are also sources of uncertainty to reproduce ISMR and its long-term trend (Hurley and Boos 2013; Sabeerali et al. 2015). Continental errors, including large cold biases over Eurasia and the subtropical deserts adjacent to India, can also affect ISMR and its long-term behavior by modulating the ISM circulation and the fast ISM response to GHG forcing (Endo et al. 2018; Terray et al. 2018; Sooraj et al. 2019). Biases in adjacent or remote regions can also impact ISMR. As an illustration, errors in the SST climatology of the eastern equatorial IO have been shown to be linked to errors in ISM simulation through Bjerknes feedback (Annamalai et al. 2017), and cold SST biases in the Arabian Sea can weaken humidity transport toward India (Levine et al. 2013). Beyond climatological errors, biases in simulated modes of interannual variability, like El Niño–Southern Oscillation (ENSO) or the Indian Ocean dipole (IOD), can also induce errors in ISMR projections (Li et al. 2017).

The skill of CGCMs at reproducing ISM climatology has increased from CMIP3 to CMIP6 (Rajendran et al. 2022; Choudhury et al. 2022). However, most current CGCMs still exhibit a large and persistent dry ISMR bias and a strong intermodel spread for ISMR projections (Sperber et al. 2013; Jain et al. 2019; Jin et al. 2020; Katzenberger et al. 2021). It is thus necessary to reduce models' uncertainties so as to strengthen our confidence in the models' projections. The main goal of this study is to provide a systematic assessment of the statistical and physical relationships between intermodel spread of ISMR changes and models' biases. A few previous studies have already discussed some aspects of these relationships but have been restricted to the possible influence of one basin or region and using CMIP5 future projections (Li et al. 2017; Shamal and Sanjay 2021). Here, we focus on the influence of precipitation and surface temperature biases over the whole tropical band on the historical changes of ISMR in the new CMIP6 database. We choose to focus on the historical period in order to take advantage of the larger number of models, each of them including more members than over the future period. The underlying questions are as follows: 1) Is there a local link between climatological biases over India and ISMR change? 2) Are there links with some remote biases over land or the tropical oceanic basins? 3) By which physical processes do local and/or remote biases influence ISMR historical evolution? Section 2 describes observational data, model simulations, and analysis methods used in this study. In section 3, we evaluate historical simulations against observations and investigate local relationships. Section 4 extends the scope of section 3 to assess relationships with remote biases over the whole tropics with the help of maximum covariance analysis (MCA). The last section presents a summary and future perspectives.

2. Data and methods

a. *Coupled simulations and validation datasets*

This study is based on the outputs of 34 CGCMs from CMIP6 (see supplemental Table S1 in the online supplemental material; Eyring et al. 2016). Most models have multiple members of the "historical" experiment (herein referred to as "historical,"

TABLE 1. Definition of the indices used in the present study. Angle brackets $\langle \cdot \rangle$ stand for spatial averaging; the superscript indicates the surface type or the atmospheric level over which the average is taken, when relevant, and the subscript the domain.

Indices	Domain and variable used
ISMR	$\langle \mathrm{Pr} \rangle^{\mathrm{Land}}_{[7^\circ\mathrm{N};30^\circ\mathrm{N}],[65^\circ\mathrm{E};95^\circ\mathrm{E}]}$
Precipitable water content over India (PRWI)	$\langle \mathrm{PRW} \rangle^{\mathrm{Land}}_{[7^\circ\mathrm{N};30^\circ\mathrm{N}],[65^\circ\mathrm{E};95^\circ\mathrm{E}]}$
Webster–Yang index (WYI)	$\langle U \rangle^{850\mathrm{hPa}}_{[0^\circ\mathrm{N};20^\circ\mathrm{N}],[40^\circ\mathrm{E};110^\circ\mathrm{E}]} - \langle U \rangle^{200\mathrm{hPa}}_{[0^\circ\mathrm{N};20^\circ\mathrm{N}],[40^\circ\mathrm{E};110^\circ\mathrm{E}]}$
Monsoon meridional circulation index (MMCI)	$\langle V \rangle^{850\mathrm{hPa}}_{[10^\circ\mathrm{N};30^\circ\mathrm{N}],[70^\circ\mathrm{E};110^\circ\mathrm{E}]} - \langle V \rangle^{200\mathrm{hPa}}_{[10^\circ\mathrm{N};30^\circ\mathrm{N}],[70^\circ\mathrm{E};110^\circ\mathrm{E}]}$
Eurasian land–ocean thermal contrast (ELOTC)	$\langle \mathrm{Tas} \rangle^{\mathrm{Land}}_{[0^\circ\mathrm{N};60^\circ\mathrm{N}],[30^\circ\mathrm{E};180^\circ]} - \langle \mathrm{Tas} \rangle^{\mathrm{Ocean}}_{[10^\circ\mathrm{S}\,60^\circ\mathrm{N}],[30^\circ\mathrm{E};180^\circ]}$
Pacific equatorial SST gradient	$\langle \mathrm{SST} \rangle_{[5^\circ\mathrm{S};5^\circ\mathrm{N}],[130^\circ\mathrm{E};170^\circ\mathrm{W}]} - \langle \mathrm{SST} \rangle_{[5^\circ\mathrm{S};5^\circ\mathrm{N}],[80^\circ\mathrm{W};140^\circ\mathrm{W}]}$

covering the period from 1850 to 2014). All these historical integrations are forced by the same time-varying external radiative forcings (both natural and anthropogenic) derived from observations, but they have different initial conditions. The monthly mean outputs used in our analysis include rainfall (Pr), precipitable water (PRW), surface temperature (Ts), near-surface air temperature (Tas), sea level pressure (SLP), and horizontal winds (U and V) at different levels.

For model validation of the precipitation field, we use the Global Precipitation Climatology Project (GPCP) monthly mean precipitation flux dataset from 1979 to 2017 (Adler et al. 2003). For surface temperature, precipitable water, and horizontal winds we use ERA-Interim (Dee et al. 2011). We also use the all-India rainfall (AIR) index, which is an area-weighted mean from a fixed ensemble of 306 rain gauge stations over India (Parthasarathy et al. 1994), and an ISMR index derived from the India Meteorological Department (IMD) rainfall dataset to monitor the observed ISMR evolution over the historical period. This last index is based on about 6329 stations (with least 90% data availability over the period) for the period 1901–2013 (Mohapatra et al. 2018).

b. Climate and ISMR indices

To understand how models' biases interact with the change of ISM rainfall and circulation, we define several indices, which serve as proxies for the main thermodynamic and dynamic components of the moisture budget (Seager et al. 2010). The different climate and dynamical indices used in this study are defined in Table 1. The overall thermodynamic change is approximated by averaging the change of the PRW change over the domain. It corresponds to the evolution of humidity integrated over the whole atmospheric column. The dynamical changes are split into zonal and meridional contributions by using the Webster–Yang index (WYI) and the monsoon meridional circulation index (MMCI), respectively (Webster and Yang 1992; Goswami et al. 1999). These indices are measures of the vertical shear of zonal and meridional winds between the 850- and 200-hPa levels, respectively. These shears are well related to the strength of the monsoon circulation and to tropospheric temperature gradients (Dai et al. 2013). Finally, we use the difference of surface temperature between part of the Eurasian continent and the surrounding oceans, later referred to as Eurasian land–ocean thermal contrast (ELOTC), to determine whether or not the large-scale surface thermal contrast is a key factor in shaping the ISM change during the historical period, as it is in projections (Jin et al. 2020). Note that thereafter, "ISMR change" refers to regionally averaged ISM rainfall (defined above as ISMR) change over the historical period (see Table 1), while ISM rainfall change refers to change in the rainfall pattern over India over the historical period. The former is an index, while the latter is a spatial pattern.

c. Methods

We define climate change over the historical period as the difference of climatological means between the end of the historical period (1979–2014) and the early industrial period (1850–75). This definition will be justified in section 3a in which we demonstrate that ISMR changes are most prominent during the last decades of the historical period. Model biases are defined as the differences between model and validation data climatologies over the 1979–2014 period during which the quality of observations and reanalysis products has greatly improved as compared to the early period. Model variability is defined as the average over the various available members of the temporal standard deviation computed over 1979–2014. Among the available datasets, we choose GPCP (ERA-Interim) to define precipitation (temperature) biases, while AIR and IMD are used to evaluate ISMR trends over the historical period. Our analysis will focus on June–September (JJAS) as it is the monsoon season and all datasets were interpolated onto a common 2.8° × 2.8° horizontal resolution by bilinear interpolation prior to the analysis. It should be noted that due to the specific focus on JJAS season, the time-lagged links between ISM changes and biases are not explored in this study. However, our results are robust if annual rather than JJAS averages are considered for the tropical SST and rainfall biases in the analysis.

For both observations and simulations, velocity potential, streamfunction, and divergent and rotational winds were calculated at different levels from horizontal winds with the spectral method (Tanaka et al. 2004). Furthermore, in order to accurately describe the low-frequency variations in the observed and simulated ISMR time series in Fig. 1, a locally weighted regression called locally estimated scatterplot smoothing (LOESS; Cleveland and Devlin 1988) was applied to the ISMR index (only for this time series). LOESS is a nonparametric method for fitting a smoothed regression curve to data through local

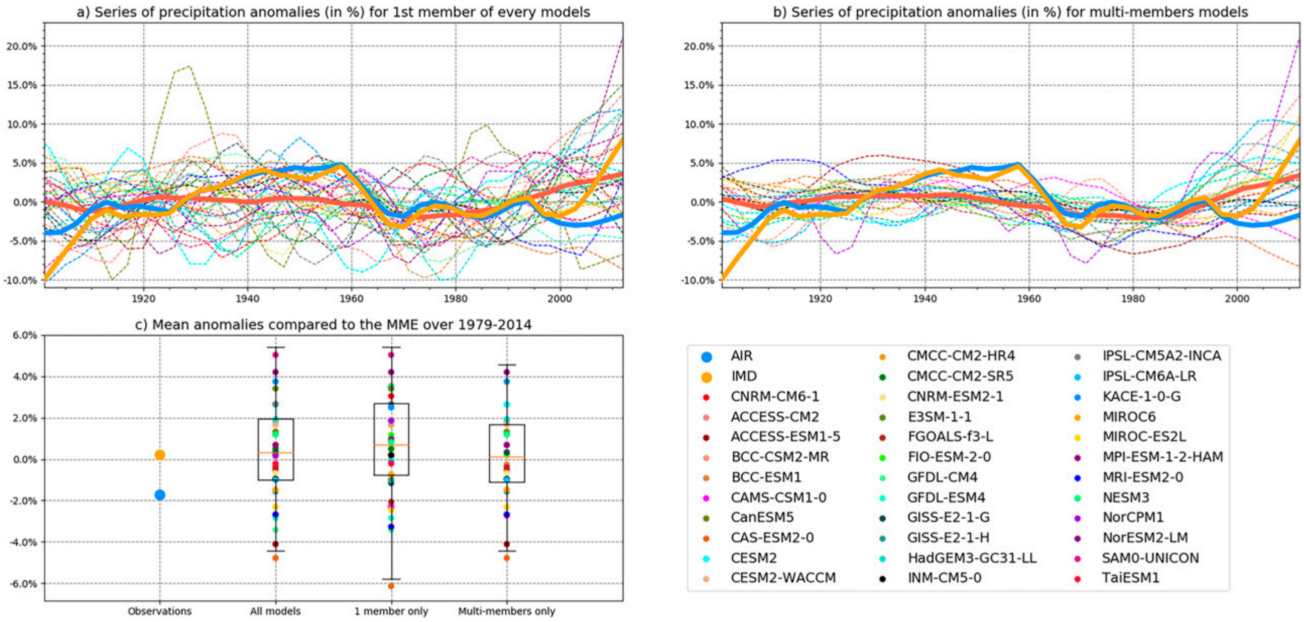

FIG. 1. (a) Low-pass-filtered ISMR time series represented as normalized anomalies and expressed in percent of the respective mean over 1901–2012 for each time series. The thin lines represent the first historical member of each of the 34 models available from the CMIP6 repository (see supplemental Table S2), while bold lines represent the MMM of these 34 first historical members (red) and the observed AIR (blue) and IMD (orange) indices, respectively. (b) As in (a), but where thin lines represent the multimember average for all models with more than one member (25 of 34 models; see supplemental Table S1 for details), and MMM is calculated on these multimembers only. (c) Mean anomalies over the 1979–2014 period relative to 1901–2012. The first column is for observations, with the same color code as in (a) and (b). The last three columns are whisker plots for three different ensembles of simulations. The first whisker column is for the multimember average for all the 34 available models, even those with only one member available. The second whisker column considers only the first member for each model [see (a)]. The third whisker column considers the multimember average for the 25 models with more than one member available [see (b)]. In all panels, the observed and simulated ISMR raw time series have been low-pass filtered with LOESS (Cleveland and Devlin 1988). See text and section 2 for details.

smoothing. We applied LOESS with a moving time window of 20 years (equivalent to a low-pass filter eliminating fluctuations with periodicities less than 20 years) to the full time series, and we chose to show the low-pass-filtered time series on the period 1901–2012, which is the common period for the observations and the simulations. The ISMR climatology over this period was then calculated for each dataset in order to express the smoothed time series as anomalies (in percentages) with respect to this climatology. Note that all other computations use the raw data without any filtering.

To investigate the first-order linear relationships between changes over the historical period and model biases as seen from climate indices, we use scatterplots and regressions. For a more systematic exploration, we use MCA, which extracts the dominant covariability patterns from two geophysical datasets (Bretherton et al. 1992; Cherry 1997). MCA calculation is described in detail in supplemental Text S1.

3. ISMR trends, tropical biases, and changes over the historical period

a. ISMR trends over the historical period

First, we document the skill of CMIP6 models in simulating the ISMR modulations over the historical period. It has been demonstrated that CMIP5 models were not skillful in this respect (Saha et al. 2014). AIR and IMD are used for observations, as they cover the whole twentieth century, and the ISMR index as defined in Table 1 is used for simulations.

AIR and IMD oscillate mainly between −5% and 5% between 1900 and 2012, except at the beginning and end of this period when variations are stronger (Fig. 1a; see the thick blue and orange lines). The correlation between AIR and IMD is significant ($r = 0.70$; $p < 0.01$), which proves an overall good agreement between our validation datasets. However, even if both observation datasets show an increase of ISMR over the recent period (2000–12; Jin and Wang 2017), there is a surprising disagreement on the magnitude of this wetting trend. This difference could possibly be related to the variable network of stations used in IMD or a too-coarse network in AIR (Lin and Huybers 2019; Singh et al. 2019). This highlights strong uncertainty on the observed recent ISMR trend and potential problems in the validation datasets.

This recent recovery of the monsoon has been attributed to an increase in atmospheric moisture content coupled to a favorable land–sea thermal contrast between East Asia and the western North Pacific Ocean (Huang et al. 2020; Rajendran et al. 2022) and between the Indian subcontinent and the IO (Jin and Wang 2017; Roxy 2017). Such evolution may also arise from the sustained increase of GHG emissions. Recent studies furthermore showed that, as sulfate aerosol mitigation policies are now applied, GHG forcing is overtaking the aerosol forcing after the 1980s (Seth et al. 2019; Allan et al. 2020). If GHGs are responsible for the recent wetting ISMR trend, the latter is likely to become more prominent in the future (Katzenberger et al. 2021).

Figure 1a also shows the first (single for models proposing only one member; see supplemental Table S2) member of historical realizations taken from all the 34 CMIP6 models available from the Earth System Grid Federation repository. Taken as a whole, this ensemble of simulations yields relatively large multidecadal variations of ISMR with an amplitude generally comparable to those found in observations (Fig. 1a). The multimodel ensemble mean (MMM) (thick red line) typically yields weaker variations than the validation datasets (from −2% to +4%), which is expected as simulated internal variability is damped by the model averaging. The relative amplitude of the drying ISMR trend during the 1950–90 period seen in both AIR and IMD (Bollasina et al. 2011; Saha et al. 2014; Salzmann et al. 2014; Roxy et al. 2015) is not well reproduced by the MMM, as in CMIP5. This result is consistent with the partial attribution of this drying trend to internal variability (Huang et al. 2020). After the 2000s, the MMM increases and peaks around +4%, which is comparable to the observed ISMR interannual variability (which is typically about 10% of the ISMR mean).

This recent recovery of ISM thus appears consistently in the MMM (computed from single or first member for each model), IMD, and AIR (Fig. 1a). This is in line with the partial attribution of this wetting trend to external forcings. However, consistent with the weaker amplitude, the slope of MMM recent trend is much weaker than the observed one. Furthermore, the single-member intermodel spread increased from the 1980s until the end of the period. Indeed, in single realizations, the anomalies are spanning from −8% to +21% toward the end of the period, while they were earlier approximately ranging between −7% and +6%.

Since the single members are influenced both by natural variability and external forcings, it is difficult to distinguish their respective contributions to the increase in the intermodel spread. To get further insights about the origin of this increase, Fig. 1b presents the temporal evolution of ISMR in multimember average for all models with more than one member (25 of 34 models). The multidecadal variability of ISMR modeled over the twentieth century is largely reduced in these multimember ensembles as expected from the averaging which damps the internal variability. The MMM is nevertheless very close to the one computed from single-member only for the whole period ($r = 0.93$), including the recent wetting period. Interestingly, the increase in the intermodel spread is still present in the multimember averages. This suggests that this spread is also associated with a biased and variable response of the models to external forcings.

To validate more quantitatively this hypothesis, we now focus on the distributions of the mean averages over the 1979–2014 period for the single-member versus multimember model sets as these time averages are used to define the climate changes (see section 2 for details) in the following sections. The two right-hand columns in Fig. 1c show that, when averaged over the 1979–2014 period, the spread of ISMR change as represented in the CMIP6 database is slightly weaker when considering only the 25 models offering multiple members of historical simulations than when considering all the 34 single or first historical realizations. Nevertheless, a two-sample version of the Smirnov–Kolmogorov test (Hodges 1958) applied to the two empirical distributions leads to the rejection of the hypothesis that these two distributions differ even at a very low confidence level (p value is 0.80).

Taking into account this result and in order to keep the model panel as large as possible to maximize the significance of our results, we consider in the following the multimember average for each of our 34 models even when only one member is available without any weighting (second column of Fig. 1c). Figure 1c illustrates that this ensemble only shows small differences with the two other ones. By using a Smirnov–Kolmogorov test as above, we could furthermore show that all these distributions are similar ($p > 0.80$). This allows us to use a multimember average for all of our models despite the fact that some of them have only one member, because the time average over the last 35 years is sufficient to damp the effect of internal variability in all cases. This also justifies our choice to give the same weight to each of the models in the rest of the study, regardless of their number of members. Finally, in order to have an overview of the relative importance of this intermodel spread with respect to internal variability, we have assessed the intramodel spread (related to internal variability) for CMIP6 models with more than one member (see supplemental Fig. S3). Interestingly, for the majority of models, the intramodel spread is lower than the intermodel spread, with the exception of the CanESM5 model.

b. *Contributions to ISMR change and spread*

To gain more insights into the physical mechanisms underlying the ISMR changes over the historical period and its intermodel spread, we now study its links with dynamical or large-scale indices (see section 2 and Table 1).

MMMs of WYI (Fig. 2a) and MMCI (Fig. 2d) changes averaged over the multimodel ensemble described above show a decrease over the historical period (see the crosses in the panels), while MMM of precipitable water content over India (PRWI) change shows a strong increase (Fig. 2e). This indicates that the small decrease in the MMM of ISMR seen in the y axis of each panel in Fig. 2 is due to a decrease in the dynamic component, which is partially compensated by the thermodynamic component. This may explain why, even if global warming and ISMR are both significantly correlated with the change in PRWI, they are not correlated with each other (Fig. 2b; $r = 0.25$; $p > 0.10$). On the other hand, the intermodel spread of PRWI is significantly correlated with the global surface temperature change among models ($r = 0.50$; $p < 0.01$; not shown), illustrating the link between thermodynamics of ISMR and global warming in agreement with the Clausius–Clapeyron relationship. Consistently, there is also a significant relationship between the intermodel spread of ISMR and PRWI changes (Fig. 2e).

The intermodel spread is also significantly related to dynamical changes with a very strong relationship between the ISMR and MMCI changes (Fig. 2d) and a weaker, but still

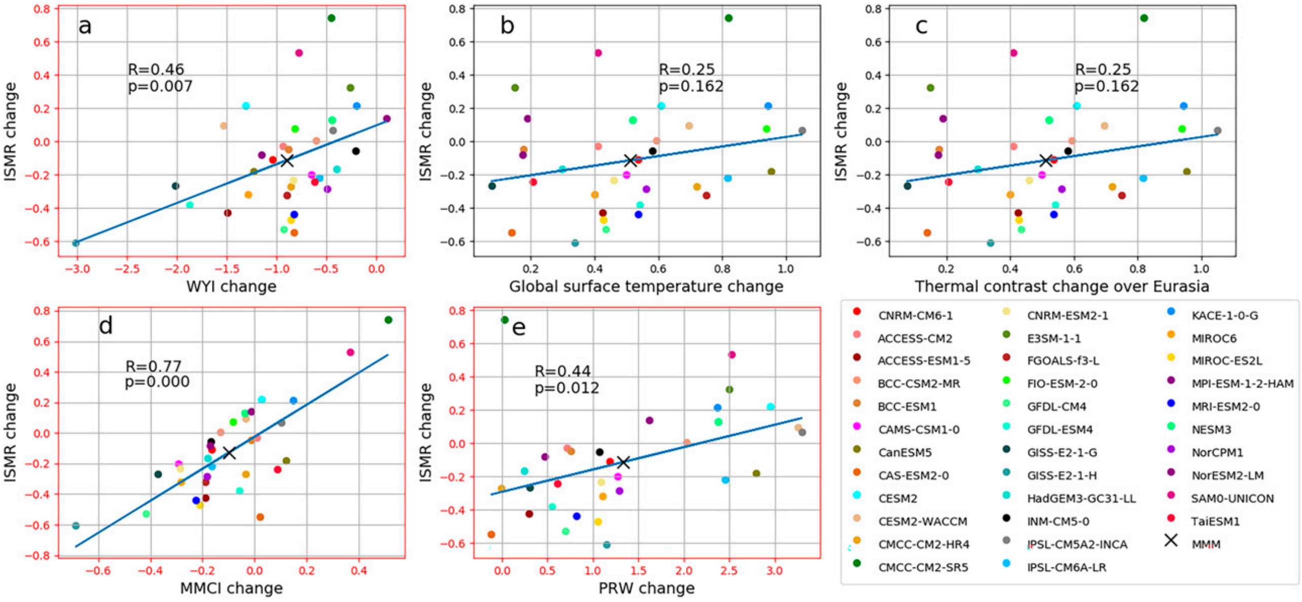

FIG. 2. Scatterplots of ISMR change (mm day^{-1}; defined in section 2 as the difference of JJAS means between 1979–2014 and 1850–1875), respectively, with changes of (a) the WYI (m s^{-1}), (b) global mean surface temperature (K), (c) ELOTC (K), (d) MMCI (m s^{-1}), and (e) PRWI (kg m^{-2}), computed over the same periods. All indices are defined in section 2. The black cross in each scatterplot marks the MMM. As explained in the text, all the 34 available CMIP6 models are used here, with 1 to 50 simulations (see Table S1). For each panel, the correlation and the corresponding p value are computed as described in section 2. The red outline of the panel means that the correlation is significant at the 95% confidence level ($p < 0.05$). Temperature and precipitation change are computed as the difference of climatological means between the end of the historical period (1979–2014) and the early industrial period (1850–75).

significant, relationship with the WYI change (Fig. 2a). However, the origin of the dispersion of the dynamic component of the ISMR remains unexplained. Indeed, in the future projections, ISMR and WYI changes are both significantly correlated with ELOTC (Jin et al. 2020), indicating a role for land–sea thermal contrast. This is not the case over the historical period (Fig. 2c for IMSR and not shown for WYI). This suggests that the mechanisms in the historical period and in projections differ. This difference may be due to the fact that aerosol forcing is strong over the historical period and does not allow for the emergence of a strong land–sea contrast.

We have shown that the intermodel spread of ISMR change is mainly related to the intermodel spread of the dynamic component. However, we lack explanations as to the origin of the intermodel spread of this dynamic component. A first approach is to look at the local scale. Hence, in the next subsection we investigate the role of the model's mean biases and variability over India to explain ISMR changes.

c. *Local relationships between ISMR bias and change over the historical period*

Figure 3 explores the linear dependence between ISMR change with local precipitation and temperature biases over India. Figures 3a and 3d show that in spite of the strong intermodel spread of ISMR biases in mean and temporal variability (e.g., standard deviation), there is no significant relationship between these biases and the ISMR change at the 95% confidence level. Hence, selecting models based on their performance in reproducing the present-day precipitation climatology and variability (Katzenberger et al. 2021) is not a discriminating criterion for how they simulate ISMR change. As for precipitation, there is also no significant relationship ($p > 0.05$) between climatological and variability biases of Indian surface temperature and ISMR change (Figs. 3b,e). On the other hand, Fig. 3c highlights a significant and expected relationship between climatological biases of surface temperature and precipitation over India. This can be explained by a reduced cooling effect (e.g., less clouds and evaporation) due to a deficit of local precipitation over India. Note, nevertheless, that an anomalous land warming could enhance the regional land–sea contrast, thereby inducing an opposite precipitation bias (Jin and Wang 2017), but this effect does not seem to dominate here, consistent with the weak correlation between ISMR and ELOTC changes (Fig. 2c).

To conclude, no obvious link was found at the local scale between the spread of local rainfall/temperature biases and ISMR change. This lack of linkage could be due to the fact that the changes in precipitation and biases are averaged over India where there are potentially inhomogeneities and error compensations for both biases and changes. It could also be that there are simply no relationships at the local scale. To discriminate between these two hypotheses, we need to zoom out from the local scale.

d. *Global changes of surface temperature and precipitation over the historical period*

Figure 4a displays the JJAS precipitation historical changes over the whole globe. Central America, Sahel, and East Asia, which are three major monsoon regions, all exhibit a strong

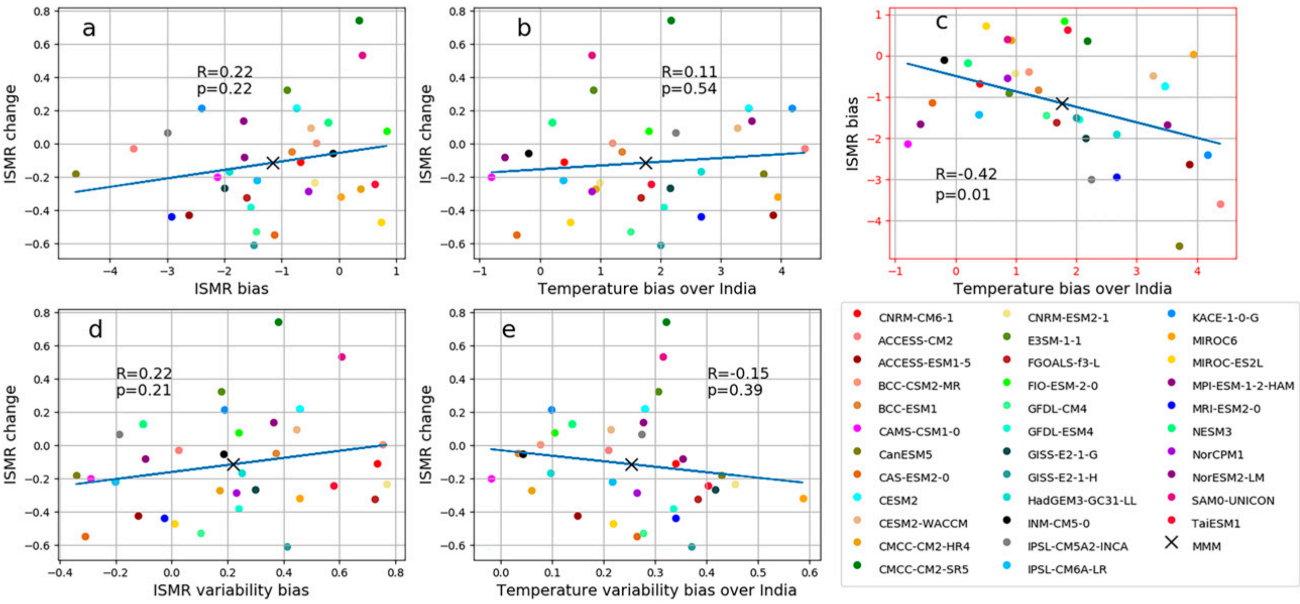

FIG. 3. Scatterplots of ISMR change (mm day^{-1}), respectively, with (a) mean ISMR bias (mm day^{-1}), (b) mean temperature bias over India (K), (d) ISMR standard deviation bias (mm day^{-1}), and (e) temperature standard deviation bias over India (K). Temperature biases are calculated over India, which corresponds to the same domain as the one used for ISMR. Temporal standard deviation in (d) and (e) is computed for each individual historical member and averaged for each model in case of several members. (c) Scatterplot of mean ISMR bias and mean surface temperature bias over India to illustrate local interaction between temperature and precipitation bias over India. The correlation and its associated p value for each pair of model series are indicated in each panel. The red outline means that the correlation is significant at the 95% confidence level ($p < 0.05$). Crosses indicate the MMM position in each scatterplot.

drying over the historical period. Figure 4a also displays a strong drying over the north subtropical Atlantic and over the Maritime Continent, both accompanied with a strong spread across models (Fig. 4b). The Pacific Ocean presents notable wetting over the South Pacific convergence zone (SPCZ) and over the western part of the ITCZ, which is located at 10°N over this region during the boreal summer and some drying in between. Furthermore, the intermodel spread of precipitation change in the Pacific Ocean is particularly strong over the warm pool and the convergence zones (SPCZ and ITCZ) forming a double ITCZ structure (Fig. 4b). Figures 4a and 4b also display a large intermodel spread of precipitation change over India, while the MMM change is not very strong and quite inhomogeneous. These features indicate a strong disagreement between models, but also indicate that averaging precipitation change over India may not be representative of ISMR change. This justifies the need to take into account the spatial pattern of rainfall changes over India when looking for relationships between biases and ISMR change.

Looking at the warming signal (Fig. 4c), an interesting feature is that the SST gradient along the equatorial Pacific (see its definition in Table 1) is enhanced toward the end of the historical period in 25 of 34 models (not related to the models with more than one member) and in the MMM (0.1 K). This latter result is at odds with the CMIP5 MMM, but it is in line with observed trends (Lian et al. 2018). Hence, CMIP6 models show a better agreement with observations than the previous generation, but they still underestimate the enhancement of the equatorial Pacific SST gradient (0.3 K). This pattern is complex and not "La Niña–like" or "El Niño–like" as discussed in Lian et al. 2018. It is rather "El Niño Modoki–like" (Ashok et al. 2007) with a stronger warming over the central Pacific, an intermediate warming over the warm pool, and a weaker warming signal over the eastern equatorial Pacific. Furthermore, the Pacific warming pattern, and hence the change in the SST gradient, is quite different between annual and JJAS mean averages (supplemental Fig. S4), highlighting that focusing on yearly ENSO patterns only may be misleading for understanding ISMR changes. It is necessary to look at the seasonal scale of change in the Pacific to fully understand the interactions with ISMR.

There is a strong intermodel spread of surface temperature change over the whole Eurasian continent and specifically over the Tibetan Plateau, which have both been suggested as important driving factors for ISMR projections (Fig. 4d; Ge et al. 2017; Wang et al. 2020). The largest spread of land temperature changes among models occurs over central Africa, North America, and north of India. Over the ocean, intermodel spread is high at mid- to high latitudes of both hemispheres and also in the eastern equatorial Pacific.

We now have an overview of the MMM spatial changes in surface temperature and precipitation over the historical period, as well as an idea of the areas with the highest disagreement between the models. In the following subsection, we will focus on the biases of these two variables and highlight the regions where the intermodel spread is important in CMIP6

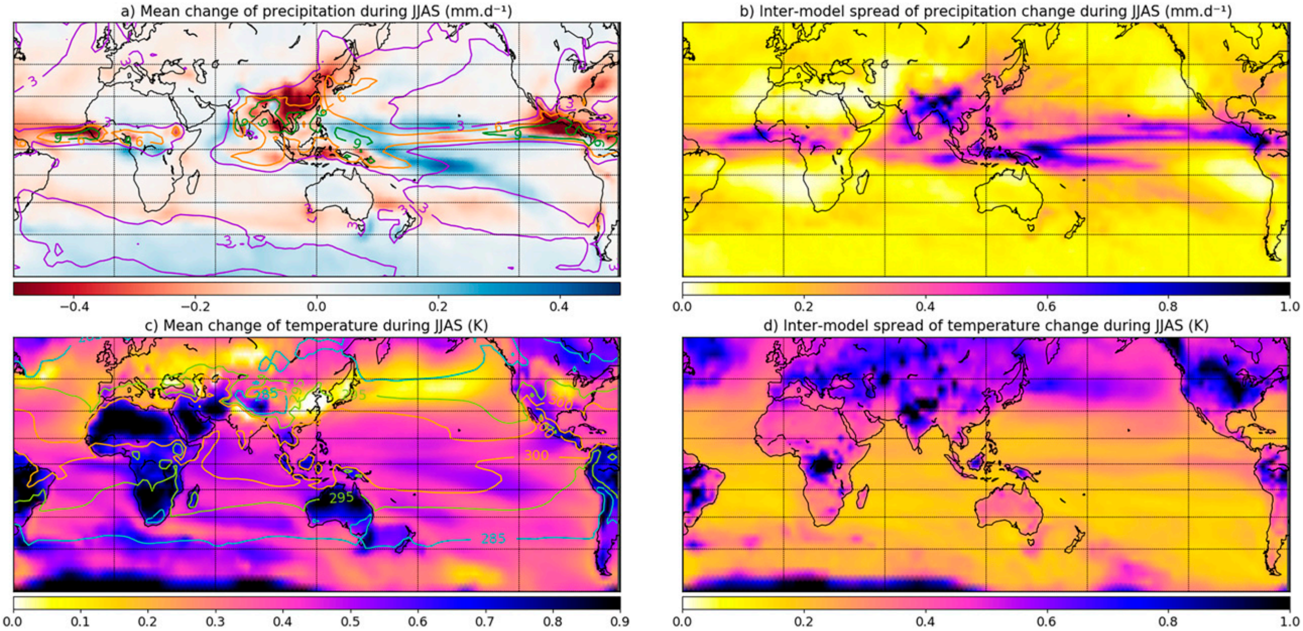

FIG. 4. JJAS MMM and intermodel spread of (top) precipitation (mm day^{-1}) and (bottom) surface temperature (K) changes computed for the 34 CMIP6 models. (a) MMM precipitation change. (b) Intermodel spread of precipitation. (c) MMM surface temperature change. (d) As in (b), but for surface temperature. Contours in (a) are for JJAS mean precipitation from GPCP (contour interval is 3 mm day^{-1}) and in (c) are for JJAS mean surface temperature from ERA-Interim (285 K, blue; 295 K, green; 300 K, orange contours). Temperature and precipitation changes are computed as the difference of climatological means between the end of the historical period (1979–2014) and the early industrial period (1850–75). See section 2 for details.

models, as we seek to establish a link with the spread in the ISMR change.

e. *An overview of climatological rainfall and temperature biases in CMIP6 models*

Figures 5a and 5b first show that India suffers on average from an important dry bias with a large intermodel spread. This dry bias is very pronounced over northern India, while it is almost absent in the south. This is consistent with the tendency of models to produce an ITCZ located 10° south of the observed location in most monsoon regions (Choudhury et al. 2022). In the Indian sector, this southward shift of the ITCZ may be due to warm SST biases over the southwest IO or along the equator (Bollasina and Ming 2013; Prodhomme et al. 2014; Annamalai et al. 2017) and/or to cold surface temperature biases over adjacent deserts (Fig. 5c; Terray et al. 2018; Sooraj et al. 2019). Both the arid regions to the west of India and the western IO have large mean biases and present a strong intermodel spread of surface temperature (Fig. 5d); they are therefore potential candidates for modulating ISMR changes.

Focusing now on remote regions, the Pacific Ocean displays an erroneous double ITCZ structure in both MMM (Fig. 5a) and intermodel spread (Fig. 5b) of precipitation bias. These errors have been typical and prominent biases of CGCMs from CMIP3 to CMIP6 even if they have been shown to be slightly reduced in CMIP6 (Tian and Dong 2020). Interestingly, both the mean and intermodel spread patterns of rainfall changes in Figs. 4a and 4b are also reminiscent of this double ITCZ bias. The equatorial Pacific is also characterized by a cold tongue bias extending from the warm pool to the eastern Pacific, and the Maritime Continent is marked by a warm bias. The upwelling regions off the Chilean and Peruvian coasts show an important warm bias that spreads northward and meets the cold tongue bias at the equator. The equatorial Atlantic also presents an important wet bias. It is attributed to the strong warm bias over the southeastern Atlantic (Fig. 5c), which causes a southeastward shift of the ITCZ over the Atlantic (Richter and Tokinaga 2020). However, as the warm Atlantic bias does not present an important intermodel spread, it is unlikely to explain the equatorial spread of precipitation alone at least in a simple linear framework. Again, continental biases, especially those over the Sahara, or erroneous combined land–ocean temperature gradients are more plausible candidates (Terray et al. 2018; Sooraj et al. 2019). Using CMIP5 models, Shamal and Sanjay (2021) have suggested that these intermodel spreads of temperature and rainfall biases in the Atlantic sector may provide a strong observational constraint for reducing the uncertainties of ISMR projections. We will test this hypothesis with CMIP6 and the historical period in the next section. Finally, Fig. 5d displays a very strong intermodel spread along with a cold bias in the MMM over the Himalayas, which may arise from the variety of the model's resolution and orography as it is a limiting factor in this region of complex orography (Lalande et al. 2021).

To conclude, given the large intermodel spread of surface temperature and rainfall biases, including both land and ocean, and the complexity in existing teleconnections to ISMR (Chowdary et al. 2021), we will next track the origins of the spread of ISMR change within the whole tropics. To this end,

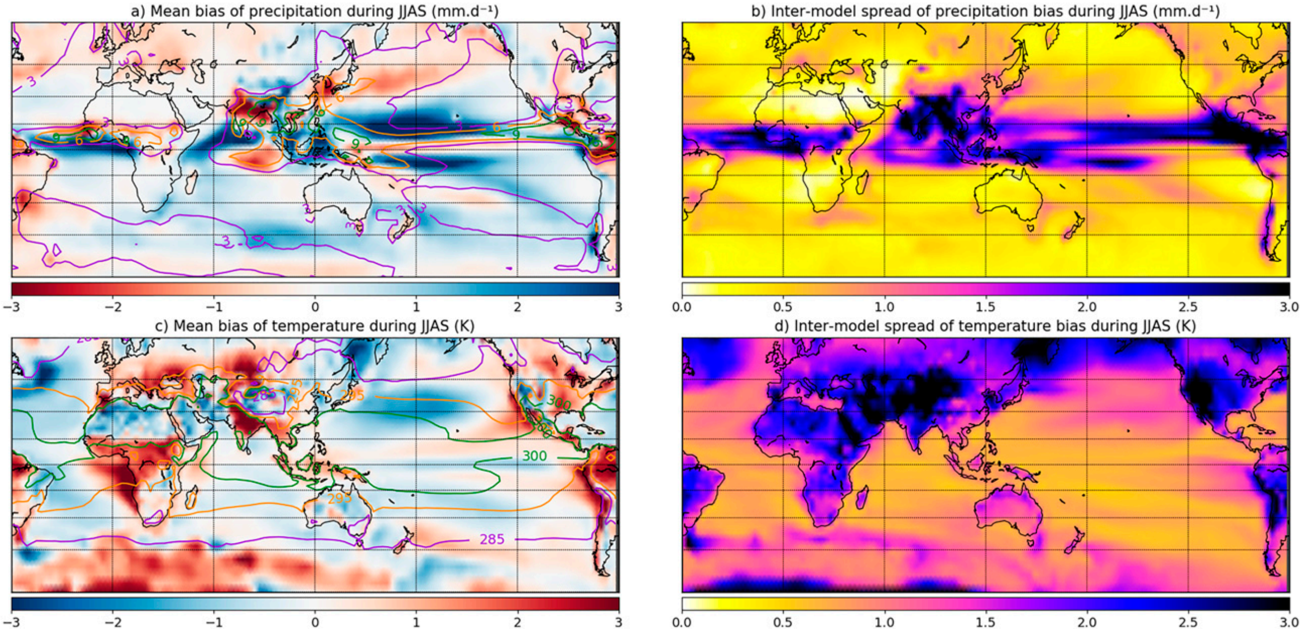

FIG. 5. Boreal summer MMM and intermodel spread of (top) precipitation (mm day^{-1}) and (bottom) temperature (K) biases computed over the 1979–2014 period for 34 CMIP6 models. (a) MMM precipitation bias with respect to GPCP. (b) Intermodel spread of precipitation. (c) MMM temperature bias with respect to ERA-Interim. (d) As in (b), but for temperature. Contours in (a) are for JJAS mean precipitation from GPCP (contour interval is 3 mm day^{-1}) and in (c) are for JJAS mean temperature from ERA-Interim (285 K, purple; 295 K, orange; 300 K, green contours).

we will investigate the dominant modes of covariance between tropical temperature or precipitation biases and ISMR changes with the help of MCAs. This method allows us to move away from spatial averaging over India and to explore the possible link between the pattern of precipitation change over India and tropical biases elsewhere.

4. Remote impact of biases on ISMR historical changes

a. *Spatial patterns of biases and rainfall changes from maximum covariance analysis*

We computed two MCAs, one between rainfall changes over India (7°–20°N and 65°–95°E; land only) and surface temperature biases within the tropical band (30°S–30°N) (Figs. 6a,b), and the other between rainfall change over India (same region) and tropical precipitation biases (Figs. 6c,d). A brief introduction to MCA is provided in Text S1 of the supplemental material for convenience, and more details can be found in Bretherton et al. (1992). We only study the leading coupled mode for each of these MCAs, as they describe a major part of the covariability between the original fields (Table 2), and they are well separated from the remaining MCA modes (not shown).

The heterogeneous maps of rainfall changes over India are spatially homogeneous and very similar in both computations (Figs. 6a,c). Consistently, the correlation between the singular variable (SV) series (e.g., expansion coefficient series) associated with the rainfall change patterns over India in both MCAs is 0.99. The SV series of precipitation changes over India in each MCA are also strongly correlated with the average index ISMR ($r = 0.95$ and 0.94; see Table 2). This latter result confirms that tropical precipitation and surface temperature biases (Figs. 6b,d) are covarying with the Indian monsoon as a whole despite the fact that MMM rainfall changes are inhomogeneous over India (Fig. 4a). The rainfall change patterns from the MCAs (Figs. 6a,c) are also very close to the first EOF mode of ISM rainfall change (not shown). The spatial structures of the leading modes from EOF and MCA are correlated with $r = 0.99$, and the explained variances by these modes are again very close (42% for the first mode of EOF and 39% for both MCAs). These features suggest that the patterns of bias identified in Figs. 6a and 6c are linked with the main mode of intermodel spread of ISM rainfall change, which further motivates a detailed analysis of these modes.

The first modes of the MCAs between surface temperature and precipitation biases with ISM rainfall changes have a square covariance fraction (SCF) of 47% and 40%, respectively, and they have similar normalized root-mean-square covariance (NC) statistics (see Text S1 in the supplemental material for a more detailed definition of this MCA statistic), suggesting that the precipitation and surface temperature biases have a statistical relationship with Indian rainfall change of similar strength (Table 2). Moreover, the correlations between the SV series corresponding to the leading patterns of precipitation and temperature biases and those of rainfall changes in each MCA are quite similar too (0.75 and 0.67; see Table 2), which corroborates that a similar strong relationship exists between biases and ISMR changes. Note that the correlation between the SV series associated with the leading bias pattern in each MCA is $r = 0.67$ ($p < 0.01$). This further shows that a linear relationship may also exist between the leading patterns of rainfall and temperature biases

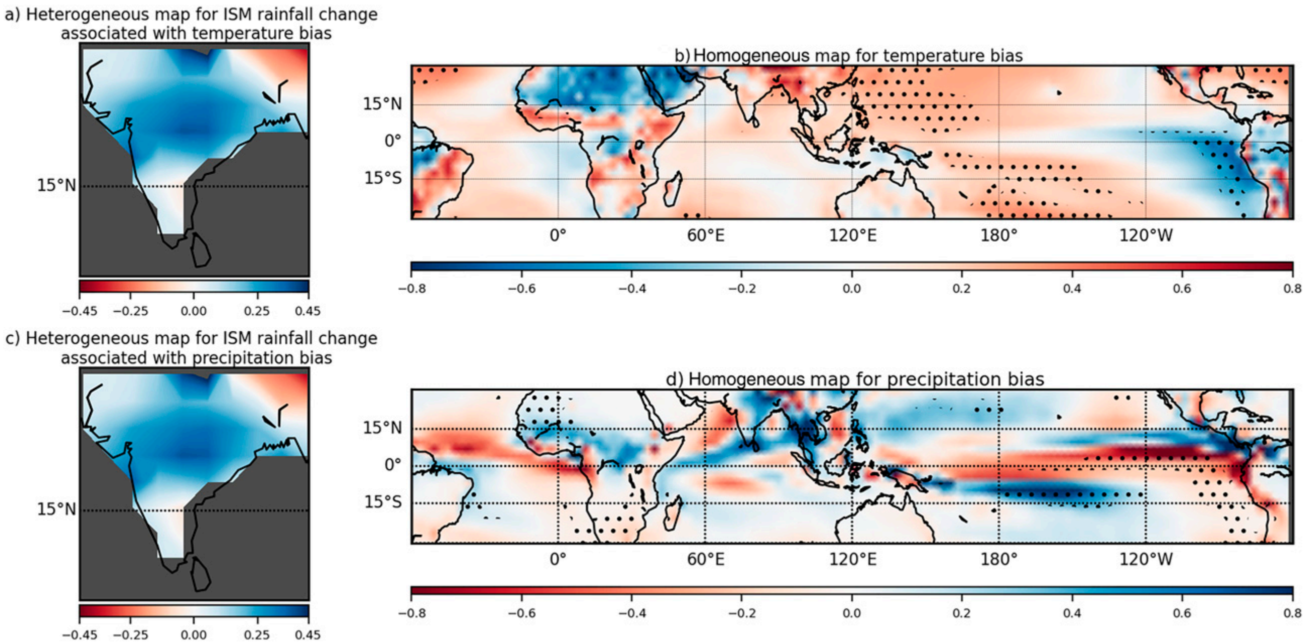

FIG. 6. (a) Heterogeneous and (b) homogeneous maps obtained from the MCA performed between the surface temperature bias of the 34 climate models and the ISM precipitation changes detected over the historical period in the same 34 models. (c),(d) As in (a) and (b), but for the MCA computed between the precipitation bias and the ISM precipitation change. Dotted points indicate significant correlations at the 95% confidence level between the respective SV and gridpoint time series. See Text S1 in the supplemental material for a short introduction to MCA or Bretherton et al. (1992) for more details on SVs (e.g., expansion coefficient series), heterogeneous and homogeneous maps, and the various statistics produced by MCA.

associated with ISM rainfall changes. In other words, this suggests the existence of coupled ocean–atmosphere and/or land–atmosphere biases, which may modulate ISMR changes over the historical period.

Associated with an increase of precipitation over India from the beginning to the end of the historical period (Fig. 6a), Fig. 6b exhibits a strong cooling over the Sahara and Arabian Deserts extending to the west of India, while the rest of India presents a strong warm bias. This spatial inhomogeneity of the intermodel temperature bias over India could explain the lack of relationship between the intermodel spread of ISMR change and Indian surface temperature bias shown in Fig. 3b. The warm bias extends to eastern and southeastern Asia, which, as mentioned earlier, experience a significant drying trend. From an oceanic perspective, Fig. 6b presents a well-defined equatorial SST gradient in the Pacific, with a cooling in the east and a warming in the west, but mainly off the equator and up to the subtropics. This pattern of SST bias in the Pacific is reminiscent of a La Niña–like SST mean pattern. Interestingly, from a statistical perspective, this La Niña–like SST pattern is significant (e.g., see the dotted areas in the Pacific) in contrast to the temperature gradient over land described above. This is physically consistent with the increase of precipitation over India in Fig. 6a as seen for the interannual time scale framework (Chowdary et al. 2021).

From the atmospheric perspective, the leading pattern of model precipitation biases presents strong signals over the

TABLE 2. Statistics of the MCAs between surface temperature or precipitation biases with Indian rainfall change shown in Fig. 6. All correlations in the last four columns are significant at the 99% confidence level. See text and Text S1 in the supplemental material for more details on the SCF and NC statistics.

	Explained variance of Indian rainfall change	SCF	NC	Correlation between SVs of rainfall change over India and ISMR change	Correlation between SV of bias and SV of rainfall change over India	Correlation between SVs of surface temperature and precipitation bias from the two MCAs	Correlation between SVs of rainfall change over India from the two MCAs
Pr bias; Indian rainfall change	39.4%	40%	12.5%	0.95	0.75	0.67	0.99
Ts bias; Indian rainfall change	39.5%	47%	12.9%	0.94	0.67		

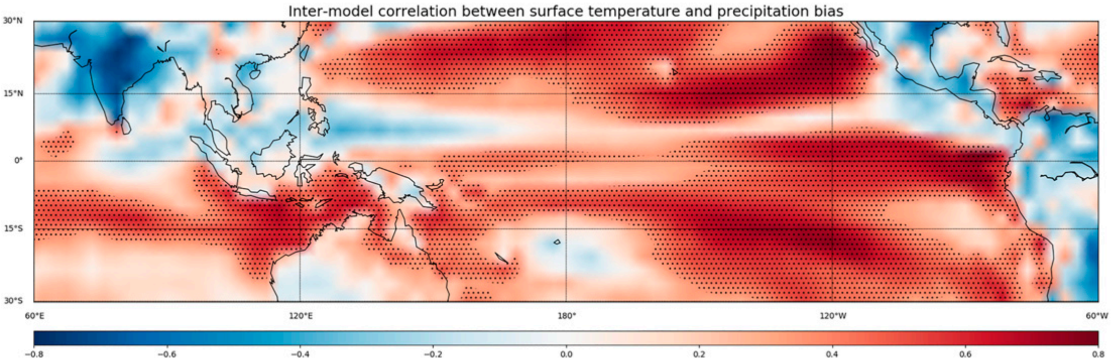

FIG. 7. Intermodel correlation between surface temperature and precipitation biases computed at every grid point in the Indo-Pacific region for the 34 CMIP6 models (see supplemental Table S2 for the list of models). Dotted points indicate grid points where the correlation is significant at the 95% confidence level.

whole tropics. First, Fig. 6d shows a double ITCZ structure over the Pacific Ocean consistent with the intermodel spread of precipitation biases discussed in section 3e. Statistical significance is moreover well defined along the equatorial Pacific and the SPCZ (Fig. 4d). Models showing a positive ISM rainfall change typically also present a strong dry bias (more precisely a reduced wet bias; see Fig. 5a) over the equatorial Atlantic, accompanied by a wet bias (e.g., a reduced dry bias) over the Sahel and central Africa, which corresponds to a northward shift of the ITCZ. This signal therefore strongly modulates the MMM rainfall bias shown in Fig. 5a over the Atlantic region. The bias pattern is complex over the IO, with a tripolar structure composed of an enhanced wet bias between 0° and 10°N, surrounded by a dry bias north and south of this band. Note that over the Indian and Atlantic regions, not many areas exhibit statistically significant gridpoint correlation in contrast to what is detected over the tropical Pacific.

To further illustrate the leading role of the tropical Pacific biases in generating intermodel spread in ISMR changes over the historical period, we computed MCAs with surface temperature and precipitation biases restricted to the tropical Pacific (see supplemental Fig. S5). The results are very similar to the Pacific structure described in Figs. 6b,d, but with higher correlations ($r > 0.85$) between the SV model series associated with the patterns of biases in each MCA. This points out the importance of Pacific biases described above and also again to the key role of ocean–atmosphere coupling in this basin for ISM rainfall changes as simulated by CMIP6 models.

As mentioned above, there is a strong relationship between the pattern of surface temperature and precipitation biases in the Indo-Pacific domain. Figure 7 explores this relationship by correlating precipitation and surface temperature biases at every grid point. The negative correlations over land are expected and consistent with the analysis of section 3c. They arise from a reduced cooling effect associated with a deficit of local precipitation and indicate that the atmosphere drives the coupling between surface temperature and precipitation biases. Over the ocean, the sign and the intensity of the correlation between these two variables are spatially variable due to the complexity of local ocean/atmosphere processes in each basin. Correlations are highest over the equatorial and subtropical areas in the Pacific. The Pacific Ocean mostly displays a positive correlation except along the Mexican coast, the Philippine Sea, and off the coast of Australia. The correlation is particularly strong in the same regions, which exhibit gridpoint statistical significance in Figs. 6b and 6d. This is especially true over the eastern Pacific, indicating that enhanced oceanic warm bias is associated with a wet bias over this region and vice versa across the models. This suggests that surface temperature biases drive the atmosphere biases over this region.

Therefore, since the biases in the tropical Pacific Ocean, particularly along the equator, are correlated with the ISM rainfall changes (Figs. 6b,d), and there is a tight coupling between the ocean and atmosphere biases over the Pacific (Fig. 7), we will focus in the following subsection on the impact of the bias affecting the equatorial Pacific SST gradient as a possible key factor for explaining the intermodel spread of historical change of this SST gradient over the equatorial Pacific and, in turn, ISMR changes.

b. *Relationship between intermodel spread of ISMR change and the equatorial SST gradient in the Pacific*

To explore the role of equatorial Pacific SST gradient biases, we first define an index of the zonal SST gradient as the SST difference between the western and eastern equatorial Pacific (see Table 1). A positive value of this zonal SST gradient index indicates a La Niña–like situation in both the SST bias and change spatial patterns over the tropical Pacific. There is a significant correlation between the SST gradient bias index and ISMR change ($r = -0.47$; $p < 0.01$), which confirms our previous interpretations on the role of tropical Pacific biases, especially along the equator, from the MCAs, and this subsection will look at the underlying mechanisms behind this statistical relationship.

First, Fig. 8a shows that models that present a La Niña–like bias have a tendency to produce a strong cooling over the equatorial eastern Pacific and a warming over the equatorial western Pacific by the end of the historical period. The correlation between the equatorial Pacific SST gradient (as defined in Table 1) bias and change confirms the existence of this strong and significant linear relationship between bias and

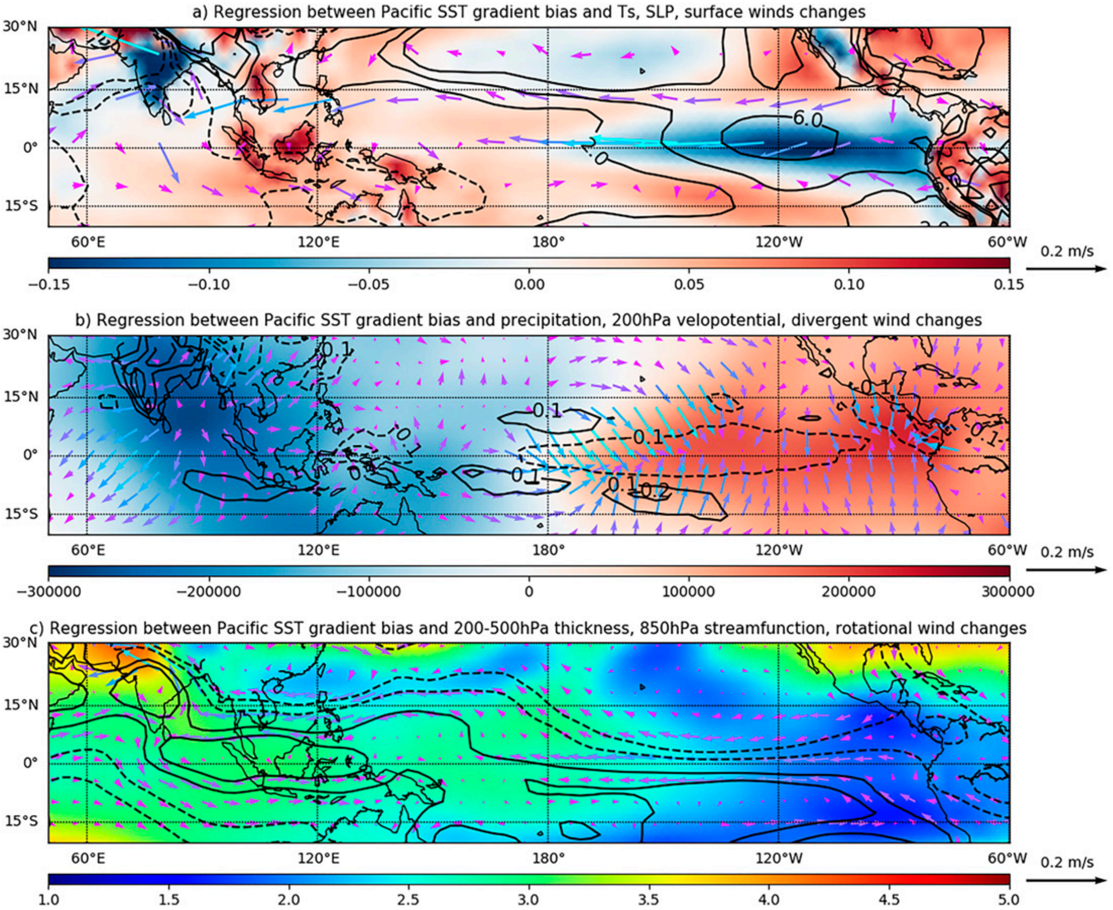

FIG. 8. Intermodel regressions against the equatorial Pacific SST gradient bias of (a) changes in SST (color shaded; K K^{-1}), sea level pressure (contour interval: 2 hPa K^{-1}) and wind at 850 hPa (vectors; m s^{-1} K^{-1}); (b) historical changes of velocity potential at 200 hPa (color shaded; m^2 s^{-1} K^{-1}), precipitation (contour interval: 0.1 mm day^{-1} K^{-1}), and divergent wind at 200 hPa (vectors; m s^{-1} K^{-1}); and (c) historical changes in 200–500-hPa thickness (color shaded; m K^{-1}), 850-hPa streamfunction (contour interval: 30 000 m^2 s^{-1} K^{-1}), and rotational wind at 850 hPa (vectors; m s^{-1} K^{-1}). The colors of the arrows in all three panels vary from purple to cyan according to the intensity of the wind speed for readability. In (a), only one vector of two is shown also for readability.

historical changes ($r = 0.66$; $p < 0.01$). In other words, models that simulate a La Niña–like SST gradient (positive gradient bias) tend to produce La Niña–like SST change over the Pacific Ocean and vice versa. According to Fig. 8, the SST gradient bias correlates more strongly with SST changes in the eastern equatorial Pacific. Furthermore, the bias of the Pacific SST gradient is more correlated with the SST bias in the eastern Pacific than in the western (supplemental Fig. S6). This suggests that, over the historical period and for CMIP6 models, the eastern equatorial Pacific plays a dominant role in shaping the change of the equatorial SST gradient as compared to the west. This is reminiscent of the ocean dynamical thermostat (ODT) mechanism (Clement et al. 1996).

Consistently, models with a La Niña–like SST gradient bias also show an increase in the SLP gradient across the Pacific via an increase in pressure in the east and a decrease in the west during the historical period (Fig. 8a). These changes in SLP and SST gradients are accompanied with an increase in easterly winds over the tropical Pacific, with all three variables being related to each other through the Bjerknes feedback (Bjerknes 1969).

These changes in surface variables are accompanied by changes at higher levels in the atmosphere (Fig. 8b) as the surface communicates with higher atmospheric levels via the latent heat release and the Walker circulation. An anomalous positive equatorial SST gradient in the Pacific induces an intensification of the Walker circulation, as well as a westward shift of its ascending branch (see supplemental Fig. S7). Indeed, Fig. 8b shows an increase in upper-level wind divergence over the Bay of Bengal and India, which implies more intense convective activity and release of latent heat. On the other hand, over the eastern Pacific we observe an increase in upper-level wind convergence, which is accompanied by an increase in subsidence and therefore a reduction in precipitation by enhanced atmospheric stability.

The intermodel spread of precipitation changes over the eastern and central Pacific, associated with the intermodel spread of the equatorial Pacific SST gradient, induces an intermodel spread of latent heat release aloft which propagates eastward in the form of a Kelvin wave over the Atlantic (not shown in Fig. 8c) and westward across the subtropical Pacific in the form of Rossby waves. The latter can be seen in Fig. 8c with the equatorially symmetric response of the tropospheric thickness change. Models that tend to show a positive bias in the SST equatorial gradient (e.g., La Niña–like anomalous pattern) are associated with an anticyclonic circulation around 15°N in the western Pacific at the end of the historical period (Fig. 8a), which promotes the moisture transport across the Bay of Bengal to India through enhanced southerlies at the surface (Figs. 8a,c). This increase of the meridional circulation can also be evidenced by the increase of the zonal tropospheric thickness gradient around India, which strengthens the vertical shear of the meridional wind according to the thermal wind relationship (Dai et al. 2013). Note that these relationships work conversely for models showing a negative bias of the SST equatorial gradient in the Pacific, as our analysis is linear. This mechanism is further supported by the correlation between the change in precipitation over the central Pacific (5°S–5°N; 180°–100°W) and the change in the MMCI ($r = -0.45$; $p < 0.01$), which was itself significantly linked to the intermodel spread of ISMR change in section 3b.

In summary, a mean bias in the equatorial Pacific SST gradient seems to modulate the ISMR change ($r = -0.47$; $p < 0.01$) by physical mechanisms very similar to those operating in the ENSO–monsoon teleconnection (Roy et al. 2019). Indeed, the intermodel spread of the equatorial Pacific SST gradient bias in the CMIP6 models modulates the historical change in this gradient, which is accompanied by cascading effects through the Bjerknes feedback, leading to a change in the Walker circulation that favors convection over India when the initial bias is more La Niña–like and vice versa. In other words, models that simulate a La Niña (El Niño)–like SST gradient tend to produce La Niña (El Niño)–like changes over the Pacific Ocean.

5. Conclusions

The impact of tropical temperature and precipitation biases on simulated changes of ISMR has been analyzed here using historical simulations of 34 coupled models from CMIP6 in order to unravel the potential roles of these biases in the large uncertainties and intermodel spread affecting ISMR simulations and projections.

a. Summary

Our results first confirm that the skill of CGCMs at reproducing ISMR climatology and trend has increased from CMIP3 to CMIP6, but the latest models still exhibit significant biases during JJAS (Jin et al. 2020; Wang et al. 2020). In particular, ISMR still suffers from a persistent mean dry bias. In terms of historical changes, the MMM from CMIP6 models still struggles to reproduce the observed post-1950 drying trend of ISMR, but the agreement of CMIP6 MMM with observations is better over the recent decades (1990–2014) during which both AIR and IMD datasets present a significant wetting trend (Jin and Wang 2017; Roxy 2017). However, both observed datasets and individual CMIP6 models disagree on the amplitude of this wetting trend. Over this wetting period, the models present a very large intermodel spread, and 40% of them produce a (nonobserved) drying trend. Our analysis demonstrates that this cannot simply be attributed to internal variability as the intermodel spread is also prominent in multimember averages in which internal variability plays a secondary role.

On a broader scale, CMIP6 models also present similar errors as previous generations: the Pacific Ocean displays an erroneous double ITCZ (Tian and Dong 2020), an equatorial Pacific cold tongue bias (Li et al. 2016), and warmer-than-observed SST in eastern boundary upwelling systems, especially in the southeast Pacific and Atlantic Oceans (Farneti et al. 2022). On an annual basis, but even more so in boreal summer, the Pacific Ocean shows an El Niño Modoki pattern of change in the historical period. However, the east–west equatorial SST gradient is increased in the MMM, suggesting also a La Niña–like pattern of change. These results are not in line with those of CMIP5, where many models agreed on an El Niño–like warming over the historical period, nor are they consistent with observations (Lian et al. 2018).

Following this assessment of the performance of the models in CMIP6, we answered the three questions that had been raised in the introduction concerning the intermodel spread of historical change ISMR:

1) Is there a local link between climatological biases over India and ISMR change? We demonstrated that temperature and rainfall climatology (and variability) biases over India cannot be used to constrain the intermodel spread of ISMR changes despite that these local biases also present a large intermodel spread. This is consistent with past investigations on CMIP5 (Racherla et al. 2012).
2) Are there links with some remote biases over land or the tropical oceanic basins? The MCAs suggest that tropical rainfall and temperature biases play a leading role in the intermodel spread of ISMR rainfall changes over the historical period, producing a similar and uniform rainfall change over India. The MCA results also confirm that the local biases are not key to reducing the uncertainties in ISMR changes. Further analysis demonstrates that remote coupled ocean–atmosphere biases in the Pacific Ocean play a dominant role. Furthermore, the strong positive correlation between local temperature and precipitation biases in the Pacific suggests that the ocean is driving the coupled biases. Consequently, we focused on the role of the bias of the equatorial SST gradient and found that the climatological background state for each model plays a pivotal role in determining the Pacific mean state change over the historical period with the eastern equatorial Pacific playing a leading role in these interactions (Fig. 6b).
3) By which physical processes do local and/or remote biases influence ISMR historical evolution? Our analysis suggests that models having a La Niña–like SST gradient bias tend to favor a La Niña–like change and, conversely, an El Niño–like bias promotes an El Niño–like change. Therefore, by modulating the change of the SST gradient

in the Pacific, the bias of this gradient impacts the local rainfall and the Walker circulation changes, which result in ISM rainfall changes through teleconnection mechanisms very similar to those associated with the ENSO–ISM teleconnection (Roy et al. 2019; Chowdary et al. 2021). The equatorial Pacific SST gradient bias also modulates changes of latent heat release (associated with the local rainfall changes) that propagate westward in the form of Rossby waves into the subtropical North Pacific Ocean. For La Niña–like models, this creates low-level anticyclonic anomalies 10° north of the Maritime Continent and changes the midtropospheric temperature gradient westward of the rainfall change in the central Pacific. Conversely, for El Niño–like models in which the Pacific equatorial SST gradient is reduced, the changes of this midtropospheric temperature gradient are reversed during the historical period. This finally leads to a modulation of the meridional monsoon circulation across the CMIP6 models, which also results in an intermodel spread of ISM rainfall and MMCI changes. The modulation of the meridional monsoon circulation by biases in the Pacific Ocean has already been suggested to play a key role in the intermodel spread of ISMR projections in CMIP5 (Li et al. 2017). However, and although the circulation patterns involved here are similar, the underlying mechanisms we suggest for the historical period are different; they involve mainly the eastern equatorial Pacific, while the role of the western Pacific is dominant in the future as diagnosed by Li et al. (2017).

b. *Discussion and perspectives*

As summarized in Lian et al. (2018), the changes of the equatorial Pacific SST gradient can be understood in an atmospheric or oceanic framework. On the one hand, the atmospheric framework links a reduction of the equatorial Pacific gradient to the weakening of the tropical and Walker circulations under a GHG forcing scenario (Held and Soden 2006). On the other hand, the oceanic framework leads to an increase of the gradient under global warming (Clement et al. 1996). The oceanic framework is based on the ODT mechanism, which refers to the damping effect of the oceanic upwelling in the eastern equatorial Pacific for a given forcing through heat divergence (Clement et al. 1996). Here, we suggest that a positive SST gradient bias is associated with an overly pronounced upwelling in the eastern Pacific, which causes an overestimation of the ODT mechanism, leading to a reinforcement of the Pacific equatorial SST gradient over the historical period and vice versa for models with a negative SST gradient bias in the equatorial Pacific. Note that a poor sampling of "observed" internal variability can also play an important additional role in the mismatch between observations and simulations. Recent results show that a correct representation of the internal variability requires large ensemble simulations, and when this is done the observed Pacific trend lies in the spread of the simulated internal variability (Watanabe et al. 2021).

Future studies should investigate in more detail how the equatorial biases in the Pacific can lead to a misrepresentation of the forced response (Lian et al. 2018) and whether these biases can be understood solely by intrinsic modeled errors of the Pacific coupled system or if these biases can be induced by remote errors, for example, those in the Atlantic or Indian basins (McGregor et al. 2018; Shamal and Sanjay 2021; Terray et al. 2021, 2023).

In a future study, the relationship between the Pacific equatorial SST gradient bias and ISMR change could be further tested using SST nudging experiments to corroborate the mechanisms that we proposed. We could also investigate whether the relationships we found over the historical period between the Pacific equatorial SST gradient biases and ISMR would still hold in CMIP projections. Indeed, we have suggested that the ODT mechanism links the equatorial Pacific gradient bias and change, but this relationship may diminish on longer time scales because the ODT mechanism is described as a rapid response of the Pacific Ocean to radiative forcing (Heede et al. 2020), as the ODT mechanism is weakening with the progressive warming of the equatorial thermocline (Luo et al. 2017).

Acknowledgments. Pascal Terray and Juliette Mignot are funded by Institut de Recherche pour le Développement (IRD; France). Analysis was done with Python (https://www.python.org/) and the STATPACK and NCSTAT softwares (https://terray.locean-ipsl.upmc.fr/software.html). This work benefited from ESPRI (https://mesocentre.ipsl.fr), which is supported by CNRS, Sorbonne University, Ecole Polytechnique, and CNES and through national and international grants. We also acknowledge funding from the ARCHANGE project of the "Make Our Planet Great Again" program (ANR-18-MPGA-0001; France) and from JPI Climate/JPI Oceans ROADMAP project (ANR-19-JPOC-003).

Data availability statement. The study is based on the outputs of CMIP6. These are publicly available upon registration on the data portal of the Earth System Grid Foundation (ESGF; https://esgf-node.ipsl.upmc.fr/search/cmip6-ipsl/). ERA-Interim is publicly accessible upon registration on the ECMWF data portal (http://apps.ecmwf.int/). The GPCP data are publicly accessible (https://psl.noaa.gov/data/gridded/data.gpcp.html).

REFERENCES

Adler, R. F., and Coauthors, 2003: The Version-2 Global Precipitation Climatology Project (GPCP) monthly precipitation analysis (1979–present). *J. Hydrometeor.*, **4**, 1147–1167, https://doi.org/10.1175/1525-7541(2003)004<1147:TVGPCP>2.0.CO;2.

Allan, R. P., and Coauthors, 2020: Advances in understanding large-scale responses of the water cycle to climate change. *Ann. N. Y. Acad. Sci.*, **1472**, 49–75, https://doi.org/10.1111/nyas.14337.

Annamalai, H., B. Taguchi, J. P. McCreary, M. Nagura, and T. Miyama, 2017: Systematic errors in South Asian monsoon simulation: Importance of equatorial Indian Ocean processes.

J. Climate, **30**, 8159–8178, https://doi.org/10.1175/JCLI-D-16-0573.1.

Ashok, K., S. K. Behera, S. A. Rao, H. Weng, and T. Yamagata, 2007: El Niño Modoki and its possible teleconnection. *J. Geophys. Res.*, **112**, C11007, https://doi.org/10.1029/2006JC003798.

Bjerknes, J., 1969: Atmospheric teleconnections from the equatorial Pacific. *Mon. Wea. Rev.*, **97**, 163–172, https://doi.org/10.1175/1520-0493(1969)097<0163:ATFTEP>2.3.CO;2.

Bollasina, M. A., and Y. Ming, 2013: The role of land-surface processes in modulating the Indian monsoon annual cycle. *Climate Dyn.*, **41**, 2497–2509–, https://doi.org/10.1007/s00382-012-1634-3.

——, ——, and V. Ramaswamy, 2011: Anthropogenic aerosols and the weakening of the South Asian summer monsoon. *Science*, **334**, 502–505, https://doi.org/10.1126/science.1204994.

Bretherton, C. S., C. Smith, and J. M. Wallace, 1992: An intercomparison of methods for finding coupled patterns in climate data. *J. Climate*, **5**, 541–560, https://doi.org/10.1175/1520-0442(1992)005<0541:AIOMFF>2.0.CO;2.

Cherry, S., 1997: Some comments on singular value decomposition analysis. *J. Climate*, **10**, 1759–1761, https://doi.org/10.1175/1520-0442(1997)010<1759:SCOSVD>2.0.CO;2.

Chinta, V., Z. Chen, Y. Du, and J. S. Chowdary, 2022: Influence of the interdecadal Pacific oscillation on South Asian and East Asian summer monsoon rainfall in CMIP6 models. *Climate Dyn.*, **58**, 1791–1809, https://doi.org/10.1007/s00382-021-05992-6.

Choudhury, B. A., P. V. Rajesh, Y. Zahan, and B. Goswami, 2022: Evolution of the Indian summer monsoon rainfall simulations from CMIP3 to CMIP6 models. *Climate Dyn.*, **58**, 2637–2662, https://doi.org/10.1007/s00382-021-06023-0.

Chowdary, J. S., A. Parekh, and C. Gnanaseelan, 2021: *Indian Summer Monsoon Variability: El Niño–Teleconnections and Beyond*. 1st ed. Elsevier, 472 pp.

Clement, A. C., R. Seager, M. A. Cane, and S. E. Zebiak, 1996: An ocean dynamical thermostat. *J. Climate*, **9**, 2190–2196, https://doi.org/10.1175/1520-0442(1996)009<2190:AODT>2.0.CO;2.

Cleveland, W. S., and S. J. Devlin, 1988: Locally weighted regression: An approach to regression analysis by local fitting. *J. Amer. Stat. Assoc.*, **83**, 596–610, https://doi.org/10.1080/01621459.1988.10478639.

Dai, A., H. Li, Y. Sun, L.-C. Hong, LinHo, C. Chou, and T. Zhou, 2013: The relative roles of upper and lower tropospheric thermal contrasts and tropical influences in driving Asian summer monsoons. *J. Geophys. Res. Atmos.*, **118**, 7024–7045, https://doi.org/10.1002/jgrd.50565.

Dee, D. P., and Coauthors, 2011: The ERA-Interim reanalysis: Configuration and performance of the data assimilation system. *Quart. J. Roy. Meteor. Soc.*, **137**, 553–597, https://doi.org/10.1002/qj.828.

Endo, H., A. Kitoh, and H. Ueda, 2018: A unique feature of the Asian summer monsoon response to global warming: The role of different land–sea thermal contrast change between the lower and upper troposphere. *SOLA*, **14**, 57–63, https://doi.org/10.2151/sola.2018-010.

Eyring, V., S. Bony, G. A. Meehl, C. A. Senior, B. Stevens, R. J. Stouffer, and K. E. Taylor, 2016: Overview of the Coupled Model Intercomparison Project phase 6 (CMIP6) experimental design and organization. *Geosci. Model Dev.*, **9**, 1937–1958, https://doi.org/10.5194/gmd-9-1937-2016.

Farneti, R., A. Stiz, and J. B. Ssebandeke, 2022: Improvements and persistent biases in the southeast tropical Atlantic in CMIP models. *npj Climate Atmos. Sci.*, **5**, 42, https://doi.org/10.1038/s41612-022-00264-4.

Gadgil, S., P. N. Vinayachandran, P. A. Francis, and S. Gadgil, 2004: Extremes of the Indian summer monsoon rainfall, ENSO and equatorial Indian Ocean oscillation. *Geophys. Res. Lett.*, **31**, L12213, https://doi.org/10.1029/2004GL019733.

Ge, F., F. Sielmann, X. Zhu, K. Fraedrich, X. Zhi, T. Peng, and L. Wang, 2017: The link between Tibetan Plateau monsoon and Indian summer precipitation: A linear diagnostic perspective. *Climate Dyn.*, **49**, 4201–4215, https://doi.org/10.1007/s00382-017-3585-1.

Goswami, B. N., V. Krishnamurthy, and H. Annmalai, 1999: A broad-scale circulation index for the interannual variability of the Indian summer monsoon. *Quart. J. Roy. Meteor. Soc.*, **125**, 611–633, https://doi.org/10.1002/qj.49712555412.

Heede, U. K., A. V. Fedorov, and N. J. Burls, 2020: Time scales and mechanisms for the tropical Pacific response to global warming: A tug of war between the ocean thermostat and weaker Walker. *J. Climate*, **33**, 6101–6118, https://doi.org/10.1175/JCLI-D-19-0690.1.

Held, I. M., and B. J. Soden, 2006: Robust responses of the hydrological cycle to global warming. *J. Climate*, **19**, 5686–5699, https://doi.org/10.1175/JCLI3990.1.

Hodges, J. L., 1958: The significance probability of the Smirnov two-sample test. *Ark. Mat.*, **3**, 469–486, https://doi.org/10.1007/BF02589501.

Huang, X., and Coauthors, 2020: The recent decline and recovery of Indian summer monsoon rainfall: Relative roles of external forcing and internal variability. *J. Climate*, **33**, 5035–5060, https://doi.org/10.1175/JCLI-D-19-0833.1.

Hurley, J. V., and W. R. Boos, 2013: Interannual variability of monsoon precipitation and local subcloud equivalent potential temperature. *J. Climate*, **26**, 9507–9527, https://doi.org/10.1175/JCLI-D-12-00229.1.

Jain, S., and V. Kumar, 2012: Trend analysis of rainfall and temperature data for India. *Curr. Sci.*, **102**, 37–49.

——, P. Salunke, S. K. Mishra, and S. Sahany, 2019: Performance of CMIP5 models in the simulation of Indian summer monsoon. *Theor. Appl. Climatol.*, **137**, 1429–1447, https://doi.org/10.1007/s00704-018-2674-3.

Jin, C., B. Wang, and J. Liu, 2020: Future changes and controlling factors of the eight regional monsoons projected by CMIP6 models. *J. Climate*, **33**, 9307–9326, https://doi.org/10.1175/JCLI-D-20-0236.1.

Jin, Q., and C. Wang, 2017: A revival of Indian summer monsoon rainfall since 2002. *Nat. Climate Change*, **7**, 587–594, https://doi.org/10.1038/nclimate3348.

Joshi, M. K., and F. Kucharski, 2017: Impact of interdecadal Pacific oscillation on Indian summer monsoon rainfall: An assessment from CMIP5 climate models. *Climate Dyn.*, **48**, 2375–2391, https://doi.org/10.1007/s00382-016-3210-8.

Katzenberger, A., J. Schewe, J. Pongratz, and A. Levermann, 2021: Robust increase of Indian monsoon rainfall and its variability under future warming in CMIP6 models. *Earth Syst. Dyn.*, **12**, 367–386, https://doi.org/10.5194/esd-12-367-2021.

Lalande, M., M. Ménégoz, G. Krinner, K. Naegeli, and S. Wunderle, 2021: Climate change in the high mountain Asia in CMIP6. *Earth Syst. Dyn.*, **12**, 1061–1098, https://doi.org/10.5194/esd-12-1061-2021.

Lau, W. K.-M., and K.-M. Kim, 2017: Competing influences of greenhouse warming and aerosols on Asian summer monsoon circulation and rainfall. *Asia-Pac. J. Atmos. Sci.*, **53**, 181–194, https://doi.org/10.1007/s13143-017-0033-4.

Levine, R. C., A. G. Turner, D. Marathayil, and G. M. Martin, 2013: The role of northern Arabian Sea surface temperature biases in CMIP5 model simulations and future projections of Indian summer monsoon rainfall. *Climate Dyn.*, **41**, 155–172, https://doi.org/10.1007/s00382-012-1656-x.

Li, G., S.-P. Xie, and Y. Du, 2015: Monsoon-induced biases of climate models over the tropical Indian Ocean. *J. Climate*, **28**, 3058–3072, https://doi.org/10.1175/JCLI-D-14-00740.1.

——, ——, C. He, and Z. Chen, 2017: Western pacific emergent constraint lowers projected increase in Indian summer monsoon rainfall. *Nat. Climate Change*, **7**, 708–712, https://doi.org/10.1038/nclimate3387.

Li, X., M. Ting, and D. E. Lee, 2018: Fast adjustments of the Asian summer monsoon to anthropogenic aerosols. *Geophys. Res. Lett.*, **45**, 1001–1010, https://doi.org/10.1002/2017GL076667.

Li, Z., and Coauthors, 2016: Aerosol and monsoon climate interactions over Asia. *Rev. Geophys.*, **54**, 866–929, https://doi.org/10.1002/2015RG000500.

Lian, T., D. Chen, J. Ying, P. Huang, and Y. Tang, 2018: Tropical Pacific trends under global warming: El Niño–like or La Niña–like? *Natl. Sci. Rev.*, **5**, 810–812, https://doi.org/10.1093/nsr/nwy134.

Lin, M., and P. Huybers, 2019: If rain falls in India and no one reports it, are historical trends in monsoon extremes biased? *Geophys. Res. Lett.*, **46**, 1681–1689, https://doi.org/10.1029/2018GL079709.

Luo, Y., J. Lu, F. Liu, and O. Garuba, 2017: The role of ocean dynamical thermostat in delaying the El Niño–like response over the equatorial Pacific to climate warming. *J. Climate*, **30**, 2811–2827, https://doi.org/10.1175/JCLI-D-16-0454.1.

Ma, J., and J.-Y. Yu, 2014: Paradox in south Asian summer monsoon circulation change: Lower tropospheric strengthening and upper tropospheric weakening. *Geophys. Res. Lett.*, **41**, 2934–2940, https://doi.org/10.1002/2014GL059891.

McGregor, S., M. F. Stuecker, J. B. Kajtar, M. H. England, and M. Collins, 2018: Model tropical Atlantic biases underpin diminished Pacific decadal variability. *Nat. Climate Change*, **8**, 493–498, https://doi.org/10.1038/s41558-018-0163-4.

Ming, Y., V. Ramaswamy, and G. Chen, 2011: A model investigation of aerosol-induced changes in boreal winter extratropical circulation. *J. Climate*, **24**, 6077–6091, https://doi.org/10.1175/2011JCLI4111.1.

Mohapatra, G. N., A. R. Beham, C. Kavyashree, S. Kavya, M. L. Singh, and J. Vaishnavi, 2018: Study of Indian summer monsoon rainfall trend during the period 1901–2013 through data mining. *Int. J. Res. Appl. Sci. Eng. Technol.*, **6**, 1701–1705, https://doi.org/10.22214/ijraset.2018.5278.

Oueslati, B., S. Bony, C. Risi, and J.-L. Dufresne, 2016: Interpreting the inter-model spread in regional precipitation projections in the tropics: Role of surface evaporation and cloud radiative effects. *Climate Dyn.*, **47**, 2801–2815, https://doi.org/10.1007/s00382-016-2998-6.

Parthasarathy, B., A. A. Munot, and D. R. Kothawale, 1994: All-India monthly and seasonal rainfall series: 1871–1993. *Theor. Appl. Climatol.*, **49**, 217–224, https://doi.org/10.1007/BF00867461.

Polson, D., M. Bollasina, G. C. Hegerl, and L. J. Wilcox, 2014: Decreased monsoon precipitation in the Northern Hemisphere due to anthropogenic aerosols. *Geophys. Res. Lett.*, **41**, 6023–6029, https://doi.org/10.1002/2014GL060811.

Prodhomme, C., P. Terray, S. Masson, T. Izumo, T. Tozuka, and T. Yamagata, 2014: Impacts of Indian Ocean SST biases on the Indian monsoon: As simulated in a global coupled model. *Climate Dyn.*, **42**, 271–290, https://doi.org/10.1007/s00382-013-1671-6.

Racherla, P. N., D. T. Shindell, and G. S. Faluvegi, 2012: The added value to global model projections of climate change by dynamical downscaling: A case study over the continental U.S. using the GISS-ModelE2 and WRF models. *J. Geophys. Res.*, **117**, D20118, https://doi.org/10.1029/2012JD018091.

Raghavan, K., and Coauthors, 2016: Deciphering the desiccation trend of the South Asian monsoon hydroclimate in a warming world. *Climate Dyn.*, **47**, 1007–1027, https://doi.org/10.1007/s00382-015-2886-5.

Rajendran, K., S. Surendran, S. J. Varghese, and A. Sathyanath, 2022: Simulation of Indian summer monsoon rainfall, interannual variability and teleconnections: Evaluation of CMIP6 models. *Climate Dyn.*, **58**, 2693–2723, https://doi.org/10.1007/s00382-021-06027-w.

Ramage, C. S., Ed., 1971: Definition of the monsoons and their extent. *Monsoon Meteorology*, International Geophysics Series, Vol. 15, Academic Press, 1–7.

Rao, S. A., and Coauthors, 2019: Monsoon mission: A targeted activity to improve monsoon prediction across scales. *Bull. Amer. Meteor. Soc.*, **100**, 2509–2532, https://doi.org/10.1175/BAMS-D-17-0330.1.

Richter, I., and H. Tokinaga, 2020: An overview of the performance of CMIP6 models in the tropical Atlantic: Mean state, variability, and remote impacts. *Climate Dyn.*, **55**, 2579–2601, https://doi.org/10.1007/s00382-020-05409-w.

Roxy, M. K., 2017: Land warming revives monsoon. *Nat. Climate Change*, **7**, 549–550, https://doi.org/10.1038/nclimate3356.

——, K. Ritika, P. Terray, R. Murtugudde, K. Ashok, and B. N. Goswami, 2015: Drying of Indian subcontinent by rapid Indian Ocean warming and a weakening land–sea thermal gradient. *Nat. Commun.*, **6**, 7423, https://doi.org/10.1038/ncomms8423.

Roy, I., R. G. Tedeschi, and M. Collins, 2019: ENSO teleconnections to the Indian summer monsoon under changing climate. *Int. J. Climatol.*, **39**, 3031–3042, https://doi.org/10.1002/joc.5999.

Sabeerali, C. T., S. A. Rao, A. R. Dhakate, K. Salunke, and B. N. Goswami, 2015: Why ensemble mean projection of South Asian monsoon rainfall by CMIP5 models is not reliable? *Climate Dyn.*, **45**, 161–174, https://doi.org/10.1007/s00382-014-2269-3.

Saha, A., S. Ghosh, A. S. Sahana, and E. P. Rao, 2014: Failure of CMIP5 climate models in simulating post-1950 decreasing trend of Indian monsoon. *Geophys. Res. Lett.*, **41**, 7323–7330, https://doi.org/10.1002/2014GL061573.

Salzmann, M., and R. Cherian, 2015: On the enhancement of the Indian summer monsoon drying by Pacific multidecadal variability during the latter half of the twentieth century. *J. Geophys. Res. Atmos.*, **120**, 9103–9118, https://doi.org/10.1002/2015JD023313.

——, H. Weser, and R. Cherian, 2014: Robust response of Asian summer monsoon to anthropogenic aerosols in CMIP5 models. *J. Geophys. Res. Atmos.*, **119**, 11 321–11 337, https://doi.org/10.1002/2014JD021783.

Seager, R., N. Naik, and G. A. Vecchi, 2010: Thermodynamic and dynamic mechanisms for large-scale changes in the hydrological cycle in response to global warming. *J. Climate*, **23**, 4651–4668, https://doi.org/10.1175/2010JCLI3655.1.

Seth, A., A. Giannini, M. Rojas, S. A. Rauscher, S. Bordoni, D. Singh, and S. J. Camargo, 2019: Monsoon responses to climate changes—connecting past, present and future. *Curr. Climate Change Rep.*, **5**, 63–79, https://doi.org/10.1007/s40641-019-00125-y.

Shamal, M., and J. Sanjay, 2021: An observational equatorial Atlantic Ocean constraint on Indian monsoon precipitation projections. *Climate Dyn.*, **57**, 209–221, https://doi.org/10.1007/s00382-021-05703-1.

Singh, D., S. Ghosh, M. K. Roxy, and S. McDermid, 2019: Indian summer monsoon: Extreme events, historical changes, and role of anthropogenic forcings. *Wiley Interdiscip. Rev. Climate Change*, **10**, e571, https://doi.org/10.1002/wcc.571.

Sooraj, K. P., P. Terray, S. Masson, and J. Crétat, 2019: Modulations of the Indian summer monsoon by the hot subtropical deserts: Insights from coupled sensitivity experiments. *Climate Dyn.*, **52**, 4527–4555, https://doi.org/10.1007/s00382-018-4396-8.

Sperber, K. R., H. Annamalai, I.-S. Kang, A. Kitoh, A. Moise, A. Turner, B. Wang, and T. Zhou, 2013: The Asian summer monsoon: An intercomparison of CMIP5 vs. CMIP3 simulations of the late 20th century. *Climate Dyn.*, **41**, 2711–2744, https://doi.org/10.1007/s00382-012-1607-6.

Swapna, P., R. Krishnan, N. Sandeep, A. G. Prajeesh, D. C. Ayantika, S. Manmeet, and R. Vellore, 2018: Long-term climate simulations using the IITM Earth System Model (IITM-ESMv2) with focus on the South Asian monsoon. *J. Adv. Model. Earth Syst.*, **10**, 1127–1149, https://doi.org/10.1029/2017MS001262.

Tanaka, H. L., N. Ishizaki, and A. Kitoh, 2004: Trend and interannual variability of Walker, monsoon and Hadley circulations defined by velocity potential in the upper troposphere. *Tellus*, **56A**, 250–269, https://doi.org/10.3402/tellusa.v56i3.14410.

Terray, P., K. P. Sooraj, S. Masson, R. P. M. Krishna, G. Samson, and A. G. Prajeesh, 2018: Towards a realistic simulation of boreal summer tropical rainfall climatology in state-of-the-art coupled models: Role of the background snow-free land albedo. *Climate Dyn.*, **50**, 3413–3439, https://doi.org/10.1007/s00382-017-3812-9.

——, ——, ——, and C. Prodhomme, 2021: Anatomy of the Indian summer monsoon and ENSO relationships in state-of-the-art CGCMs: Role of the tropical Indian Ocean. *Climate Dyn.*, **56**, 329–356, https://doi.org/10.1007/s00382-020-05484-z.

——, L. Joseph, and K. Sooraj, 2023: Anatomy of the Indian summer monsoon and ENSO relationship in a state-of-the-art CGCM: Role of the tropical Atlantic Ocean. *Climate Dyn.*, **60**, 1559–1582, https://doi.org/10.1007/s00382-022-06397-9.

Tian, B., and X. Dong, 2020: The double-ITCZ bias in CMIP3, CMIP5, and CMIP6 models based on annual mean precipitation. *Geophys. Res. Lett.*, **47**, e2020GL087232, https://doi.org/10.1029/2020GL087232.

Vecchi, G. A., and B. J. Soden, 2007: Global warming and the weakening of the tropical circulation. *J. Climate*, **20**, 4316–4340, https://doi.org/10.1175/JCLI4258.1.

Vibhute, A., S. Halder, P. Singh, A. Parekh, J. S. Chowdary, and C. Gnanaseelan, 2020: Decadal variability of tropical Indian Ocean sea surface temperature and its impact on the Indian summer monsoon. *Theor. Appl. Climatol.*, **141**, 551–566, https://doi.org/10.1007/s00704-020-03216-1.

Wang, B., C. Jin, and J. Liu, 2020: Understanding future change of global monsoons projected by CMIP6 models. *J. Climate*, **33**, 6471–6489, https://doi.org/10.1175/JCLI-D-19-0993.1.

Wang, M., and Coauthors, 2015: A multiscale modeling framework model (superparameterized CAM5) with a higher-order turbulence closure: Model description and low-cloud simulations. *J. Adv. Model. Earth Syst.*, **7**, 484–509, https://doi.org/10.1002/2014MS000375.

Watanabe, M., J.-L. Dufresne, Y. Kosaka, T. Mauritsen, and H. Tatebe, 2021: Enhanced warming constrained by past trends in equatorial Pacific sea surface temperature gradient. *Nat. Climate Change*, **11**, 33–37, https://doi.org/10.1038/s41558-020-00933-3.

Webster, P. J., and S. Yang, 1992: Monsoon and ENSO: Selectively interactive systems. *Quart. J. Roy. Meteor. Soc.*, **118**, 877–926, https://doi.org/10.1002/qj.49711850705.

Wilcox, L. J., E. J. Highwood, and N. J. Dunstone, 2013: The influence of anthropogenic aerosol on multi-decadal variations of historical global climate. *Environ. Res. Lett.*, **8**, 024033, https://doi.org/10.1088/1748-9326/8/2/024033.

Zhou, T., and Coauthors, 2016: GMMIP (v1.0) contribution to CMIP6: Global monsoons model inter-comparison project. *Geosci. Model Dev.*, **9**, 3589–3604, https://doi.org/10.5194/gmd-9-3589-2016.

3.3 To go further: the case of the historical response of the Sahel

In this section, we will apply the methodology used earlier for the Indian monsoon to the case of the Sahelian monsoon in order to assess possible links between the inter-model spread of its response to anthropogenic forcing over the historical period and the temperature and rainfall biases elsewhere. A small technical accident that occurred in the summer of 2022 will nevertheless modify the models we will use this time. Indeed, the servers hosting the data used in the first article burnt down, so the same models as those used in Chapter 4 are used here instead of those used in Section 3.1 for ISM. This new set includes 32 models, 26 of which are common to those used in the original study (see Table.2.1 in Chapter 2). The change is therefore minimal but no secrets between us!

3.3.1 Sahel rainfall trend over the historical period

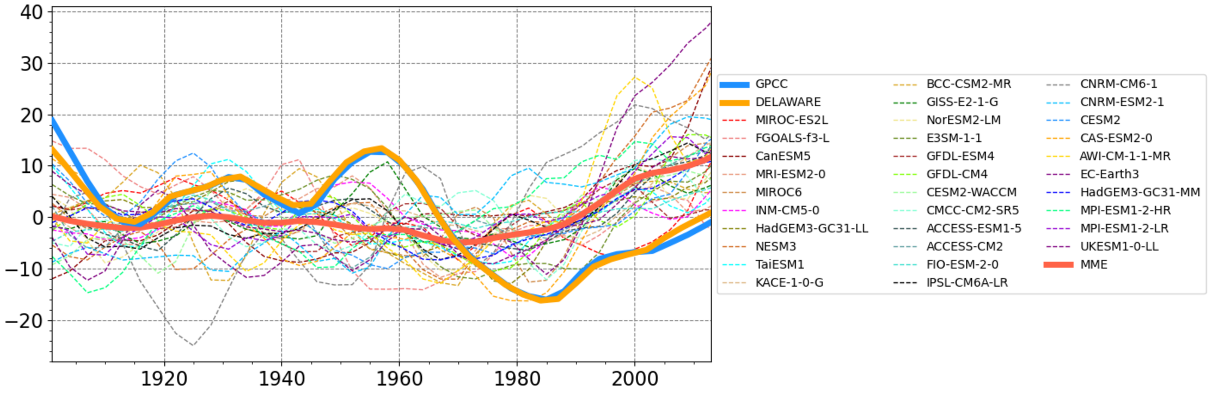

Figure 3.1: This figure is equivalent to Fig.1a of the article, but for the simulated and observed Sahel precipitation trends. Low-pass-filtered (with LOESS) Sahel precipitation time series are represented as normalized anomalies and expressed in percent of the respective mean over 1901–2013 for each time series. The thin lines represent the first historical member of each of the 32 models available, while bold lines represent the MMM of these 32 first historical members (red), the observed GPCC (blue) and DELAWARE (orange).

We use two observed precipitation datasets, namely GPCC and DELAWARE, which provide station-based rainfall observations over the Sahel from the beginning of 20th century to the present. GPCC and DELAWARE mainly fluctuate between -15% and 15% except at the very beginning of the period where GPCC and DELAWARE has a maximum (Figure.3.1). These two sets of observations agree remarkably well over the whole period, both in terms of the temporality of the trends, which is confirmed by their strong correlation (p-value=0.99), and in terms of amplitude with variations of the same order of magnitude. The drying trend from the 1960s to the 1980s (Dai et al., 2004;Greene et al., 2009)is clearly visible here, with a drop in precipitation of around 30% over the period. From the 1980s onwards, there is a partial revival of monsoonal rainfall in the Sahel with a strong positive trend to the present day (Lebel and Ali, 2009) on which GPCC and DELAWARE agree very well. Thus, while the low-frequency fluctuations of Sahel rainfall are quite different from those of ISM in the first part of the observed record, both systems experience increased monsoon rainfall during the recent decades.

As will be discussed again in Chapter 4, the 1960-1980 drought includes probably both a human-induced component and one related to internal variability. During this period, the anthropogenic component is thought to consist mainly of land-atmosphere feedback (J. G. Charney, 1975;Kucharski et al., 2013) and aerosols (Dong and Sutton, 2015;Giannini and Kaplan, 2019), while teleconnections driven by the Atlantic ocean decadal mode of internal variability (e.g., AMV, see Chapter 1) may also play a role (Martin and Thorncroft, 2014). Their respective magnitude is still hotly debated (Janicot et al., 2015), as well as the "real" internal character of the AMV (e.g., Qin et al., 2020). As for the partial recovery of precipitation, it could be linked to the reduced effect of aerosols in connection with environmental policies in the 1980s (Seth et al., 2019) and to the concomitant increasing influence of GHGs which could globally favor Sahelian monsoon precipitation despite conflicting effects as for the ISM (Chou and Neelin, 2004;Biasutti, 2013.

The thick orange line in Figure.3.1 represents the MMM which fluctuates between -5% and 12%. The sharp fall in rainfall from the 1960s to the 1980s does not seem to be reproduced by the MMM, especially in terms of amplitude, although Ndiaye et al., 2022 show a significant correlation over the same period between MMM and observations. The lowest value is -5% compared to -15% in the observations, and this minimum is reached around 1970 whereas in the observations this is the time when the drying trend is strongest and the minimum occurs only after 1980. This result is consistent with the partial attribution of the drought to internal variability, which is largely attenuated in the MMM (Martin and Thorncroft, 2014). On the other hand, the monsoon renewal trend is very well reproduced by the MMM with an increase of 13% over the period 1980-2013, which is also found in the GPCC and DELAWARE observations. This indicates that this trend seems to be linked to anthropogenic forcing, notably GHGs, as this trend of increasing Sahelian precipitation is prolonged in the projections (see Chapter 4 and also Z. Chen et al., 2020).

Concerning the first members of each of our 32 models, we note that they have a variability, at least for some of them, fairly close in amplitude to that of the observations up to the 1980s, although not reaching the highest values, oscillating between -10% and +10%. Nevertheless, the inter-model spread increases sharply after the 1980s, with values ranging from -2% to +38% at the end of the period. Based on the results of the previous paper focusing on ISM and also investigations reported in Chapter 4 on the relative roles of internal variability and anthropogenic forcing in the inter-model spread of Sahel rainfall projections, we assume that the 35-year averaging used to define the historical change, strongly attenuates the internal variability and that the inter-model spread over the period is mainly related to a variable response of the models to the external forcings, although we only use one member for each model.

Since the historical changes and biases of global temperature and precipitation have been already presented and discussed in the published article (see especially Figure 4 and Figure 5 in Section 2 of Chapter 3) and assuming that the small changes in the sets of models do not disrupt them, we now go straight to the results of the MCAs exploring the links between the Sahel rainfall change and the temperatures and rainfall biases across the models. As a reminder, by using MCAs, we want to answer the following question: is there a link between local or remote climatological biases (during boreal summer) in the models and the way they simulate the historical rainfall response in the Sahel?

3.3.2 Local and remote impacts of temperature and precipitation biases on Sahel rainfall historical changes

MCAs are performed over a slightly larger area ([20W;20E],[3N;20N], land only) than the canonical Sahel domain ([20W;20E],[10N;20N], land only) in order to better capture meridional shifts movements of the precipitation band and the ITCZ position.

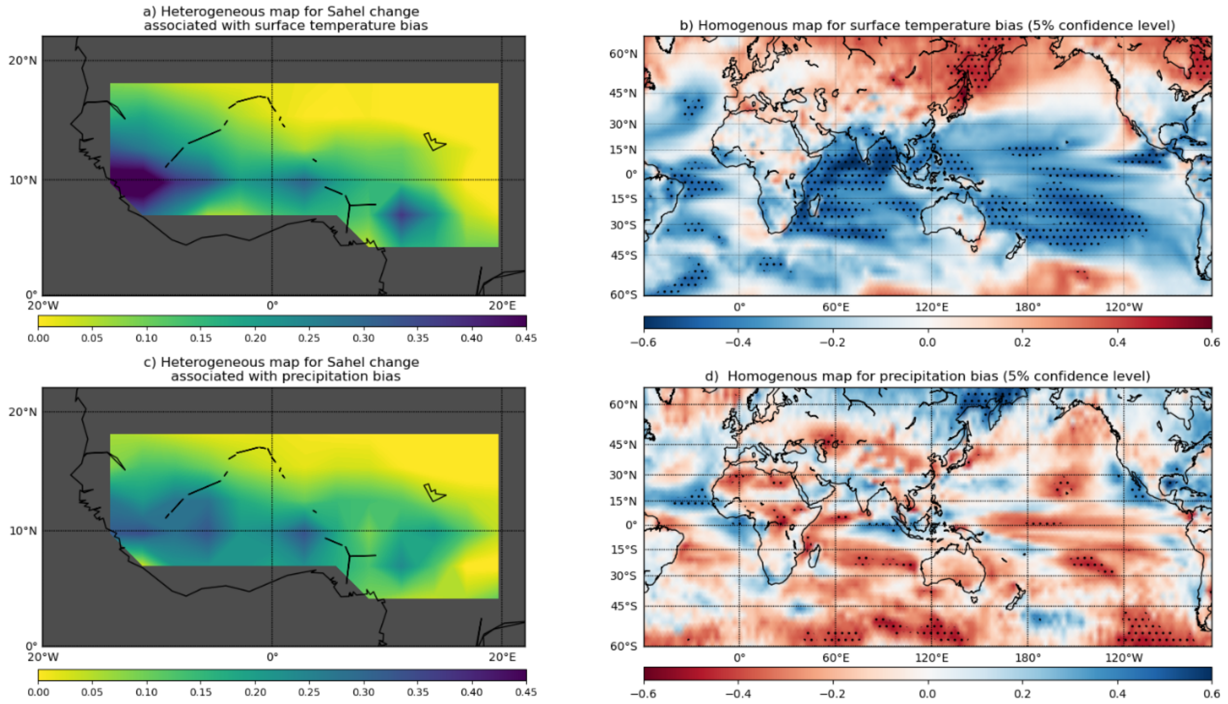

Figure 3.2: (a) Heterogeneous and (b) homogeneous maps obtained from the MCA performed between the Sahel precipitation changes detected over the historical period and the surface temperature bias during boreal summer. (c),(d) As in (a) and (b), but for the MCA computed between the Sahel precipitation change and the precipitation bias during boreal summer. Dotted points indicate significant point-wise correlations at the 95% confidence level between the respective SV and gridpoint time series.

The heterogeneous rainfall maps of the Sahel rainfall change (Figure.3.2ac) show a predominantly meridional modulation of rainfall, with an intensification of rainfall in the southern Sahel and little change in the north. However, this modulation is more pronounced in the western part of the domain than in the eastern part, particularly when the MCA is computed with surface temperature biases (Figure.3.2a). The statistics for the MCAs are presented in Table.3.1. They show values of the same order of magnitude to those found in the case of India's historical change, except that the explained variance of the Sahel change is a bit lower here (33% compared to 39% previously). The change in precipitation over the Sahel from the MCAs is also very close to the first mode of the EOF for this same field, with r=0.97, and very similar explained variances (33% for the MCA, 35% for the EOF). This suggests that the precipitation and temperature bias patterns identified through the MCA are related to the main inter-model spread mode of historical precipitation change in the Sahel.

These MCA modes have a SCF of 41% and 40% with surface temperature and precipitation biases, respectively, and they have similar NC statistics (Table.3.1). This suggests that the precipitation and surface temperature biases have a statistical relationship with Sahel rainfall change of similar strength . Moreover, the correlations between the SV series corresponding to the leading patterns of precipitation and temperature biases and those of rainfall changes in each MCA are quite similar too (0.74 and 0.67; see Table.3.1), which corroborates that a similar strong relationship exists between biases and Sahel rainfall changes. These results are in agreement with the fact that bias modes from the MCAs are strongly related (r=0.69, p-value<0.01).

Table 3.1: Statistics of the MCA between precipitation bias and Sahel historical precipitation change (Figure.3.2). Correlation is between the SV of Sahel rainfall change and the SV of the associated bias.

	Explained variance of Sahel rainfall change	SCF(%)	NC(%)	Correlation
Pr bias; Sahel rainfall change	32%	40%	13%	0.67
Ts bias; Sahel rainfall change	33%	41%	13%	0.74

On a regional scale, models having a wet bias off the coast of Senegal and over the gulf of Guinea show a general increase of Sahel rainfall over the historical period (Figure.3.2d). Interestingly, from the perspective of the MCA modes displayed in Figure.3.2ac, these wet biases are not directly related to local SST biases, but to cold biases in the western tropical Atlantic. On a more tropical scale, the precipitation bias mode (Figure.3.2d) seems to be linked with an intensification of the Walker circulation in the Indo-Pacific regions, with a pattern of excessive precipitation over the maritime continent framed by dry biases over the western Indian Ocean and the Pacific Ocean. Note, however, that the rainfall patterns shown in Figure.3.2d are only weakly significant over the equatorial Pacific and Indian oceans. Finally, on the global scale, The temperature bias pattern (Figure.3.2b) shows a more significant large-scale structure than its precipitation counterpart, with a broad SST cold bias covering the whole Tropics. This cold bias is particularly pronounced over the western Indian Ocean from 40°S to 15°N. We also note that at high northern latitudes, a warm bias also emerges. This suggests that the inter-model spread of historical response of Sahel rainfall is partly associated with the inter-model spread of the inter-hemispheric temperature gradient during boreal summer across the models and that this relationship is mainly driven by the tropical SST bias in the models. Consistent with this hypothesis, there is a good spatial correspondence between cold SST and dry biases South of the Equator in the MCA modes displayed in Figure.3.2c and Figure.3.2d. However, this link is not seen in the North Hemisphere as the homogeneous map of rainfall bias does not show a northward shift of the ITCZ (Figure.3.2d).

To try to better understand the links between the biases and the responses, we also carried out MCAs between historical precipitation changes in the Sahel and global changes in precipitation and surface temperature. The modes over the Sahel are identical to those found with the biases (Figure.3.2ac, r=0.98), and thus we show only the global change modes in Figure.3.3 We can see that an increase in precipitation over the Sahel over the historical period is well associated with a sharp rise in the inter-hemispheric temperature gradient (Figure.3.3a). This result linking the inter-hemispheric temperature gradient and Sahel precipitation is in line with previous studies (Hwang et al, 2013; Schneider et al, 2014) and also echoes what we will present in Chapter 4 in the context of the projections. From the perspective of precipitation changes (Figure.3.3b), no global pattern seems to emerge. Indeed, while a strong correlation is found in the Sahel region by design, the homogeneous rainfall map is very patchy. Yet, Some significant correlations are found in East Asia and Southeast Pacific. Consequently, the inter-model spread of historical Sahel rainfall change does not appear to be regulated by tropical dynamics as was the case for India.

a) Homogenous map for surface temperature change (5% confidence level)

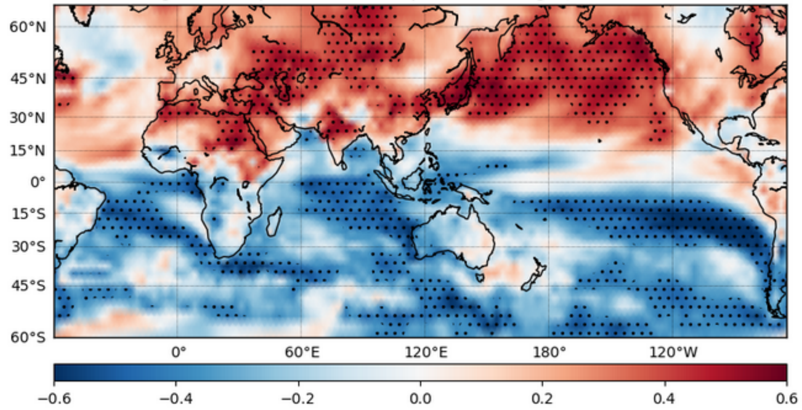

b) Homogenous map for precipitation change (5% confidence level)

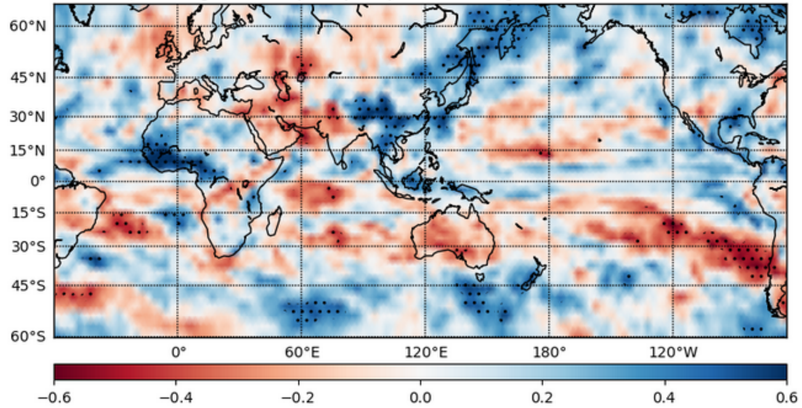

Figure 3.3: (a) homogeneous maps obtained from the MCA performed between the surface temperature change and the Sahel precipitation changes detected over the historical period. (b) same as (a), but for the MCA computed between the global precipitation change and the Sahel precipitation change. Dotted points indicate significant correlations at the 95% confidence level between the respective SV and gridpoint time series.

To summarize, we have identified, on one hand, a global surface temperature response mode reflecting a modulation of the inter-hemispheric temperature gradient across the models and, on the other hand, modes in precipitation and temperature biases also suggesting the role of the inter-hemispheric temperature gradient, all of which are linked to the same mode of precipitation change in the Sahel. As we seek to explain the connections between the identified biases and the historical response of the Sahel, we can question whether there is a link between the identified bias mode and the global temperature change mode. Figure.3.4 shows that there is only a modest relationship between the identified bias mode and the global temperature change, which suggests that the bias mode is not linked to the historical temperature change mode despite both of them being linked to a modulation of the inter-hemispheric temperature gradient at the global scale. In other words, these two modes appear as independent sources of the inter-model spread of the Sahel rainfall response during the historical period.

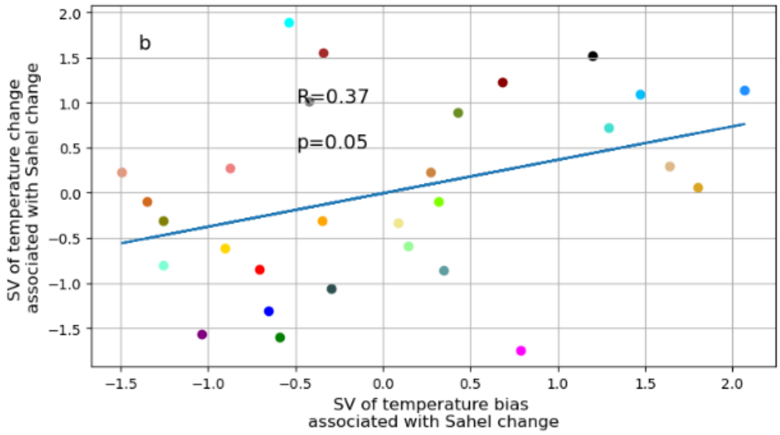

Figure 3.4: Scatterplots of SV of global temperature change with SV of global temperature bias.

To better understand the mechanisms underlying the statistical relationships we have identified, further diagnostics would be necessary, such as analyzing cloud cover or radiative balance variables. However, this goes beyond the scope of this supplement (and the available time to complete this manuscript). It is thus left for future studies.

While this section can be frustrating as it raises more questions than it provides answers, it illustrates the difficulty in establishing links between model biases and historical responses, in this case, regarding the Sahelian monsoon. However, this issue is quite general in nature. It also highlights the fact that monsoons are highly distinct systems that do not necessarily exhibit similar behavior, challenging the notion of a global monsoon. Despite not being able to reach definitive conclusions regarding the biases, we have highlighted that the inter-model spread of the Sahel’s historical response is strongly linked to how models simulate the response of the inter-hemispheric gradient. Spoiler alert: this will also apply to projections and appears to be a consistent feature over time.

Inter-model Spread of Future Indian and Sahelian Monsoon Rainfall in CMIP6

4

The aim of this chapter is to study the inter-model spread that affects the projections of the Indian and Sahelian monsoons under the assumption of the strongest emissions scenario (SSP5-8.5), which results in the strongest anthropogenic responses. In particular, we seek to understand the mechanisms underlying the varied responses of the two monsoons across the models. The results obtained on the Sahel monsoon have been the topic of an under-review article in Journal of Climate in 2023 (see section 4.2) and are summarized below. The focus on the Indian monsoon is detailed in section 4.3.

4.1 Sources of uncertainty in Sahelian rainfall projections under global warming in CMIP6: objectives and summary

This chapter is based on a large set of 32 coupled models from the CMIP6 exercise, comprising between 1 and 50 members each (see Annex 2). First, we show that precipitation change in the Sahel at the end of the 21st century (i.e. 2064-2099) is highly uncertain in CMIP6 in agreement with previous studies (Monerie et al., 2017;Z. Zhang and Li, 2022), with one-third of models showing a decrease in precipitation and two-thirds an intensification. For the Multi-Model Mean (MMM), our results are also in line with previous studies, as we find a dipolar response over the Sahel, with a decrease in precipitation over the western Sahel and an increase over the central Sahel (Monerie et al., 2017;Almazroui et al., 2020). On a more global scale, the MMM response shows a dipolar response of precipitation along the Equator in the Indo-Pacific zone, with a decrease in precipitation over the eastern Indian Ocean and an increase over the central to eastern Pacific. This dipolar response is in agreement with the El Niño-like response in SST over the Pacific Ocean. However, both the precipitation and SST response over the Indo-Pacific present strong uncertainties across the models. From the point of view of temperature changes, the continents show a very strong inter-model spread, notably over the Sahara and Eurasia, which have both been pointed out as drivers of change in the Sahelian monsoon (Park et al., 2015;Z. Zhang and Li, 2022). But the area with the greatest uncertainty is the northern Atlantic Ocean, which has also been suggested to be an inter-model spread generator for Sahelian precipitation response (Z. Zhang and Li, 2022).

After providing an overview of the MMM changes and associated uncertainties, we use MCAs with global precipitation and temperature changes to identify the sources of inter-model spread in Sahel rainfall change at a global scale. In order to ensure that the extracted MCA modes are mainly linked to the different models' responses to anthropogenic forcings rather than internal variability, we perform two sets of twin MCAs: the first considering only one member for each model, and the second in which we average all available members for each model before computing the covariance matrix between the two fields as was done in Chapter 3. The fact that almost identical modes are obtained from these two approaches allows us to demonstrate that (i) the long-term averaging (2064-2099) used to define changes effectively dampens internal variability (a feature already observed in Chapter 3), and (ii) the inter-model spread is indeed mostly attributable to forced response. For the remainder, to simplify calculations, especially those with wind and geopotential at different levels, we will only use one member per model based on these preliminary investigations. Furthermore, we note that the analysis is performed on a more extended region than the strict canonical definition of the Sahel region. The extended region may rather be called the west african region. This extended region was indeed defined so as to better capture the meridional shifts of the maximum summer rainfall. Given the results which indeed primarily highlight meridional shifts within the Sahel region, and the seasonal analysis performed only over the season of the Sahel monsoon, we will use the term Sahel monsoon and Sahel region in all this chapter to name the changes in summer rainfall identified over the western Africa.

The MCAs show that changes in tropical precipitation and global surface temperature patterns modulate zonally the Sahel rainfall change. The strong correlation between the two MCAs suggests that coupled ocean-atmosphere and land-atmosphere changes are responsible for the Sahelian change's uncertainty. In order to compare our results with previous studies, we focus on the impact of temperature changes and identify two major sources of uncertainty: the inter-hemispheric gradient and the equatorial Pacific mean-state during boreal summer. These two factors are strongly correlated with Sahel rainfall change, but not significantly correlated with each other, allowing us to consider them as independent in a first approximation.

The next step is to address the following question: what are the physical processes that connect these sources of uncertainty in the models' response to Sahelian rainfall change?

Case of the inter-hemispheric gradient change

The more pronounced the inter-hemispheric temperature gradient (e.g., with a positive anomaly in the North and a negative anomaly in the South), the further north the ITCZ shifts and the greater the precipitation in the Sahel, in accordance with the energy framework (Schneider et al., 2014). Additionally, as the ITCZ moves northward and the inter-hemispheric SLP gradient is enhanced, the West African Westerly Jet (WAWJ; Pu and Cook, 2010), a surface jet at 15°N off the African coast, becomes stronger. Since this jet brings moisture to the Sahel, the stronger it is, the greater the monsoon precipitation tends to be.

Case of the equatorial Pacific change

The change in the mean-state of the equatorial Pacific has two main impacts. Firstly, it affects the large-scale zonal circulations in the Tropics (Trenberth et al., 1998). Models that exhibit a La Niña-like anomalous sea surface temperature (SST) change show a stronger westward shift of the Walker circulation compared to the MMM, which has an El Niño-like pattern as noted above. This favors anomalous upper-tropospheric divergence over the Sahel and promotes local convection. The situation is reversed for El Niño-like models. Secondly, SST changes in the equatorial Indo-Pacific region modulate the intensity and position of tropospheric warming by influencing the positions of latent heat release sources. This, in turn, generates tropical Kelvin and extratropical Rossby waves that modify the meridional mid-tropospheric temperature gradient around the Sahel. Consequently, there are changes in the upper-level zonal circulation over the Sahel, particularly in the intensity of the Tropical Easterly Jet (TEJ). The strength of the TEJ then influences upper-level divergence and vertical zonal wind shear, thereby impacting convection in the region (Nicholson, 2009).

Lastly, after identifying these two sources of uncertainty, the final step is to quantify their respective contributions to the inter-model spread of Sahelian precipitation changes. While we initially considered these sources to be independent in a first approximation based on statistical considerations, we ultimately demonstrate that their interactions account for 12% of the uncertainty in Sahel precipitation change. Using attribution methods and a bilinear regression model, we allocate this portion to each of our indices and ultimately show that among the 62% of inter-model spread in Sahel precipitation change that we are able to explain, 40% are explained by the inter-hemispheric gradient change and 22% are explained by the equatorial Pacific change.

4.2 Article *in extenso*, under review in Journal of Climate

Additional material for this article can be found in the second section of the appendix!

Sources of uncertainty in Sahel rainfall projections under global warming in CMIP6

Marcellin Guilbert[a], Pascal Terray[a], Juliette Mignot[a], Luther Ollier[a], Guillaume Gastineau[a]

[a] *Laboratoire d'Océanographie et du Climat: Expérimentations et Approches Numériques, Institut Pierre-Simon Laplace, Sorbonne Université/CNRS/IRD/MNHN, Paris, France*

Corresponding author: Marcellin Guilbert, marcellin.guilbert@locean.ipsl.fr

ABSTRACT

The Sahel is one of the most vulnerable regions to climate change. Robust estimation of future changes in the Sahel monsoon is therefore essential for effective climate change adaptation. Unfortunately, state-of-the-art climate models show large uncertainties in their projections of Sahel rainfall, even concerning the sign of changes toward the end of the 21st century. In this study, we use 32 models from CMIP6 to identify the sources of this large inter-model spread of Sahel rainfall. By using Maximum Covariance Analysis, we first highlight two key drivers of this spread during boreal summer: the inter-hemispheric temperature gradient and equatorial Pacific Sea Surface Temperature (SST) changes. Next, we unravel the physical mechanisms behind their statistical relationships with Sahel rainfall changes, which bear strong similarities with those operating at decadal and interannual timescales. Firstly, the modulation of the inter-hemispheric temperature gradient across the models leads to varying latitudinal positions of the ITCZ and, consequently, varying Sahel rainfall intensity. The greater the gradient, the more pronounced the northward shift of the ITCZ, resulting in a spatially homogeneous increase in precipitation over the Sahel. Secondly, models that exhibit less warming than others in the equatorial Pacific, thereby projecting a more "La Niña-like" mean state, simulate enhanced precipitation over the central Sahel in the future through a shift in the Walker circulation and a modulation of the Tropical Easterly Jet (TEJ) via the propagation of Rossby and Kelvin waves. The situation is reversed for models exhibiting an enhanced El-Niño-like SST change. Finally, we show that these two physically based indices collectively explain 62% of Sahel rainfall change uncertainty: 40% due to the inter-hemispheric temperature gradient and 22% through equatorial Pacific SST.

KEYWORDS : MONSOON, CLIMATE CHANGE, TELECONNECTIONS, MODEL UNCERTAINTY

1. Introduction

The Sahel experiences a rainy season from June to September (JJAS) associated with the northward migration of the InterTropical Convergence Zone (ITCZ) (Nicholson 2013), while the rest of the year is practically entirely dry. The Sahel monsoon is characterized by a complex vertical structure of the atmospheric circulation (Shekhar and Boos 2017; Akinsanola and Zhou 2019). In the lower troposphere, southwesterly winds bring moisture from the tropical Atlantic (Sultan and Janicot 2003), while, in the middle (500 hPa) and upper troposphere (200 hPa), the circulation is dominated, respectively, by the African Easterly Jet (AEJ) and the Tropical Easterly Jet (Nicholson 2009). The Sahel monsoon provides most of the water resources for predominantly rainfed agriculture, which is the main source of income for the region (Sultan and Gaetani 2016). Coupled with the exponential growth of the population and the ongoing desertification process (Wei et al. 2017), Sahel is one of the most vulnerable places to climate change in the world (Sylla et al. 2016).

The long-lasting Sahel drought in the 1970s and 1980s has offered a glimpse of the potential climate impacts of human activities on this region. Indeed, many studies have established the existence of a human-induced component in the drought, mainly related to land surface atmosphere feedbacks (Charney et al. 1975; Kucharski et al. 2013) and anthropogenic aerosols (Dong and Sutton 2015; Giannini and Kaplan 2019; Ndiaye et al. 2022). The latter have an impact on Sahel rainfall through the anomalous inter-hemispheric radiative imbalance they induce (Hwang et al. 2013; Schneider et al. 2014) and via their effects on anomalous Sea Surface Temperature (SST) patterns, especially in the Atlantic ocean (Giannini and Kaplan 2019; Hirasawa et al. 2020). However, as the internal component of the Atlantic Multidecadal Oscillation can lead to similar anomalous SST patterns (Martin and Thorncroft 2014) and a partial recovery of the the West African Monsoon (WAM) has been observed since the early 2000s (Lebel and Ali 2009), the magnitude of the human-induced component of the 1980s drought is still hotly debated (Janicot et al. 2015). At the same time, the reduction in aerosols emissions around the North Atlantic that resulted from environmental legislation during the 1980s (Seth et al. 2019; Biasutti 2019), combined to their short atmospheric lifetime, may also have reversed the anomalous inter-hemispheric radiative imbalance (Giannini and Kaplan 2019) and thereby played a role in the recent recovery. While most studies focus on the Atlantic, Park et al. (2016) suggest that rising SSTs in the Mediterranean may also be a driver in the Sahel monsoon recovery.

Finally, Greenhouse gases (GHGs) emissions could have also contributed to the observed modulations, yet with two opposing effects (Chou and Neelin 2004; Marvel et al. 2020; Monerie et al. 2022). On the one hand, by increasing the specific humidity according to the Clausius-Clapeyron relationship and by strengthening the Saharan shallow meridional circulation associated with a warmer Sahara and a stronger Sahara Heat Low (Cook and Vizy 2015; Wei et al. 2017; Terray et al. 2018), GHG forcing could increase local precipitation by promoting moisture convergence (Sooraj et al. 2019) and shifting the rainbelt northward in a warming climate (Byrne et al. 2018). On the other hand, the stabilization of the tropical troposphere and the dry air intrusions from the Sahara linked to GHGs could make convection more difficult in this transition zone (Chou and Neelin 2004; Biasutti 2013; Hill 2019). Thus, GHGs forcing promotes several contradictory effects, primarily in terms of dynamical response, but also through interactions between the dynamic and thermodynamic responses (Chen et al. 2020).

In a nutshell, the historical period illustrates that there are many factors potentially influencing the Sahel rainfall, each with different and sometimes contradictory effects, ranging from regional to global scales. This complexity might be partly reflected in the substantial disagreement between coupled model projections, persisting from Coupled Model Intercomparison Project (CMIP) 3 to CMIP6, with an inter-model spread larger than the mean multi-model change, and some CMIP models projecting a drying and others a wettening of the Sahel (Monerie et al. 2017b; Zhang and Li 2022). As the forcing at the end of the 21st century is dominated by GHGs, the large inter-model spread probably comes mainly from the opposing GHG effects described above (Biasutti 2019). More specifically, a recent study had suggested that the main source of inter-model spread in the projections does not seem to come from the thermodynamic response, but rather from the dynamic one, for which climate models have difficulty in reaching a robust agreement (Kent et al. 2015; Monerie et al. 2020b; Zhang and Li 2022). This dynamical disagreement among models' projections has been mainly linked to teleconnections arising from anomalous SSTs in various oceanic basins, but also to the persistent difficulties of CMIP coupled models to capture realistically the main processes driving the WAM (Roehrig et al. 2013). Park et al. (2015) and Monerie et al. (2020b) suggested that the spread in the relative warming between the Northern Hemisphere and the Tropics modulates the strength of the Sahara Heat Low (SHL) and the low-level monsoon circulation. Some studies specifically highlight the role of individual oceanic basins. Regarding the Atlantic Ocean, it is suggested that differential warming between the tropical and North Atlantic regions is a key player (Zhang and Li 2022). Beyond its role in the revival of the Sahel monsoon in the recent decades, Park et al. (2016) also identified Mediterranean warming as a key factor in shaping the future of the Sahel monsoon. Finally, a link between model biases in various regions of the world over the current period and the inter-model spread of the future Sahel monsoon has also been put forward by several studies (Roehrig et al. 2013; Yan et al. 2019). As an illustration, Yan et al. (2019) indicate a strong relationship between the uncertainties of future Sahel monsoon rainfall and the inter-model spread of summer precipitation biases in South Asia and the North-West Pacific (NWP), suggesting that this relationship stem from the diversity of deep convection parameterizations used by the models.

In this study, we use Maximum Covariance Analysis (MCA) to objectively analyse the relationships between the projected Sahel rainfall and projected global surface temperatures and rainfall (including both land and ocean) across CMIP6 models. The underlying questions are : 1) Can we revisit the factors explaining the projected Sahel rainfall uncertainties from an objective analysis of the projected changes at the ocean-atmosphere-land surface ? 2) By what physical processes are these factors related to Sahel rainfall? 3) How much uncertainty can they explain? Section 2 describes models and analysis methods used in this study. Section 3 provides a systematic evaluation of the statistical relationship between the inter-model spread of Sahel rainfall and global surface temperature and rainfall changes by the end of the 21st century in the CMIP6 models. Section 4 examines the physical processes linking the influencing large-scale drivers and regions found in Section 3 to Sahel rainfall, the amount of uncertainty they explain and their respective individual contributions to it. The last section presents a summary and future perspectives.

2. Data and methods

a) *Coupled simulations, validation datasets and climate indices*

This study is based on the high emission Shared Socio-economic Pathways 8.5 (SSP5-8.5) scenario experiments, and uses outputs of 32 CGCMs from CMIP6 (see supplementary Table S1; Eyring et al. 2016). Here, in most of our statistical analyses, we use only one simulation member for each model, but we also checked in a preliminary step that our main results are not sensitive to the multi-members averaging, which imply that the inter-model spread is largely driven by differences in the forced response of the models (see Section 4a). The monthly mean outputs used in our analysis are rainfall (Pr), surface temperature (Ts), near-surface air temperature (Tas), Sea Level Pressure (SLP), horizontal winds (U and V) and geopotential (Zg) at different levels.

Table 1 summarizes the different climate indices and regions used in our analysis. In addition to definitions of the whole Sahel region, or parts of it (Monerie et al. 2021), and the canonical Nino3.4 index, it includes an interhemispheric temperature gradient, a northern hemisphere differential warming and a northern minus tropical Atlantic SST index, all defined in previous studies as important drivers of the Sahel rainfall changes (Park et al. 2015; Monerie et al. 2020a; Zhang and Li 2022). Note also that our inter-hemispheric temperature gradient is defined with respect to the latitude 15°N because our focus is on the boreal summer season (e.g. from June to September). However, our results remain valid if we define this gradient with respect to the Equator instead (not shown). A tropospheric thickness gradient is also introduced and will be used in Section 5b when discussing the influence of the equatorial Pacific on the TEJ.

Regions / Indices	Domain and variable used when relevant
Canonical Sahel	[10N;20N], [20W;20E], land only
Extended Sahel	[3N;20N], [20W;20E], land only
Western Sahel	[10N;20N], [20W;5W], land only
Central Sahel	[10N;20N], [5W;20E], land only
Niño3.4	$< SST >_{[5S;5N],\ [170W,120W]}$
Inter-hemispheric temperature gradient	$< Ts >_{[15N;90N],[0;360]} - < Ts >_{[90S;15N],[0;360]}$
Northern hemisphere differential warming	$< SST >_{[30N;75N],[0;360]} - < SST >_{[20S;20N],[0;360]}$
Northern minus tropical Atlantic SST change	$< SST >_{[45N;65N],[40W;10W]} - < SST >_{[20S;10N],[40W;10W]}$
Thickness gradient around Sahel	$< Zg^{200hPa}\text{-}Zg^{850hPa} >_{[20N;30N],[20W;20E]} - < Zg^{200hPa}\text{-}Zg^{850hPa} >_{[0;10N],[20W;20E]}$

TABLE 1. Definition of the indices used in the present study. < > stands for spatial averaging over the subscript domain. The superscript indicates the surface type or the atmospheric level over which the average is taken, when relevant.

b) Methods

Our analysis will focus on June-September (JJAS) as it is the rainy season for the Sahel. We define the change of a given variable associated with global warming as the difference between the future climatology defined over the period [2064-2099] using SSP5-8.5 experiment and the present simulated climatology computed over the period [1979-2014] using historical experiment. In the following, all changes are normalized by the corresponding global mean surface temperature increase for each model, so that we look at responses for a same level of warming among models. This choice will be discussed in more details and validated in Section 4. All datasets were interpolated onto a common 2.8°x2.8° horizontal resolution by bilinear interpolation prior to the analysis, which is the coarsest spatial resolution among the 32 models. Velocity potential used in Section 5 is calculated at different levels from horizontal winds with the spectral method (Tanaka et al. 2004).

In order to investigate the first order linear relationships between changes seen from climate indices, we use scatter plots and correlation/regression analyses across the various models. P-values of correlations are calculated using Student t-test with 31 degrees of freedom, given the use of 32 GCMs and thus assuming that they are independent. Yet, for a more systematic exploration, we use MCA, which extracts the dominant co-variability patterns from two geophysical datasets (Bretherton et al. 1992; Cherry 1997). We will use quantities such as Squared Covariance Fraction (SCF) and Normalized root-mean-square Covariance (NC), the former being an indicator of the importance of a mode within a MCA, while the latter is a metric that allows to compare the importance of modes from different MCAs. Further details about the MCA and its metrics are given in supplementary Text S1. We compute the significance of the MCA statistics by using a bootstrap resampling MCA scheme with 500 shuffles (e.g., in each shuffle, the rows of one of the matrix fields are randomly permuted before recomputing the covariance matrix and the MCA). The idea is to generate a large number of independent realizations of the covariance matrix under the assumption that the two fields are independent of each other in order to assess the confidence level of the obtained signal as seen by the MCA statistics.

To capture the entire main mode of Sahel precipitation change with the MCA, we use an extended region compared to the canonical Sahel definition, called "extended Sahel" in Table 1. This enables us to better capture the meridional shifts of the ITCZ than over the canonical Sahel region. Note, however, that the first MCA modes obtained by using the canonical or extended boxes are almost identical (r=0.99), illustrating the robustness of the leading MCA patterns with respect to the choice of the Sahel boundaries.

Finally, in Section 5, we use three statistical methods to estimate the relative contributions of the different factors that explain the inter-model spread in rainfall change over the Sahel. First, we use a Permutation Feature Importance (PFI) method (Fisher et al. 2019) to get a measure of how much the accuracy of the regression model depends on the information in each input variable. Technically, all variables are held constant except one for which random permutations are made. The difference in the sum of squared residuals (SSR) between the output of the regression model when using the initial input data versus the randomly permuted variable is evaluated. This is repeated 10,000 times for each variable and the median of the SSR distributions for each variable are compared to obtain the relative contribution of the given input data. Second, we construct a Random Forest model fitting the data. We also use a similarity measure of variable importance (Breiman 2001) to assess the results of our first method. From each constructed tree, we randomly permute one of the input variables and run down the corresponding tree. Then, we compare the resulting output with the correct one to get a mis-regression rate. This is similar to the PFI method, but adapted to the method of random forest. Thirdly and finally, we use a Dominance Analysis (Azen and Budescu 2003), which computes the variable's individual effect as well as its effect in the presence of other variables to identify its relative contribution to the full regression model. For bilinear regression, this corresponds to the average between the individual contribution and the incremental contribution resulting from the interactions with the other factor.

3. Global changes of surface temperature and precipitation over the 21st century

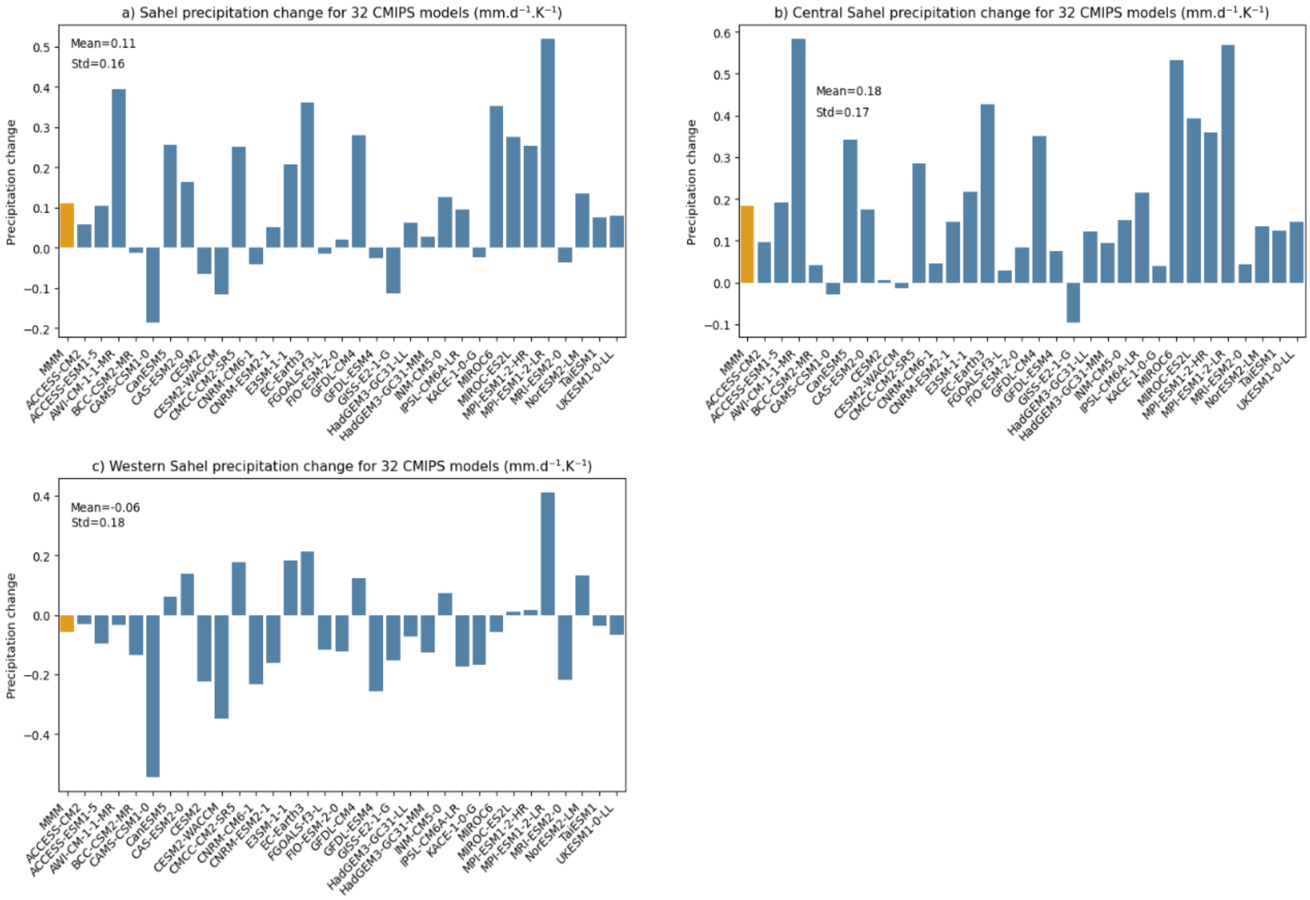

Fig. 1. Rainfall change (JJAS) computed on (a) the Sahel canonical domain, (b) Central Sahel and (c) Western Sahel for 32 CMIP6 models and their Multi-Models Mean (MMM; left orange bar). All the model changes are scaled by the global surface temperature change in each model as explained in Section 2. Units is mm.d^{-1}.K^{-1}. See Table 1 for indices definitions.

In agreement with previous studies (Monerie et al. 2017b; Zhang and Li 2022), Fig.1 illustrates that CMIP6 models show a wide range of responses of the Sahel monsoon to climate change towards the end of the 21st century in the SSP5-8.5 simulations. The multi-model mean (MMM; 0.11 mm.d-^{1}.K-^{1}) results from an increase in precipitation over the central Sahel (MMM;0.18 mm.d-^{1}.K-^{1}) and a reduction over the western Sahel (MMM; -0.06 mm.d-^{1}.K-^{1}), which is consistent with the dipolar pattern as seen in previous CMIP models (Monerie et al. 2017a; Almazroui et al. 2020; Monerie et al. 2021). The intermodel spread is the same for the Western and Central Sahel regions and therefore for the whole region (about 0.17 mm.d^{-1}.K^{-1}; see the statistics in the upper left corner of each panel in Fig.1). It is larger than the MMM especially for Western Sahel. There is a general agreement on the sign of the projected change for central Sahel but with a largely varying amplitude. However, there is no agreement on the sign of the projected change for Western Sahel and Sahel as a whole: one third of the models predict a reduction in precipitation and two thirds an increase. As we seek to establish links between the inter-model spread of Sahel precipitation change and changes elsewhere, we present first an overview of the MMM changes of global surface temperature and precipitation, as well as an outlook of the areas of greatest disagreement between the models regarding the change of these two variables.

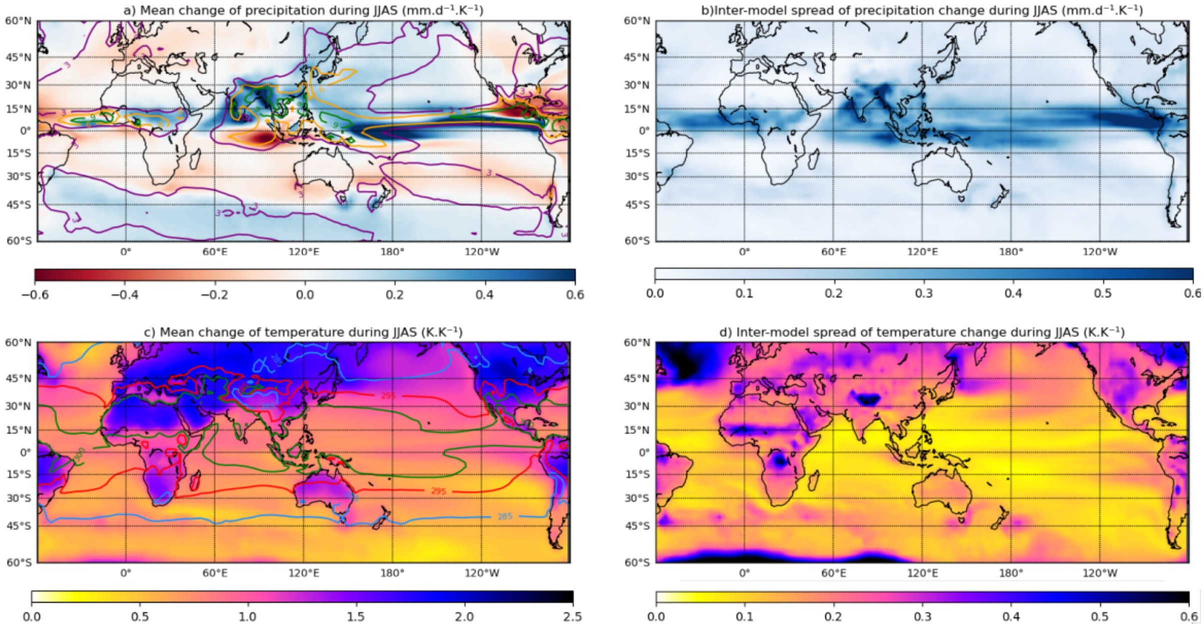

Fig. 2. JJAS MMM and inter-model spread of scaled precipitation (mm.d^{-1}.K^{-1}, top) and surface temperature (K.K^{-1}, bottom) changes computed for the 32 CMIP6 models. (a) MMM precipitation change, (b) inter-model spread of precipitation. (c) and (d) are the same as (a) and (b), respectively, but for surface temperature. Contours in (a) are for JJAS precipitation present day (1979 to 2014) observed climatology (Global Precipitation Climatology Project (GPCP) monthly mean precipitation flux dataset (Adler et al. 2003), contour interval is 3 mm.day^{-1}) and in (c) for JJAS surface temperature present day climatology (ERA-Interim reanalysis (Dee et al. 2011), 285K blue, 295K red, 300K green contours). Temperature and precipitation changes are computed as the difference of climatological means between the end of the century (2064-2099) and the end of the historical period (1979-2014). See Section 2 for details.

Fig.2a displays the JJAS precipitation changes over the 21st century in the SSP5-8.5 scenario, as defined in Section 2. As expected the main changes take place in the Tropics. Over the Sahel, we find a dipolar zonal rainfall pattern as in previous generations of CMIP (Roehrig et al. 2013; Monerie et al. 2013, 2021), with a decrease in rainfall over the western part of the Sahel and an intensification over the rest of the region in agreement with Fig.1. This rainfall zonal gradient over land is in fact part of a larger quadrupole rainfall pattern in the tropical Atlantic-WAM region (Fig.2a). Sahel rainfall presents one of the largest uncertainties in relative precipitation change and large disagreement regarding the sign of the change (Figs.1 and 2b; AR6). This large uncertainty is also a characteristic of the whole quadrupole rainfall pattern described above. The other monsoon regions around the world tend to show an increase of precipitation in the future, except Central America (Fig.2a). There is a large uncertainty about the magnitude of change over all monsoon regions, not only the Sahel, but the relative changes are the highest for the Sahel (Chen et al. 2020).

Overall, Fig.2a shows that the most important changes in precipitation over the ocean occur in the Pacific ITCZ, which shows both a strong intensification and an asymmetric double ITCZ structure. Fig.2a displays also a precipitation zonal dipole around the maritime continent, with an intensification of precipitation in the central and eastern Pacific and a decrease in precipitation in the southeastern Indian Ocean. This feature is consistent with the emergence of an Indian Ocean Dipole (IOD) mean state changes in the SSP5-8.5 scenario of CMIP6 (see Fig.8.6 in Cherchi et al. 2021). This Indo-pacific dipole is also consistent with the evolution towards an El Niño-like mean SST state in the Indo-pacific region in the SSP5-8.5 scenario (Fig.2c; see also Lian et al. 2019; Cherchi et al. 2021). There is also a strong inter-model spread across the Pacific, more pronounced in the eastern part of the basin (Fig.2b), which is also consistent with the large inter-model spread affecting the American monsoon in CMIP5 (Pascale et al. 2017).

In terms of temperature (Fig.2c), it is no surprise that the continents are warming more than the oceans, and also that lands in the Northern Hemisphere are warming more than in the southern one during boreal summer. Over land, the greatest uncertainties are found in the Himalayas, the Sahel and Central Africa (Fig.2d). There are, in particular, large uncertainties over the Sahara and Europe, which have both been pointed out as regions that may influence the Sahel monsoon (Cook and Vizy 2015; Biasutti 2019; Zhang and Li 2022). Uncertainties are less pronounced over the Asian monsoon regions, which is surprising given the uncertainties in precipitation described above, but may be explained by the fact that the temperature changes are mainly controlled by the precipitation changes in this region (Guilbert et al. 2023). Turning now to the SSTs (Fig.2c; supplementary Fig.S1), one of the major robust changes over CMIP generations of models is that the mean state of the Pacific tends to be more El Niño-like, with a more pronounced warming in the east of the basin. The mean state of the Indian Ocean is more positive IOD-like, which is consistent with the strong coupling between the two oceanic basins (Lian et al. 2019; Cherchi et al. 2021). Large uncertainties regarding the amplitude of the eastern Pacific warming persist nonetheless (Fig. 2d), similarly to the historical period (Guilbert et al. 2023). Model uncertainties are largest around the South Pole (supplementary Fig.S1) and in the northern Atlantic subpolar gyre, where inter-model spread maxima are found (Fig.2d). Overall, uncertainty is much stronger for the northern hemisphere and the North Atlantic than for the tropical SSTs.

Given the large inter-model spread of surface temperature and precipitation changes, and the complex teleconnections linking the Sahel rainfall with the rest of the globe (Janicot et al. 2011; Martin et al. 2014; Giannini and Kaplan 2019; Nakanishi et al. 2021), we will track in the following section the main sources of inter-model spread of Sahel rainfall change on a global scale, by using a series of MCA analyses.

4. Sources of Sahel precipitation change uncertainties

a) *Global temperature and precipitation changes associated with Sahel rainfall*

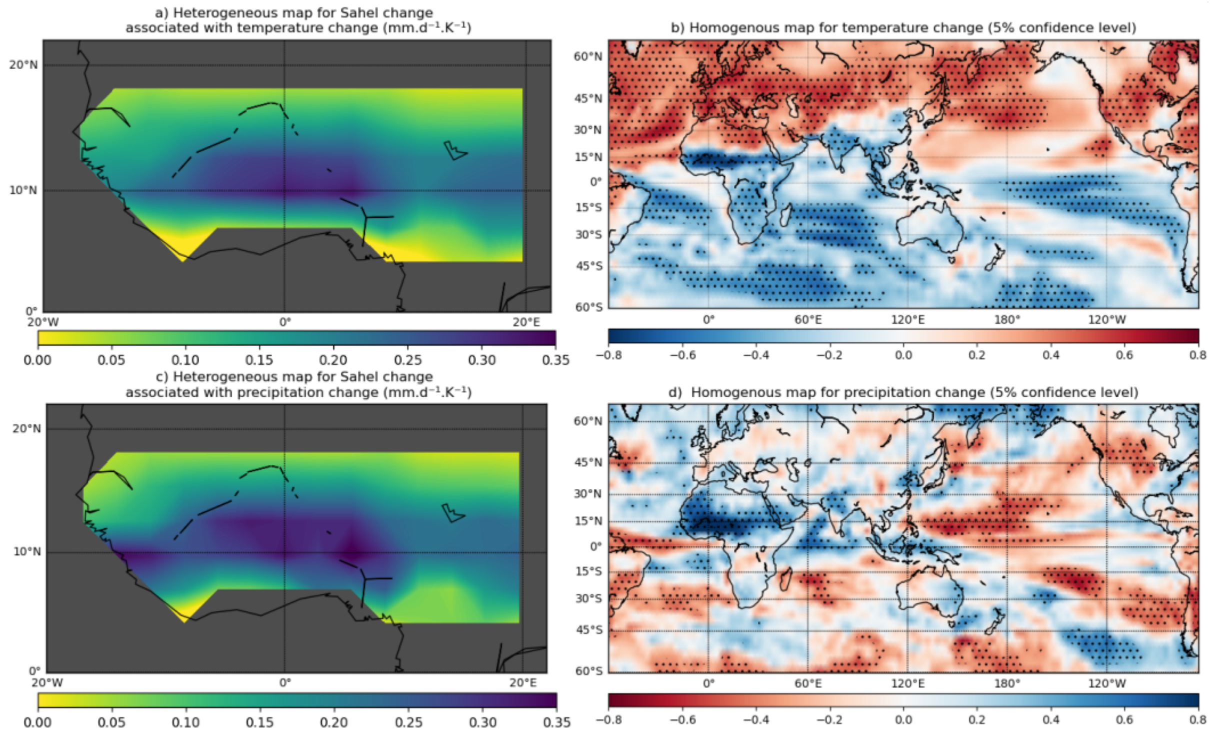

Fig. 3. Heterogeneous (a) and homogeneous (b) maps obtained from the MCA analysis performed between the scaled surface temperature change (K.K^{-1}) of the 32 climate models and the scaled Sahel precipitation changes (mm.d^{-1}.K^{-1}) in the same 32 models. (c) and (d): same as (a) and (b) for the MCA between the precipitation change (mm.d^{-1}.K^{-1}) and the Sahel precipitation change (mm.d^{-1}.K^{-1}). Precipitation and temperature fields are scaled by global temperature change (see text and Section 2 for details). Dotted points indicate pointwise correlations significant at the 95% confidence level between the respective Singular Variable (SV) and grid-point model series using a Student test and 31 degrees of freedom (Section 2). See Text.S1 in the supplemental material for a short introduction to MCA.

We compute two MCAs, one between changes in precipitation over the extended Sahel region and changes in global surface temperature (Figs.3a,b), and the other onebetween changes in precipitation over the extended Sahel and global precipitation changes (Figs. 3c,d). First, in a preliminary analysis, to assess the influence of internal variability on our MCA results, we recompute the two MCAs by considering all members available for each model and averaging them before computing the covariance matrix (see Fig.S3). The extreme similarity between Fig.3 and Fig.S3 shows that internal variability does not play an important role, as damping it by considering multi-member averages in the MCAs has no notable impact on the relationships highlighted by the MCAs. This shows that the inter-model spread of Sahel rainfall change as computed from the difference between two 35-year periods is mainly dominated by uncertainty in the models' response to external forcing, not internal variability, in agreement with (Monerie et al. 2021).

Second, in order to assess the possible influence of the climate sensitivity of the models on the MCA results, we also performed the MCAs both with and without global temperature scaling (see Fig.S4). The precipitation change MCA patterns over the Sahel or globally are again robust (Fig.3.a,b,c and Fig.S4.a,b,c), as they remain unchanged whether the temperature scaling is applied or not. However, as global warming is a very strong signal and is an important amplifying factor of the inter-model surface temperature spread (compare Fig.2 and Fig.S2), it influences the first temperature MCA pattern (Fig.3b and Fig.S4.b) even though it has no impact on the corresponding rainfall change in the Sahel, as we have just discussed (Figs.3a,c and Figs.S4a,c). This phenomenon is also well illustrated by the strong and significant relationship between the global warming series across the models and the unscaled temperature change SV ($r=0.90$), while the unscaled Sahel rainfall change SV shows no significant relationship with this global temperature series ($r=0.20$, P-value>0.20). Thus, given that the climate sensitivity of each of the models can artificially blur the signal of interest for the Sahel, we have chosen to work with scaled quantities, as also done in many previous studies (Kent et al. 2015; Li et al. 2017; Zhang and Li 2022). This allows to eliminate the effect of the large spread of ECS in CMIP6 models (e.g. Meehl et al. 2020; Zelinka et al. 2020) as an additional source of inter-model difference. This amounts to an analysis of climate responses between models for the same level of warming.

We study only the leading mode for each of these MCAs, as they describe most of the covariability between the original fields (Table 2) and they explain much more inter-model spread of Sahel rainfall change than the second MCA mode (51% against 17%). The Square Covariance Fraction (SCF) and Normalized root-mean-square Covariance (NC) statistics characterizing the strength of the coupling in the MCA (see Text. S1 for a more detailed definition of these MCA statistics) are strong (see Table 2) and significant at the 1% level for the leading modes, which again corroborates the reliability of these modes.

The associated heterogeneous maps (see Text. S1) of rainfall changes over extended Sahel are similar in both computations (Figs.3a,c). The spatial loadings are fairly homogeneous and positive, but with weaker values at the edges of the domain. Consistently, the correlations between the Singular Variable series (SV; e.g. expansion coefficient series from the MCA) associated with the rainfall change patterns over the extended Sahel (Fig.3a and Fig.3c respectively), and precipitation averaged over the canonical Sahel are respectively 0.99 and 0.94.

Finally, the rainfall changes patterns from the MCAs (Figs.3a,c) are also very close to the first Empirical Orthogonal Function (EOF) mode of Sahel rainfall change (not shown): the leading modes from EOF and MCA are correlated with r=0.99 and the variance explained by these modes are again very close (51% for the first mode of EOF and 50% for both MCAs) despite that the MCA is designed to maximize the covariance between the two fields rather than the explained variances of the fields.

These results further motivate a detailed analysis of the covariability of these modes of inter-model spread of Sahel rainfall change with local and remote factors. The correlations between the SV series of the main modes of precipitation and temperature changes (Fig.3b and Fig.3d) and those of the Sahel precipitation change (Fig. 3a and Fig. 3c) highlight strong and similar statistical relationships within the two pairs of fields (0.89 and 0.80 respectively; see Table 2). This suggests first that projected precipitation and surface temperature inter-model spreads have relationships of rather equivalent strength with the inter-model spread of Sahel rainfall change and, second, the existence of regional or global ocean-atmosphere and/or land-atmosphere couplings that modulate the Sahel rainfall projections across the models. Consistently, there is a significant linear relationship between the main precipitation and temperature change patterns (Fig.3b and Fig.3d) associated with Sahel precipitation changes (r=0.70).

Fig.3b shows that associated with an intensification of Sahel rainfall, there is a strong global contrast between the northern and southern hemispheres with an anomalous warming north of 15°N and an anomalous cooling south of 15°N during boreal summer. This inter-hemispheric temperature gradient is superimposed on the global (uniform) warming simulated by all models, not shown here as it has been eliminated by the temperature scaling. In a global energetic framework of the ITCZ (Schneider et al. 2014; Byrne et al. 2018; Biasutti et al. 2018), such inter-hemispheric temperature gradient is associated with an inter-hemispheric radiative imbalance and a migration of the Hadley cell system and the associated ITCZ towards the warmer hemisphere. The lower branch of the Hadley circulation indeed transports moisture towards the warmer hemisphere, which is materialized by the migration of the ITCZ. It allows energy to be transported towards the cooler hemisphere along its reinforced upper branch to compensate for the energy imbalance. Fig.S5 corroborates the involvement of the lower branch of the Hadley cell by showing a well defined strengthening of subtropical highs and trade winds in all oceanic basins of the Southern Hemisphere. Note that the inter-hemispheric temperature and SLP gradients and the associated inter-hemispheric low-level atmospheric flow are particularly well defined in the Atlantic sector as expected. Moreover, the associated strengthening of the Southern Hemisphere trade winds is consistent with the significant cooling observed at the margins of subtropical highs in the Southern hemisphere in all three oceanic basins (Fig.3b).

In addition to this large-scale inter-hemispheric signature, there is an anomalous equatorial cooling over the eastern and central Pacific (Fig.3b) that modulates significantly the El-Niño like signal found in the MMM (Fig.2c, see also Lian et al. 2019, Fredriksen et al. 2020). This suggests that models with a more La Niña-like temperature change in the tropical Pacific tend to project an intensification of precipitation in the Sahel (Fig.3b). This is plausible given the strong negative correlation found in observations between El Niño-Southern Oscillation (ENSO) and rainfall in the Sahel on interannual time scales (Joly and Voldoire 2009; Janicot et al. 2011). In the observations and at interannual timescales, such SST anomalies exert an influence on the atmosphere by shifting the heat sources associated with deep convection, with the upper tropospheric heating propagating through the Tropics in the form of Kelvin and Rossby waves (Trenberth et al. 1998). Yet, it remains to be proven that similar mechanisms are at work for explaining a part of the inter-model spread of Sahel rainfall projections, and that they apply in the case of changes in the mean state of the equatorial Pacific rather than in ENSO variability (see below). Note that the anomalous cooling occurring in the southeastern tropical Pacific could be related to both the emergence of this La Niña-like pattern and the strengthening of the subtropical anticyclone discussed above (see Fig.S5), and therefore be related to both the near global inter-hemispheric gradient and the ENSO-like mean-state. This aspect is further detailed in Subsection 4b below.

From the rainfall perspective, Fig.3d shows a large rainfall modulation over the entire Sahel band. Along the western side of Africa, it extends in latitude up to 30°N. Along the equatorial Atlantic, Fig.3d displays a band of decreasing rainfall which could be associated with the increase in Sahel rainfall. In this case, it could be interpreted as a northeastward shift of the ITCZ, which would be partly consistent with the inter-hemispheric surface temperature and

SLP patterns described above. Nevertheless, Fig.3d shows that this northward migration of the ITCZ is not found in other basins, suggesting that there are other important factors besides the inter-hemispheric temperature gradient. In connection with the MCA analysis we have conducted on global temperature changes (Fig.3b), one can consider the modulation of equatorial Pacific SSTs, which are known to exert a strong influence on tropical precipitation and could dominate over the inter-hemispheric temperature gradient in these regions. For example, Fig.3d shows that the Arabian sea and India also experience anomalously strong rainfall for models projecting a wet Sahel. This feature is consistent with the role of central Pacific SSTs if we assume that the mechanisms involved in interannual variability also apply to changes, which remains to be proven (see Section 5b). Indeed, the Indian and African monsoons covary under the influence of ENSO in the observations (Madhavan et al. 2022). Accordingly, the Pacific Ocean presents a strong signal of precipitation change, with stronger than average precipitation over the Maritime Continent and the Indian region, but a weaker precipitation over the NWP monsoon area, all of which are consistent with the variability of Indo-Pacific precipitation during La Niña events (Timmermann et al. 2018; Tao et al. 2022). However, even if the intensification of precipitation over the western part of the Indo-Pacific region is consistent with an enhanced zonal circulation, the most significant signal is the drying on the northwestern part of the Pacific Ocean, which is under the influence of the NWP monsoon system. Therefore, rainfall changes in the Indo-Pacific region could also be related to a westward shift in the zonal circulation rather than an intensification alone. Finally, Fig. 3d shows a drying in the vicinity of the Southern Hemisphere subtropical highs in each of the three ocean basins, which is consistent with a strengthening of the Hadley cells and supports the importance of the inter-hemispheric temperature gradient described above.

To conclude, the MCA analyses highlight an increased inter-hemispheric gradient and an ENSO-like signature as important factors in explaining the differential response of Sahel rainfall in the CMIP6 projections.

	Explained variances of Extended Sahel rainfall change by the first leading mode in each MCA	SCF	NC	Correlations between the first SVs of rainfall change over extended Sahel and Sahel averaged precipitation change	Correlation between first SV of global change and first SV of rainfall change over Sahel	Correlation between the first SVs of global precipitation and surface temperature change from the two MCAs (Figs.3bd)	Correlation between the first SVs of rainfall change over the Extended Sahel from the two MCAs (Figs.3ac)
MCA: global Pr change with Sahel rainfall change	51 %	68 %	22 %	0,93	0,89	0,70	0,99
MCA: global Ts change with Sahel rainfall change	49 %	79 %	25 %	0,95	0,80		

TABLE 2. Statistics associated with the MCAs between surface temperature or precipitation changes with Sahel rainfall change shown in Fig.3. All correlations in the last four columns are significant at the 99% confidence level considering each model independent. See text and Text.S1 in the supplemental material for more details on the SCF and NC statistics.

b) *Performance of averaged temperature indices in explaining Sahel rainfall change*

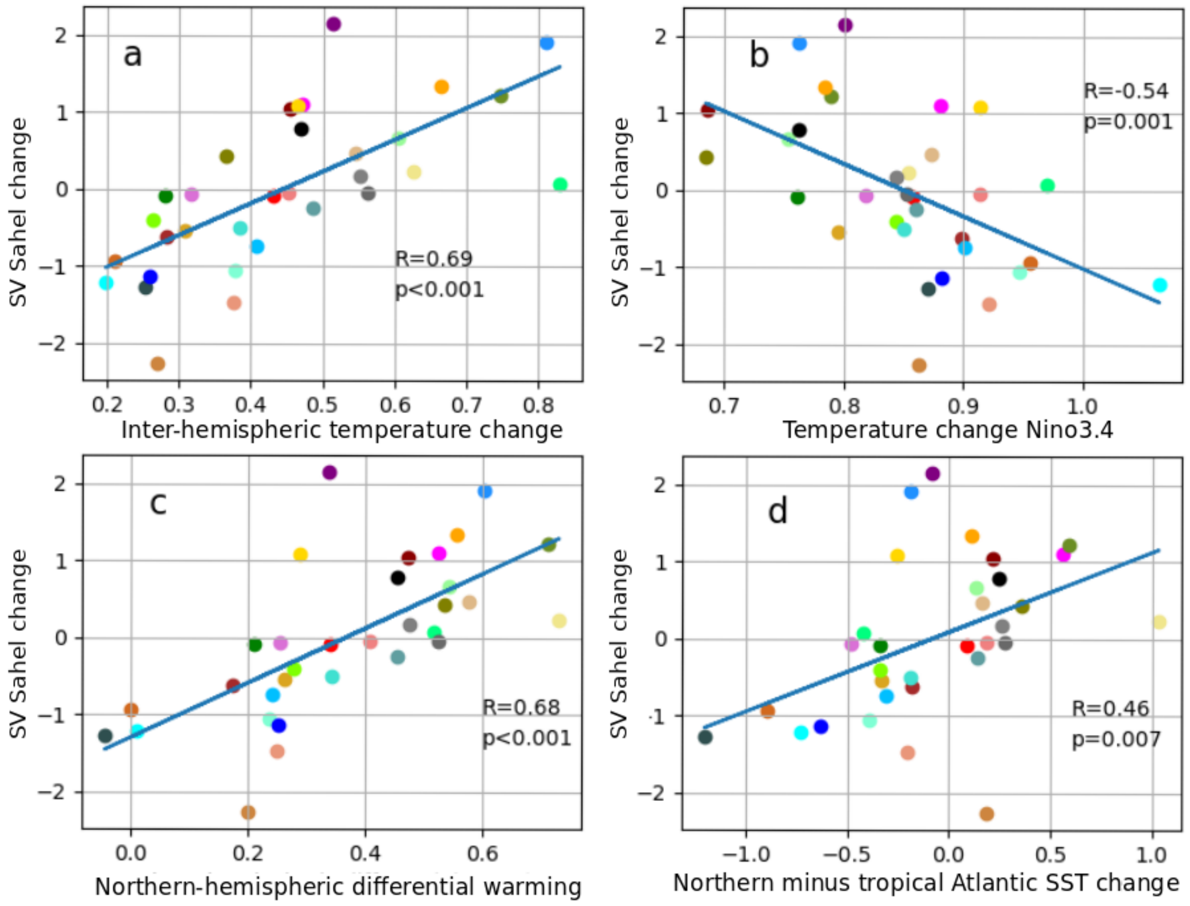

Fig. 4. Scatterplots of SV Sahel change ($mm.d^{-1}.K^{-1}$, from Fig.3a), respectively, with (a) inter-hemispheric temperature change ($K.K^{-1}$), (b) Niño3.4 temperature change ($K.K^{-1}$), (c) northern-hemispheric SST differential warming ($K.K^{-1}$), (d) northern minus tropical Atlantic SST change ($K.K^{-1}$). The definition of each index can be found in Section 2 and Table 1. All model series are scaled by the global temperature change in each model. The correlation and its associated P-value for each pair of model series are indicated in each panel.

In view of the consistent results between the two MCAs, we choose to focus on selected key temperature indices representing well defined modes of variability or physical processes to explain the inter-model spread of Sahel precipitation change. The inter-hemispheric temperature gradient index has a strong correlation with the Sahel rainfall change spread (Fig.4a), stronger than the Niño3.4 index (Fig.4b), both being significant at the 99% significance level. Note that if we extend the regression line in Fig.4a to a zero change in the inter-hemispheric temperature gradient, i.e., uniform warming, this relationship predicts a drier Sahel, which is consistent with the results of Chou and Neelin (2004), Held et al. (2005) or Gaetani et al. (2017) describing a stabilization of the tropical troposphere, and also with the dry air intrusions from the Sahara due the uneven atmospheric boundary layer moisture increase between convective and non convective regions, known as the upped-ante mechanism. Other indices, mostly inspired from previous studies (defined in Table 1), such as the northern-hemispheric differential warming (Park et al. 2015) or differential warming between north and tropical Atlantic SSTs (Zhang and Li 2022) are also displayed, respectively, in Figs.4c and 4d. The differential warming between north and tropical Atlantic SSTs show consistent, but weaker correlation with the inter-model spread of Sahel precipitation change, whereas the index derived by Park et al. (2015) yields a correlation very close to the inter-hemispheric gradient index defined here.

Fig.4b confirms that the inter-model spread of Niño3.4 SST change is also significantly correlated with the inter-model spread of Sahel precipitation change. Interestingly, the inter-hemispheric temperature gradient is not significantly correlated with temperature change over Niño3.4 ($r=-0.25$, P-value=0.17), unlike both the Northern Hemisphere differential warming and the northern minus tropical Atlantic SST gradient (their correlations with Niño3.4 are, respectively, $r=-0.49$ (P-value<0.01) and $r=-0.42$ (P-value=0.02). This supports the choice of the inter-hemispheric temperature gradient and Niño3.4 SST as key indices to explain the Sahel rainfall change in the rest of the study. Furthermore, they are associated with well-defined modes of variability which are both known to be important for Sahel variability at interannual and/or decadal or centennial timescales (Joly and Voldoire 2009; Biasutti et al. 2018). This makes them both plausible candidates from the point of view of physical processes in addition to their statistical relevance for explaining the inter-model spread of Sahel rainfall projections.

In order to check for the existence of other potential drivers, we compute regression analyses of the SV of the Sahel precipitation change with surface temperature change after removing the effect of the inter-hemispheric temperature gradient index alone (top, Fig. S6) and of the effect of both the inter-hemispheric temperature gradient and Niño3.4 indices (bottom, Fig. S6). The results show that when we remove the linear contributions of both indices, there is almost no significant correlation left over the globe between surface temperature changes and

Sahel rainfall changes, except over the Sahel itself. The inter-hemispheric temperature gradient alone is however not sufficient to remove all the signal with the temperature changes, especially in the Pacific (bottom, Fig. S6).

5. Mechanisms of future Sahel rainfall uncertainties

a) Inter-hemispheric gradient change and Sahel rainfall

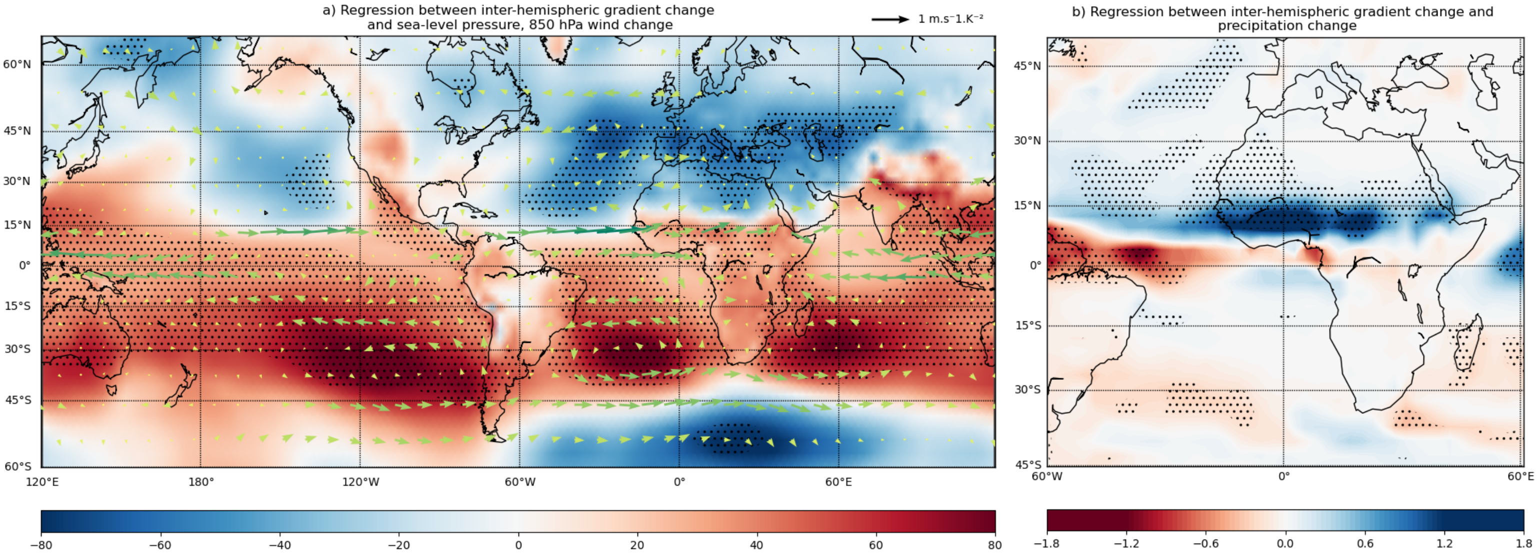

Fig. 5. Inter-model regressions against the inter-hemispheric temperature gradient change of (a): changes in SLP (color shaded, Pa.K^{-2}) and wind at 850 hPa (vectors, m.s^{-1}.K^{-2}); (b) precipitation change (color shaded : 0,1 mm.d^{-1}.K^{-2}). The colors of the arrows vary from green to yellow according to the intensity of the wind speed for readability. On panel (a), only 1 vector out of 3 is shown also for readability and dotted points indicate grid-points where the regression with sea-level pressure change is significant at the 95% confidence level. On panel (b), dotted points indicate grid-points where the regression with precipitation change is significant at the 95% confidence level.

Figure 5a shows that the models with an enhanced inter-hemispheric gradient in the future with respect to the MMM tend to produce an intensification of the subtropical highs in the Southern Hemisphere and a reduction of those in the Northern Hemisphere in all oceanic basins as compared to the MMM. Consistently, the trade-winds in the south subtropics and the eastward low-level anomalous flow at about 15°N towards the West African, Indian and American monsoons regions are both stronger when the inter-hemispheric temperature gradient is enhanced. Note that these low-level wind, temperature and SLP gradients between the two hemispheres are reminiscent of the positive wind-evaporation-SST feedback linking the SST gradient and the cross-gradient flow in the Tropics at the interannual and decadal time scales (Chang et al. 1997; Chiang and Vimont 2004). This suggests that local coupled ocean-atmosphere interactions may also sustain this wind regime changes in both the Pacific and Atlantic basins.

These patterns of SLP and low-level wind changes are broadly similar to those associated with the first leading MCA mode of Sahel rainfall illustrated in Fig.S5, especially in the Southern Hemisphere. This is further confirmed by the associated precipitation change (Fig. 5b), which depicts a northward shift of the ITCZ in the Atlantic sector, with a homogeneous intensification of precipitation over the Sahel and a decrease along the equator. An additional mechanism that may link an anomalously strong inter-hemispheric gradient change to enhanced precipitation change over the Sahel is the intensification of the West African Westerly Jet (WAWJ), leading to an increase in moisture convergence over the Sahel (Grodsky et al. 2003; Pu and Cook 2010). This is in agreement with previous studies such as Park et al. (2015) or Zhang and Li (2022), which point, respectively, to an amplification of low pressure over the Sahara or over Western Europe as the origin of these westerly wind anomalies. These regions are also highlighted in Fig.5a, but we emphasize here that the northward migration of the ITCZ could be also a key factor in the intensification of the WAWJ. Indeed, when the Atlantic ITCZ is shifted northwards, the southerly winds are stronger, which reinforces the eastward acceleration by the Coriolis force as they cross the Equator and reach the west coast of Africa, consequently reinforcing the WAWJ (Pu and Cook 2012).

Some differences between the SLP and wind anomalous patterns in the Northern Hemisphere in Fig.S5 and those associated with the globally enhanced meridional temperature gradient in Fig.5a are nevertheless noteworthy. Although both figures show high-pressure anomalies over the NWP, as well as the low-pressure anomalies over North Africa and Europe, these are more pronounced in Fig.S5 than in Fig.5a, as can be seen from the loss of significance over certain parts of these regions. This suggests that other mechanisms are at work to complete the picture, notably from the influence of the equatorial Pacific SSTs that we highlighted earlier.

b) Teleconnection between Niño3.4 *and Sahel rainfall*

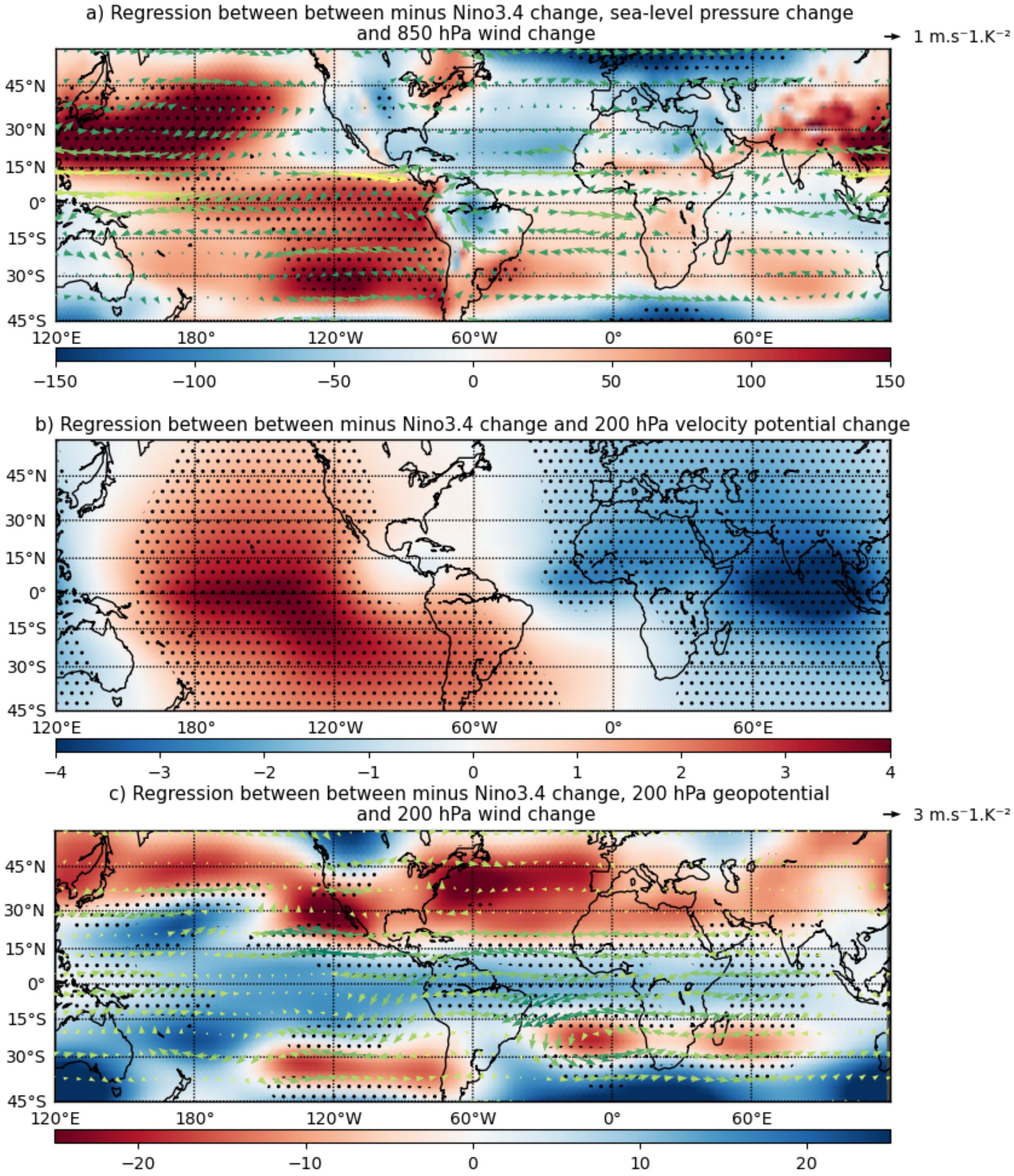

Fig. 6. Inter-model regressions against minus Niño3.4 temperature change of (a): SLP changes (color shaded, Pa.K^{-1}) and 850 hPa winds (vectors); (b) change of velocity potential at 200 hPa (color shaded, x10^{6} m^{2}.s^{-1}.K^{-2}); (c) 200 hPa geopotential change (color shaded : m^{2}.s^{-2}.K^{-2}) and winds (vectors). “Minus Nino3.4” refers to the fact that we have taken the opposite of Nino3.4 in order to have a positive modulation of rainfall over the Sahel as in the MCA patterns of Fig. 3a and c.

In order to facilitate the comparison with the MCA results which display an intensification of Sahel rainfall (Fig.3ac), Figs. 6-8 show regressions with the opposite (minus) of the Niño3.4 index, thus featuring anomalous La Niña patterns. Note that this is an approximation within the linear framework of our study, as the (observed) El Niño/La Niña patterns are not simply opposite to each other, as we imply here (Su et al. 2010).

In the Tropics, a classic mechanism for remote large-scale teleconnections at interannual timescales arises from the fact that ENSO is associated with an eastward migration of the Indo-Pacific warm pool causing the Walker circulation to shift zonally (Trenberth et al. 1998; Joly and Voldoire 2009; Roy et al. 2019). The hypothesis that similar mechanisms are at work here for explaining a part of the inter-model spread of Sahel rainfall change is suggested by Fig.6. This is firstly seen via the surface variables changes associated with the inter-model changes in the (minus) Niño3.4 index shown in Fig.6a. Models with a La Niña-like change in the equatorial Pacific with respect to the MMM show a stronger and significant intensification of the subtropical anticyclone in the southeast Pacific and of the pressure gradient along the Equator, resulting in an intensification of the trade winds from 30°S to 5°N. To the west of the basin, there are also strong positive pressure anomalies around 30°N, which lead to strong anticyclonic circulation anomalies corresponding to a drastic weakening of the NWP monsoon during boreal summer. Taken together, these features strongly enhance wind and moisture convergence from the Pacific towards the Maritime Continent and the Indian Ocean, especially along the Equator, but also over South Asia as shown in Fig.7. Coupled with the westerly low-level wind anomalies over the Atlantic Ocean and Africa between 0° and 15°N, there is a strong low-level moisture convergence anomaly over the African-Indian region materialized by precipitation anomalies (Fig.7). This illustrates a zonal shift of convection in the Indo-Pacific sector which is very similar to what is observed traditionally during developing La Niña events, with a weak NWP monsoon, and conversely during El Niños (Wang et al. 2001; Chou et al. 2003; Crétat et al. 2017).

Fig.6b further illustrates the pronounced shift of the Walker circulation from the perspective of the upper troposphere. It shows stronger than average velocity potential changes at 200hPa over the Pacific Ocean which correspond to anomalous convergence above the Pacific Ocean and, thus, a weaker convection for anomalous La Niña-like changes. Conversely, weaker than average changes of the velocity potential extending from the Indian Ocean to western Africa correspond to increased upper level divergence associated with heavier rainfall over the Sahel and Indian sector (Fig.7). Therefore, through interactions with the large-scale circulation, a change in SST toward a more La Niña-like mean state in the Pacific Ocean in a particular model (see Supplementary Fig.S7, Lian et al. 2019) tends to produce amplified rainfall over the Sahel in this model compared to the MMM. This large-scale mechanism is broadly consistent with the rainfall changes observed in Fig.3d, which shows increased rainfall from West Africa to the Maritime Continent, and a decrease over the Pacific Ocean.

This link between Pacific mean state change and Sahel rainfall could also occur through the modulation of upper tropospheric jets (Nicholson 2009). Fig.6c shows that a La Niña-like SST change tends to produce easterly wind anomalies at 200 hPa from 120E to 90E which are symmetric about the Equator. This corresponds to a strong enhancement of the TEJ located between 5°N and 10°N. Such conditions are favorable to enhanced Sahel rainfall as an enhanced TEJ promotes uplift and upper-level divergence (Nicholson 2009). Furthermore, it is known that an increase of the vertical shear of the summer mean flow may be a primary factor leading to the northward propagation of the intra-seasonal convection and the rainfall band (Jiang et al. 2004; Bickle et al. 2021). The symmetry of 200 hPa dynamical features with respect to the equator first suggests that these upper-level zonal wind anomalies may be caused by the eastward propagation of a Kelvin wave from the equatorial Pacific. Consistent with this view, Fig.6c shows 200 hPa geopotential anomalies extending along the Equator from the equatorial Pacific to Africa, reminiscent of a Kelvin wave signature from a Matsuno-Gill type response (Gill 1980). However, these equatorial 200 hPa geopotential anomalies are not statistically significant. Furthermore, the Kelvin wave response is centered at the Equator and decreases exponentially away from the Equator while the TEJ position is at 10-15°N. Therefore the Kelvin wave response does not seem to be sufficient to explain the

TEJ anomalies on their own. Nonetheless, Fig.6 also suggests an additional pathway which may explain how models showing a more La Niña-like mean state than the MMM may also simulate an enhanced TEJ and thus WAM. The 200 hPa geopotential anomalies (Fig.6c) associated with the minus Niño3.4 index exhibit anomalous maxima and minima centers over the North Pacific, North America and the North Atlantic, which appear to be consistent with the extratropical teleconnections mediated through Rossby wave propagation associated with ENSO in observations and models (Trenberth et al. 1998; García-Serrano et al. 2017). The positive 200 hPa geopotential anomalies above the North Atlantic produced by this extratropical wave train can modulate tropospheric properties above 15°N and, thus, the TEJ. Indeed, although 200 hPa geopotential changes around the Sahel related to the minus Niño3.4 index are not individually significantly, the geopotential thickness (between 200 and 850 hPa) gradient around the Sahel (see Section 2 and Table 1 for details) is significantly linked to the (minus) Niño3.4 index ($r=0.46$, $p<0.01$). Via the thermal wind relationship, this tropospheric thickness gradient is also strongly related to the vertical wind shear over the Sahel, itself largely driven by the TEJ (not shown). Therefore, a change of the Pacific mean state could be linked to a change in the TEJ via both tropical and extratropical pathways, resulting in modulation of Sahel rainfall by promoting or inhibiting deep convection.

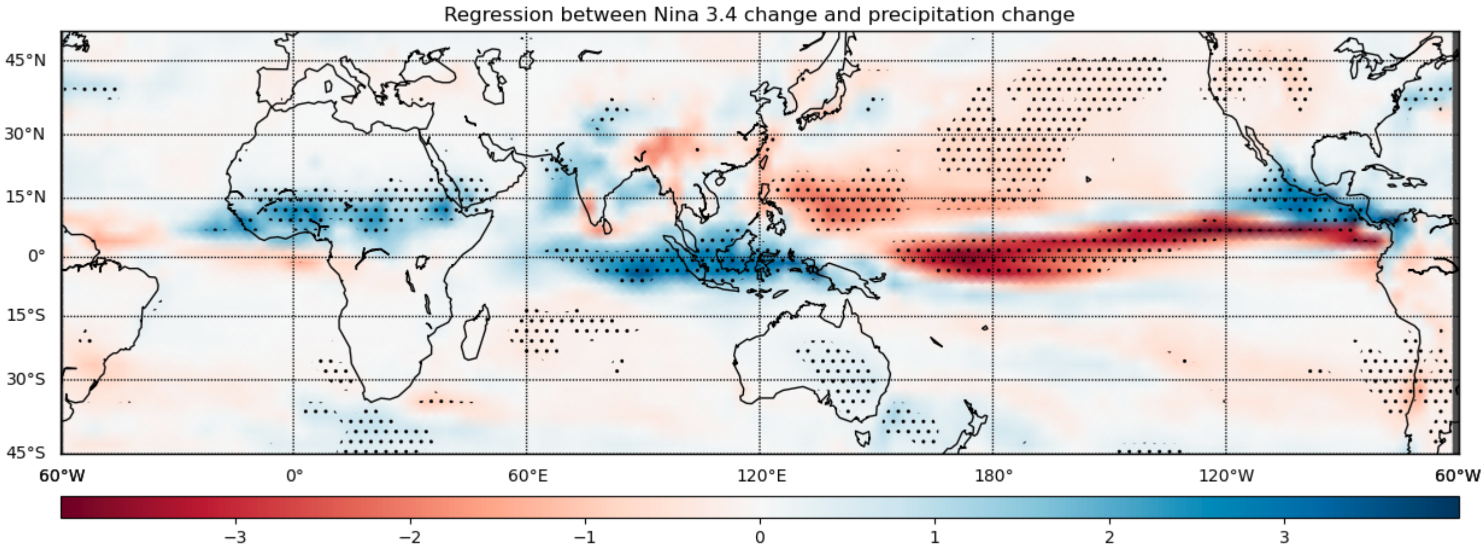

Fig.7. Inter-model regression of precipitation change against minus Niño3.4 temperature change ($mm.d^{-1}.K^{-2}$)

c) Respective contributions of the inter-hemispheric gradient and Niño3.4 index to the inter-model spread of Sahel rainfall

The sources of uncertainty in Sahel precipitation that we have highlighted have so far been considered as independent to first order. Nevertheless, although not statistically significant, there is still a correlation between the two indices ($r=-0.25$, P-value=0.17) which have thus some cross effects. In order to quantify their global and collective contributions to the inter-model spread of Sahel rainfall, we first use a bilinear regression model with these two indices. The parameters of the bilinear model is computed using a least squares optimization which aims to minimize the sum of the squared differences between the target variable and the values predicted by the model with the two explanatory variables. In our case, the target variable is the SV of precipitation change in the Sahel, and the predictor variables are the changes in the inter-hemispheric temperature gradient and Nino3.4 SST. This simple bilinear model explains 62% of the inter-model spread of the SV of Sahel precipitation change ($R^2=0.62$, $r=0.79$), which is very close to the inter-model spread explained by the temperature pattern from the MCA ($R^2=0.64$, $r=0.80$). Similar results are obtained when we consider the precipitation change average over the Sahel canonical domain (not shown). In other words, the two indices taken together explain a very similar amount of future Sahel rainfall change spread as the first MCA mode shown in Fig.3.

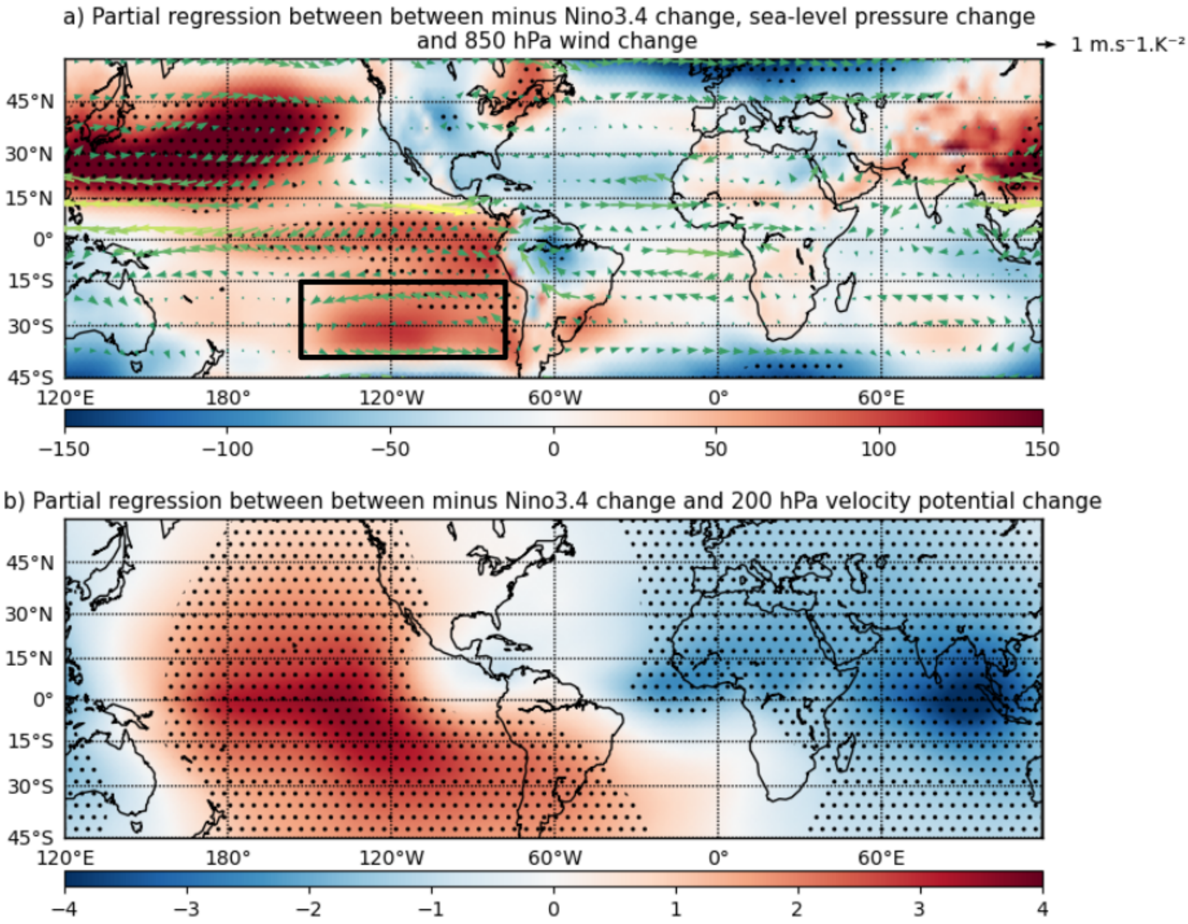

Fig. 8. Partial correlation between minus Niño3.4 index change with changes in (a) SLP and 850 hPa winds -; (b) 200 hPa velocity potential; excluding in all variables their linear dependance to the inter-hemispheric temperature change (see Section 2 for details). Dotted points indicate significant correlations at the 95% confidence level. The black square emphasizes the area that lost intensity and significance compared to Fig.6a.

Next, to estimate the individual contribution of the interhemispheric temperature gradient and the equatorial Pacific SST change to the uncertainty, we use partial regressions that allow to isolate the effect of one index by removing the linear contribution of the other. The contributions of the inter-hemispheric gradient and Nino3.4, assuming the other factor is held constant, are estimated to be 34% and 16%, respectively. What remains of the 62% of the spread explained by the bilinear model, i.e. 12%, corresponds to the role of the interactions between the two indices. This redundancy is not small and therefore can’t be overlooked. This is illustrated first by the comparison between Figs.8a and 6a, which shows that the strength of the subtropical anticyclone in the South-East Pacific Ocean (see the black box in Fig.8a) decreases considerably and loses significance when considering the 'pure' influence of the minus Niño3.4 index after the removal of the linear contribution of the inter-hemispheric gradient. Similarly, in the upper-troposphere (compared Fig.8b with Fig.6b): the anomalous pattern is the same, but the amplitude of the velocity potential anomalies are smaller when the contribution from the inter-hemispheric temperature gradient is removed.

Finally, to estimate the individual contributions from the two indices, which correspond to the "pure" contribution of each of them, plus a part of the interactions, we use three different attribution methods as described in Section 2. As shown in Table 3, the three methods give very similar results, which gives confidence in the robustness of the results. By averaging the results of the three methods, we find that 40% of the inter-model spread of precipitation change over the Sahel is explained by the inter-hemispheric gradient and 22% by the SST Pacific mean state. This corresponds, on average over the methods, to an equal distribution of the 12% of the interactions to each of the two indices. Thus, we confirm, as previously supposed, that the inter-hemispheric gradient is the main source of uncertainty, and that the the tropical Pacific mean state is a secondary, but critical, source of uncertainty for Sahel rainfall projection and its spatial modulation, which may also positively interact with the inter-hemispheric gradient. Our results are consistent with Monerie et al. (2021) who shows that the fast response of the Sahel precipitation is associated with a reinforced inter-hemispheric gradient of temperature and explains most of the uncertainty. Moreover, our estimate of the inter-model spread of the change in precipitation in the Sahel explained by Nino3.4 is also consistent with the part explained by the slow response of the Sahel precipitation in Monerie et al (2021), which may be partly associated with the equatorial Pacific according to the same study.

	Dominance analysis	*Permutation Feature Importance*	*Random forest attribution*
Niño3.4 estimated contribution	*23%*	*22%*	*20%*
Inter-hemispheric gradient estimated contribution	*39%*	*40%*	*42%*

TABLE 3. Relative contributions of Niño3.4 and inter-hemispheric gradient to the inter-model spread of the SV of Sahel rainfall change, estimated with three different attribution methods (see Section 2 for details).

6. Conclusions and discussion

The response of Sahel monsoon rainfall to global warming suffers from large uncertainties which have not decreased from CMIP3 to CMIP6 (Monerie et al. 2020a; Zhang and Li 2022), and the origins of this inter-model spread are not yet well understood. In this study, we analyze 32 coupled models from CMIP6 under a high emission scenario (SSP5-8.5) in order to revisit the sources of Sahel rainfall change uncertainties at the end of the 21st century.

Our results first confirm that Sahel rainfall change in CMIP6 still suffers from large uncertainties with one third of the models projecting a decrease in precipitation and two thirds an intensification. We also confirm that these uncertainties are mainly due to the dynamic component of the monsoon as the scaled and unscaled (by the global temperature) pattern from the MCAs are broadly similar. The MMM change of Sahel precipitation exhibits a dipolar pattern with an increase over the central Sahel and a decrease in the western Sahel as in previous CMIP generations (Monerie et al. 2017b; Almazroui et al. 2020), but this zonal contrast is not apparent in the inter-model spread, which is fairly homogeneous over the Sahel. This suggests that mechanisms responsible for this spread induce primarily zonally homogeneous changes, which will be confirmed later by the predominant role of the inter-hemispheric temperature gradient.

On a broader scale, CMIP6 models also present large uncertainties regarding precipitation and SST change over the Pacific ocean. Indeed, although the models agree on a rather El-Niño-like warming in the equatorial Pacific, the magnitude of this change is highly uncertain (Lian et al. 2019; Fredriksen et al. 2020). The Sahara and Eurasia also show a large inter-model spread of surface temperature changes. This is consistent with previous studies and suggests that they are also potential drivers of the change of the Sahel monsoon under global warming across the models (Park et al. 2015; Zhang and Li 2022). Finally, the largest surface temperature uncertainty is found over the North Atlantic ocean, which has been suggested as another important source of uncertainty for Sahel precipitation change (Park et al. 2015; Monerie et al. 2020b; Bellomo et al. 2021; Zhang and Li 2022). Following this overview of the changes and related uncertainties from the models in CMIP6, we answered the three questions that had been raised in the introduction concerning the inter-model spread of Sahel rainfall change :

1. Can we revisit and improve the factors explaining the projected Sahel rainfall uncertainties from an objective analysis of the projected changes at the ocean-atmosphere-land surface ?

   The MCAs show that changes in tropical precipitation and surface temperature both zonally modulate the change in Sahel precipitation. However, this modulation is more important in the central Sahel than at the eastern and western edges of the region. The close correspondence among the two MCA analyses demonstrate that coupled ocean-atmosphere and land-atmosphere changes are linked to the uncertainties in Sahel rainfall change. In order to compare our results with previous studies, we choose to focus on the impact of surface temperatures which highlights two major sources of uncertainties: an inter-hemispheric temperature gradient and the equatorial Pacific mean-state represented here by a Niño3.4 index. In addition to being strongly correlated with Sahel precipitation change, these two indices are not significantly correlated with each other, which allows us to consider them as two independent sources of uncertainty in a first statistical approximation. It should be remembered that MCAs can be used to demonstrate relationships, but not causality. Causality arises from the physical mechanisms described below.

2. By what physical processes are these factors related to Sahel rainfall?

   The major processes which link the inter-model spread of Sahel rainfall change to the two factors mentioned above are summarized in Fig.9.

   a) The inter-hemispheric temperature gradient impacts Sahel rainfall change by modulating the position of the ITCZ. Based on the energetic framework and the assumption that this gradient is a good proxy for the radiative imbalance between the two hemispheres during boreal summer (Schneider et al. 2014; Byrne et al. 2018), an increased inter-hemispheric gradient results in a northward shift of the ITCZ and stronger rainfall over the Sahel. The associated rainfall modulation is homogeneous over the Sahel, which has been a factor of exclusion of this large-scale differential warming for explaining the inter-model spread of Sahel rainfall in previous studies (Park et al. 2015). Here we can rehabilitate this source of uncertainty because we demonstrate that the zonal contrast in the inter-model spread of Sahel rainfall changes is secondary in CMIP6 and also because the spatial rainfall modulation in the Sahel itself is provided by the change in the equatorial Pacific mean-state.

   b) The change in the equatorial Pacific mean-state has an impact firstly via the large-scale overturning zonal circulations in the Tropics. Indeed, for the models exhibiting a La-Niña-like anomalous SST change, the Walker circulation is strongly shifted westward compared to the MMM (which is El-Niño-like), creating anomalous divergence in the upper-troposphere that extends over the Sahel and promotes local convection. The situation is reversed for El-Niño-like models. Secondly, by modulating the latent heat release, SST changes in the equatorial Pacific modulate both the intensity and position of tropospheric warming and, subsequently, generate tropical Kelvin and extra-tropical Rossby waves that modify the meridional mid-tropospheric temperature gradient around the Sahel. This ultimately leads to changes in the upper-level zonal circulation over the Sahel and in particular of the TEJ intensity. The strength of the TEJ in turn modulates upper-level divergence and the vertical zonal wind shear, and hence convection over the region (Nicholson 2009). The minus Niño3.4 index produces more intense rainfall modulation over Central Sahel, and therefore seems responsible for the spatial signature of monsoon rainfall change over the Sahel (Fig.S8).

3. How much uncertainty can they explain?

Although the two sources of uncertainty are not significantly correlated, we demonstrate that there are nevertheless plausible physical interactions between them, notably mediated by the strength of the subtropical anticyclone in the southeast Pacific. These interactions account for 12% of the uncertainty of rainfall change in the Sahel according to a bilinear regression model. However, by using attribution methods, we were able to distribute this share between the two indices and, finally, estimate their respective full contributions. Of the 62% of the inter-model spread of rainfall change in the Sahel explained by the bilinear regression: 40% are explained by the inter-hemispheric gradient and 22% by Niño3.4. Finally, the overall performance of the bilinear model is equivalent to what is obtained from the multivariate MCA optimization, and is, thus, unlikely to be further significantly improved by using only linear relationships and surface temperature indices.

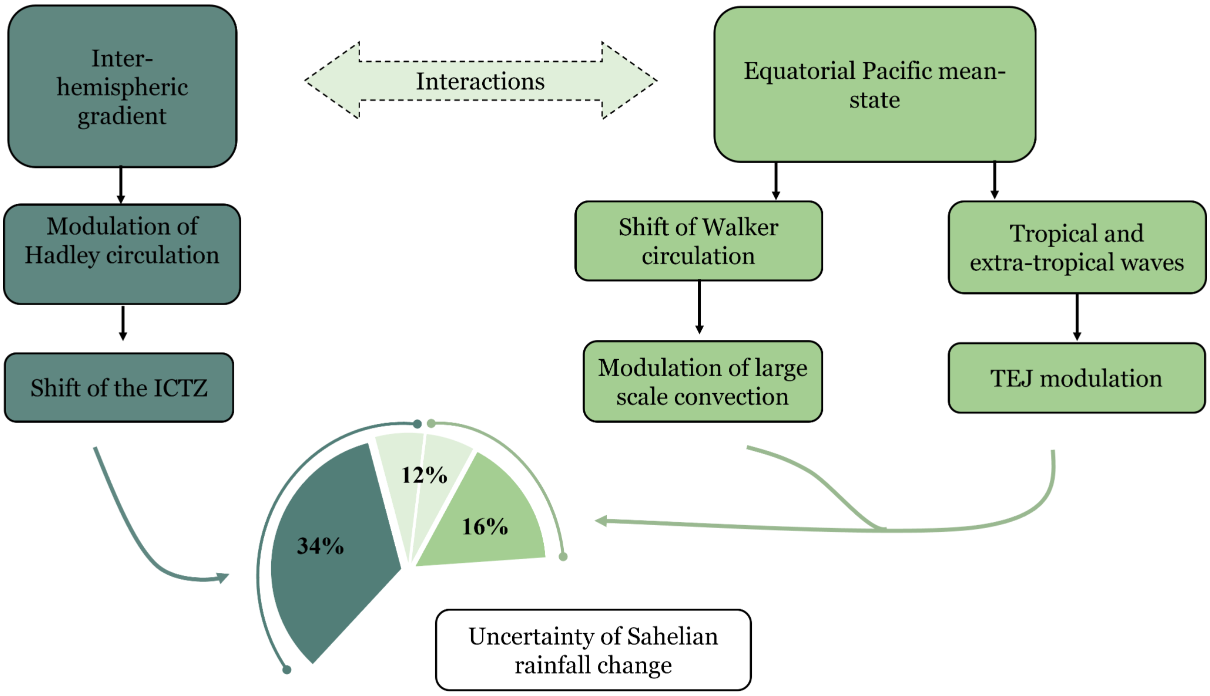

Fig. 9. Schematic diagram showing the processes by which the inter-hemispheric gradient and Niño3.4 anomalous warming patterns modulate the inter-model spread of Sahel rainfall change and their respective contributions to this inter-model spread.

The relationship between the inter-hemispheric gradient, equatorial Pacific SST and Sahel rainfall change could be further tested using SST nudging experiments. Further understanding of the mechanisms could also be obtained by using a moisture budget analysis (Chou et al. 2009; Chen et al. 2020). As our study focused on the sources of uncertainty in the change of the Sahel monsoon under SSP5-8.5 scenario, one could also extend it to the historical period and other scenarios to verify if the sources of uncertainty we have highlighted are still relevant and robust, and also to determine their time of emergence. Regarding its key role in Sahel rainfall uncertainty and its importance for global climate, further work should focus on the inter-hemispheric temperature gradient change and the radiative imbalance between the two hemispheres during boreal summer. Chung and Soden (2017) showed that by modulating cloud properties, anthropogenic aerosol can be critical in shaping future inter-hemispheric temperature change at least in near future. A future study should also address the sources of uncertainty in SST change in the equatorial Pacific as it plays a pivotal role in the Tropics. Such uncertainties have been linked to model biases in the Pacific itself (Guilbert et al. 2023) or to biases in other basins (McGregor et al. 2018; Marathe et al. 2021; Terray et al. 2021), with equatorial undercurrent and inter-basin interactions suggested to be key to reduce these models biases (Coats and Karnauskas 2017). Finally, as we have so far mainly used interannual to decadal variability mechanisms to link our indices to Sahel rainfall change, improving present day performance at simulating Sahel rainfall variability could be critical to further reduce the disagreement between models projections and predictions.

Acknowledgments.

Pascal Terray and Juliette Mignot are funded by Institut de Recherche pour le Développement (IRD, France) and supported by ANR-19-JPOC-003 JPI climate/JPI ocean ROADMAP. Analysis was done with Python (https://www.python.org/) and the STATPACK and NCSTAT softwares (https://terray.locean-ipsl.upmc.fr/software.html). This work benefited from the ESPRI computing and data centre (https://mesocentre.ipsl.fr) which is supported by CNRS, Sorbonne University, Ecole Polytechnique and CNES and through national and international grants.

Data Availability Statement.

The study is based on the outputs of CMIP6. These are publicly available upon registration on the Data Portal of the Earth System Grid Foundation (ESGF: https://esgf-node.ipsl.upmc.fr/search/cmip6-ipsl/). ERA-Interim publicly accessible upon registration on the ECMWF Data Portal (http://apps.ecmwf.int/). The GPCP data are publicly accessible (https://psl.noaa.gov/data/gridded/data.gpcp.html).

REFERENCES

Adler, R. F., and Coauthors, 2003: The Version-2 Global Precipitation Climatology Project (GPCP) Monthly Precipitation Analysis (1979–Present). *J. Hydrometeorol.*, **4**, 1147–1167, https://doi.org/10.1175/1525-7541(2003)004<1147:TVGPCP>2.0.CO;2.

Akinsanola, A. A., and W. Zhou, 2019: Ensemble-based CMIP5 simulations of West African summer monsoon rainfall: current climate and future changes. *Theor. Appl. Climatol.*, **136**, 1021–1031, https://doi.org/10.1007/s00704-018-2516-3.

Almazroui, M., F. Saeed, S. Saeed, M. Nazrul Islam, M. Ismail, N. A. B. Klutse, and M. H. Siddiqui, 2020: Projected Change in Temperature and Precipitation Over Africa from CMIP6. *Earth Syst. Environ.*, **4**, 455–475, https://doi.org/10.1007/s41748-020-00161-x.

Azen, R., and D. Budescu, 2003: The Dominance Analysis Approach for Comparing Predictors in Multiple Regression. *Psychol. Methods*, **8**, 129–148, https://doi.org/10.1037/1082-989X.8.2.129.

Bellomo, K., M. Angeloni, S. Corti, and J. von Hardenberg, 2021: Future climate change shaped by inter-model differences in Atlantic meridional overturning circulation response. *Nat. Commun.*, **12**, 3659, https://doi.org/10.1038/s41467-021-24015-w.

Biasutti, M., 2013: Forced Sahel rainfall trends in the CMIP5 archive. *J. Geophys. Res. Atmospheres*, **118**, 1613–1623, https://doi.org/10.1002/jgrd.50206.

Biasutti, M., 2019: Rainfall trends in the African Sahel: Characteristics, processes, and causes. *WIREs Clim. Change*, **10**, e591, https://doi.org/10.1002/wcc.591.

——, and Coauthors, 2018: Global energetics and local physics as drivers of past, present and future monsoons. *Nat. Geosci.*, **11**, 392–400, https://doi.org/10.1038/s41561-018-0137-1.

Bickle, M. E., J. H. Marsham, A. N. Ross, D. P. Rowell, D. J. Parker, and C. M. Taylor, 2021: Understanding mechanisms for trends in Sahelian squall lines: Roles of thermodynamics and shear. *Q. J. R. Meteorol. Soc.*, **147**, 983–1006, https://doi.org/10.1002/qj.3955.

Breiman, L., 2001: Random Forests. *Mach. Learn.*, **45**, 5–32, https://doi.org/10.1023/A:1010933404324.

Bretherton, C. S., C. Smith, and J. M. Wallace, 1992: An intercomparison of methods for finding coupled patterns in climate data. *J. Clim.*, **5**, 541–560, https://doi.org/10.1175/1520-0442(1992)005<0541:AIOMFF>2.0.CO;2.

Byrne, M. P., A. G. Pendergrass, A. D. Rapp, and K. R. Wodzicki, 2018: Response of the Intertropical Convergence Zone to Climate Change: Location, Width, and Strength. *Curr. Clim. Change Rep.*, **4**, 355–370, https://doi.org/10.1007/s40641-018-0110-5.

Chang, P., L. Ji, and H. Li, 1997: A decadal climate variation in the tropical Atlantic Ocean from thermodynamic air-sea interactions. *Nature*, **385**, 516–518, https://doi.org/10.1038/385516a0.

Charney, J., P. H. Stone, and W. J. Quirk, 1975: Drought in the Sahara: A Biogeophysical Feedback Mechanism. *Science*, **187**, 434–435, https://doi.org/10.1126/science.187.4175.434.

Chen, Z., T. Zhou, L. Zhang, X. Chen, W. Zhang, and J. Jiang, 2020: Global land monsoon precipitation changes in CMIP6 projections. *Geophys. Res. Lett.*, **47**, e2019GL086902, https://doi.org/10.1029/2019GL086902.

Cherchi, A., P. Terray, S. B Ratna, S. Sankar, K. Sooraj, and S. Behera, 2021: Indian Ocean Dipole influence on Indian summer monsoon and ENSO: A review.

Cherry, S., 1997: Some comments on singular value decomposition analysis. *J. Clim.*, **10**, 1759–1761, https://doi.org/10.1175/1520-0442(1997)010<1759:SCOSVD>2.0.CO;2.

Chiang, J. C. H., and D. J. Vimont, 2004: Analogous Pacific and Atlantic Meridional Modes of Tropical Atmosphere–Ocean Variability. *J. Clim.*, **17**, 4143–4158, https://doi.org/10.1175/JCLI4953.1.

Chou, C., and J. D. Neelin, 2004: Mechanisms of Global Warming Impacts on Regional Tropical Precipitation. *J. Clim.*, **17**, 2688–2701, https://doi.org/10.1175/1520-0442(2004)017<2688:MOGWIO>2.0.CO;2.

——, J.-Y. Tu, and J.-Y. Yu, 2003: Interannual Variability of the Western North Pacific Summer Monsoon: Differences between ENSO and Non-ENSO Years. *J. Clim.*, **16**, 2275–2287, https://doi.org/10.1175/2761.1.

——, J. D. Neelin, C.-A. Chen, and J.-Y. Tu, 2009: Evaluating the "Rich-Get-Richer" Mechanism in Tropical Precipitation Change under Global Warming. *J. Clim.*, **22**, 1982–2005, https://doi.org/10.1175/2008JCLI2471.1.

Chung, E.-S., and B. Soden, 2017: Hemispheric climate shifts driven by anthropogenic aerosol–cloud interactions. *Nat. Geosci.*, **10**, https://doi.org/10.1038/ngeo2988.

Coats, S., and K. Karnauskas, 2017: Are simulated and observed 20 th century tropical Pacific sea surface temperature trends significant relative to internal variability?: Tropical Pacific SST trends in CGCMs. *Geophys. Res. Lett.*, **44**, https://doi.org/10.1002/2017GL074622.

Cook, K. H., and E. K. Vizy, 2015: Detection and Analysis of an Amplified Warming of the Sahara Desert. *J. Clim.*, **28**, 6560–6580, https://doi.org/10.1175/JCLI-D-14-00230.1.

Crétat, J., P. Terray, S. Masson, K. P. Sooraj, and M. K. Roxy, 2017: Indian Ocean and Indian summer monsoon: relationships without ENSO in ocean–atmosphere coupled simulations. *Clim. Dyn.*, **49**, 1429–1448, https://doi.org/10.1007/s00382-016-3387-x.

Dee, D. P., and Coauthors, 2011: The ERA-Interim reanalysis: configuration and performance of the data assimilation system. *Q. J. R. Meteorol. Soc.*, **137**, 553–597, https://doi.org/10.1002/qj.828.

Dong, B., and R. Sutton, 2015: Dominant role of greenhouse-gas forcing in the recovery of Sahel rainfall. *Nat. Clim. Change*, **5**, 757–760, https://doi.org/10.1038/nclimate2664.

Eyring, V., S. Bony, G. A. Meehl, C. A. Senior, B. Stevens, R. J. Stouffer, and K. E. Taylor, 2016: Overview of the Coupled Model Intercomparison Project Phase 6 (CMIP6) experimental design and organization. *Geosci. Model Dev.*, **9**, 1937–1958, https://doi.org/10.5194/gmd-9-1937-2016.

Fisher, A., C. Rudin, and F. Dominici, 2019: All Models are Wrong, but Many are Useful: Learning a Variable's Importance by Studying an Entire Class of Prediction Models Simultaneously. https://doi.org/10.48550/arXiv.1801.01489.

Fredriksen, H.-B., J. Berner, A. C. Subramanian, and A. Capotondi, 2020: How Does El Niño–Southern Oscillation Change Under Global Warming—A First Look at CMIP6. *Geophys. Res. Lett.*, **47**, e2020GL090640, https://doi.org/10.1029/2020GL090640.

Gaetani, M., C. Flamant, S. Bastin, S. Janicot, C. Lavaysse, F. Hourdin, P. Braconnot, and S. Bony, 2017: West African monsoon dynamics and precipitation: the competition between global SST warming and CO2 increase in CMIP5 idealized simulations. *Clim. Dyn.*, **48**, 1353–1373, https://doi.org/10.1007/s00382-016-3146-z.

García-Serrano, J., C. Cassou, H. Douville, A. Giannini, and F. J. Doblas-Reyes, 2017: Revisiting the ENSO Teleconnection to the Tropical North Atlantic. *J. Clim.*, **30**, 6945–6957, https://doi.org/10.1175/JCLI-D-16-0641.1.

Giannini, A., and A. Kaplan, 2019: The role of aerosols and greenhouse gases in Sahel drought and recovery. *Clim. Change*, **152**, 449–466, https://doi.org/10.1007/s10584-018-2341-9.

Gill, A. E., 1980: Some simple solutions for heat-induced tropical circulation. *Q. J. R. Meteorol. Soc.*, **106**, 447–462, https://doi.org/10.1002/qj.49710644905.

Grodsky, S. A., J. A. Carton, and S. Nigam, 2003: Near surface westerly wind jet in the Atlantic ITCZ. *Geophys. Res. Lett.*, **30**, https://doi.org/10.1029/2003GL017867.

Guilbert, M., P. Terray, and J. Mignot, 2023: Intermodel spread of historical Indian monsoon rainfall change in CMIP6: The role of the tropical Pacific mean-state. *J. Clim.*, **1**, 1–42, https://doi.org/10.1175/JCLI-D-22-0585.1.

Held, I. M., T. L. Delworth, J. Lu, K. L. Findell, and T. R. Knutson, 2005: Simulation of Sahel drought in the 20th and 21st centuries. *Proc. Natl. Acad. Sci.*, **102**, 17891–17896, https://doi.org/10.1073/pnas.0509057102.

Hill, S., 2019: Theories for Past and Future Monsoon Rainfall Changes. *Curr. Clim. Change Rep.*, **5**, 1–12, https://doi.org/10.1007/s40641-019-00137-8.

Hirasawa, H., P. Kushner, M. Sigmond, J. Fyfe, and C. Deser, 2020: Anthropogenic Aerosols

Dominate Forced Multidecadal Sahel Precipitation Change through Distinct Atmospheric and Oceanic Drivers. *J. Clim.*, **33**, 1–56, https://doi.org/10.1175/JCLI-D-19-0829.1.

Hwang, Y.-T., D. M. W. Frierson, and S. M. Kang, 2013: Anthropogenic sulfate aerosol and the southward shift of tropical precipitation in the late 20th century. *Geophys. Res. Lett.*, **40**, 2845–2850, https://doi.org/10.1002/grl.50502.

Janicot, S., and Coauthors, 2011: Intraseasonal variability of the West African monsoon. *Atmospheric Sci. Lett.*, **12**, 58–66, https://doi.org/10.1002/asl.280.

Janicot, S., and Coauthors, 2015: The Recent Partial Recovery in Sahel Rainfall: A Fingerprint of Greenhouse Gases Forcing? *GEWEX News*, **27**, 11–15.

Jiang, X., T. Li, and B. Wang, 2004: Structures and Mechanisms of the Northward Propagating Boreal Summer Intraseasonal Oscillation. *J. Clim.*, **17**, 1022–1039, https://doi.org/10.1175/1520-0442(2004)017<1022:SAMOTN>2.0.CO;2.

Joly, M., and A. Voldoire, 2009: Influence of ENSO on the West African Monsoon: Temporal Aspects and Atmospheric Processes. *J. Clim.*, **22**, 3193–3210, https://doi.org/10.1175/2008JCLI2450.1.

Kent, C., R. Chadwick, and D. P. Rowell, 2015: Understanding Uncertainties in Future Projections of Seasonal Tropical Precipitation. *J. Clim.*, **28**, 4390–4413, https://doi.org/10.1175/JCLI-D-14-00613.1.

Kucharski, F., N. Zeng, and E. Kalnay, 2013: A further assessment of vegetation feedback on decadal Sahel rainfall variability. *Clim. Dyn.*, **40**, 1453–1466, https://doi.org/10.1007/s00382-012-1397-x.

Lebel, T., and A. Ali, 2009: Recent trends in the Central and Western Sahel rainfall regime (1990–2007). *J. Hydrol.*, **375**, 52–64, https://doi.org/10.1016/j.jhydrol.2008.11.030.

Li, G., S.-P. Xie, C. He, and Z. Chen, 2017: Western Pacific emergent constraint lowers projected increase in Indian summer monsoon rainfall. *Nat. Clim. Change*, **7**, 708–712, https://doi.org/10.1038/nclimate3387.

Lian, T., D. Chen, J. Ying, P. Huang, and Y. Tang, 2019: Tropical Pacific trends under global warming: El Niño-like or La Niña-like? *Natl. Sci. Rev.*, **5**, https://doi.org/10.1093/nsr/nwy134.

Madhavan, M., L. Ravisankar, K. Thirumalai, and R. Ramesh, 2022: Coherent Indian Summer Monsoon and Sahel Rainfall Variability Revealed by Ethiopian Rainfall δ 18 O. *J. Geophys. Res. Atmospheres*, **127**, https://doi.org/10.1029/2022JD037160.

Marathe, S., P. Terray, and A. Karumuri, 2021: Tropical Indian Ocean and ENSO relationships in a changed climate. *Clim. Dyn.*, **56**, 3255–3276, https://doi.org/10.1007/s00382-021-05641-y.

Martin, E. R., and C. D. Thorncroft, 2014: The impact of the AMO on the West African monsoon annual cycle. *Q. J. R. Meteorol. Soc.*, **140**, 31–46, https://doi.org/10.1002/qj.2107.

——, C. Thorncroft, and B. B. B. Booth, 2014: The Multidecadal Atlantic SST—Sahel Rainfall Teleconnection in CMIP5 Simulations. *J. Clim.*, **27**, 784–806, https://doi.org/10.1175/JCLI-D-13-00242.1.

Marvel, K., M. Biasutti, and C. Bonfils, 2020: Fingerprints of external forcings on Sahel rainfall: aerosols, greenhouse gases, and model-observation discrepancies. *Environ. Res. Lett.*, **15**, 084023, https://doi.org/10.1088/1748-9326/ab858e.

McGregor, S., M. F. Stuecker, J. B. Kajtar, M. H. England, and M. Collins, 2018: Model tropical Atlantic biases underpin diminished Pacific decadal variability. *Nat. Clim. Change*, **8**, 493–498, https://doi.org/10.1038/s41558-018-0163-4.

Meehl, G. A., C. A. Senior, V. Eyring, G. Flato, J.-F. Lamarque, R. J. Stouffer, K. E. Taylor, and M. Schlund, 2020: Context for interpreting equilibrium climate sensitivity and transient climate response from the CMIP6 Earth system models. *Sci. Adv.*, **6**, eaba1981, https://doi.org/10.1126/sciadv.aba1981.

Monerie, P.-A., B. Fontaine, and P. Roucou, 2013: Mid-century effects of Climate Change on African monsoon dynamics using the A1B emission scenario. *Int. J. Climatol.*, **33**, 881–896, https://doi.org/10.1002/joc.3476.

——, E. Sanchez-Gomez, and J. Boé, 2017a: On the range of future Sahel precipitation projections and the selection of a sub-sample of CMIP5 models for impact studies. *Clim. Dyn.*, **48**, 2751–2770, https://doi.org/10.1007/s00382-016-3236-y.

——, ——, B. Pohl, J. Robson, and B. Dong, 2017b: Impact of internal variability on projections of Sahel precipitation change. *Environ. Res. Lett.*, **12**, 114003, https://doi.org/10.1088/1748-9326/aa8cda.

——, ——, M. Gaetani, E. Mohino, and B. Dong, 2020a: Future evolution of the Sahel precipitation zonal contrast in CESM1. *Clim. Dyn.*, **55**, 2801–2821, https://doi.org/10.1007/s00382-020-05417-w.

——, C. M. Wainwright, M. Sidibe, and A. A. Akinsanola, 2020b: Model uncertainties in climate change impacts on Sahel precipitation in ensembles of CMIP5 and CMIP6 simulations. *Clim. Dyn.*, **55**, 1385–1401, https://doi.org/10.1007/s00382-020-05332-0.

——, B. Pohl, and M. Gaetani, 2021: The fast response of Sahel precipitation to climate change allows effective mitigation action. *Npj Clim. Atmospheric Sci.*, **4**, 1–8, https://doi.org/10.1038/s41612-021-00179-6.

——, L. J. Wilcox, and A. G. Turner, 2022: Effects of Anthropogenic Aerosol and Greenhouse Gas Emissions on Northern Hemisphere Monsoon Precipitation: Mechanisms and Uncertainty. *J. Clim.*, **35**, 2305–2326, https://doi.org/10.1175/JCLI-D-21-0412.1.

Nakanishi, T., Y. Tachibana, and Y. Ando, 2021: Possible semi-circumglobal teleconnection across Eurasia driven by deep convection over the Sahel. *Clim. Dyn.*, **57**, 2287–2299, https://doi.org/10.1007/s00382-021-05804-x.

Ndiaye, C. D., E. Mohino, J. Mignot, and S. M. Sall, 2022: On the Detection of Externally Forced Decadal Modulations of the Sahel Rainfall over the Whole Twentieth Century in the CMIP6 Ensemble. *J. Clim.*, **35**, 3339–3354, https://doi.org/10.1175/JCLI-D-21-0585.1.

Nicholson, S., 2013: The West African Sahel: A Review of Recent Studies on the Rainfall Regime and Its Interannual Variability. *ISRN Meteorol.*, **2013**, https://doi.org/10.1155/2013/453521.

Nicholson, S. E., 2009: A revised picture of the structure of the “monsoon” and land ITCZ over West Africa. *Clim. Dyn.*, **32**, 1155–1171, https://doi.org/10.1007/s00382-008-0514-3.

Park, J., J. Bader, and D. Matei, 2016: Anthropogenic Mediterranean warming essential driver for present and future Sahel rainfall. *Nat. Clim. Change*, **6**, 941–945, https://doi.org/10.1038/nclimate3065.

Park, J.-Y., J. Bader, and D. Matei, 2015: Northern-hemispheric differential warming is the key to understanding the discrepancies in the projected Sahel rainfall. *Nat. Commun.*, **6**, 5985, https://doi.org/10.1038/ncomms6985.

Pascale, S., W. R. Boos, S. Bordoni, T. L. Delworth, S. B. Kapnick, H. Murakami, G. A. Vecchi, and W. Zhang, 2017: Weakening of the North American monsoon with global warming. *Nat. Clim. Change*, **7**, 806–812, https://doi.org/10.1038/nclimate3412.

Pu, B., and K. H. Cook, 2010: Dynamics of the West African Westerly Jet. *J. Clim.*, **23**, 6263–6276, https://doi.org/10.1175/2010JCLI3648.1.

——, and ——, 2012: Role of the West African Westerly Jet in Sahel Rainfall Variations. *J. Clim.*, **25**, 2880–2896, https://doi.org/10.1175/JCLI-D-11-00394.1.

Roehrig, R., D. Bouniol, F. Guichard, F. Hourdin, and J.-L. Redelsperger, 2013: The Present and Future of the West African Monsoon: A Process-Oriented Assessment of CMIP5 Simulations along the AMMA Transect. *J. Clim.*, **26**, 6471–6505, https://doi.org/10.1175/JCLI-D-12-00505.1.

Roy, I., R. G. Tedeschi, and M. Collins, 2019: ENSO teleconnections to the Indian summer monsoon under changing climate. *Int. J. Climatol.*, **39**, 3031–3042, https://doi.org/10.1002/joc.5999.

Schneider, T., T. Bischoff, and G. H. Haug, 2014: Migrations and dynamics of the intertropical convergence zone. *Nature*, **513**, 45–53, https://doi.org/10.1038/nature13636.

Seth, A., A. Giannini, M. Rojas, S. A. Rauscher, S. Bordoni, D. Singh, and S. J. Camargo, 2019: Monsoon responses to climate changes—connecting past, present and future. *Curr. Clim. Change Rep.*, **5**, 63–79, https://doi.org/10.1007/s40641-019-00125-y.

Shekhar, R., and W. R. Boos, 2017: Weakening and Shifting of the Saharan Shallow Meridional Circulation during Wet Years of the West African Monsoon. *J. Clim.*, **30**, 7399–7422, https://doi.org/10.1175/JCLI-D-16-0696.1.

Sooraj, K. P., P. Terray, S. Masson, and J. Crétat, 2019: Modulations of the Indian summer monsoon by the hot subtropical deserts: insights from coupled sensitivity experiments. *Clim. Dyn.*, **52**, 4527–4555, https://doi.org/10.1007/s00382-018-4396-8.

Su, J., R. Zhang, T. Li, X. Rong, J.-S. Kug, and C.-C. Hong, 2010: Causes of the El Niño and La Niña Amplitude Asymmetry in the Equatorial Eastern Pacific. *J. Clim.*, **23**, 605–617, https://doi.org/10.1175/2009JCLI2894.1.

Sultan, B., and S. Janicot, 2003: The West African Monsoon Dynamics. Part II: The “Preonset” and “Onset” of the Summer Monsoon. *J. Clim.*, **16**, 3407–3427, https://doi.org/10.1175/1520-0442(2003)016<3407:TWAMDP>2.0.CO;2.

——, and M. Gaetani, 2016: Agriculture in West Africa in the Twenty-First Century: Climate Change and Impacts Scenarios, and Potential for Adaptation. *Front. Plant Sci.*, **7**.

Sylla, M. B., P. M. Nikiema, P. Gibba, I. Kebe, and N. A. B. Klutse, 2016: Climate Change over West Africa: Recent Trends and Future Projections. *Adaptation to Climate Change and Variability in Rural West Africa*, J.A. Yaro and J. Hesselberg, Eds., Springer International Publishing, 25–40.

Tanaka, H. L., N. Ishizaki, and A. Kitoh, 2004: Trend and interannual variability of Walker, monsoon and Hadley circulations defined by velocity potential in the upper troposphere. *Tellus A*, **56**, 250–269, https://doi.org/10.1111/j.1600-0870.2004.00049.x.

Tao, W., X. Kong, L. Yong, Y. Wang, and D. Danhong, 2022: Diversity of Northwest Pacific atmospheric circulation anomalies during post-ENSO summer. *Front. Environ. Sci.*, **10**, 1068155, https://doi.org/10.3389/fenvs.2022.1068155.

Terray, P., K. P. Sooraj, S. Masson, R. P. M. Krishna, G. Samson, and A. G. Prajeesh, 2018: Towards a realistic simulation of boreal summer tropical rainfall climatology in state-of-the-art coupled models: role of the background snow-free land albedo. *Clim. Dyn.*, **50**, 3413–3439, https://doi.org/10.1007/s00382-017-3812-9.

Terray, P., K. P. Sooraj, S. Masson, and C. Prodhomme, 2021: Anatomy of the Indian Summer Monsoon and ENSO relationships in state-of-the-art CGCMs: role of the tropical Indian Ocean. *Clim. Dyn.*, **56**, 329–356, https://doi.org/10.1007/s00382-020-05484-z.

Timmermann, A., and Coauthors, 2018: El Niño–Southern Oscillation complexity. *Nature*, **559**, 535–545, https://doi.org/10.1038/s41586-018-0252-6.

Trenberth, K. E., G. W. Branstator, D. Karoly, A. Kumar, N.-C. Lau, and C. Ropelewski, 1998: Progress during TOGA in understanding and modeling global teleconnections associated with tropical sea surface temperatures. *J. Geophys. Res. Oceans*, **103**, 14291–14324, https://doi.org/10.1029/97JC01444.

Wang, B., R. Wu, and K.-M. Lau, 2001: Interannual Variability of the Asian Summer Monsoon: Contrasts between the Indian and the Western North Pacific–East Asian Monsoons. *J. Clim.*, **14**, 4073–4090, https://doi.org/10.1175/1520-0442(2001)014<4073:IVOTAS>2.0.CO;2.

Wei, N., L. Zhou, Y. Dai, G. Xia, and W. Hua, 2017: Observational evidence for desert amplification using multiple satellite datasets. *Sci. Rep.*, **7**, 2043, https://doi.org/10.1038/s41598-017-02064-w.

Yan, Y., R. Lu, and C. Li, 2019: Relationship between the Future Projections of Sahel Rainfall and the Simulation Biases of Present South Asian and Western North Pacific Rainfall in Summer. *J. Clim.*, **32**, 1327–1343, https://doi.org/10.1175/JCLI-D-17-0846.1.

Zelinka, M. D., T. A. Myers, D. T. McCoy, S. Po-Chedley, P. M. Caldwell, P. Ceppi, S. A. Klein, and K. E. Taylor, 2020: Causes of Higher Climate Sensitivity in CMIP6 Models.

Geophys. Res. Lett., **47**, e2019GL085782, https://doi.org/10.1029/2019GL085782.

Zhang, Z., and G. Li, 2022: Uncertainty in the projected changes of Sahel summer rainfall under global warming in CMIP5 and CMIP6 multi-model ensembles. *Clim. Dyn.*, **59**, 1–19, https://doi.org/10.1007/s00382-022-06284-3.

4.3 To go further: the case of future Indian rainfall

You've probably got an idea of what's to come in this section, haven't you? That's right! We're going to try and extend the study we did on Sahel monsoon projections to the case of India. Indeed, numerous studies have examined the nature of the uncertainty in the projections of the Indian monsoon, and have shown that it is mainly linked to its dynamic response (G. Li et al., 2017;Z. Chen et al., 2020). But, regardless of the thermodynamic or dynamic nature of the uncertainty, few studies to our knowledge have sought to answer the following question: what is the source of uncertainty in the Indian monsoon?

The projected changes of global temperature and precipitation and their related inter-model spread have been already presented and discussed in Section.4.2 (see especially Figure 2 in the article above). We now go straight to the results of the MCAs exploring the links between the Indian rainfall change and global temperatures and rainfall changes across the models.

Note that based on the results of the Section 2 of Chapter 4, we will also use a single member per model in the case of India, assuming that the inter-model spread of Indian rainfall change as computed from the difference between two 35-years is mainly dominated by uncertainty in models' response to external forcings, a feature already observed for the historical changes in Chapter 3.

4.3.1 Global temperature and precipitation changes associated with Indian rainfall projected change

Firstly, the domain we're working on is slightly truncated compared with the Indian domain we used in Chapter 3. Indeed, when using the same domain as in Chapter 3 to compute the MCAs shown in Figure.4.1, few points in the north-eastern part of the domain monopolized the entire covariance due to their very large inter-model spread (not shown), and made the pattern of change over India less robust and dependent on whether or not we scaled by global temperature increases. We therefore slightly reduced the domain on its eastern edge (85°E instead of 95°E) to ignore the few over-represented points, making the MCAs independent of global warming ($r=0.15$, $p\text{-value}<0.30$) as in the case of the Sahel.

The heterogeneous maps of the ISM rainfall change (Figure.4.1ac) show a relatively homogeneous intensification of rainfall in the core monsoon zone (corresponding to the position of the monsoon trough) in both the MCAs involving the global temperature and rainfall changes, still with lower values on the edges of the domain . The statistics for the two MCAs are presented in Table.4.1. First, they show values significantly lower than those found in the case of Sahel projected change, with, in particular, a lower explained variance of the change in monsoon rainfall : 26% of ISM change in both cases (temperature and precipitation changes)here compared to 50% in the case of Sahel changes. The explanation lies in the fact that in both cases, the first two MCA modes are almost "degenerated" in terms of explained variance: the first explains 26% in both cases, while

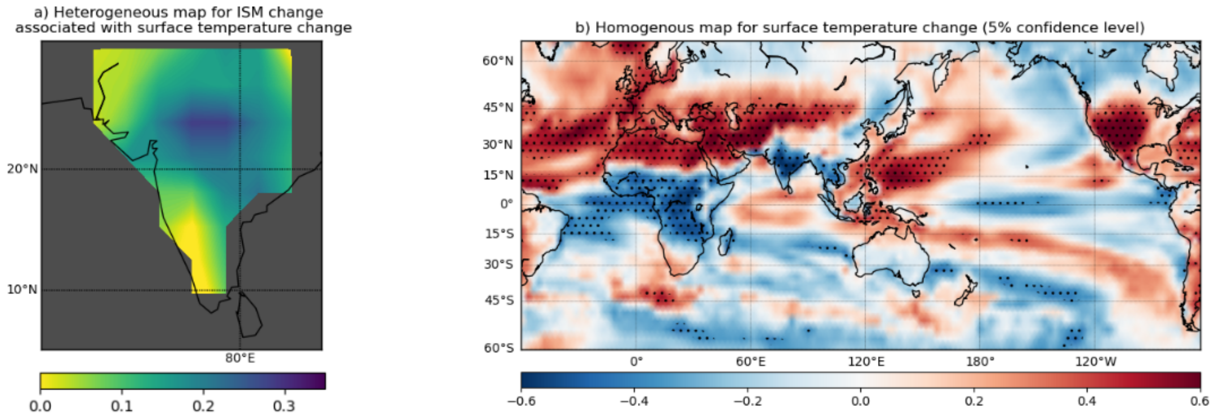

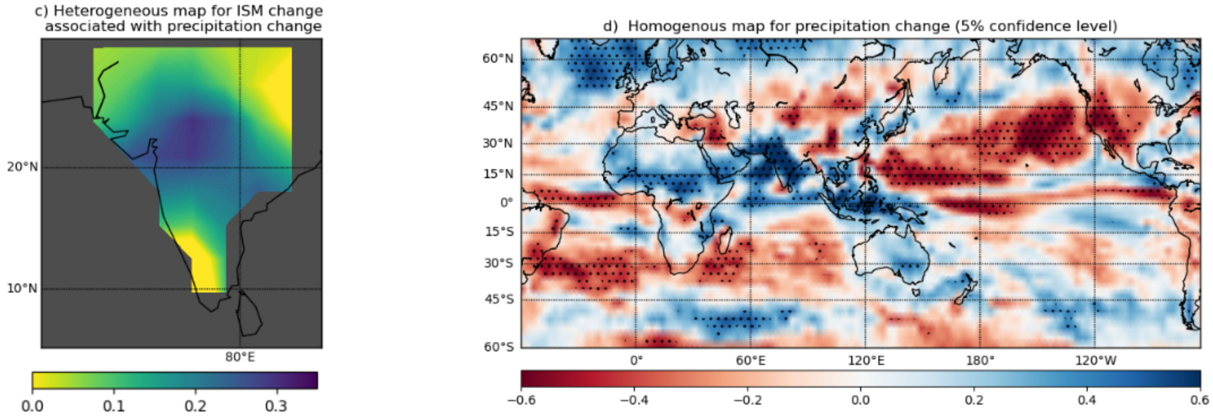

Figure 4.1: Heterogeneous (a) and homogeneous (b) maps obtained from the MCA analysis performed between the scaled surface temperature change ($K.K^{-1}$) of the 32 climate models and the scaled ISM precipitation changes ($mm.d^{-1}.K^{-1}$) in the same 32 models. (c) and (d): same as (a) and (b) for the MCA between the precipitation change ($mm.d^{-1}.K^{-1}$) and the ISM precipitation change ($mm.d^{-1}.K^{-1}$). Dotted points indicate pointwise correlations significant at the 95% confidence level between the respective Singular Variable (SV) and grid-point model series using a Student test with 31 degrees of freedom.

the second explains 24%. However, the SCF, which is a metric of relative importance of modes in a given MCA (see Section 2), is much higher in mode 1 than in mode 2 (48% vs. 24%). Consequently, this first mode is the most likely to interact with changes in precipitation and temperature on a global scale, which is why we will be working on the leading MCA mode.

The correlations between the SV series of the main MCA modes of precipitation and temperature changes (Figure.4.1b and Figure.4.1d) and those of the ISM rainfall change (Figure.4.1 and Figure.4.1) highlight strong statistical relationships within the two pairs of fields (0.84 and 0.72 respectively; see Table.4.1). This suggests the existence of regional or global ocean-atmosphere and/or land-atmosphere couplings that modulate ISM rainfall projections across the models. Consistently, there is a significant linear relationship between the SV series featuring the main homogeneous precipitation and temperature change patterns (Figure.4.1b and Figure.4.1d) associated with ISM precipitation changes (r=0.65, see Table.4.1) in the two MCAs.

Figure.4.1b shows a strong meridional temperature gradient between the desert zones of the Northern Hemisphere, from the Sahara to Pakistan, and the tropical Africa-Atlantic region. This pattern is reminiscent of the meridional global temperature gradient identified for the Sahel monsoon. Yet, it is much more localized on continental regions: it is not significant

Table 4.1: Statistics associated with the MCAs between surface temperature or precipitation changes with ISM rainfall change shown in Figure.4.1. All correlations in the last four columns are significant at the 99% confidence level.

	Explained variances of ISM rainfall change	SCF	NC	Correlation between SV of global change and SV of ISM rainfall change (Figure.4.1ac)	Correlation between the SV of global precipitation and surface temperature change (Figure.4.1bd)
Global Pr change with ISM rainfall change	27%	48 %	17 %	0,84	0,65
Global Ts change with ISM rainfall change	25 %	43 %	15 %	0.72	

over the Pacific and particularly marked over the desertic African-Arabia region. Furthermore, the important role of desert areas in the Northern Hemisphere is also highlighted by the high significance of the eastern United States, which was not identified in the literature as connected to the Indian monsoon region, but is highlighted because it is also an arid zone. Samson et al., 2017, Terray et al., 2018 and Sooraj et al., 2019, using different coupled models and experimental setups, showed that the desert surface albedo to the west of India is crucial for Indian monsoon biases and for modulating the India rainfall changes, challenging the view that the monsoon circulation at mid- and upper-levels is driving the monsoon. Our present results seem to extend this finding for Indian monsoon projections, although we are not looking directly at albedo but at its effect on surface temperatures. We may also wonder why these arid regions are not an important source of inter-model spread for the Indian monsoon during the historical period covered in Chapter 3. We conjecture that this factor becomes increasingly important and discriminant for a strong anthropogenic forcing only. This hypothesis can be tested by analyzing a scenario with moderate emissions such as the SSP2-4.5, but this interesting extension of the present results is left for a future study. We also note that this meridional temperature gradient extends over the Atlantic Ocean, with warm anomalies between 15°N and 45°N and cold anomalies in the equatorial Atlantic. The cold anomalies both over land and ocean could be linked to the atmospheric response of the Sahel Monsoon due to the increased meridional SLP gradient driven by the strong warm temperature anomalies of the adjacent arid regions if we consider the continental response to be the dominant signal, which is likely due to its extension and consistency (cf. arid zone of the United States). This interpretation is also consistent with albedo perturbation's experiments analyzed in Sooraj et al., 2019. Note that there are also strong warm anomalies in the NWP extending towards the maritime continent, and cold anomalies along the equatorial Pacific, suggesting the emergence of an anomalous La Niña-like horseshoe SST pattern in the tropical Pacific as in the historical period (see Chapter 3), . The significance in the tropical Pacific is nevertheless very low compared to the regional meridional temperature gradient driven by the arid regions to the west

From the rainfall perspective, Figure.4.1d shows a large coherent rainfall modulation extending from the entire Sahel band to the Indian subcontinent and the adjacent oceanic regions (North Arabian Sea and

Bay of Bengal). Along the equatorial Atlantic, Figure.4.1d displays a band of decreasing rainfall which could be associated with the increase in Sahel rainfall. In this case, it could be interpreted as a shift of the ITCZ, which would be consistent with the surface temperature gradient and its effect on the surface circulation mediated by the associated SLP gradient described above. In this sense, we see that the uncertainties of the Sahelian and Indian monsoons' future changes appear to be partly linked, since their precipitation modulation is evolving hand in hand in response to the regional temperature changes. The Pacific is marked by a strong negative precipitation anomaly covering the entire northern part of the basin. This is consistent with the forcing (e.g. strengthening) of the Northern Pacific subtropical anticyclone in response to the enhanced monsoon rainfall to its west over India and West Africa Rodwell and Hoskins, 2001) and the zonal planetary-scale perspective of the Northern summer monsoons (T.-C. Chen, 2003). Furthermore, Terray et al., 2018 have demonstrated that such a zonal response in the Northern Subtropics can be triggered by temperature changes over the arid regions of Africa and Asia. Along the Equator, we note a precipitation dipole between the maritime continent and the western equatorial Pacific, which is consistent with the temperature signature indicating a strengthening of the SST gradient across the Pacific as during the historical period.

4.3.2 Performance of averaged temperature indices in explaining ISM rainfall change

In view of the consistent results between the two MCAs of Figure.4.1 and in order to remain within the same framework as the Sahel study, we have chosen to focus on temperature change indices. We compute an African temperature gradient index, solely based on continental temperature, because of the consistency of the signals for desert areas highlighted above, and the uniform response over tropical Africa (see Table.4.2 for definition). To compare the sources of uncertainties of the Sahelian and Indian monsoons we also use the inter-hemispheric temperature gradient change we used in the previous section.

We can see that the African temperature gradient is very strongly correlated with the ISM change spread (Figure.4.2b). Note that if we extend the regression line in Figure.4.2b to a zero change in the African temperature gradient, i.e., uniform warming, this relationship predicts a drier ISM, which is consistent with the results of Chou and Neelin, 2004, Held and Soden, 2006 describing a stabilization of the tropical troposphere. The inter-hemispheric gradient also shows a significant relationship (Figure.4.2a) , albeit much weaker, which illustrates that the sources of inter-model spread are not exactly the same in the case of the Sahelian and Indian monsoons, as expected from the MCAs. The Sahel monsoon uncertainty across the models is mainly driven by the interhemispheric temperature gradient, while the Indian monsoon is mainly associated with zonal contrasts driven by the uncertainty of the temperature over the arid regions across the models. Nevertheless, there is a strong correlation between the two temperature gradient indices we used, as illustrated in Figure.4.2c, which is to be expected since the African temperature gradient is a subset of the inter-hemispheric gradient. Consequently, although the sources of uncertainty for the two monsoons are different,

Table 4.2: Definition of the indices used in the present study. < > stands for spatial averaging over the subscript domain. The superscript indicates the surface type or the atmospheric level over which the average is taken, when relevant.

Regions/Indices	Domain and variable used when relevant
ISM	[65E;85E], [7N;30N]
Inter-hemispheric temperature gradient	*<Ts >[15N;90N],[0;360] - <Ts >[90S;15N],[0;360]*
Tropical Africa temperature change	*<Ts >[15S;15N],[20W;40E] land only*
Deserts temperature change	*<Ts >[20N;45N],[20W;65E] land only*
Africa temperature gradient change	Deserts temperature change - Tropical Africa temperature change

they are strongly related, and the uncertainties of the Sahelian and Indian monsoons are therefore also strongly related. This is corroborated by the strong and positive correlation between the SVs of Indian and Sahelian precipitation changes (r=0.58, not shown), which illustrates that the uncertainties of these two monsoons across the models are partly related.

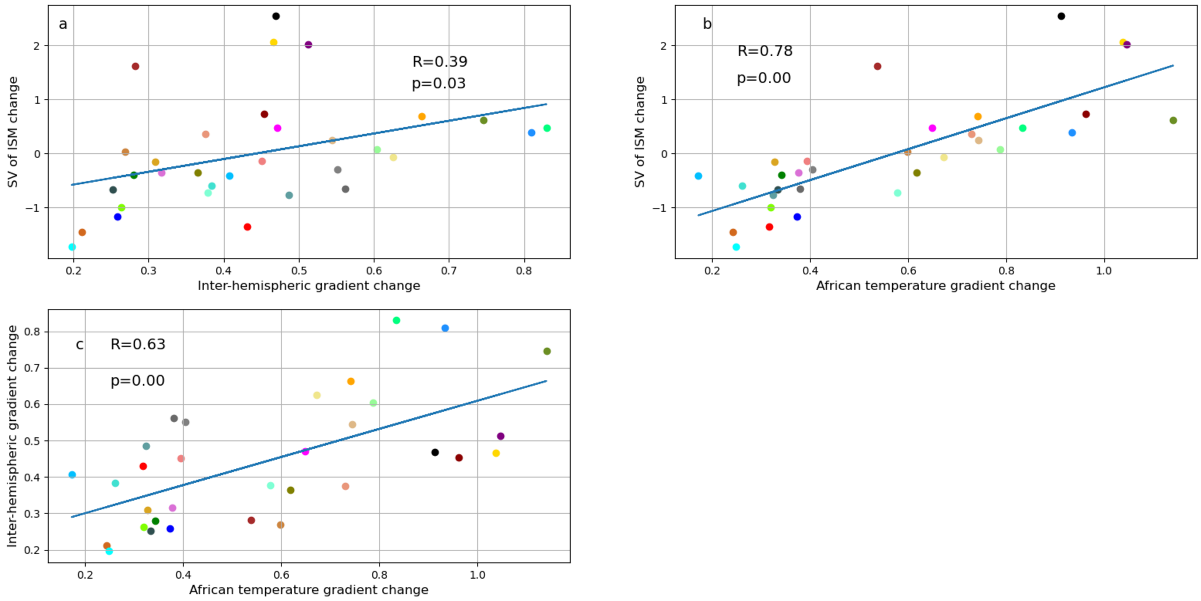

Figure 4.2: Scatterplots of SV of ISM change ($mm.d^{-1}.K^{-1}$, from Figure.2.1a), respectively, with (a) inter-hemispheric temperature change ($K.K^{-1}$), (b) African temperature gradient change ($K.K^{-1}$). (c) Scatterplot between inter-hemispheric temperature change ($K.K^{-1}$) and African gradient change ($K.K^{-1}$). The definition of each index can be found in Table.4.2. All model series are scaled by the global temperature change in each model. The correlation and its associated P-value for each pair of model series are indicated in each panel.

As the source of uncertainty we have highlighted is a large-scale factor, we can also look individually at the two regions that make it up, namely the deserts and tropical Africa, to see if we can also explain the inter-model spread of ISM precipitation change by more regional mechanisms and solely by the role of the deserts suggested above.

As we see in Figure.4.3, and as expected from the MCAs and previous results, both components of the large scale temperature index have strong and largely significant correlations with inter-model spread of ISM precipitation change (Figure.4.3ab). However, we note the presence of two outliers in the relationship linking the deserts to the Indian monsoon, one of which is MIROC6, which has already been mentioned as having significant and very serious problems with continental temperatures in CMIP6 (Kamworapan et al., 2021). We thus propose to remove them in our analysis. Note these models are not outliers in terms of the large-scale index of African temperature gradient (Figure.4.2b), and removing them does not affect the relationship we highlighted earlier (r=0.79 vs r=0.78 previously, not shown), probably because they affect most land areas. Similarly, the relationship linking tropical African temperatures to the ISM is unchanged when removing the two models, as shown in Figure.4.3bd. However, Figure.4.3c now highlights a very strong relationship between the desert response and the ISM which is almost equivalent to that of the African large-scale index. This result raises an alternative and more local view of the sources of uncertainty of the ISM response. This regional subtropical index is in line with previous studies showing the existence of relationships between subtropical deserts and the Indian monsoon and a planetary-scale zonal perspective of the monsoons (Rodwell and Hoskins, 1996;Rodwell and Hoskins, 2001;T.-C. Chen, 2003;Sooraj et al., 2019), which is in sharp contrast with the Hadley and energetic perspectives (Schneider et al., 2014) well adapted to the Sahel monsoon. Here we extend these contrasting views and results to model projections. These different results also show the complexity of the relationships that can drive the ISM response and uncertainties across the models, and the possible interaction between factors of different spatial scales, given that the large-scale and regional visions we have proposed coexist and mutually interact.

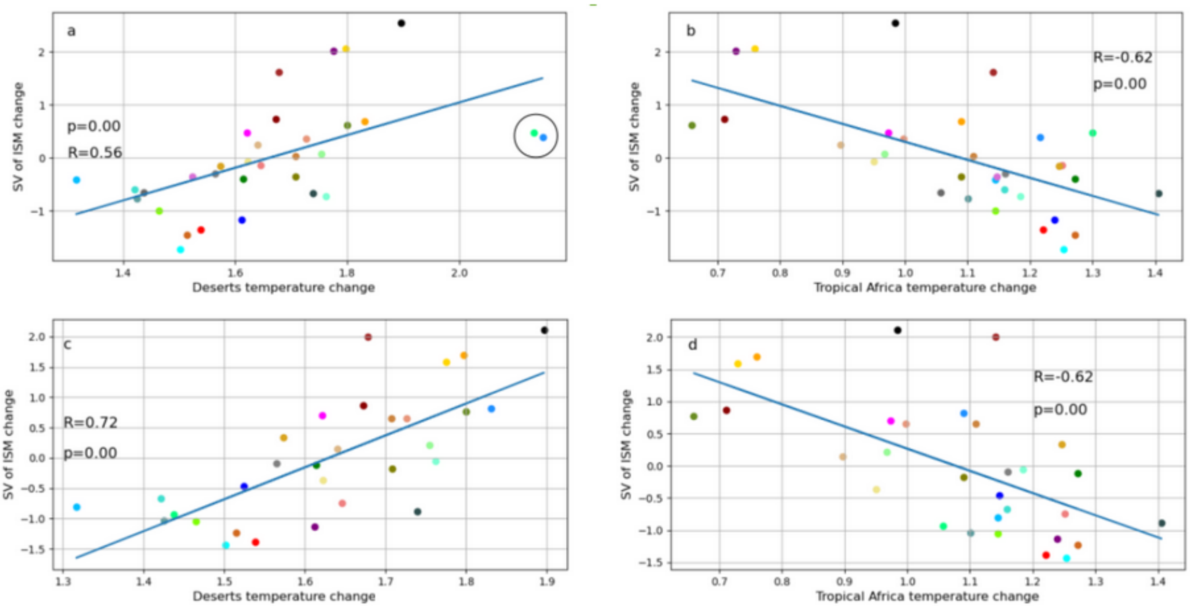

Figure 4.3: Scatterplots of SV of ISM change ($mm.d^{-1}.K^{-1}$, from Figure.4.1a), respectively, with (a) deserts temperature change ($K.K^{-1}$), (b) tropical Africa temperature change ($K.K^{-1}$). (c) and (d), same as (a) an (b) but without the circled outliers. The definition of each index can be found in Table 2. All model series are scaled by the global temperature change in each model. The correlation and its associated P-value for each pair of model series are indicated in each panel.

4.3.3 Atmospheric mechanisms of future ISM rainfall uncertainties

In light of the previous results, and in order to go beyond the statistical relationship, we propose here to further explore the physical mechanisms that can link the inter-model spread of the temperature response of subtropical deserts to the inter-model spread of the ISM rainfall change.

Figure.4.4a shows that models with anomalous warm response over subtropical deserts consistently exhibit a low-pressure anomaly at their surface, corresponding to an intensification of the Heat Low extending from the Sahara to the Arabian Peninsula. Associated with this reinforced Heat Low, there is a significant intensification of winds coming from the Gulf of Guinea. Note that, the extended Sahelian region we studied previously covers the western part of the North African monsoon as defined in AR6. The latter indeed extends almost to the East Coast of Africa (see Fig.1.11). Consistent with these strengthened monsoon winds circulating on the southern flank of the Heat Low in agreement with geostrophic balance, Figure.4.4b demonstrates enhanced precipitation between 10°N and 15°N, indicating an intensification of the African monsoon due to increased moisture flux inland. Next, the winds encounter the Ethiopian Highlands around 40°E, where the generation of topographic waves is observed. The winds deflect northward upon reaching the massif and then deflect southward once the relief is surpassed. The winds, reinforced by the Heat Low, then reach the Indian Ocean and interact with the Indian monsoon circulation by reinforcing the Somali jet off the African coast and the zonal flux over the Arabian Sea. The strong acceleration of surface winds over the northeastern part of the Indian Ocean also increases the moisture flux towards India, resulting in increased precipitation over the western Arabian Sea, on the windward side of the Ghats, and along the monsoon trough in the Indo-Gangetic plains (Figure.4.4a), as illustrated in Figure.4.4b. This mechanism is very similar to the one linking the Sahelian and Indian monsoons with the Heat Low in previous studies (Rodwell and Hoskins, 1996;Biasutti, 2019). However, it has never been explored in projections and is likely to explain the strong relationship between the uncertainties of Sahelian and Indian precipitation changes that we have already mentioned (r=0.58). Thus, whether considering the large-scale index (African gradient) or a more regional perspective (deserts), we find the intertwined fate of the Indian and Sahelian monsoons and the contrasting, but not contradicting, effects of the "meridional" and "zonal" large-scale theories of the monsoons (T.-C. Chen, 2003;Schneider et al., 2014).

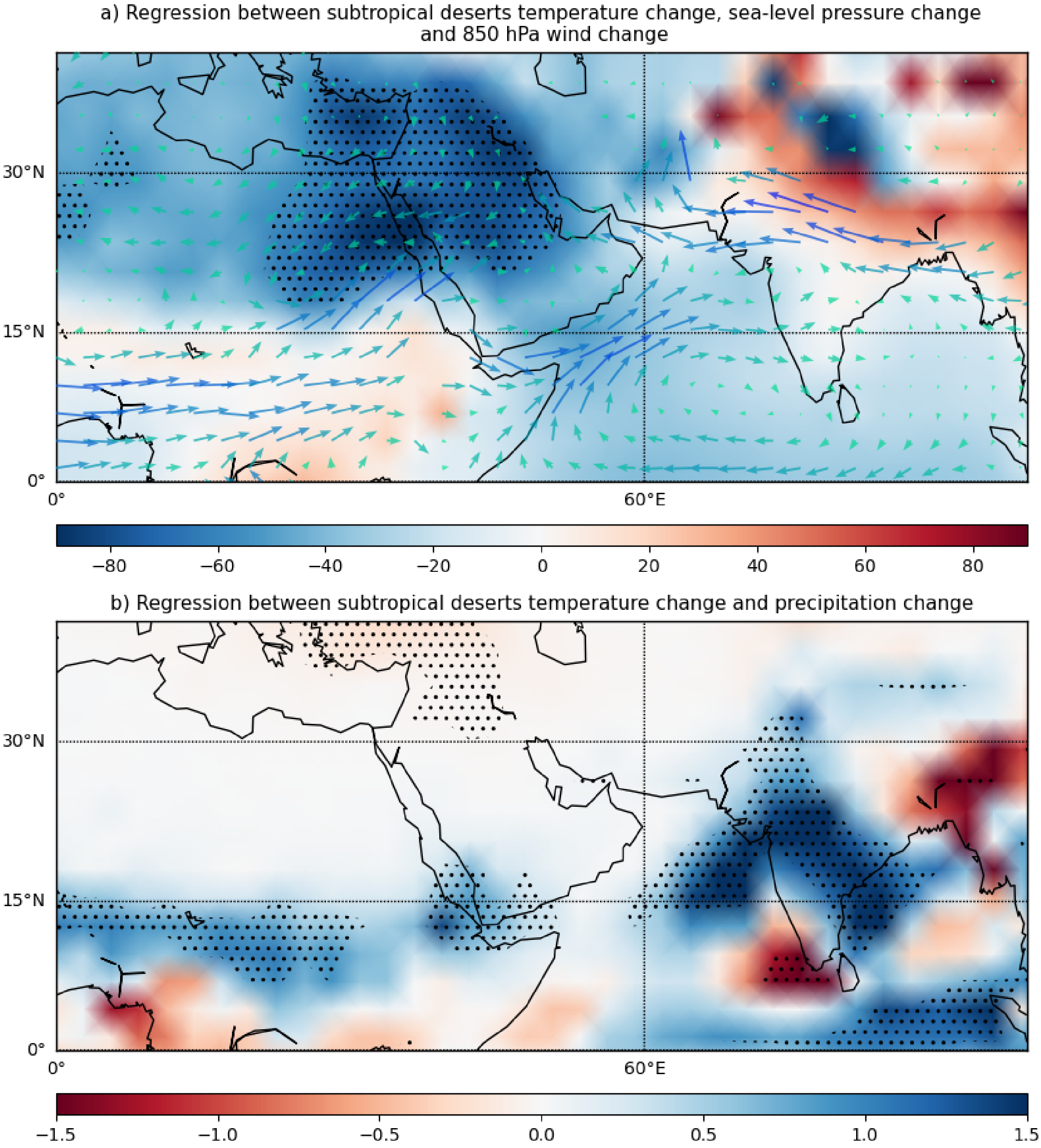

Figure 4.4: Inter-model regressions against the subtropical deserts temperature change of (a): changes in SLP (color shaded, $Pa.K^{-2}$) and wind at 850 hPa (vectors, $m.s^{-1}.K^{-2}$); (b) precipitation change (color shaded : 0,1 $mm.d^{-1}.K^{-2}$). The colors of the arrows vary from blue to green according to the intensity of the wind speed for readability. On panel (a)dotted points indicate grid-points where the regression with SLP change is significant at the 95% confidence level. On panel (b), dotted points indicate grid-points where the regression with precipitation change is significant at the 95% confidence level.

CONCLUSIONS AND PERSPECTIVES

Conclusion and perspectives | 5

Precipitation, through the water cycle, is an integral part of the energy balance of the climate system. However, mankind is modifying the latter by introducing anthropogenic forcings, notably greenhouse gasses. As a result, precipitation is changing so that the energy balance of the atmosphere (or surface) remains in equilibrium (O'Gorman et al., 2012;Allan et al., 2020). On a global scale and based mainly on theoretical arguments, this translates into a ~3%/°C increase in precipitation (Held and Soden, 2006). This is less than the increase in specific humidity directly expected from global warming through the Clausius-Clapeyron relationship which amounts to ~7%/°C. This difference must reflect, among other things, a slowdown in circulation, particularly in the Tropics (Ma et al., 2018), but this differential signal between specific humidity and precipitation is not yet clearly seen in the observations (Wentz et al., 2007). Moreover, this response of precipitation to anthropogenic forcing is highly variable from one region to another (Allan et al., 2020), and in this thesis we have focused on the case of the monsoons over India and the Sahel. In these regions, monsoon rainfall accounts for around 80% of annual precipitation for populations living mainly on rain-fed agriculture. Projecting monsoon changes is therefore essential for these regions, which could be home to more than two billion people by 2100. In line with paleoclimatic studies that link monsoon precipitation to global mean surface temperature, notably with stronger monsoons during interglacial eras such as the mid-Holocene (Mohapatra et al., 2018;Braconnot et al., 2019), models project an average increase in Sahelian and Indian monsoon precipitation by the end of the 21st century (Z. Chen et al., 2020). However, there is a significant inter-model spread regarding the amplitude of this change for both monsoons. This is described as the model uncertainty of the monsoon response to climate change, and it tends to persist in each successive generation of models and to increase with higher-emission scenarios (Monerie et al., 2017;Katzenberger et al., 2021;Z. Zhang and Li, 2022). Many studies have focused on deciphering the origins of this inter-model spread and this uncertainty has been predominantly attributed to the dynamic response of the monsoon, i.e., how its circulation changes, while the mean response is mainly explained by thermodynamics factors (Z. Chen et al., 2020;Monerie et al., 2021;Z. Zhang and Li, 2022). Other studies have sought to determine whether model errors during the current period, known as biases, could explain this inter-model spread in monsoon responses (G. Li et al., 2017;Yan et al., 2019). Finally, some studies have sought relationships between model uncertainties directly within the projections, in order to identify whether certain model disagreements at the local or global scale could have an impact on the monsoons (Park et al., 2015;Z. Zhang and Li, 2022). This is the backdrop to our studies, whose mission is to describe the response to anthropogenic forcing of the Indian and Sahelian monsoons, but more specifically to revisit the origins of their uncertainties, both during the historical period and in climate projections of the next 80 years, using simulations from climate models that participated in the last CMIP6 exercise. In doing so, we also illustrate how difficult it is to design robust precipitation Emergent Constraints (ECs), e.g. to find a physically-explainable relationship between model simulations of a past climate variable and projections of a future climate variable (Ferguglia et al., 2023).

The first introductory chapter set the stage and reminded us of the fundamentals about the climate system, monsoons and climate models. In Chapter 2, you were introduced to the data and simulations we used, as well as the arsenal of statistical methods to explore them, especially the jungle of CMIP6 multi-model and multi-member simulations. Chapter 3 was dedicated to the historical period, where we provided explanations or insights into the origins of the inter-model spread in summer precipitation responses over the Sahel and India. Chapter 4 was the futuristic alter ego of the previous chapter, where we provided explanations for the uncertainties in the precipitation response in the Sahel and India within the context of a high-emission scenario. Finally, for dessert, this last chapter offers a synthesis of the obtained results, seasoned with perspectives fueled by our findings and the new questions they have raised.

5.1 Synthesis

5.1.1 The historical period

Based on a set of 34 coupled models that participated to the CMIP6 exercise, we showed that both the mean response and the inter-model spread of the Indian Summer Monsoon (ISM) rainfall intensify towards the end of the historical period, and that this intensification is primarily driven by the response of the climate models to various external forcings rather than internal variability. This has also been an opportunity to highlight uncertainty within observed datasets of Indian precipitation, which demonstrate certain limitations of observational data. We then confirmed that the uncertainty in the historical response of the Indian monsoon is linked to the uncertainty in its dynamical response, primarily the meridional component of its circulation.

Biases in tropical precipitation and surface temperature, both locally and remotely, were explored as potential influencers of the forced ISM change over the historical period. However, the analysis reveals no significant relationship with local (i.e. around and in India) variables and thus expands the investigation to remote links. Precipitation and temperature biases in the tropical Pacific have emerged as key modulators of the inter-model spread of the historical ISM response during the 20th century. In particular, the bias in the equatorial Pacific SST gradient drives the inter-model spread of the ISM response, with models exhibiting El Niño-like biases also producing El Niño-like changes over the historical period. This bias in the SST gradient affects the monsoon response by influencing the Walker circulation and generating upper tropospheric anomalies that propagate as Rossby waves, ultimately impacting the atmospheric circulation and precipitation patterns in the Indo-Pacific region. These findings shed light on the complex dynamics underlying the uncertainty in historical response of the Indian monsoon. They also underline their links to remote biases in the tropical Pacific rather than with local or regional factors such as the land-sea contrast in the Indian region or the warming of the Indian Ocean (Hurley and Boos, 2013;Levine et al., 2013;Annamalai et al., 2017). Overall, these results are consistent with recent investigations by Wilks et al.(2022) which show that both the simulated enhanced warming in the eastern equatorial Pacific and the inter-model spread associated with this warming by CMIP5 and CMIP6 models can be partly explained by local model biases in the tropical Pacific.

We then replicated the same study on the historical response of Sahelian precipitation. Similar to India, both the mean response and inter-model spread also increase towards the end of the period. Based on the previous results and investigations on SSP5-8.5 projections discussed below, we assume that this inter-model spread is primarily due to the different forced responses of the models rather than internal variability.

Again and surprisingly, the statistical analysis shows that local biases do not seem to have an impact on the inter-model spread of the historical response of Sahel precipitation. However, the study of remote biases reveals strong statistical relationships, primarily with a large cold SST bias in the Tropics, particularly marked in the Indian Ocean. We then identify that the spread of the historical Sahel response is also strongly linked to the historical response of the inter-hemispheric temperature gradient, without being able to link it unambiguously to temperature or precipitation biases across the models. Thus, unlike the case of India, we have not been able to find a physically-explained relationship between biases and a remote response of temperature or precipitation that would influence the Sahel through teleconnections. However, we did find patterns related to inter-hemispheric temperature gradient in both the historical period and the high-emission scenario. In any case note that this additional analysis is preliminary and was conducted for illustrative purposes and would warrant further investigation, which is left to my successors, or perhaps myself after my vacations!

5.1.2 Projections under SSP5-8.5 scenario

Based on 32 coupled models from the CMIP6 exercise, we then focused on the uncertainties of future Sahelian precipitation changes in the context of global warming. The analysis reveals that there are strong uncertainties in the precipitation projections for the Sahel by the end of the 21st century (2064-2099) among the CMIP6 models, with one-third of the models indicating a decrease in precipitation, while the remaining two-thirds show an intensification. These findings align with previous studies that have also highlighted the uncertainty in Sahelian precipitation projections (Monerie et al., 2017;Biasutti, 2019;Z. Zhang and Li, 2022). As we did for the historical period, we showed that the inter-model spread of Sahel monsoon rainfall intensifies over time, and that this intensification is primarily driven by the various forced responses of the climate models rather than internal variability.

The analysis then explored the sources of these inter-model spread in Sahelian rainfall changes using MCAs based on global precipitation and temperature changes as simulated by the recent CMIP6 models.

The MCAs reveal strong correlations between changes in tropical precipitation, large-scale surface temperature, and Sahelian rainfall during boreal summer. These findings suggest that coupled and remote ocean-atmosphere and land-atmosphere interactions contribute to the uncertainty in Sahelian precipitation projections. The study further investigates two major sources of uncertainty: the change in inter-hemispheric temperature gradient and the future mean-state of the equatorial Pacific, which have already been detected, respectively, as potential drivers of the inter-model spread responses of the Sahelian and Indian monsoons during the historical period (see section a) above). The inter-hemispheric gradient influences the northward shift of the ITCZ and the strength of the West African Westerly Jet (WAWJ; Pu and Cook, 2010), both of which impact precipitation in the Sahel. The mean-state of the equatorial Pacific affects the Walker circulation, which influences upper-level divergence, vertical zonal wind shear and local convection over the Sahel. Additionally, changes in SST in the equatorial Pacific modulate the intensity and position of tropospheric warming, leading to tropical and extratropical waves which modulate the strength of the Tropical Easterly Jet (TEJ) over the Sahel. Finally, attribution methods and bilinear regression techniques show that we can explain 62% of the inter-model spread of Sahel rainfall change with these two sources of uncertainty: 40% with the changes in the inter-hemispheric temperature gradient and 22% with the changes in the equatorial Pacific.

We then replicated the same study on the projected change of ISM precipitation based on the previous results and investigations on SSP5-8.5 projections, and we assume again that this inter-model spread is primarily due to the different forced responses of the models rather than internal variability. The MCAs reveal a strong relationship between the surface temperature response over the northern subtropical deserts, from the Sahara to Pakistan, and the ISM response. This temperature response is also found to be important for the African monsoon responses. This result is consistent with previous studies that have shown the existence of a connection between subtropical deserts and ISM, supporting the concept of a planetary-scale zonal perspective of the monsoons (Rodwell and Hoskins, 1996;Rodwell and Hoskins, 2001;Samson et al., 2017;Terray et al., 2018). We then explore the mechanisms underlying these relationships between deserts and the ISM across the models in the projections. We demonstrate that models exhibiting greater surface warming over northern subtropical deserts tend to have a strengthened heat low over the region. The winds around the heat low strengthen through geostrophy, increasing the moisture flux towards the Sahel and intensifying the ISM circulation, particularly the Somali jet off the African coast and the monsoon winds over the Arabian Sea, which also enhance the moisture flux towards India and consequently increase ISM precipitation. This mechanism is very similar to the one linking the Heat Low to the Indian and Sahelian monsoons, but here in the context of projections (Biasutti, 2019;Samson et al., 2017), illustrating the intertwined uncertainties linking the two monsoons.

5.2 Perspectives

And now what? This is the final question we will ask in this manuscript, where we will open up possibilities and try to provide good (or bad) ideas to extend our studies.

5.2.1 Cross-perspective on our studies: the link between biases, historical and projected monsoon responses

Concerning the fate of the Sahelian monsoon over the historical period (section 3, chapter 3), we identified the importance of a large bias in tropical SSTs. While we were not able to explore more thoroughly how these biases are linked to the inter-model spread of the historical response, we propose here to check first whether this relationship persists over time, i.e. in future projections. This is indeed a necessary condition for implementing robust techniques such as emergent constraints to reduce model uncertainty (G. Li et al., 2017;Ferguglia et al., 2023).

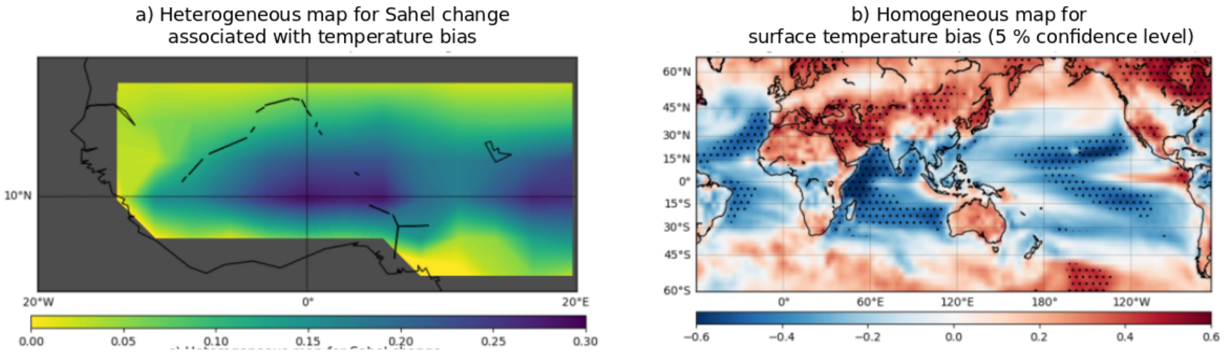
a) Heterogeneous map for Sahel change associated with temperature bias

b) Homogeneous map for surface temperature bias (5 % confidence level)

Figure 5.1: (a) Heterogeneous and (b) homogeneous maps obtained from the MCA performed between the projected Sahel precipitation changes and the surface temperature bias during boreal summer across the models. Dotted points indicate significant point-wise correlations at the 95% confidence level between the respective SV and the grid-point series across the models.

Therefore, we replicate the analysis we conducted in Section 3 of Chapter 3, but this time we examine the relationships between biases and the future response of the Sahelian monsoon (Fig.5.1). The MCA mode of projected Sahel rainfall change shows a homogeneous modulation of response (Fig.5.1a), while historical change showed mainly a modulation of precipitation over the western Sahel (see figure 2 of Section 3 from Chapter 3). However, we observe that for both historical and projected Sahel rainfall change, the associated patterns of temperature biases are very similar and are, in particular, dominated by negative SST anomalies over the Indian Ocean, tropical Atlantic and tropical Pacific. Warm biases in the Mediterranean Sea, Arabic Peninsula and Pakistan seem to be also associated with future changes of the Sahel monsoon (Fig. 5.1). The correlation between the corresponding singular vectors (SVs) of temperature biases is highly significant (r=0.56, p-value<0.01), thereby confirming the relative similarity between the two temperature bias patterns. Consequently, the potential role of cold SST biases in the Indian and Pacific oceans in particular, and tropical Atlantic to a lesser extent, appear to be fairly stationary for the Sahelian monsoon, making it particularly interesting for developing a possible robust EC for reducing the inter-model spread associated with this monsoon system.

What about the ISM? In the historical period, we emphasized the importance of the bias in the equatorial Pacific SST gradient, but does this bias stand the test of time (Ferguglia et al., 2023)? As for the Sahel, we also reproduce the MCAs we carried out in Section 2 of Chapter 3, but this time we focus on the link between biases and the projected response of the ISM. Afterwards, I promise we are almost done with the MCAs!

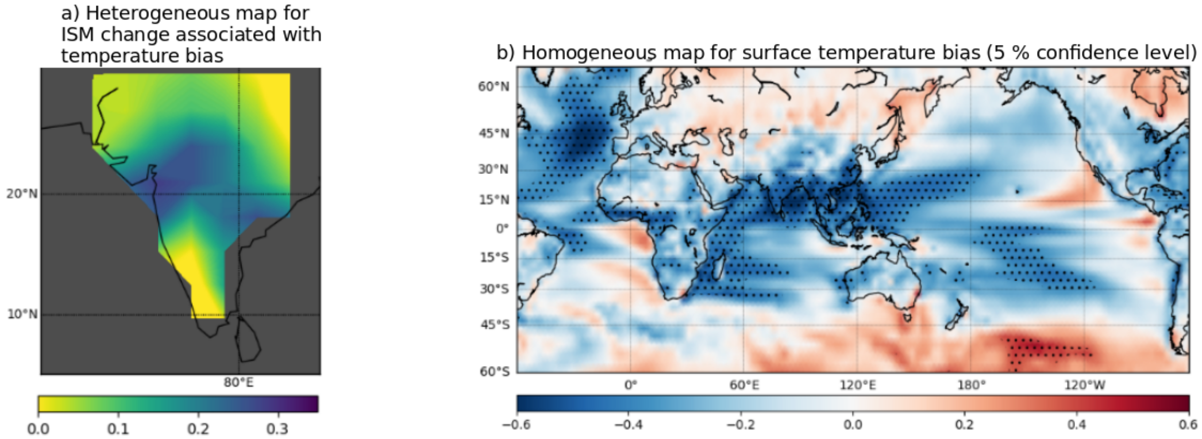

Figure 5.2: (a) Heterogeneous and (b) homogeneous maps obtained from the MCA performed between the projected ISM precipitation changes and the surface temperature bias during boreal summer. Dotted points indicate significant point-wise correlations at the 95% confidence level between the respective SV and gridpoint series across the models.

The biases that are linked to the ISM rainfall spread in the future are concentrated in the western Indian Ocean, north Atlantic and the western tropical and south Pacific (Figure 5.2b). This pattern is very different from the tropical Pacific pattern identified in Chapter 3 , which highlights the role of the equatorial Pacific SST gradient (See Figure 6 in Section 2 from Chapter 3). The relationship we identified in the historical period is therefore not stationary and cannot be used to reduce the uncertainties in the ISM projections. To explain this failure, we have first to reckon that the domain used for the ISM region is slightly different from the one used over the historical period, for the reasons explained in Chapter 4. This may partly explain the discrepancies. This is also in agreement with certain hypotheses we made in Section 2 of Chapter 3. Indeed, we suggested that the Ocean Dynamical Thermostat (ODT, Clement et al., 1996) was one of the mechanisms at play in the bias-ISM response during the historical period. However, this mechanism is a rapid response of the Pacific Ocean (Heede et al., 2020) that weakens as the Pacific thermocline warms (Luo et al., 2017). Thus, in a scenario of high emissions and consequently strong warming of the Pacific thermocline, this mechanism potentially becomes negligible, which is consistent with the absence of a relationship between equatorial SST gradient bias and the projected ISM precipitation change. Finally, it is interesting to observe that the surface temperature biases over the subtropical deserts are not emerging in Fig.5.2.b while the inter-model spread of surface temperature changes are tightly associated with the future ISM changes across the models (see Figure 1 in Section 3 from Chapter 4). This illustrates again the challenges associated with the design of robust ECs, at least for the ISM, which may be partly due to the role of aerosols, which are important during the historical period, but much less so in the high-emission scenario, which is dominated by GHGs forcing. This raises the question of whether using DAMIP (The Detection and Attribution Model Intercomparison Project;

Gillett et al., 2016) to build robust EC from the historical period is a better strategy, than using standard historical simulations to better constrain the future model uncertainties which are tightly linked to the GHGs by design.

However, the temperature biases associated with the ISM projections (Figure 5.2b) exhibit significant similarities to the ones we highlighted for the future response of the Sahelian monsoon over the oceans (Fig.5.1b). We confirm this by correlating the SVs of temperature biases derived from these MCAs and show that there is a very strong and highly significant correlation (r=0.82, p-value<0.01). Therefore, it seems that a common bias in the current SST climatology, in particular in terms of homogeneous biases in the western indian ocean and off-equatorial Pacific and Atlantic oceans, is associated with the inter-model spread of the projections of both monsoons, in addition to being stationary in the case of the Sahel. This result, along with those from Section 3 of Chapter 4, seems to indicate that the inter-model spreads of both the Sahel and Indian monsoons share an intertwined fate in the projections. It is therefore crucial to better understand the physical origins, if any, of this statistical relationship in order to reduce the uncertainty in the monsoon projections.

To take this a step further, we could for example look at the radiative balance of the Tropics and/or clouds parameters and distributions, as these variables have the potential to generate tropic-scale patterns, and are known to be a major source of uncertainty in climate models (Vial et al., 2013;Schneider et al., 2017). Recent studies have proposed a semi-automatic analysis of the impact of these parameters in one coupled model (Peatier et al., 2022). Such analysis applied to different coupled models could help diagnosing the origins of the SST bias across the models. This could also be of interest in understanding the inter-model spread of the inter-hemispheric gradient or the response of subtropical deserts, which we have highlighted as key parameters for monsoon projection. Finally, it can be very instructive to look at the dependence of these various relationships with respect to anthropogenic forcing and the DAMIP simulations can be again very useful for this task.

5.2.2 Another step towards understanding physics.

Next, we propose here a few avenues for further exploration of the physical mechanisms underlying the relationships we have highlighted in this thesis.

Variability and forced responses

In our studies, most of the mechanisms linking model responses to anthropogenic forcing that we have identified are similar to well-known existing interannual to decadal variability mechanisms. More generally, we can question the link between interannual variability and the response to anthropogenic forcings in climate models, in the sense that model performance in simulating variability could be a critical parameter for constraining uncertainties in the models' forced response. To explore this type of question, we could employ the same MCA-based methodology but focus on variability biases instead of mean-state biases across the models.

For example, given the relationships we have highlighted between future precipitation uncertainty in the Sahel (or alternatively historical ISM precipitation) and the equatorial Pacific, it could be that the relationships are even more pronounced when considering the inter-model spread of simulated variability.

The impact of land feedback

In chapter 4, we were able to attribute more than 60% of the inter-model spread of Sahel rainfall projected change to the response of the inter-hemispheric gradient and the equatorial Pacific. The partial correlation maps (Appendix 2, Fig.S3) show an absence of significant links between Sahel rainfall change and temperatures, outside of the Sahel itself, when excluding the linear dependance to the two explaining factors. Consequently, it appears that there are no other remote relationships and the logical next step would be to investigate whether local factors such soil's humidity, which can sustain a local temperature-evaporation rainfall feedback, could explain the remaining residual inter-model spread of Sahel rainfall. Since land-atmosphere feedback is known to be a strong modulator of the forced response of the Sahelian monsoon (Kucharski et al., 2013), studying them could prove valuable in reducing the uncertainty of the forced response, notably by using the LUMIP simulations (Lawrence et al., 2016).

Single model exploration

Using a single coupled model, such as the in-house IPSL model for example, to conduct nudging or sensitivity experiments could also enable us to verify some of the mechanisms proposed in different chapters and delve further into their understanding. For example, to test our results from Chapters 3 and 4, we could use a pacemaker experiment on the equatorial Pacific. In a pacemaker experiment, climate is forced into a specific region while being allowed to evolve freely elsewhere (Deser et al., 2017). So, by prescribing different SST gradients in the equatorial Pacific, we could study the effect of its historical or future changes, in particular on the response of the ISM and Sahelian monsoons, and verify the teleconnection mechanisms we propose. Such experiments have been successful to analyze teleconnections from the Tropical Pacific and to demonstrate the role of the tropical Pacific in the global warming hiatus during the period 1998–2013 (Kosaka and Xie, 2013;Deser et al., 2017). Working with a single model (or at least less models) would also allow us to assess more easily moisture budgets, something that is not feasible with large model ensembles due to the lack of certain variables, or high-frequency outputs, for evaluating all the terms of the water budget for many models in the CMIP databases.

5.2.3 Another step towards improving the models

In this thesis, we stated several times that the aim was to reduce uncertainties in monsoon projections. This also involves improving the models, and we propose here a few ways of transferring our results, which have identified certain critical points, into constraints for the models development. Let's get down to the modelers' business and get our hands dirty! Intrinsic uncertainty of climate models comes to a large extent from the fact that many aspects of the climate are represented with parameterizations that summarize the effect of missing processes, such as those happening on scales that are smaller than the model grid sizes. The parameterizations in turn involve many parameters, sometimes poorly estimated from observations, that have to be calibrated. Among many steps, the development of climate models thus implies constraining these parameters. For this, modelers typically use a few metrics based on large-scale variables such as near-global mean temperature, summer Arctic sea-ice extent (e.g. Mauritsen and Roeckner, 2020; Hourdin et al., 2017; Schmidt et al., 2017; Senior et al., 2020; Mignot et al., 2021). Our results suggest that specific patterns such as the tropical SST bias identified to influence both ISM and Sahelian monsoon projections should be added to this list of target metrics. At Institut Pierre Simon Laplace (IPSL), the climate modeling group is currently testing a semi-automatic tuning protocol for the forthcoming IPSL-CM7 model, following Hourdin et al (2023). Highlighting such impactful bias patterns is, thus, particularly timely. However, this will lead only to a reduction of the inter-model spread if other modeling groups use the same kind of semi-automatic tuning. This is obviously a huge collective task for the future!

5.2.4 Other futures, other monsoons

Finally, we have studied the responses of the monsoons for the high-emission scenario, but it would also be interesting to verify if the relationships we have found are applicable to scenarios where anthropogenic forcing is lower, in order to assess their robustness and the validity of potential ECs. Another possibility would be to test our methodology on other monsoons. In particular, the South American monsoon could be an interesting system to study, as there is considerable uncertainty regarding its future in high-emission scenarios, with just as many models projecting an increase as a decrease in precipitation (Z. Chen et al., 2020). Constraining these projections could be essential insofar as this region constitutes a biodiversity hotspot and also because drier conditions, can push the rainforest ecosystem past a tipping point, beyond which there is rapid land surface degradation, a sharp reduction in atmospheric moisture recycling, an increase in the fraction of precipitation that runs off, and a further shift towards a drier climate (Staal et al., 2015;Ruiz-Vásquez et al., 2020).

APPENDIX

Supplementary materials 6

6.1 Supplementary material of *Intermodel spread of historical Indian monsoon rainfall change in CMIP6: The role of the tropical Pacific mean-state.*

Intermodel spread of historical Indian monsoon rainfall change in CMIP6: The role of the tropical Pacific mean-state

Marcellin Guilbert[a], Pascal Terray[a], Juliette Mignot[a]

[a] *Laboratoire d'Océanographie et du Climat: Expérimentations et Approches Numériques, Institut Pierre-Simon Laplace, Sorbonne Université/CNRS/IRD/MNHN, Paris, France*

Corresponding author: Marcellin Guilbert, marcellin.guilbert@locean.ipsl.fr

S1: introduction to Maximum Covariance Analysis (MCA)

MCA aims at estimating the covariance matrix between two fields and computing the Singular Value Decomposition (SVD) of this covariance matrix by defining pairs of spatial patterns ranked in decreasing order by the Squared Covariance Fraction (SCF) they describe (Bretherton et al. 1992). Usually, the two fields are geophysical datasets with the same time dimension, but with different space dimensions, and the covariance matrix has dimensions corresponding to the space dimensions of the two fields. Here, we use a «model» dimension rather than a time dimension, as we want to describe the statistical relationships between the inter-model spread of precipitation change over India and tropical temperature or rainfall biases. Hence in our case, the « model » dimension is 34 and this corresponds to the number of CGCMs we use (see Table S1). Note that due to the small number of models compared to the "spatial" dimensions of the bias fields, the covariance matrix is singular. For this reason, we only focus on the 1st mode from the MCAs. By doing so, we also avoid the problems of interpretation related to the orthogonality constraints, inherent to the higher MCA modes (Cherry 1997).

The MCA results in « model » series and spatial patterns for both investigated fields (e.g. rainfall change over India and tropical temperature/rainfall bias). For each field, the 1st Singular variable (SV) is the projection of the original field onto the 1st singular vector of the SVD of the covariance matrix, thus it is a « model » series whose length is the number of models used (i.e. 34). The SV series are the Expansion Coefficient (time) series in the terminology of Bretherton et al. (1992).

Using the 1st SVs, two types of regression maps can be generated : the 1st homogeneous map, which is the regression map of a given input field and its 1st SV, and the 1st heterogeneous map, which is the regression map between a given input field and the 1st SV of the other field. The heterogeneous map indicates how one field can be predicted from the SV time series of the other field at the grid-point level. Here, as we are interested in how the inter-model spread of temperature (or rainfall) bias can explain the inter-model spread of ISM rainfall change, we will use homogenous maps for the biases and heterogeneous maps for ISM rainfall change (see figure 6 in the main text). Another relevant measure of the significance of the patterns obtained with MCA is given by the fraction of domain-integrated variance of each field explained by the SVs. This metric quantifies how well each pattern retrieves the variability of the original fields.

Finally, the SCF is used for comparing the relative importance of modes in a given MCA while the correlation value (r) between the 1st SVs of the two fields and the Normalized root-mean-square Covariance (NC) allows us to assess how the coupled patterns associated with a MCA mode are related (Zhang et al. 1998).

Bretherton, C. S., C. Smith, and J. M. Wallace, 1992: An intercomparison of methods for finding coupled patterns in climate data. *J. Clim.*, **5**, 541–560, https://doi.org/10.1175/1520-0442(1992)005<0541:AIOMFF>2.0.CO;2.

Cherry, S., 1997: Some comments on singular value decomposition analysis. *J. Clim.*, **10**, 1759–1761, https://doi.org/10.1175/1520-0442(1997)010<1759:SCOSVD>2.0.CO;2.

Zhang, Y., J. R. Norris, and J. M. Wallace, 1998: Seasonality of large-scale atmosphere–ocean interaction over the North Pacific. *J. Clim.*, **11**, 2473–2481, https://doi.org/10.1175/1520-0442(1998)011<2473:SOLSAO>2.0.CO;2.

Model name	Modeling center, country	Spatial atmospheric resolution (Lon x Lat)	Number of historical members used
BCC-ESM1	BCC, China	2.815° x 2.815°	3
BCC-CSM2-MR	BCC, China	1.125° x 1.125°	3
NESM3	NUIST, China	1.875° x 1.875°	5
GISS-E2-1-G	NASA-GISS, USA	2.5° x 2.0°	10
GISS-E2-1-H	NASA-GISS, USA	2.5° x 2.0°	10
NorESM2-LM	NCC, Norway	2.5° x 1.875°	3
NorCPM1	NCC, Norway	2.5° x 1.875°	1
IPSL-CM5A2-INCA	IPSL, France	3.75° x 3.75°	1
IPSL-CM6A-LR	IPSL, France	2.5° x 1.125°	32
HadGEM3-GC31-LL	MOHC, UK	1.875° x 1.25°	4
E3SM-1-1	E3SM-Project, DOE, USA	1.0° x 1.0°	1
CanESM5	CCCma, Canada	2.8125° x 2.8125°	25
CNRM-ESM2-1	CNRM-CERFACS, France	1.4° x 1.4°	11
CNRM-CM6-1	CNRM-CERFACS, France	1.4° x 1.4°	30
FGOALS-f3-L	CAS, China	1.0° x 1.0°	2
CAMS-CSM1-0	CAMS, China	1.125° x 1.125°	2
MIROC-ES2L	MIROC, Japan	2.8° x 2.8°	10

MIROC6	MIROC, Japan	1.4° x 1.4°	50
GFDL-ESM4	NOAA-GFDL, USA	1.25°x1.0°	1
GFDL-CM4	NOAA-GFDL, USA	1.25°x1.0°	1
MRI-ESM2-0	MRI, Japan	1.125° x 1.125°	5
CAS-ESM2-0	CAS,China	1.4° x 1.4°	2
INM-CM5-0	INM, Russia	2.0° x 1.5°	9
SAM0-UNICON	SNU, Korea	1.25° x 0.9375°	1
CESM2	NCAR, USA	1.25° x 0.9375°	6
CESM2-WACCM	NCAR, USA	1.25° x 0.9375°	3
ACCESS-CM2	CSIRO, Australia	1.875° x 1.25°	3
ACCESS-ESM1-5	CSIRO, Australia	1.875° x 1.25°	20
FIO-ESM2-0	FIO, China	1.875° x 1.25°	2
TaiESM1	AS-RCEC, China	1.875° x 1.25°	1
KACE-1-0-G	NIMS-KMA, Korea	1.875° x 1.25°	3
CMCC-CM2-HR4	CMCC, Italy	1.25° x 0.9375°	1
CMCC-CM2-HR4	CMCC, Italy	1.0° x 1.0°	1
MPI-ESM-1-2-HAM	Hammoz Consortium	1.875° x 1.875°	2

S2. List of CMIP6 models and simulations used in the present study.

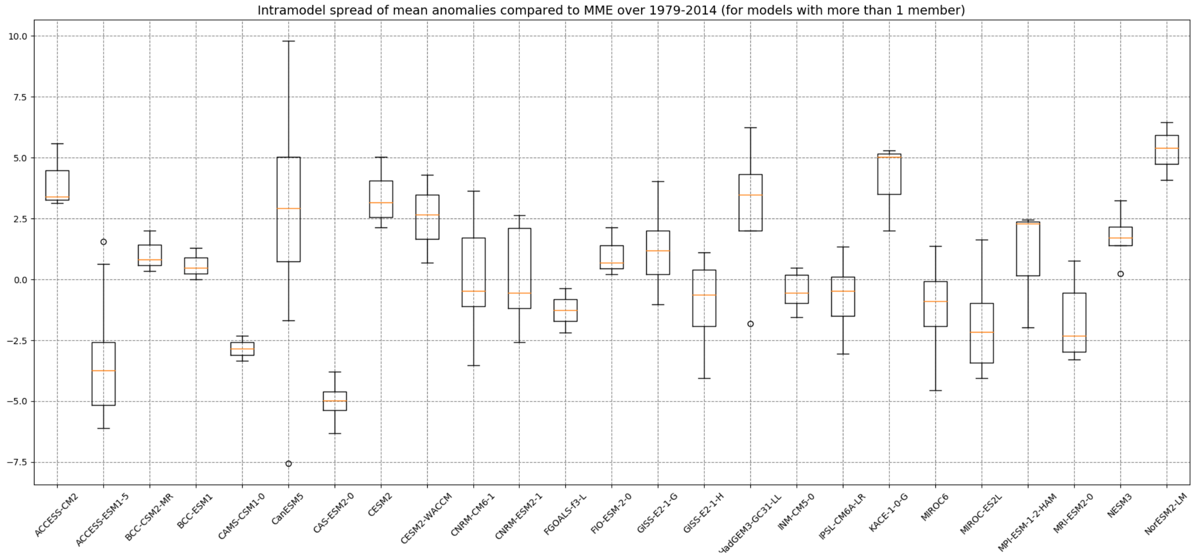

S3: boxplots of the mean anomalies over the 1979-2014 period relative to 1901-2012 of ISMR (in % as in Fig. 1) for each member for CMIP6 models with more than one member.

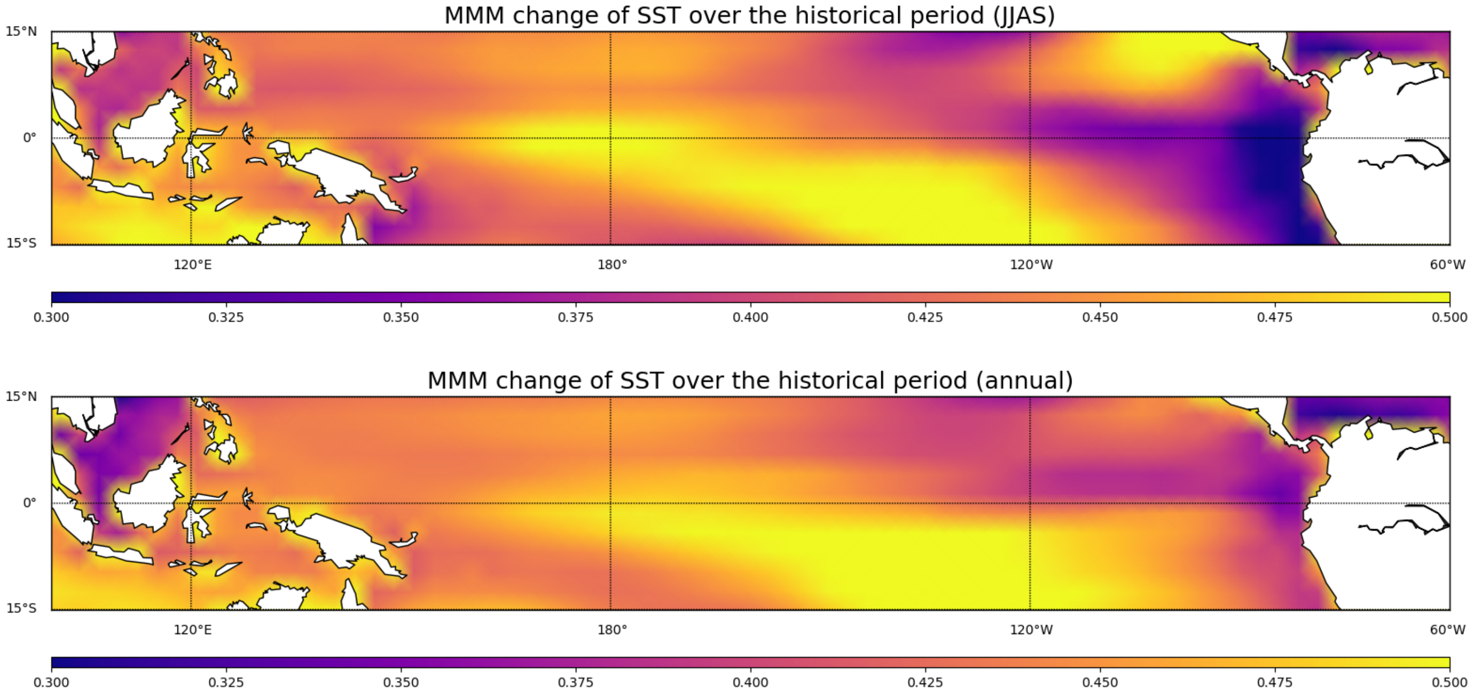

S4: MMM change of SST (K) computed over JJAS (top) and annually (bottom) in the tropical Pacific.

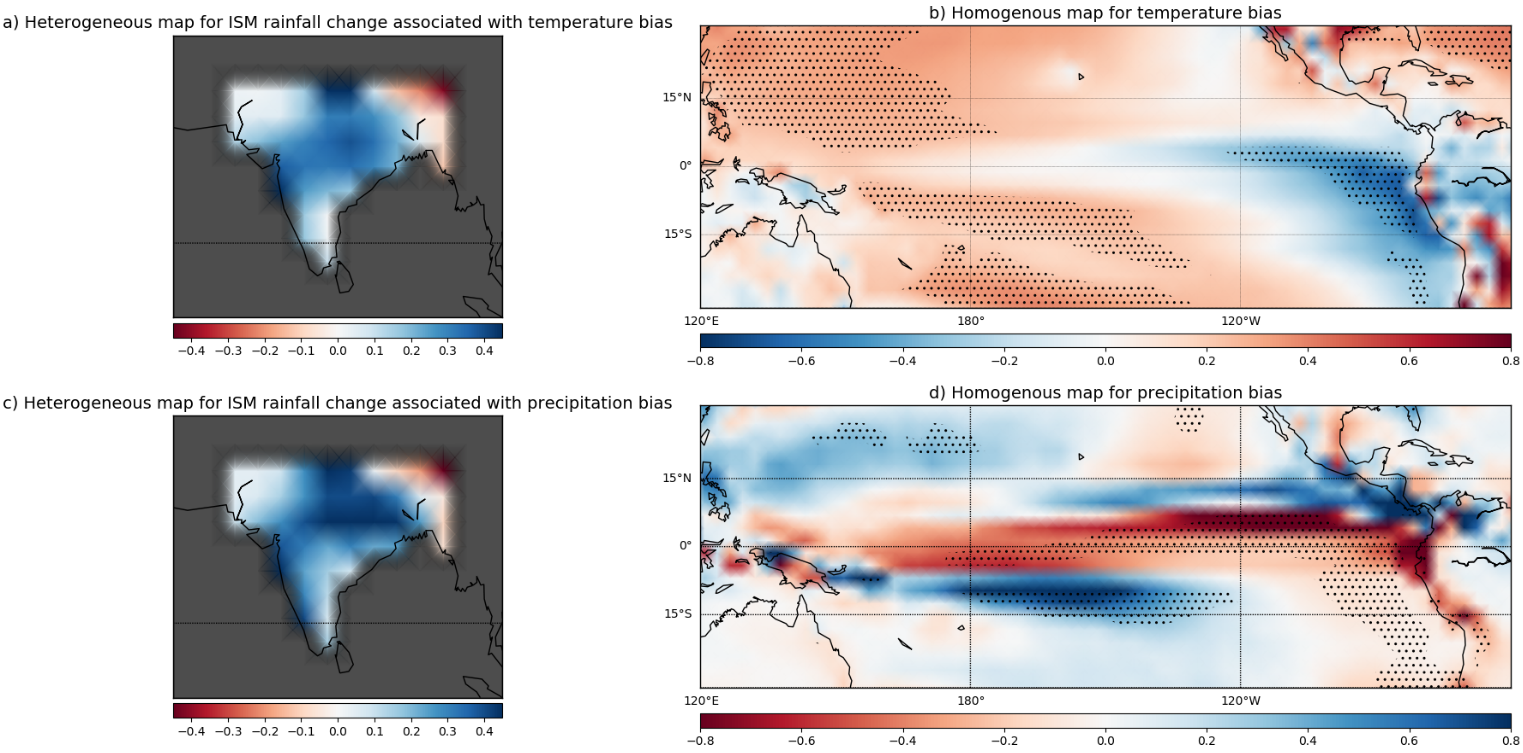
a) Heterogeneous map for ISM rainfall change associated with temperature bias

b) Homogenous map for temperature bias

c) Heterogeneous map for ISM rainfall change associated with precipitation bias

d) Homogenous map for precipitation bias

S5: MCA analyses as Fig.6 in the main text, but the domain for the temperature and precipitation bias fields in the MCAs is restricted to the tropical Pacific Ocean.

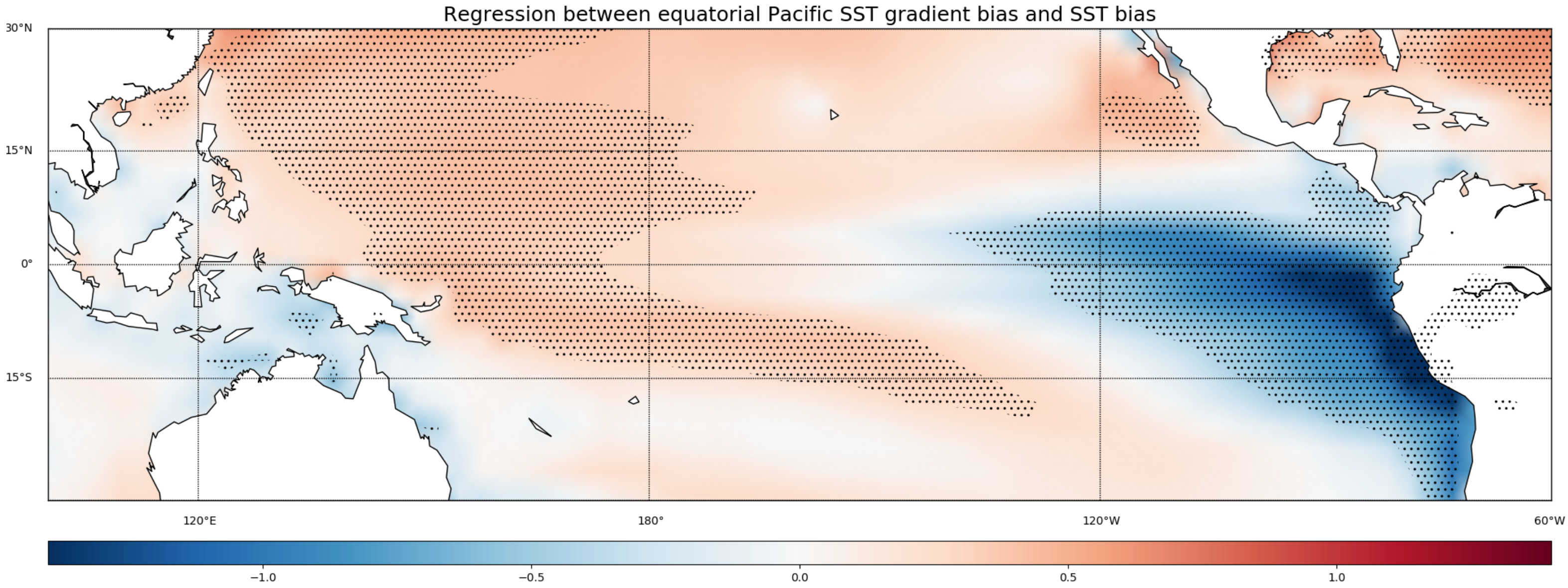

S6 : regression between the equatorial Pacific SST gradient bias and the SST bias (K.K^{-1}). Dotted points indicate significant correlations at the 95% confidence level .

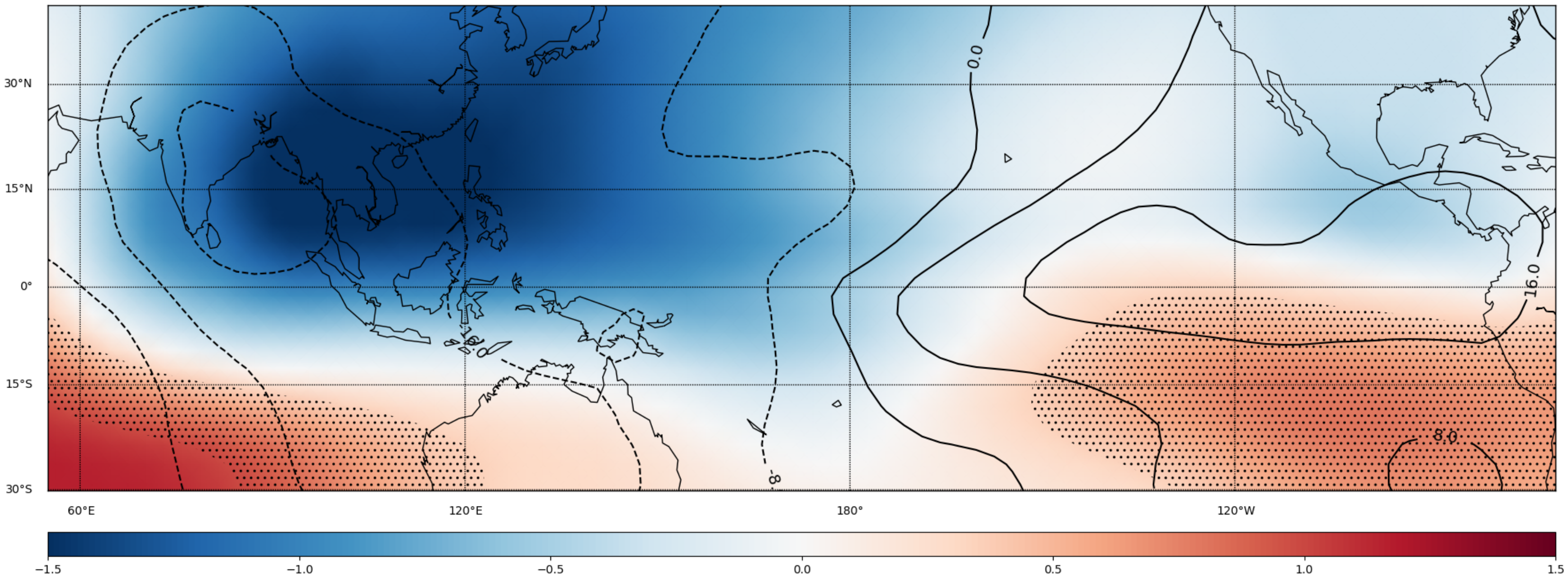

S7: MMM of velocity potential climatology (1979-2014) at 200 hPa (x10^7 $m^2.s^{-1}$, color shaded) and regression of the 200-hPa velocity potential change over the historical period onto the bias of the equatorial Pacific SST gradient bias (contour lines : 8x10^4 $m^2.s^{-1}.K^{-1}$). Note that the contour lines on the Western Pacific are not centered on the minimum of the MMM, which indicates a westward shift.

6.2 Supplementary material of *Sources of uncertainty in Sahel rainfall projections under global warming in CMIP6. Supplementary material*

Sources of uncertainty in Sahelian rainfall projections under global warming in CMIP6

Marcellin Guilbert[a], Pascal Terray[a], Juliette Mignot[a], Luther Ollier[a] , Guillaume Gastineau[a]

[a] *Laboratoire d'Océanographie et du Climat: Expérimentations et Approches Numériques, Institut Pierre-Simon Laplace, Sorbonne Université/CNRS/IRD/MNHN, Paris, France*

Corresponding author: Marcellin Guilbert, marcellin.guilbert@locean.ipsl.fr

S1: introduction to Maximum Covariance Analysis (MCA)

Maximum Covariance Analysis (MCA) is a statistical method whose aim is to find the main modes of covariability between two fields, i.e. the main modes by which they interact. In our case, we are trying to find out how Sahel rainfall change varies with global precipitation/surface temperature change in CMIP6 models. MCA aims at estimating the covariance matrix between two fields and computing the Singular Value Decomposition (SVD) of this covariance matrix by defining pairs of spatial patterns ranked in decreasing order by the Squared Covariance Fraction (SCF) they describe (Bretherton et al. 1992). Usually, the two fields are geophysical datasets with the same time dimension, but with different space dimensions, and the covariance matrix has dimensions corresponding to the space dimensions of the two fields. Here, we use a «model» dimension rather than a time dimension, as we want to describe the statistical relationships between the inter-model spread of precipitation change over the Sahel and global surface temperature and rainfall changes. Hence in our case, the « model » dimension is 32 and this corresponds to the number of CGCMs we use (see Table S1). Note that due to the small number of models compared to the “spatial” dimensions of the global change fields, the covariance matrix is singular. For this reason, we only focus on the 1st mode from the MCAs. By doing so, we also avoid the problems of interpretation related to the orthogonality constraints, inherent to the higher MCA modes (Cherry 1997).

The MCA results in « model » series and spatial patterns for both investigated fields (e.g. rainfall change over the Sahel and global temperature/rainfall change). For each field, the 1st Singular variable (SV) is the projection of the original field onto the 1st singular vector of the SVD of the covariance matrix, thus it is a « model » series whose length is the number of models used (i.e. 32). The SV series are the Expansion Coefficient (time) series in the terminology of Bretherton et al. (1992).

Using the 1st SVs, two types of regression maps can be generated : the 1st homogeneous map, which is the regression map of a given input field and its 1st SV, and the 1st heterogeneous map, which is the regression map between a given input field and the 1st SV of the other field. The heterogeneous map indicates how one field can be predicted from the SV time series of the other field at the grid-point level. Here, as we are interested in how the inter-model spread of temperature (or rainfall) change can explain the inter-model spread of Sahel rainfall change, we will use homogeneous maps for the global changes and heterogeneous maps for Sahel rainfall change (see figure 6 in the main text). Another relevant measure of the significance of the patterns obtained with MCA is given by the fraction of domain-integrated variance of each field explained by the SVs. This metric quantifies how well each pattern retrieves the variability of the original fields.

Finally, the SCF is used for comparing the relative importance of modes in a given MCA while the correlation value (r) between the 1st SVs of the two fields and the Normalized root-mean-square Covariance (NC) allows us to assess how the coupled patterns associated with a MCA mode are related (Zhang et al. 1998).

Bretherton, C. S., C. Smith, and J. M. Wallace, 1992: An intercomparison of methods for finding coupled patterns in climate data. *J. Clim.*, **5**, 541–560, https://doi.org/10.1175/1520-0442(1992)005<0541:AIOMFF>2.0.CO;2.

Cherry, S., 1997: Some comments on singular value decomposition analysis. *J. Clim.*, **10**, 1759–1761, https://doi.org/10.1175/1520-0442(1997)010<1759:SCOSVD>2.0.CO;2.

Zhang, Y., J. R. Norris, and J. M. Wallace, 1998: Seasonality of large-scale atmosphere–ocean interaction over the North Pacific. *J. Clim.*, **11**, 2473–2481, https://doi.org/10.1175/1520-0442(1998)011<2473:SOLSAO>2.0.CO;2

Model name	Modeling center, country	Spatial atmospheric resolution (Lon x Lat)	ECS	Members
BCC-CSM2-MR	BCC, China	1.125° x 1.125°	3.02	1
GISS-E2-1-G	NASA-GISS, USA	2.5° x 2.0°	2.71	1
NorESM2-LM	NCC, Norway	2.5° x 1.875°	2.56	1
IPSL-CM6A-LR	IPSL, France	2.5° x 1.125°	4.70	7
HadGEM3-GC31-LL	MOHC, UK	1.875° x 1.25°	5.55	4
HadGEM3-GC31-MM	MOHC, UK	0.83° x 0.55°	5.44	4
UKESM1-0-LL	MOHC, UK	1.875° x 1.25°	5.36	3
E3SM-1-1	E3SM-Project, DOE, USA	1.0° x 1.0°	5.31	1
CanESM5	CCCma, Canada	2.8° x 2.8°	5.64	25
CNRM-ESM2-1	CNRM-CERFACS, France	1.4° x 1.4°	4.79	6
CNRM-CM6-1	CNRM-CERFACS, France	1.4° x 1.4°	4.90	5
FGOALS-f3-L	CAS, China	1.0° x 1.0°	2.98	1

CAMS-CSM1-0	CAMS, China	1.125° x 1.125°	2.29	2
MIROC-ES2L	MIROC, Japan	2.8° x 2.8°	2.66	6
MIROC6	MIROC, Japan	1.4° x 1.4°	2.60	50
GFDL-ESM4	NOAA-GFDL, USA	1.25°x1.0°	2.65	1
GFDL-CM4	NOAA-GFDL, USA	1.25°x1.0°	3.89	1
MRI-ESM2-0	MRI, Japan	1.125° x 1.125°	3.13	1
CAS-ESM2-0	CAS,China	1.4° x 1.4°		2
INM-CM5-0	INM, Russia	2.0° x 1.5°	1.92	1
CESM2	NCAR, USA	1.25° x 0.9375°	5.15	4
CESM2-WACCM	NCAR, USA	1.25° x 0.9375°	4.68	3
ACCESS-CM2	CSIRO, Australia	1.875° x 1.25°	4.66	3
ACCESS-ESM1-5	CSIRO, Australia	1.875° x 1.25°	3.88	9
FIO-ESM2-0	FIO, China	1.875° x 1.25°		2
TaiESM1	AS-RCEC, China	1.875° x 1.25°	4.36	1
KACE-1-0-G	NIMS-KMA, Korea	1.875° x 1.25°	4.93	3
CMCC-CM2-SR5	CMCC, Italy	1.25° x 0.9375°	3.55	1
EC-Earth3	EC-Earth consortium	0.7° x 0.7°	4.26	3
MPI-ESM1-2-LR	MPI, Germany	1.875°x1.25°	3.03	2

MPI-ESM1-2-HR	MPI, Germany	0.9375° x 0.9375°	2.98	10
AWI-CM-1-1-MR	AWI, Germany	0.9375° x 0.9375°	3.16	3

S2: List of CMIP6 models and simulations used in the present study.

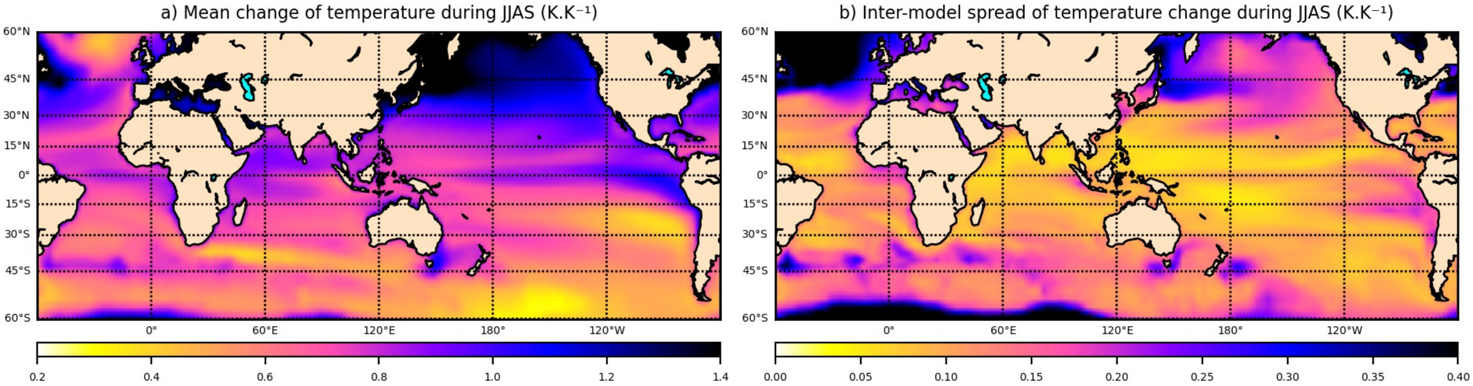

a) Mean change of temperature during JJAS (K.K⁻¹)

b) Inter-model spread of temperature change during JJAS (K.K⁻¹)

Fig. S1. (a) MMM temperature change (K.K^{-1}), (b) inter-model spread of temperature change(K.K^{-1}), during JJAS and ocean-only. Computed for the 32 CMIP6 models.

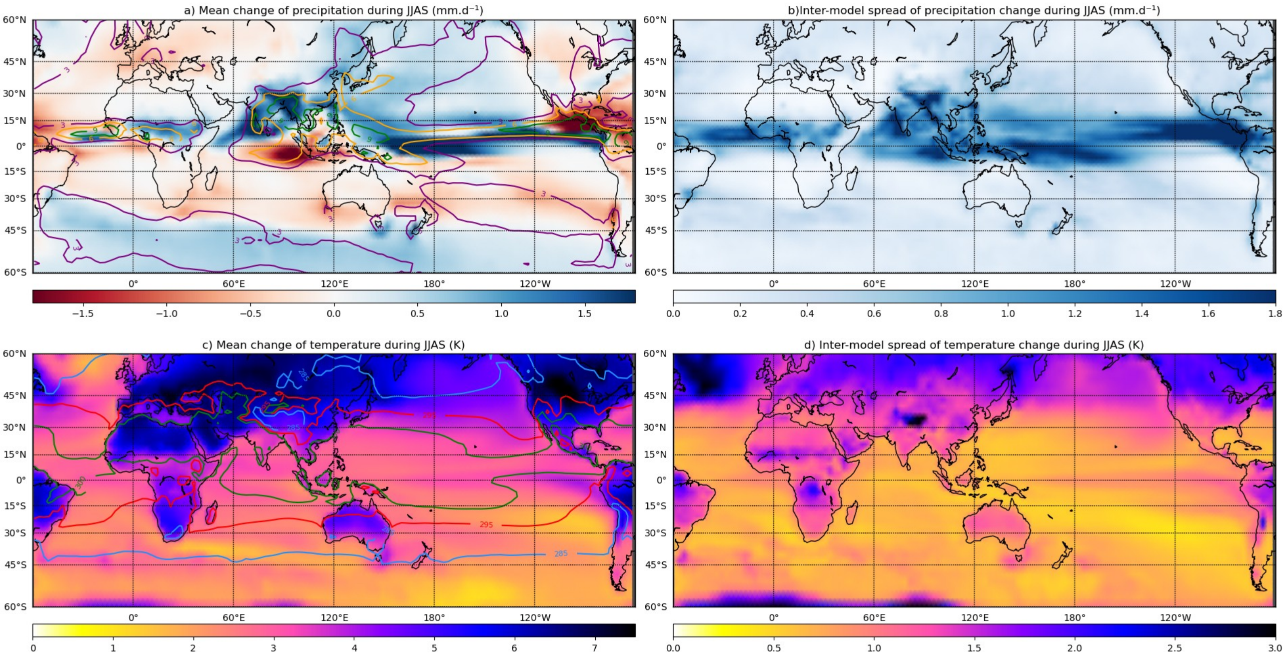

Fig.S2: same as Fig.2 but without the scaling by global temperature change.

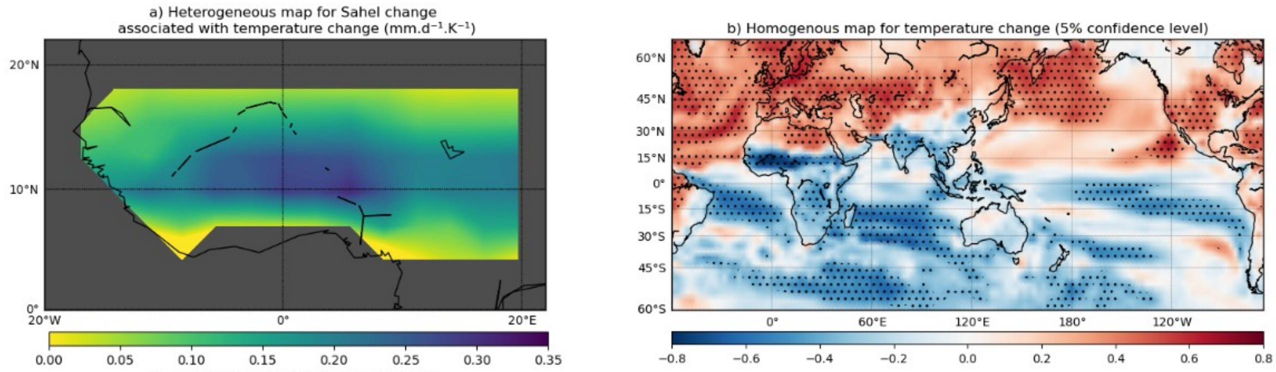

a) Heterogeneous map for Sahel change associated with temperature change (mm.d^{-1}.K^{-1})

b) Homogenous map for temperature change (5% confidence level)

c) Heterogeneous map for Sahel change associated with precipitation change (mm.d^{-1}.K^{-1})

d) Homogenous map for precipitation change (5% confidence level)

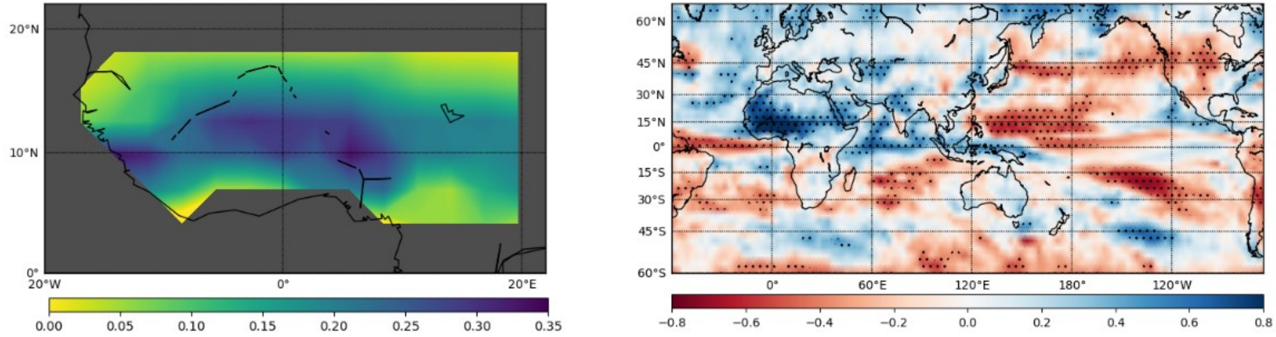

Fig.S3: same as Fig.3 but multi-members average are considered for all models with more than one member.

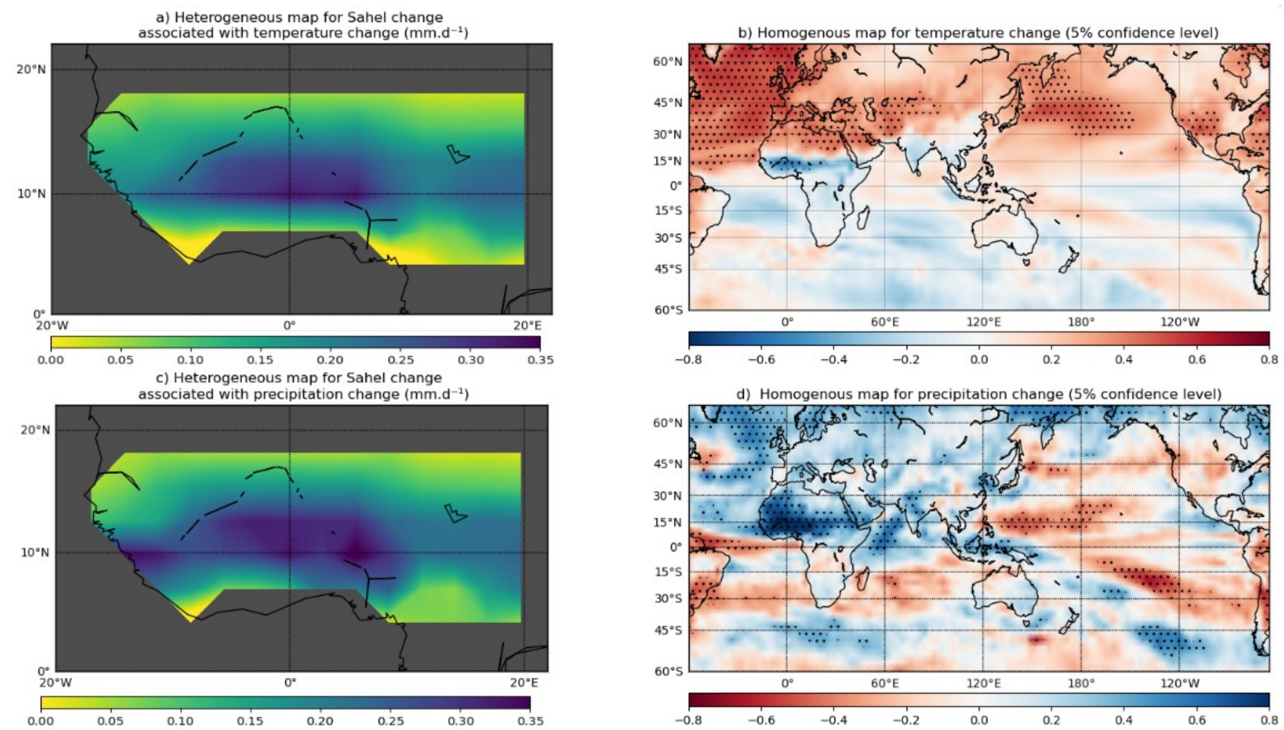

Fig.S4: same as Fig.3 but with unscaled temperature and precipitation fields.

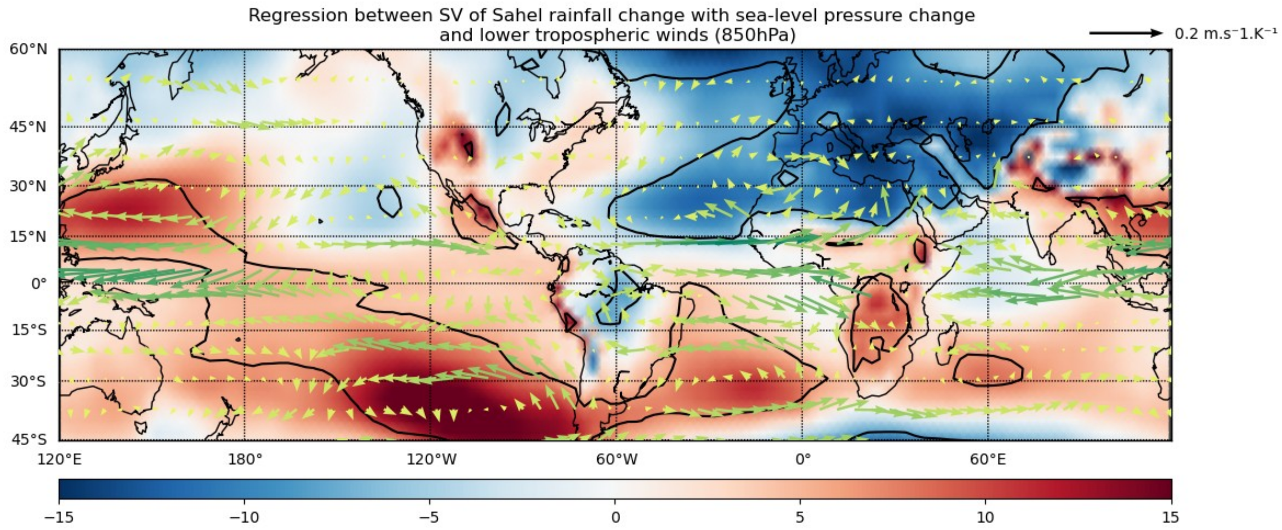

Fig.S5. Regression between SV of Sahel rainfall change with sea-level pressure change and lower-tropospheric winds (850hPa). Contour line indicate significant correlations at the 95% confidence level

a) Partial regression between SV of Sahel rainfall change and temperature change (inter-hemispheric gradient excluded)

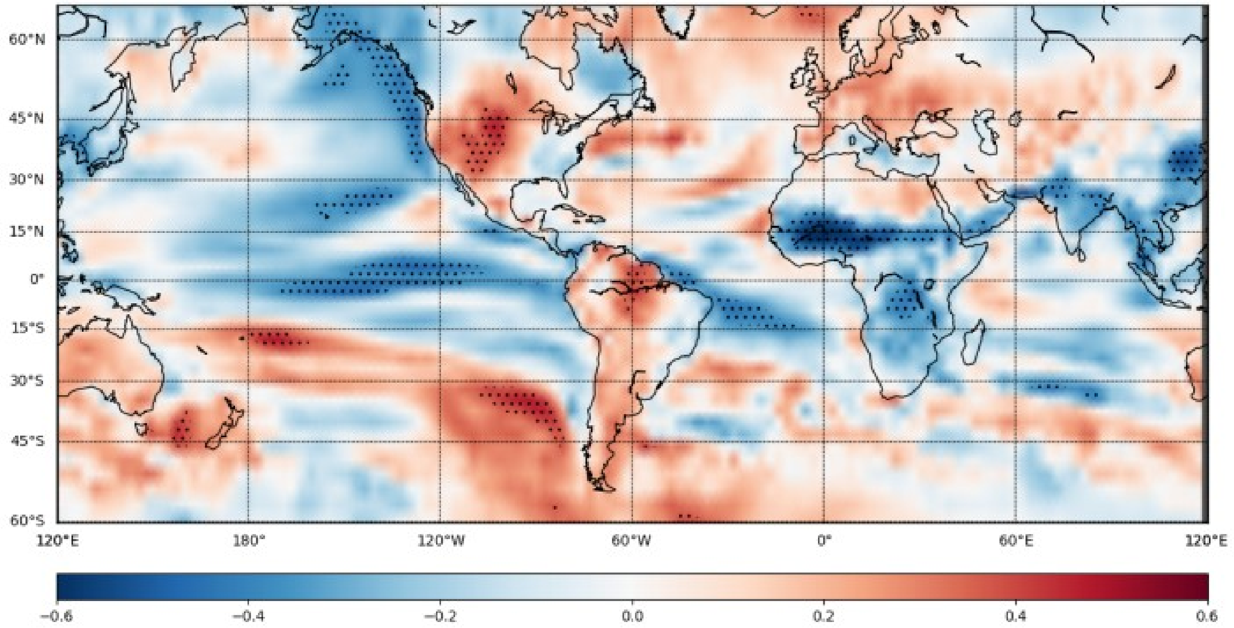

b) Partial regression between SV of Sahel rainfall change and temperature change (inter-hemispheric gradient and Nino3.4 excluded)

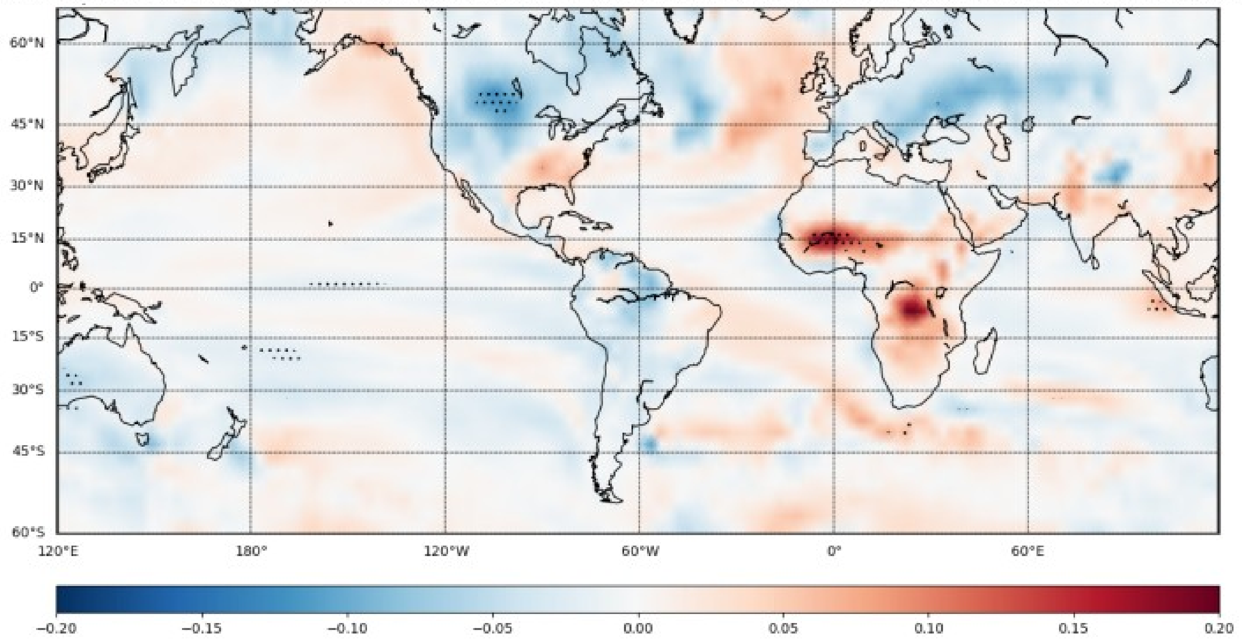

Fig.S6. Partial correlation between SV of Sahel rainfall change with temperature change, excluding in both their linear dependance (a) to the inter-hemispheric temperature change, (b)t o the inter-hemispheric temperature change and Nino3.4 change (see Section 2 for details). Dotted points indicate significant correlations at the 95% confidence level.

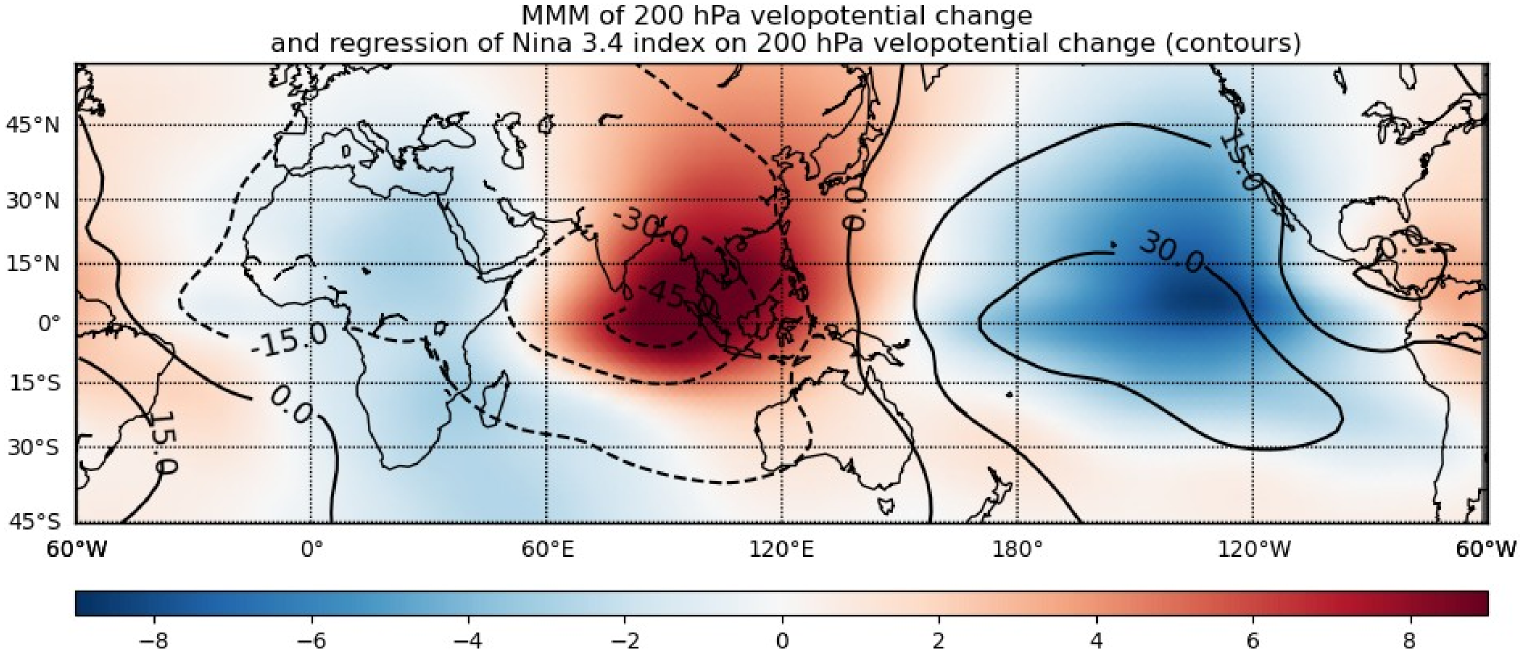

MMM of 200 hPa velopotential change
and regression of Nina 3.4 index on 200 hPa velopotential change (contours)

Fig.S7.MMM of velocity potential change at 200 hPa ($x10^5$ $m^2.s^{-1}.K^{-1}$, color shaded) and regression of the 200-hPa velocity potential change over onto the Nina 3.4 index (contour lines : $x10^5$ $m^2.s^{-1}.K^{-2}$). Note that the contour lines seems to oppose the MMM change.

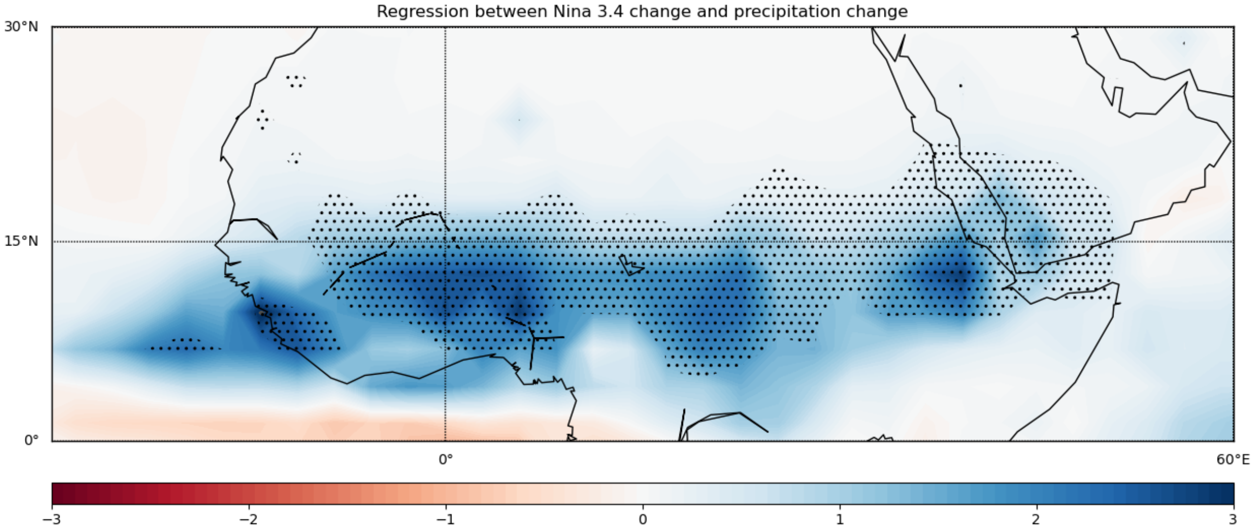

Fig.S8. Inter-model regression against minus Niño3.4 (see Niña3.4 in Section 2) temperature change of precipitation change (mm.d^{-1}.K^{-2})

List of acronyms

AEJ: African Easterly Jet
AIR: All-India Rainfall
AMOC: Atlantic Meridional Overturning Circulation
AMV: Atlantic Meridional Variability
CGCM: Coupled Global Circulation Model
CMIP: Coupled Model Intercomparison Project
DAMIP: Detection and Attribution Model Intercomparison Project
EC: Expansion Coefficient
ECMWF: European Center for Medium-ranged Weather Forecasting
ENSO: El-Nino Southern Oscillation
ERAi: ERA Interim
FAO: Food and Agriculture Organization of the United Nations
GDP: Gross Domestic Product
GHG: Greenhouse Gas
GPCC: Global Precipitation Climatology Centre
GPCP : Global Precipitation Climatology Project
IMD: India Meteorological Department
IPCC: Intergovernmental Panel on Climate Change
IPO: Interdecadal Pacific Oscillation
IPSL: Institut Pierre-Simon Laplace
ISM: Indian Summer Monsoon
ITCZ: Inter-Tropical Convergence Zone
LUMIP: Land Use Model Intercomparison Project
MCA: Maximum Covariance Analysis
MMM: Multi-Model Mean
NAF: North African monsoon
NC: Normalized root-mean-square Covariance
NOAA: National Oceanographic and Atmospheric Administration
ODT: Ocean Dynamical Thermostat
PCA: Principal Component Analysis
SAS: South Asian monsoon
SCF: Squared Covariance Fraction
SLP: Sea-level Pressure
SST: Sea Surface Temperature
SV: Singular Value
SVD: Singular Value Decomposition
TEJ: Tropical Easterly Jet

Bibliography

The part no one reads

Adler, R. F., Huffman, G. J., Chang, A., Ferraro, R., Xie, P.-P., Janowiak, J., Rudolf, B., Schneider, U., Curtis, S., Bolvin, D., et al. (2003). The version-2 global precipitation climatology project (gpcp) monthly precipitation analysis (1979–present). *Journal of hydrometeorology*, *4*(6), 1147–1167 (cited on page 43).

Allan, R. P., Barlow, M., Byrne, M. P., Cherchi, A., Douville, H., Fowler, H. J., Gan, T. Y., Pendergrass, A. G., Rosenfeld, D., Swann, A. L., et al. (2020). Advances in understanding large-scale responses of the water cycle to climate change. *Annals of the New York Academy of Sciences*, *1472*(1), 49–75 (cited on pages 29, 135).

Almazroui, M., Saeed, F., Saeed, S., Nazrul Islam, M., Ismail, M., Klutse, N. A. B., & Siddiqui, M. H. (2020). Projected change in temperature and precipitation over africa from cmip6. *Earth Systems and Environment*, *4*, 455–475 (cited on page 81).

Annamalai, H., Taguchi, B., McCreary, J. P., Nagura, M., & Miyama, T. (2017). Systematic errors in south asian monsoon simulation: Importance of equatorial indian ocean processes. *Journal of Climate*, *30*(20), 8159–8178 (cited on page 137).

Balaji, V., Couvreux, F., Deshayes, J., Gautrais, J., Hourdin, F., & Rio, C. (2022). Are general circulation models obsolete? *Proceedings of the National Academy of Sciences*, *119*(47), e2202075119 (cited on page 33).

Baldocchi, D. (2014). Measuring fluxes of trace gases and energy between ecosystems and the atmosphere–the state and future of the eddy covariance method. *Global change biology*, *20*(12), 3600–3609 (cited on page 30).

Bellomo, K., Angeloni, M., Corti, S., & von Hardenberg, J. (2021). Future climate change shaped by inter-model differences in atlantic meridional overturning circulation response. *Nature Communications*, *12*(1), 3659 (cited on page 27).

Biasutti, M. (2013). Forced sahel rainfall trends in the cmip5 archive. *Journal of Geophysical Research: Atmospheres*, *118*(4), 1613–1623 (cited on pages 28, 76).

Biasutti, M. (2019). Rainfall trends in the african sahel: Characteristics, processes, and causes. *Wiley Interdisciplinary Reviews: Climate Change*, *10*(4), e591 (cited on pages 22, 26, 27, 131, 137, 138).

Bjerknes, J. (1969). Atmospheric teleconnections from the equatorial pacific. *Monthly weather review*, *97*(3), 163–172 (cited on page 13).

Bjerknes, V. (1904). Das problem der wettervorhersage, betrachtet vom standpunkte der mechanik und der physik. *Meteor. Z.*, *21*, 1–7 (cited on page 32).

Bollasina, M. A., Ming, Y., & Ramaswamy, V. (2011). Anthropogenic aerosols and the weakening of the south asian summer monsoon. *science*, *334*(6055), 502–505 (cited on page 28).

Braconnot, P., Crétat, J., Marti, O., Balkanski, Y., Caubel, A., Cozic, A., Foujols, M.-A., & Sanogo, S. (2019). Impact of multiscale variability on last 6,000 years indian and west african monsoon rain. *Geophysical Research Letters*, *46*(23), 14021–14029 (cited on page 135).

Bretherton, C. S., Smith, C., & Wallace, J. M. (1992). An intercomparison of methods for finding coupled patterns in climate data. *Journal of climate*, *5*(6), 541–560 (cited on page 50).

Chadwick, R., Ackerley, D., Ogura, T., & Dommenget, D. (2019). Separating the influences of land warming, the direct co2 effect, the plant physiological effect, and sst warming on regional precipitation changes. *Journal of Geophysical Research: Atmospheres*, *124*(2), 624–640 (cited on page 30).

Charney, J., Quirk, W. J., Chow, S.-.-h., & Kornfield, J. (1977). A comparative study of the effects of albedo change on drought in semi–arid regions. *Journal of the atmospheric sciences*, *34*(9), 1366–1385 (cited on page 30).

Charney, J. G. (1975). Dynamics of deserts and drought in the sahel. *Quarterly Journal of the Royal Meteorological Society*, *101*(428), 193–202 (cited on page 76).

Chen, T.-C. (2003). Maintenance of summer monsoon circulations: A planetary-scale perspective. *Journal of climate*, *16*(12), 2022–2037 (cited on pages 128, 130, 131).

Chen, Z., Zhou, T., Zhang, L., Chen, X., Zhang, W., & Jiang, J. (2020). Global land monsoon precipitation changes in cmip6 projections. *Geophysical Research Letters*, *47*(14), e2019GL086902 (cited on pages 38, 76, 125, 135, 143).

Cherry, S. (1997). Some comments on singular value decomposition analysis. *Journal of Climate*, *10*(7), 1759–1761 (cited on page 51).

Chiang, J. C., & Friedman, A. R. (2012). Extratropical cooling, interhemispheric thermal gradients, and tropical climate change. *Annual Review of Earth and Planetary Sciences*, *40*, 383–412 (cited on page 29).

Chou, C., & Neelin, J. D. (2004). Mechanisms of global warming impacts on regional tropical precipitation. *Journal of climate*, *17*(13), 2688–2701 (cited on pages 76, 128).

Clement, A. C., Seager, R., Cane, M. A., & Zebiak, S. E. (1996). An ocean dynamical thermostat. *Journal of Climate*, *9*(9), 2190–2196 (cited on page 140).

Cleveland, W. S., & Devlin, S. J. (1988). Locally weighted regression: An approach to regression analysis by local fitting. *Journal of the American statistical association*, *83*(403), 596–610 (cited on page 49).

Dai, A., Lamb, P. J., Trenberth, K. E., Hulme, M., Jones, P. D., & Xie, P. (2004). The recent sahel drought is real. *International Journal of Climatology: A Journal of the Royal Meteorological Society*, *24*(11), 1323–1331 (cited on page 75).

Dai, A., Li, H., Sun, Y., Hong, L.-C., LinHo, Chou, C., & Zhou, T. (2013). The relative roles of upper and lower tropospheric thermal contrasts and tropical influences in driving asian summer monsoons. *Journal of Geophysical Research: Atmospheres*, *118*(13), 7024–7045 (cited on pages 19, 20).

Dee, D. P., Uppala, S. M., Simmons, A. J., Berrisford, P., Poli, P., Kobayashi, S., Andrae, U., Balmaseda, M., Balsamo, G., Bauer, d. P., et al. (2011). The era-interim reanalysis: Configuration and performance of the data assimilation system. *Quarterly Journal of the royal meteorological society*, *137*(656), 553–597 (cited on page 45).

Deser, C., Alexander, M. A., Xie, S.-P., & Phillips, A. S. (2010). Sea surface temperature variability: Patterns and mechanisms. *Annual review of marine science*, *2*, 115–143 (cited on page 26).

Deser, C., Guo, R., & Lehner, F. (2017). The relative contributions of tropical pacific sea surface temperatures and atmospheric internal variability to the recent global warming hiatus. *Geophysical Research Letters*, *44*(15), 7945–7954 (cited on pages 8, 142).

Deser, C., Phillips, A. S., Simpson, I. R., Rosenbloom, N., Coleman, D., Lehner, F., Pendergrass, A. G., DiNezio, P., & Stevenson, S. (2020). Isolating the evolving contributions of anthropogenic aerosols and greenhouse gases: A new cesm1 large ensemble community resource. *Journal of climate*, *33*(18), 7835–7858 (cited on page 48).

Dong, B., & Sutton, R. (2015). Dominant role of greenhouse-gas forcing in the recovery of sahel rainfall. *Nature Climate Change*, *5*(8), 757–760 (cited on page 76).

Eyring, V., Bony, S., Meehl, G. A., Senior, C. A., Stevens, B., Stouffer, R. J., & Taylor, K. E. (2016). Overview of the coupled model intercomparison project phase 6 (cmip6) experimental design and organization. *Geoscientific Model Development*, *9*(5), 1937–1958 (cited on page 46).

Ferguglia, O., von Hardenberg, J., & Palazzi, E. (2023). Robustness of precipitation emergent constraints in cmip6 models. *Climate Dynamics*, 1–12 (cited on pages 136, 139, 140).

Giannini, A., & Kaplan, A. (2019). The role of aerosols and greenhouse gases in sahel drought and recovery. *Climatic Change*, *152*(3-4), 449–466 (cited on page 76).

Gillett, N. P., Shiogama, H., Funke, B., Hegerl, G., Knutti, R., Matthes, K., Santer, B. D., Stone, D., & Tebaldi, C. (2016). The detection and attribution model intercomparison project (damip v1. 0) contribution to cmip6. *Geoscientific Model Development*, *9*(10), 3685–3697 (cited on page 141).

Graft, H., Kirchner, I., Robock, A., & Schult, I. (1993). Pinatubo eruption winter climate effects: Model versus observations. *Climate Dynamics*, *9*, 81–93 (cited on page 7).

Greene, A. M., Giannini, A., & Zebiak, S. E. (2009). Drought return times in the sahel: A question of attribution. *Geophysical Research Letters*, *36*(12) (cited on page 75).

Heede, U. K., Fedorov, A. V., & Burls, N. J. (2020). Time scales and mechanisms for the tropical pacific response to global warming: A tug of war between the ocean thermostat and weaker walker. *Journal of Climate*, *33*(14), 6101–6118 (cited on page 140).

Held, I. M. (2013). The cause of the pause. *Nature*, *501*(7467), 318–319 (cited on page 8).

Held, I. M., & Soden, B. J. (2006). Robust responses of the hydrological cycle to global warming. *Journal of climate*, *19*(21), 5686–5699 (cited on pages 34, 128, 135).

Hourdin, F., Mauritsen, T., Gettelman, A., Golaz, J.-C., Balaji, V., Duan, Q., Folini, D., Ji, D., Klocke, D., Qian, Y., et al. (2017). The art and science of climate model tuning. *Bulletin of the American Meteorological Society*, *98*(3), 589–602 (cited on pages 34, 143).

Huang, X., Zhou, T., Turner, A., Dai, A., Chen, X., Clark, R., Jiang, J., Man, W., Murphy, J., Rostron, J., et al. (2020). The recent decline and recovery of indian summer monsoon rainfall: Relative roles of external forcing and internal variability. *Journal of Climate*, *33*(12), 5035–5060 (cited on page 26).

Hurley, J. V., & Boos, W. R. (2013). Interannual variability of monsoon precipitation and local subcloud equivalent potential temperature. *Journal of Climate*, *26*(23), 9507–9527 (cited on page 137).

Janicot, S., Gaetani, M., Hourdin, F., Giannini, A., Biasutti, M., Mohino, E., Xue, Y., Boone, A., Gaye, A., Salack, S., et al. (2015). The recent partial recovery in sahel rainfall: A fingerprint of greenhouse gases forcing. *Gewex News*, *27*(4), 11–15 (cited on page 76).

Janicot, S., Trzaska, S., & Poccard, I. (2001). Summer sahel-enso teleconnection and decadal time scale sst variations. *Climate Dynamics*, *18*, 303–320 (cited on page 14).

Kamworapan, S., Thao, P. T. B., Gheewala, S. H., Pimonsree, S., & Prueksakorn, K. (2021). Evaluation of cmip6 gcms for simulations of temperature over thailand and nearby areas in the early 21st century. *Heliyon*, *7*(11) (cited on page 129).

Katzenberger, A., Schewe, J., Pongratz, J., & Levermann, A. (2021). Robust increase of indian monsoon rainfall and its variability under future warming in cmip6 models. *Earth System Dynamics*, *12*(2), 367–386 (cited on page 135).

Kay, J. E., Deser, C., Phillips, A., Mai, A., Hannay, C., Strand, G., Arblaster, J. M., Bates, S., Danabasoglu, G., Edwards, J., et al. (2015). The community earth system model (cesm) large ensemble project: A community resource for studying climate change in the presence of internal climate variability. *Bulletin of the American Meteorological Society*, *96*(8), 1333–1349 (cited on page 48).

Knight, J. R., Allan, R. J., Folland, C. K., Vellinga, M., & Mann, M. E. (2005). A signature of persistent natural thermohaline circulation cycles in observed climate. *Geophysical Research Letters*, *32*(20) (cited on page 27).

Koppen, W. (1936). Das geographische system de klimate. *Handbuch der klimatologie* (cited on page 4).

Kosaka, Y., & Xie, S.-P. (2013). Recent global-warming hiatus tied to equatorial pacific surface cooling. *Nature*, *501*(7467), 403–407 (cited on page 142).

Kucharski, F., Zeng, N., & Kalnay, E. (2013). A further assessment of vegetation feedback on decadal sahel rainfall variability. *Climate dynamics*, *40*, 1453–1466 (cited on pages 76, 142).

Lau, W. K., & Kim, K.-M. (2010). Fingerprinting the impacts of aerosols on long-term trends of the indian summer monsoon regional rainfall. *Geophysical Research Letters*, *37*(16) (cited on page 28).

Lawrence, D. M., Hurtt, G. C., Arneth, A., Brovkin, V., Calvin, K. V., Jones, A. D., Jones, C. D., Lawrence, P. J., de Noblet-Ducoudré, N., Pongratz, J., et al. (2016). The land use model intercomparison project (lumip) contribution to cmip6: Rationale and experimental design. *Geoscientific Model Development*, *9*(9), 2973–2998 (cited on page 142).

Lawrimore, J. H., Menne, M. J., Gleason, B. E., Williams, C. N., Wuertz, D. B., Vose, R. S., & Rennie, J. (2011). An overview of the global historical climatology network monthly mean temperature data set, version 3. *Journal of Geophysical Research: Atmospheres*, *116*(D19) (cited on page 45).

Lebel, T., & Ali, A. (2009). Recent trends in the central and western sahel rainfall regime (1990–2007). *Journal of hydrology*, *375*(1-2), 52–64 (cited on page 75).

Lehner, F., Deser, C., Maher, N., Marotzke, J., Fischer, E. M., Brunner, L., Knutti, R., & Hawkins, E. (2020). Partitioning climate projection uncertainty with multiple large ensembles and cmip5/6. *Earth System Dynamics*, *11*(2), 491–508 (cited on pages 35–37).

Levine, R. C., Turner, A. G., Marathayil, D., & Martin, G. M. (2013). The role of northern arabian sea surface temperature biases in cmip5 model simulations and future projections of indian summer monsoon rainfall. *Climate Dynamics*, *41*, 155–172 (cited on page 137).

Li, G., Xie, S.-P., He, C., & Chen, Z. (2017). Western pacific emergent constraint lowers projected increase in indian summer monsoon rainfall. *Nature Climate Change*, *7*(10), 708–712 (cited on pages 29, 40, 56, 125, 135, 139).

Li, X., Ting, M., & Lee, D. E. (2018). Fast adjustments of the asian summer monsoon to anthropogenic aerosols. *Geophysical Research Letters*, *45*(2), 1001–1010 (cited on page 28).

Lin, M., & Huybers, P. (2019). If rain falls in india and no one reports it, are historical trends in monsoon extremes biased? *Geophysical Research Letters*, *46*(3), 1681–1689 (cited on page 44).

Luo, Y., Lu, J., Liu, F., & Garuba, O. (2017). The role of ocean dynamical thermostat in delaying the el niño–like response over the equatorial pacific to climate warming. *Journal of Climate*, *30*(8), 2811–2827 (cited on page 140).

Lutgens, F., & Tarbuck, E. (2001). The atmosphereeighth ed. (Cited on page 11).

Ma, J., Chadwick, R., Seo, K.-H., Dong, C., Huang, G., Foltz, G. R., & Jiang, J. H. (2018). Responses of the tropical atmospheric circulation to climate change and connection to the hydrological cycle. *Annual Review of Earth and Planetary Sciences*, *46*, 549–580 (cited on page 135).

Maher, N., Milinski, S., & Ludwig, R. (2021). Large ensemble climate model simulations: Introduction, overview, and future prospects for utilising multiple types of large ensemble. *Earth System Dynamics*, *12*(2), 401–418 (cited on page 35).

Martin, E. R., & Thorncroft, C. D. (2014). The impact of the amo on the west african monsoon annual cycle. *Quarterly Journal of the Royal Meteorological Society*, *140*(678), 31–46 (cited on page 76).

Mauritsen, T., & Roeckner, E. (2020). Tuning the mpi-esm1. 2 global climate model to improve the match with instrumental record warming by lowering its climate sensitivity. *Journal of Advances in Modeling Earth Systems*, *12*(5), e2019MS002037 (cited on page 143).

Menne, M. J., Durre, I., Vose, R. S., Gleason, B. E., & Houston, T. G. (2012). An overview of the global historical climatology network-daily database. *Journal of atmospheric and oceanic technology*, *29*(7), 897–910 (cited on page 45).

Mignot, J., Hourdin, F., Deshayes, J., Boucher, O., Gastineau, G., Musat, I., Vancoppenolle, M., Servonnat, J., Caubel, A., Chéruy, F., et al. (2021). The tuning strategy of ipsl-cm6a-lr. *Journal of Advances in Modeling Earth Systems*, *13*(5), e2020MS002340 (cited on page 143).

Mohapatra, G., Beham, A., Kavyashree, C., Kavya, S., Singh, M., Vaishnavi, J., et al. (2018). Study of indian summer monsoon rainfall trend during the period 1901-2013 through data mining. *International Journal for Research in Applied Science and Engineering Technology*, *6*(5), 1701–1705 (cited on pages 44, 135).

Monerie, P.-A., Pohl, B., & Gaetani, M. (2021). The fast response of sahel precipitation to climate change allows effective mitigation action. *npj climate and atmospheric science*, *4*(1), 24 (cited on page 135).

Monerie, P.-A., Sanchez-Gomez, E., & Boé, J. (2017). On the range of future sahel precipitation projections and the selection of a sub-sample of cmip5 models for impact studies. *Climate Dynamics*, *48*(7-8), 2751–2770 (cited on pages 38, 81, 135, 137).

Morice, C. P., Kennedy, J. J., Rayner, N. A., & Jones, P. D. (2012). Quantifying uncertainties in global and regional temperature change using an ensemble of observational estimates: The hadcrut4 data set. *Journal of Geophysical Research: Atmospheres*, *117*(D8) (cited on page 8).

Ndiaye, C. D., Mohino, E., Mignot, J., & Sall, S. M. (2022). On the detection of externally forced decadal modulations of the sahel rainfall over the whole twentieth century in the cmip6 ensemble. *Journal of Climate*, *35*(21), 6939–6954 (cited on page 76).

Nicholson, S. E. (2009). A revised picture of the structure of the "monsoon" and land itcz over west africa. *Climate Dynamics*, *32*, 1155–1171 (cited on page 83).

O'Gorman, P. A., Allan, R. P., Byrne, M. P., & Previdi, M. (2012). Energetic constraints on precipitation under climate change. *Surveys in geophysics*, *33*, 585–608 (cited on page 135).

Park, J.-Y., Bader, J., & Matei, D. (2015). Northern-hemispheric differential warming is the key to understanding the discrepancies in the projected sahel rainfall. *Nature communications*, *6*(1), 5985 (cited on pages 40, 81, 135).

Parthasarathy, B., Munot, A., & Kothawale, D. (1994). All-india monthly and seasonal rainfall series: 1871–1993. *Theoretical and Applied Climatology*, *49*, 217–224 (cited on page 44).

Peatier, S., Sanderson, B., Terray, L., & Roehrig, R. (2022). Investigating parametric dependence of climate feedbacks in the atmospheric component of cnrm-cm6-1. *Geophysical Research Letters*, *49*(9), e2021GL095084 (cited on pages 34, 141).

Peterson, T. C., & Vose, R. S. (1997). An overview of the global historical climatology network temperature database. *Bulletin of the American Meteorological Society*, *78*(12), 2837–2850 (cited on page 45).

Power, S., Lengaigne, M., Capotondi, A., Khodri, M., Vialard, J., Jebri, B., Guilyardi, E., McGregor, S., Kug, J.-S., Newman, M., et al. (2021). Decadal climate variability in the tropical pacific: Characteristics, causes, predictability, and prospects. *Science*, *374*(6563), eaay9165 (cited on page 26).

Pu, B., & Cook, K. H. (2010). Dynamics of the west african westerly jet. *Journal of Climate*, *23*(23), 6263–6276 (cited on pages 82, 138).

Qin, M., Dai, A., & Hua, W. (2020). Quantifying contributions of internal variability and external forcing to atlantic multidecadal variability since 1870. *Geophysical Research Letters*, *47*(22), e2020GL089504 (cited on pages 27, 76).

Rodwell, M. J., & Hoskins, B. J. (1996). Monsoons and the dynamics of deserts. *Quarterly Journal of the Royal Meteorological Society*, *122*(534), 1385–1404 (cited on pages 130, 131, 138).

Rodwell, M. J., & Hoskins, B. J. (2001). Subtropical anticyclones and summer monsoons. *Journal of Climate*, *14*(15), 3192–3211 (cited on pages 128, 130, 138).

Roxy, M. K. (2017). Land warming revives monsoon. *Nature Climate Change*, *7*(8), 549–550 (cited on page 39).

Rudolf, B., Hauschild, H., Rueth, W., & Schneider, U. (1994). Terrestrial precipitation analysis: Operational method and required density of point measurements. *Global precipitations and climate change*, 173–186 (cited on page 45).

Ruiz-Vásquez, M., Arias, P. A., Martınez, J. A., & Espinoza, J. C. (2020). Effects of amazon basin deforestation on regional atmospheric circulation and water vapor transport towards tropical south america. *Climate Dynamics*, *54*, 4169–4189 (cited on page 143).

Samson, G., Masson, S., Durand, F., Terray, P., Berthet, S., & Jullien, S. (2017). Roles of land surface albedo and horizontal resolution on the indian summer monsoon biases in a coupled ocean–atmosphere tropical-channel model. *Climate dynamics*, *48*, 1571–1594 (cited on pages 127, 138).

Sandeep, N., Swapna, P., Krishnan, R., Farneti, R., Kucharski, F., Modi, A., Prajeesh, A., Ayantika, D., & Manmeet, S. (2022). On the weakening association between south asian monsoon and atlantic multidecadal oscillation. *Climate Dynamics*, *59*(9-10), 2531–2547 (cited on page 27).

Schmidt, G. A., Bader, D., Donner, L. J., Elsaesser, G. S., Golaz, J.-C., Hannay, C., Molod, A., Neale, R. B., & Saha, S. (2017). Practice and philosophy of climate model tuning across six us modeling centers. *Geoscientific Model Development*, *10*(9), 3207–3223 (cited on page 143).

Schneider, T., Bischoff, T., & Haug, G. H. (2014). Migrations and dynamics of the intertropical convergence zone. *Nature*, *513*(7516), 45–53 (cited on pages 23, 82, 130, 131).

Schneider, T., Teixeira, J., Bretherton, C. S., Brient, F., Pressel, K. G., Schär, C., & Siebesma, A. P. (2017). Climate goals and computing the future of clouds. *Nature Climate Change*, *7*(1), 3–5 (cited on pages 34, 141).

Senior, C. A., Jones, C. G., Wood, R. A., Sellar, A., Belcher, S., Klein-Tank, A., Sutton, R., Walton, J., Lawrence, B., Andrews, T., et al. (2020). Uk community earth system modeling for cmip6. *Journal of Advances in Modeling Earth Systems*, *12*(9), e2019MS002004 (cited on page 143).

Seth, A., Giannini, A., Rojas, M., Rauscher, S. A., Bordoni, S., Singh, D., & Camargo, S. J. (2019). Monsoon responses to climate changes—connecting past, present and future. *Current Climate Change Reports*, *5*, 63–79 (cited on page 76).

Singh, D., Ghosh, S., Roxy, M. K., & McDermid, S. (2019). Indian summer monsoon: Extreme events, historical changes, and role of anthropogenic forcings. *Wiley Interdisciplinary Reviews: Climate Change*, *10*(2), e571 (cited on page 44).

Sooraj, K., Terray, P., Masson, S., & Crétat, J. (2019). Modulations of the indian summer monsoon by the hot subtropical deserts: Insights from coupled sensitivity experiments. *Climate Dynamics*, *52*, 4527–4555 (cited on pages 127, 130).

Staal, A., Dekker, S. C., Hirota, M., & van Nes, E. H. (2015). Synergistic effects of drought and deforestation on the resilience of the south-eastern amazon rainforest. *Ecological Complexity*, *22*, 65–75 (cited on page 143).

Terray, P., Sooraj, K., Masson, S., Krishna, R., Samson, G., & Prajeesh, A. (2018). Towards a realistic simulation of boreal summer tropical rainfall climatology in state-of-the-art coupled models: Role of the background snow-free land albedo. *Climate Dynamics*, *50*, 3413–3439 (cited on pages 127, 128, 138).

Trenberth, K. E., Branstator, G. W., Karoly, D., Kumar, A., Lau, N.-C., & Ropelewski, C. (1998). Progress during toga in understanding and modeling global teleconnections associated with tropical sea surface temperatures. *Journal of Geophysical Research: Oceans*, *103*(C7), 14291–14324 (cited on pages 14, 82).

Turner, A. G., Bhat, G., Martin, G., Parker, D. J., Taylor, C., Mitra, A. K., Tripathi, S. N., Milton, S., Rajagopal, E., Evans, J. G., et al. (2020). Interaction of convective organization with monsoon precipitation, atmosphere, surface and sea: The 2016 incompass field campaign in india. *Quarterly Journal of the Royal Meteorological Society*, *146*(731), 2828–2852 (cited on page 39).

Vial, J., Dufresne, J.-L., & Bony, S. (2013). On the interpretation of inter-model spread in cmip5 climate sensitivity estimates. *Climate Dynamics*, *41*, 3339–3362 (cited on pages 34, 141).

Von Storch, H., & Navarra, A. (1999). *Analysis of climate variability: Applications of statistical techniques*. Springer Science & Business Media. (Cited on pages 48, 49).

Wang, B., Liu, J., Kim, H.-J., Webster, P. J., & Yim, S.-Y. (2012). Recent change of the global monsoon precipitation (1979–2008). *Climate Dynamics*, *39*, 1123–1135 (cited on page 16).

Wang, B., Yim, S.-Y., Lee, J.-Y., Liu, J., & Ha, K.-J. (2014). Future change of asian-australian monsoon under rcp 4.5 anthropogenic warming scenario. *Climate dynamics*, *42*, 83–100 (cited on page 29).

Webster, P. J., Magana, V. O., Palmer, T., Shukla, J., Tomas, R., Yanai, M., & Yasunari, T. (1998). Monsoons: Processes, predictability, and the prospects for prediction. *Journal of Geophysical Research: Oceans*, *103*(C7), 14451–14510 (cited on pages 14, 15).

Wentz, F. J., Ricciardulli, L., Hilburn, K., & Mears, C. (2007). How much more rain will global warming bring? *Science*, *317*(5835), 233–235 (cited on page 135).

Yan, Y., Lu, R., & Li, C. (2019). Relationship between the future projections of sahel rainfall and the simulation biases of present south asian and western north pacific rainfall in summer. *Journal of Climate*, *32*(4), 1327–1343 (cited on page 135).

Zhang, Y., Norris, J. R., & Wallace, J. M. (1998). Seasonality of large-scale atmosphere–ocean interaction over the north pacific. *Journal of Climate*, *11*(10), 2473–2481 (cited on page 51).

Zhang, Z., & Li, G. (2022). Uncertainty in the projected changes of sahel summer rainfall under global warming in cmip5 and cmip6 multi-model ensembles. *Climate Dynamics*, *59*(11-12), 3579–3597 (cited on pages 38–40, 81, 135, 137).

Zuo, Z., & Zhang, K. (2023). Link between the land–sea thermal contrast and the asian summer monsoon. *Journal of Climate*, *36*(1), 213–225 (cited on page 29).